

## DISSERTATION

# The Fundamental Parameter Approach of Quantitative XRFA Investigation of Photoelectric Absorption Coefficients

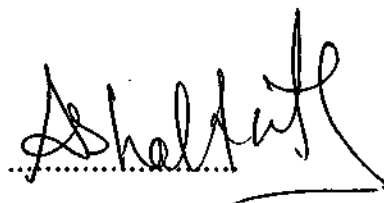
Ausgeführt zum Zwecke der Erlangung des akademischen Grades eines  
Doktors der technischen Wissenschaften unter der Anleitung von

**Univ. Prof. Dr. Horst Ebel**  
Institutsnummer: 138  
Institut für Festkörperphysik

eingereicht an der Technischen Universität Wien  
Fakultät für Technische Naturwissenschaften und Informatik

von  
**Abdallah A. Shaltout**  
Matrikelnummer: 9927156  
Penzingerstraße 150-166/26/2, 1140 Wien

Wien, im Juni 2003



بِسْمِ اللَّهِ الرَّحْمَنِ الرَّحِيمِ  
 وَقَدْ خَلَقْنَا الْإِنْسَانَ مِنْ سُلَالَةٍ مِنْ طِينٍ (١٢) ثُمَّ جَعَلْنَاهُ نُطْقَةً فِي قَرَارٍ مَكِينٍ (١٣) ثُمَّ خَلَقْنَا  
 النُّطْقَةَ عِلاَقَةً فَخَلَقْنَا الْمَلَقَةَ مُضْغَةً فَخَلَقْنَا الْمُضْغَةَ عِظَامًا فَكَسَوْنَا الْعِظَامَ لَحْمًا ثُمَّ أَنْشَأْنَاهُ خَلْقًا آخَرَ  
 فَتَبَارَكَ اللَّهُ أَحْسَنُ الْخَالِقِينَ (١٤) (المؤمنون)



Im Namen Allahs,  
 des Allerbarmers, des Barmherzigen

Und wahrlich, Wir erschufen den Menschen aus einer Substanz aus Lehm(12). Alsdann setzten Wir ihn als Samentropfen an eine sichere Ruhestätte(13). Dann bildeten Wir den Tropfen zu einem Blutklumpen; dann bildeten Wir den Blutklumpen zu einem Fleischklumpen; dann bildeten Wir aus dem Fleischklumpen Knochen; dann bekleideten Wir die Knochen mit Fleisch; dann entwickelten Wir es zu einer anderen Schöpfung. So sei denn Allah gepriesen, der beste Schöpfer(14). **Al-Mu'minun**



In the Name of Allah,  
 Most Gracious, Most Merciful

Verily We created man from a product of wet earth(12). Then placed him as a drop (of seed) in a safe lodging(13). Then fashioned We the drop a clot, then fashioned We the clot a little lump, then fashioned We the little lump bones, then clothed the bones with flesh, and then produced it as another creation. So blessed be Allah, the Best of creators!(14). **Al-Mu'minun**

## Deutsche Kurzfassung der Dissertation

Die vorliegende Arbeit befasst sich mit aktuellen Problemen der quantitativen Röntgenfluoreszenzanalyse auf der Basis des fundamentalen Parameter Ansatzes. Zur Einführung in die Thematik werden zunächst die wesentlichen charakteristischen Größen anhand der Beispiele der Röntgenröhrenspektren, der Detektoreffizienz und des analytischen Ansatzes für Mehrstoffsysteme unter Berücksichtigung der Primär- und der Sekundäranregung erörtert. Als wesentlicher Parameter mit dem dringenden Bedarf nach einer umfassenden Überprüfung stellt sich dabei der photoelektrische Wirkungsquerschnitt dar.

Um einen möglichst vollständigen Überblick über den derzeitigen Wissensstand zu erlangen, werden die photoelektrischen Wirkungsquerschnitte und die kohärenten und die inkohärenten Streuquerschnitte im Quantenenergiebereich von 1 bis 300 keV für die chemischen Elemente mit den Ordnungszahlen von  $Z=1$  bis  $Z=94$  aus den Tabellen und den Datenbanken von HubbeU, McMaster, MUCALL, Scofield, XCOM, Elam, Sasaki, Henke, Cullen und Chantier untersucht. Eine Korrektur, Vervollständigung und gezielte Anpassung an die Erfordernisse fundamentaler Parameterprogramme für quantitative energie- und wellenlängendispersive Röntgenanalytik, sowie Elektronenstrahlmikroanalyse, Röntgenphotoelektronenspektrometrie und die Analytik mittels Messung der durch Röntgenstrahlung ausgelösten Elektronenemission trägt zur wesentlichen Verbesserung der Qualität und der Darstellung der Datensätze photoelektrischer Wirkungsquerschnitte bei.

In den bei der Entwicklung von einschlägigen Rechenprogrammen häufig verwendeten McMaster-Tafeln fehlen die chemischen Elemente  $Z=84, 85, 87, 88, 89, 91$  und  $93$ . Diese mußten ergänzt werden, wobei die photoelektrischen Wirkungsquerschnitte der Schalen und der Subschalen aus den Tabellen von Scofield, die Streuquerschnitte aus der Elam-Datei und die Kantenpositionen aus den Tabellen von Bearden in die McMaster Darstellung Eingang fanden. Die Polynom Anpassungen der Elemente von  $Z=61$  bis  $69$  im N-Bereich sind falsch. Eine Korrekturmöglichkeit bietet die Ausgleichsrechnung an tabellierte Werte im betrachteten Quantenenergiebereich. Darüber hinaus sind in den McMaster Tabellen von der Gesamtheit der M- und N-Kanten nur die  $M_1$ - und  $N_1$ -Kanten energiemäßig spezifiziert. Ebenso fehlen die zugehörigen Kantensprünge. Diese fehlenden Daten werden in der vorliegenden Arbeit durch Daten aus den Bearden-Tabellen und durch Extrapolation der jeweiligen Subschalen Wirkungsquerschnitte erarbeitet. Ein generelles Problem aller Dateien stellt der Verlauf im Bereiche der Absorptionskanten dar. Aus dem Vergleich der einzelnen Datenwerke und den Ergebnissen von Messungen im kantennahen Bereich geht hervor, dass nach dem derzeitigen Wissensstand für die Anwendung der Daten in fundamentalen Parameter Programmen ein Sägezahnverlauf die bestmögliche Beschreibung darstellt. Anhand der Theorie zur Beschreibung der Anregung charakteristischer K- und L-Strahlungen wird gezeigt, dass das Konzept der Absorptionskantensprünge bereits bei L-Strahlungen zu deutlichen Fehlern Anlass gibt. Aus diesem Grunde wurde ein allgemein zugänglicher Algorithmus (Internet) auf der Basis der Scofield Daten in Polynomdarstellung entwickelt, der sägezahnförmige Kantenstrukturen und die Beschreibung aller Subschalenquerschnitte gestattet. Die Kantenpositionen entsprechen dem derzeit aktuellen Datenmaterial.

Die Ergebnisse bei der Anwendung auf die quantitative Analyse binärer und ternärer Proben bestätigt die Qualität der neu entwickelten Datenbeschreibung .

## ABSTRACT

The present work describes some actual problems of quantitative x-ray fluorescence analysis by means of the fundamental parameter approach. To perform this task, some of the main parameters are discussed in detail. These parameters are photoelectric cross sections, coherent and incoherent scattering cross sections, mass absorption cross sections and the variation of the x-ray tube voltage.

Photoelectric cross sections, coherent and incoherent scattering cross sections and mass absorption cross sections in the energy range from 1 to 300 keV for the elements from  $Z=1$  to 94 considering ten different data bases are studied. These are data bases given by Hubbell, McMaster, Mucall, Scofield, Xcom, Ekm, Sasaki, Henke, Cullen and Chander's data bases. These data bases have been developed also for an application in fundamental parameter programs for quantitative x-ray analysis (Energy Dispersive X-Ray Fluorescence Analysis (EDXRFA), Electron Probe Microanalysis (EPMA), X-Ray Photoelectron Spectroscopy (XPS) and Total Electron Yield (TEY)). In addition a comparison is performed between different data bases.

In McMaster's data base, the missing elements ( $Z=84, 85, 87, 88, 89, 91,$  and  $93$ ) are added by using photoelectric cross sections of Scofield's data base, coherent as well as incoherent scattering cross sections of Elam's data base and the absorption edges of Bearden. Also, the N-fit coefficients of the elements from  $Z=61$  to  $69$  are wrong in McMaster data base, therefore, linear least squares fits are used to recalculate the N-fit coefficients of these elements. Additionally, in the McMaster tables the positions of the M- and N-edges of all elements with the exception of the  $M_1$ - and  $N_1$ - edges are not defined as well as the jump ratio of the edges. In the present work, the M- and N-edges and the related jump ratios are calculated. To include the missing N-edges, Bearden's values of energy edges are used. In Scofield's data base, modifications include check and correction of edge positions, description of  $M_4$  and  $M_5$ -ranges of elements from  $Z=61$  upwards by sawtooth responses and reduction of data by introduction of least squares fits of fifth order. In order to calculate the mass absorption coefficients from Scofield's data base, coherent and incoherent scattering cross sections have to be taken from Elam's numerical data. This revised version of Scofield's data base is recommended for quantitative x-ray analysis programs.

The detector efficiency of both EPMA and EDXRFA was calculated theoretically. Consequently, a comparison between experimental and theoretical x-ray tube spectra at 30 keV indicated the validity of the computed detector efficiencies. A precise calculation of correction factor and solid angle is performed in order to decrease the systematic errors in the fundamental parameter programs. By using the mentioned new set of fundamental parameters, a quantitative analysis of binary and ternary alloys was performed. The comparison between computed and expected compositions confirms the quality of the modified fundamental parameters.

## الملخص العربي

يركز العمل الحالي على عملية التحليل الكمي للأشعة السينية الفلورية وذلك عن طريق التحليل النظري باستخدام العوامل الأساسية. لإنجاز هذا العمل فقد تم تطوير عدد من العوامل الأساسية. هذه العوامل هي المقاطع العرضية الكهروضوئية ومقاطع التبعثر العرضية المتماسكة والمتفككة بالإضافة (الى المقاطع العرضية المتماسكة والمتفككة). المقاطع العرضية الكهروضوئية وللمتفككة والمتفككة بالإضافة (الى المقاطع العرضية المتماسكة والمتفككة). المقاطع العرضية الكهروضوئية وللمتفككة والمتفككة بالإضافة (الى المقاطع العرضية المتماسكة والمتفككة). المقاطع العرضية الكهروضوئية وللمتفككة والمتفككة بالإضافة (الى المقاطع العرضية المتماسكة والمتفككة).

في مدى الطاقة من 1 الي 300 كيلو إلكترون فولت تم دراسة المقاطع العرضية الكهروضوئية ومقاطع التبعثر العرضية المتماسكة والمتفككة والمقاطع العرضية الكلية في عشرة قواعد بيانات مختلفة وذلك للعناصر الكيميائية ذات العدد الذري من 1 الى 94. قواعد بيانات الأشعة السينية المستخدمة هي قواعد بيانات التجريبي (المقاسة عمليا) وقواعد بيانات مك ماستر وقواعد بيانات ميوكال وقواعد بيانات إسكوفيلد وقواعد بيانات إكس كوم وقواعد بيانات إيلام وقواعد بيانات ساساكي وقواعد بيانات إكس كي وقواعد بيانات كالتن وأخيرا قواعد بيانات شانتر. تم تطوير قواعد البيانات المذكورة خصيصا حتى يمكن استخدامها فيما بعد في البرامج النظرية لعملية التحليل الكمي بالأشعة السينية الفلورية. وبهذا فيمكن استخدامها أى من قواعد البيانات المذكورة في كل من المجالات الآتية: مجال تحليل الأشعة السينية الفلورية باستخدام تفريق الطاقة (XRFA) ومجال التحليل الدقيق باستخدام الإلكترون الموجه (EPMA) ومجال التحليل باستخدام الإلكترون الضوئي المصاحب للأشعة السينية (XPS) ومجال التحليل باستخدام التحصيل الإلكتروني (TEY). إضافة إلى ذلك فقد تم عمل مقارنة بين كل من قواعد البيانات المذكورة.

تعديلات مؤثرة تم إدخالها على قواعد بيانات كل من مك ماستر و"كوفيلد. ففي قواعد بيانات مك ماستر تم إضافة العناصر الكمومية المفقودة ذات الأعداد الذرية 84, 85, 87, 88, 89, 91 و93. وإضافة هذه العناصر فقد استخدم المقاطع العرضية الكهروضوئية لإسكوفيلد ومقاطع التبعثر العرضية المتماسكة والمتفككة لإيلام وحافات امتصاص الطاقة لبيردن. أيضا فقد وجد أن معاملات المقاطع العرضية الكهروضوئية عند مدى الطاقة الخاص بالمدار N وذلك للعناصر الكمومية ذات الأعداد الذرية من 61 إلى 69, غير صحيحة في قواعد بيانات مك ماستر. ولذلك فقد تم إعادة حساب هذه المعاملات وتصحيحها. أيضا فإن جميع قيم حافات امتصاص الطاقة ونسب القفز المتعلقة للمدارين N, M غير معرفتي قواعد بيانات مك ماستر وذلك باستثناء المدارين الفرعيين  $M_1, N_1$ . ولذلك فقد تم في هذا العمل حساب جميع قيم حافات امتصاص الطاقة ونسب القفز المتعلقة بكل منها. بالإضافة قيم حافات امتصاص الطاقة ونسب القفز المتعلقة للمدارين N, M فقد تم استخدام قيم حافات امتصاص الطاقة المقاسة تجريبيا بواسطة بيردن.

Lai في قواعد بيانات إسكوفيلد، فقد تم تدقيق وتصحيح جميع قيم حافات امتصاص الطاقة وخاصة عند حافتي امتصاص الخاصة بالمدارين الفرعيين  $M_4, M_5$ . وللحصول على أفضل قيم لمعاملات المقاطع العرضية الكهروضوئية والتي تغطي جميع المقاطع تماما للقيم الأصلية لإسكوفيلد، فقد تم حساب هذه المعاملات باستخدام درجة التقريب الخامسة والحادية عشرة للمعادلة العرضية للامتصاص  $K_{eff}$  فقد تم الاستعانة بمقاطع التبعثر العرضية المتماسكة والمتفككة لإيلام وحافات امتصاص الطاقة لبيردن بدلا من حافات امتصاص الطاقة لإسكوفيلد. من ثم فإننا نوصي باستخدام قواعد بيانات إسكوفيلد المعدلة في البرامج النظرية للتحليل الكمي باستخدام الأشعة السينية الفلورية.

أضا فقد تم نظريا حساب كفاءة كاشف الأشعة السينية والمنتز من في كلامن جهاز تحليل الأشعة السينية الفلورية باستخدام تفريق الطاقة (XRFA) وجهاز التحليل الدقيق باستخدام الإلكترون الموجه (EPMA). وبناء على ذلك تم حساب كلا من معامل التبعثر وحج ومقدار الزاوية المحسمة وذلك لتقليل نسبة الخطأ عند استخدام هذه العوامل الأساسية في برامج التحليل الكمي. بالإضافة إلى ذلك فقد تم أيضا عمل مقارنة بين ما يه أنبوب الأشعة السينية نظريا ومما يراقده وجد توافق بين الحسابات النظرية. ومع استخدام العوامل الأساسية الجديدة التي تم التوصل إليها في عملية التحليل الكمي للسبائك الثنائية والثلاثية ومقارنة ذلك بالنتائج العملية، فإن النتائج تؤكد كفاءة ودقة العوامل الأساسية التي تم التوصل إليها.

## ACNOWLEDGMENT

Thanks to my God for helping me to complete this work. This work was accomplished under the supervision of Univ. Prof. Dr. Horst Ebel, Institute of Solid State Physics, Vienna University of Technology. I am grateful for his support of both scientific and administrative nature.

I am indebted to Univ. Prof. Dr. Maria Ebel, Institute of Solid State Physics, Vienna University of Technology for her help in the beginning and in the final revision of my thesis. Also, I am indebted to Univ. Prof. Dr. Johann Wernisch, Institute of Solid State Physics, Vienna University of Technology for his help in the experimental measurements in the Electron Probe Micro Analyser (EPMA). Finally, I am indebted to Robert Svagera, Institute of Solid State Physics, Vienna University of Technology for discussions during the progress of this work.

I am indebted to Dr. Theresia Laubichler and Mag. Brigitte Moerth-Cikanek, Österreichische Orient-Gesellschaft Hammer-Purgstall for financial support during the last two years.

I cannot forget my family, my parent's memory, my brothers Mohamed and Mahmoud Shaltout, my wife Eman Nassar, my daughter Maria and my son Motasem.

I would like also to express my gratitude to the following authorities

- Institute of Solid State Physics, Vienna University of Technology, Wiedner Hauptstraße, 8-10/138, Austria
- Österreichische Orient-Gesellschaft Hammer-Purgstall, 1010 Wien, Dominikanerbastei 6/6, Austria

# CONTENTS

## INTRODUCTION

Introduction	1
--------------	---

### CHAPTER 1

#### THEORETICAL BASIS OF X-RAY SPECTRA AND THE FUNDAMENTAL PARAMETER APPROACH

1.1	Fundamental Parameters	5
1.1.1	X-Ray Cross Sections	5
1.1.1.1	X-Ray Scattering	5
1.1.1.2	Photoelectric Effect	9
1.1.1.3	X-Ray Absorption	9
1.1.2	Fluorescence Yield	11
1.1.3	Transition Probability	13
1.2	Theoretical Bases of X-Ray Tube Spectra	14
1.2.1	The Continuous X-Radiation,(Bremsstrahlung)	14
1.2.2	The Characteristic X-Ray Radiation	18
1.3	Theoretical Bases of the Fundamental Parameter Approach	20
1.3.1	The Primary Fluorescence.	20
1.3.2	The Secondary Fluorescence	24
1.3.3	The Tertiary Fluorescence	28
1.3.4	Iteration Procedure	29
1.4	Si(Li) Detector	30
1.4.1	Detector Efficiency	31
1.4.1.1	Detector Efficiency ofEDXRF-KEVEX 0700	32
1.4.1.2	Detector Efficiency ofEPMA	33

### CHAPTER 2

#### QUANTITATIVE ANALYSIS USING FUNDAMENTAL PARAMETER APPROACH

2.1	X-Ray Tube Spectra	35
2.1.1	Comparison Between Theoretical and Experimental Continuous X-Ray Spectra	36
2.2	Solid Angle	38
2.3	Correction Factor	41
2.4	Quantitative Analysis of Binary Alloys Using Fundamental Parameter Approach	44
2.4.1	Cu-Zn Binary Alloy	44
2.4.2	Au-Ni Binary Alloys	45
2.4.3	Al-Cu Binary Alloy	47
2.4.3.1	Quantitative Analysis Results	49
2.5	The Effect of X-Ray Tube Voltage Variation on the Results of Quantitative Analysis of a Ternary Alloy Cu-Zn-Pb	50
2.6	Cu-Zn-Pb Quantitative Analysis Using Theoretical and Experimental X-ray Spectra	54

**CHAPTER 3**  
**UNCERTAINTIES IN THE DATABASES OF**  
**X-RAY CROSS SECTIONS**

3.1	The Experimental Database	58
3.2	McMaster Database	63
3.2.1	Errors in the McMaster Database	64
3.2.2	Edge Energies and the Related Jump Ratios	70
3.2.3	Shaltout's Corrected Version of McMaster Database	73
3.2.4	Previous Description of McMaster Database, (MUCAL Program)	73
3.3	Scofield's Database	75
3.3.1	Description of Scofield's Database	75
3.3.2	Criticisms	78
3.3.3	Least Squares Fitting of Scofield Data	80
3.3.4	Comparison between Edge Energy Values of Scofield and Bearden	87
3.4	XCOM Database	89
3.5	Elam's Database	91
3.6	Cullen's Database	93
3.6.1	EPICSHOW program	96
3.7	Henke's Database	98
3.8	Sasaki's Database	100
3.9	Chantler's Database	101
3.10	Comparisons between the Available Databases	102
3.11	Published Paper	103
3.11.1	Abstract	103
3.11.2	Introduction	103
3.11.3	Comparison of Different Databases	104
3.11.4	Modification of Scofield's Database	112

**CHAPTER 4**  
**THE COMPUTING ALGORITHMS**

4.1	SCOFFT.BAS	116
4.2	MOMMCM.BAS	119

<b>REFERENCES</b>	<b>140</b>
-------------------	------------



## INTRODUCTION

The history of x-ray fluorescence dates back to the discovery of x-rays. In 1895 the German physicist Roentgen discovered x-rays while studying cathode rays in a gas discharge. He realized that some new kind of radiation was emitted by the discharge volume to make material fluorescent. He did not know that it was a particularly short wavelength electromagnetic radiation. So he called the mystery radiation "x-rays". X-rays can be defined as electromagnetic radiation of wavelengths from approximately 0.01 to 20 nm. X-rays were widely applied in medical and industrial radiography and fluoroscopy within the first years after their discovery.

X-rays are produced when high energy electrons are stopped in matter (Bremsstrahlung) or when electron transitions occur in the inner shells of atoms (characteristic radiation). Other sources of x-radiation are from "accelerated" electrons (synchrotron radiation), radioactive elements ( $\gamma$ -rays) and high temperature plasmas from stars (black body radiation).

The simplest way to decelerate electrons abruptly is to bring them to a sudden stop by directing a beam of them onto a metal target. These electrons are emitted by thermal emission from a hot cathode, accelerated to a kinetic energy of some keV and after that directed onto the metal target.

Moseley[1, 2] established the basis for qualitative x-ray spectrochemical analysis in 1913. He discovered for the first time a systematic correlation between wavelengths (frequency) of characteristic radiations of the chemical elements and their atomic number. From this correlation he predicted the existence of three unknown elements (Tc, Pm and Re). The present work concentrates on the application of x-ray spectrometry to elemental analysis.

Since 1950, the use of x-ray spectrometry for elemental analysis became widespread. Until the late 1960s, all spectrometers were wavelength dispersive x-ray fluorescence spectrometers. In the early 1970s energy dispersive x-ray fluorescence spectrometry became available. In conventional x-ray spectrometry, the spectral region of interest is 0.02 ~ 2 nm. All of the early work in x-ray spectrometry was done by electron excitation and this technique is still used in electron probe micro analysis. Nowadays, different kinds of x-ray excitation are used, such as x-ray photons from tubes or secondary targets,  $\gamma$ -rays, proton source and synchrotron source. When x-rays interact with matter, they can be either absorbed by the atoms or scattered. The following processes are of interest for x-ray analysis:

- **Photoelectric absorption**

An x-ray photon is absorbed by the atom by transferring its energy to one or even more electrons of the atom. If the photon has sufficient energy, an electron can be removed from the inner shells, creating a vacancy as shown in Fig. 1(a).

- **X-ray fluorescence**

As a consequence of photoelectric absorption, there are one or even more vacancies in the atom. These vacancies cause an unstable state of the atom. As the atom returns to its ground state, electrons from the outer shells are transferred to the inner shells. The atom emits electromagnetic radiation with energies depending on the binding energy of the electrons. Many such transitions take place in one atom and a number of characteristic energies can be detected by exciting a single atom. The process of emission of characteristic x-rays after photoelectric absorption is called "X-Ray Fluorescence". Figs. 1(b) and (c) show the processes for K and L radiation. The characteristic x-rays are labeled K, L, M, or N to denote the shells they originated from. The designation alpha ( $\alpha$ ), beta ( $\beta$ ) and gamma ( $\gamma$ ) is made to mark the intensity of the corresponding

radiation. Thus,  $K_{\alpha}$  has the highest signal strength of K-radiations and is produced from a transition of an electron from  $L_{2,3}$  to K, and similarly  $K_{\beta}$  transitions are produced from transitions of an electron from M or N to K. Since within the shells there are multiple orbits of higher and lower binding energy, further designation is made such as  $\alpha_1, \alpha_2, \beta_1, \beta_2$  in order to denote transitions of electrons from these orbits into the same shell (K). The wavelength of the radiations  $\lambda$  emitted from any one transition can be determined from the following equation.

$$E = h\nu = \frac{hc}{\lambda} \quad (1)$$

Where  $E$  is the difference in binding energy of an electron in its final and excited states,  $h$  is Planck's constant,  $c$  is the velocity of light and  $V$  is the frequency of the radiation. Equation 1 can be expressed as:

$$E_{keV} = \frac{1.2398}{\lambda_{nm}} \quad (2)$$

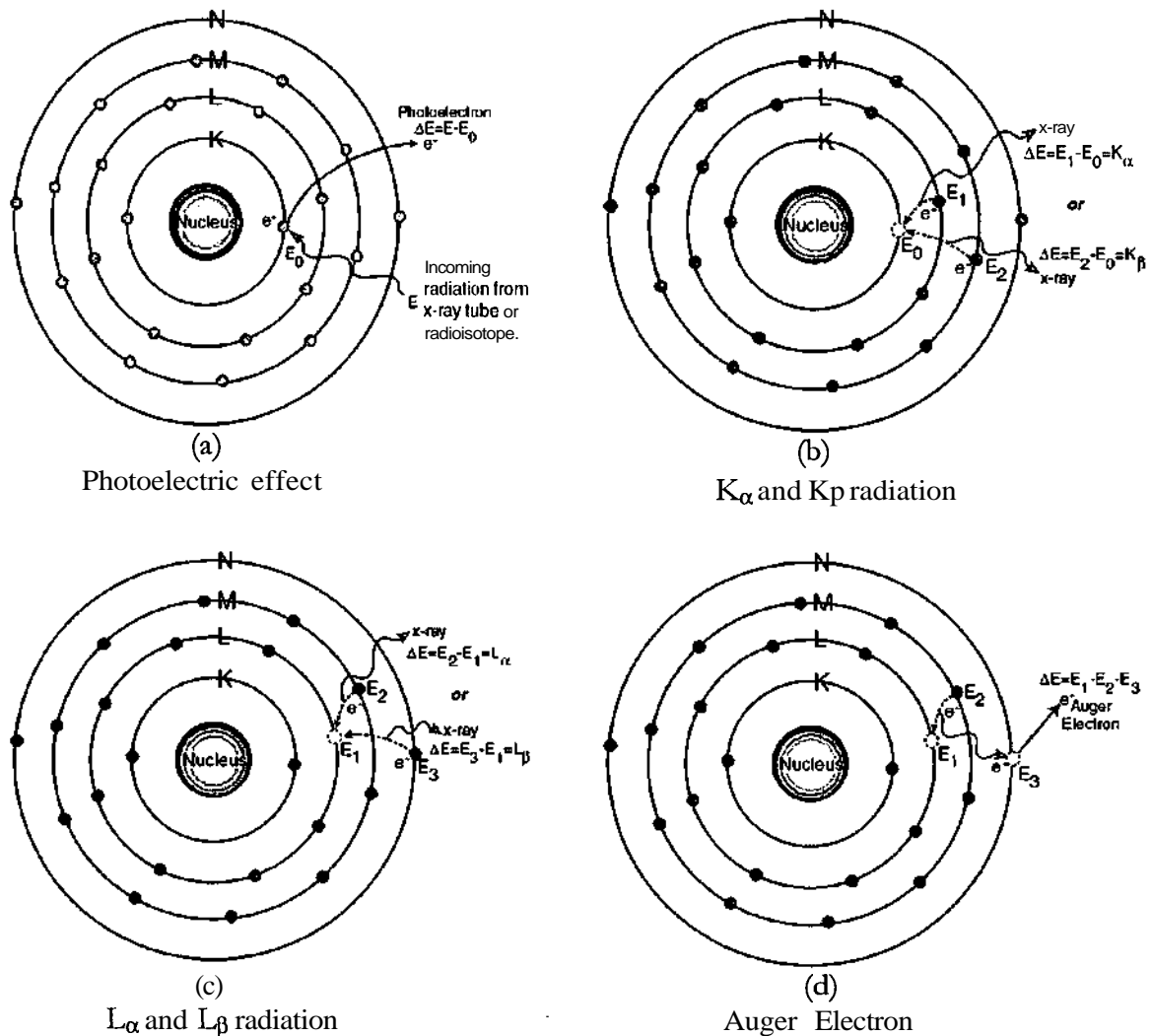


Fig. 1. X-ray fluorescence processes in Titanium, (a)- Photoelectric effect, (b)- K radiation, (c)- L radiation, (d)- Auger electron

- **Auger electrons**

Sometimes, as the atom returns to its ground state, instead of emitting characteristic x-rays it transfers the energy directly to one of the outer electrons, causing it to be ejected from the atom. The ejected electron is called "Auger electron" as illustrated in Fig. 1(d). This process is a competing process to x-ray fluorescence. Auger electrons are more probable for low Z elements than for high Z elements.

X-ray fluorescence is an important method of elemental analysis that assesses the presence and the concentration of various elements. The method does not destroy the sample and is suitable for routine analysis. Elements from Uranium down to Beryllium can be detected at levels of a few  $\mu\text{g/g}$  or even less. In the last years, much progress has been made in the field of Energy Dispersive X-Ray Fluorescence Spectrometry, (EDXRFS) as well as Wavelength Dispersive X-Ray Fluorescence Spectrometry, (WDXRFS).

There are mainly two different methods of quantitative analysis available in x-ray fluorescence Spectrometry, namely comparison to standards and mathematical methods based on the theory of x-ray fluorescence. The standard methods classify into a lot of different categories: One of them is a calibration standard method. The greater portion of quantitative x-ray fluorescence Spectrometry was carried out using calibration standard analysis. Calibration standards are used to set up calibration curves which are used to determine chemical composition from measured x-ray characteristic line intensities from unknown samples. This method is still widely employed and does not require big computation facilities. Another method is the standard addition method where, the analyte concentration is altered quantitatively in the sample itself. This method provides excellent data in powder and solution analysis, but it does not work successfully in bulk sample analysis where the use of the standard is practically impossible. There are other different methods such as, thin film methods (the specimens are thin films and the absorption enhancement effects substantially disappear), comparison standard methods (the analyte line intensity from the sample is compared with that from standards having the same shape as the samples and nearly the same analyte concentration and matrix), internal standard and standardization with scattered x-rays.

A wide spread of computers is resulting in new computation approaches in x-ray fluorescence analysis. In addition, they become of interest for an improvement of empirical relationships between characteristic x-rays and chemical composition. Attempts have been made at absolute x-ray spectrometric analysis by conversion of intensity data to analytical data by wholly mathematical means. The calculations require knowledge of:

- The spectral distribution of the primary x-ray beam. The problem of a proper description of the spectral distribution of primary radiation avoided the development of absolute intensity-concentration algorithms until 1968.
- Mass absorption coefficients of the specimen for each primary x-ray beam and for analyte lines.
- Conversion efficiencies of each primary wavelength to each matrix element line.
- Efficiency of the spectrometer for detection of the analyte lines.
- The fluorescence yield as well as the transition probabilities.

The derivation of the basic mathematical equation is based on the assumption that the specimen is homogeneous, infinitely thick and has a plane surface. The calculation used to convert the measured intensities to concentration is extremely complex and must be done by computer simulations. Gillam and Heal[3] were the first to provide an algorithm that included secondary fluorescence. Sherman[4] described the basic mathematical relationship between the intensity of a characteristic x-ray wavelength and the chemical composition in multicomponent systems. He derived for the first time the intensity-concentration relationship for elements with

high atomic numbers. The intensity-concentration relationship for elements of lower atomic number were corrected for enhancement by the spectra of the elements of higher atomic numbers (secondary excitation). Lucas-Tooth and Price[5] suggested a linear expression relating the concentration of the elements in different specimen to its intensity. Shiraiwa and Fujino[6,7] extended Sherman's work by adding tertiary excitation.

There are different approaches used to derive analyte concentrations from the measured spectra, such as graphic calculations, empirical calculations, correction for absorption, calculations with polynomial equations and fundamental parameter methods.

The fundamental parameter method permits the calculation of analytical composition from the measured analyte line intensities and the different values of the fundamental parameters such as absorption coefficients, fluorescent yields, transition probabilities, ...etc. No calibration standards are required. The fundamental parameter method uses the spectral distribution instead of simple monochromatic spectra. This distribution can be estimated theoretically or it may be measured from a given x-ray tube target. Matrix absorption and analyte line excitation by matrix elements are entered into the equation explicitly for each specimen. Analyte concentration is calculated by iteration. The advantages of the fundamental parameters methods are that the limited composition ranges of the regression methods can be avoided and that no intermediate standard or empirical coefficient is required for any matrix. The main limitations are the spectral distribution of the primary x-ray beam, although it may vary with the age of the x-ray tube as well as the uncertainty in mass absorption coefficients and fluorescence yield data. Several fundamental parameters methods were developed. Criss and Birks[8] published details of their fundamental parameter approach. In this work, the fundamental parameter method was used which is based on the previous theoretical description of the x-ray tube spectra as well as characteristic  $K_{\alpha}$ ,  $K_{\beta}$  and  $L_{\alpha}$  radiations [51, 9].

Pella[51] and Ebel[9] published the theoretical description of continuous radiation of the x-ray tube spectra as well as characteristic  $K_{\alpha}$ ,  $K_{\beta}$  and  $L_{\alpha}$  radiations. The present work depends basically on this theoretical description for quantitative analysis using the fundamental parameter approach. Therefore, the present work deals with the following tasks:

- The uncertainties of the mass absorption coefficient values are one of the main sources of error in the fundamental parameter approaches. To overcome this problem, a new description of the numerical values of different mass absorption coefficients data bases is the main task. The data bases of McMaster, Scofield, Xcom, Elam, Henke, Sasaki, Chantler and Cullen are considered as well as the complete experimental data base.
- Description of the detector efficiencies.
- Comparisons between the theoretical and experimental data of x-ray continuum as well as the characteristic x-radiation.
- Quantitative analysis using fundamental parameters approaches based on the mentioned description[51, 9] of x-ray tube spectra and characteristic radiation for different types of alloys. In addition, the effect of x-ray tube voltage variation on the results of quantitative analysis was studied.

# CHAPTER 1

## THEORETICAL BASIS OF X-RAY SPECTRA AND THE FUNDAMENTAL PARAMETER APPROACH

### 1.1 Fundamental Parameters

The fundamental parameters are required to calculate x-ray emission (primary, secondary and tertiary). A well defined set of fundamental parameters leads to a precise description of the theoretical x-ray emission. Some of these fundamental parameters are x-ray absorption, fluorescence yield, transition probability, x-ray tube spectra and detector efficiency.

#### 1.1.1 X-Ray Cross Sections

Generally, when a beam of x-rays interacts with the specimen, the intensity is attenuated and several types of interaction occur. In the energy range of x-ray fluorescence spectrometry, two types of interaction are of interest, photoelectric absorption and x-ray scattering. The x-ray scattering consists of two types namely, Compton scatter (incoherent or modified or inelastic scatter) where a fraction of the incident x-ray photon energy is transferred to a loosely bound electron of the atom and Rayleigh scatter (coherent or unmodified or elastic scatter) where no energy is lost in the interaction process. The transmitted x-ray beam which represents the fraction of the photons which passes through the specimen without interaction is described by using the mass absorption coefficient. A part of the photo absorbed x-rays causes fluorescence. The x-ray interaction with the specimen depends on the energy of the incident x-radiation, atomic number and the crystalline structure of the specimen. To understand the interaction of the x-radiation with the specimen, the interaction of x-rays with a single free electron has to be discussed followed by the interaction of x-rays with multielectron atoms.

##### 1.1.1.1 X-Ray Scattering

As mentioned above, there are two main types of x-ray scattering, coherent and incoherent scattering. The effective coherent and incoherent scattering interaction is proportional to the sum of individual scatter contributions from each element in the specimen. Coherent and incoherent scattering can be used to estimate both background and mass absorption coefficients for trace elements in selected spectral regions[10, 11]. A power function relation between the mass absorption coefficient and incoherent scattering coefficient of Rh  $K_{\alpha}$  was theoretically predicted[12] over a wide range of atomic numbers

$$\mu_{\lambda} - I_{\lambda}^{-n} \quad (1.1)$$

where  $\mu_{\lambda}$  and  $I_{\lambda}^{-n}$  are mass absorption coefficient and scattering intensity, for wavelength  $\lambda$  and values of the exponent  $n$  depend on the kind of radiations used.

Also, the coherent and incoherent scattering can be used to normalize x-ray fluorescent intensities and reducing both instrumental errors and errors arising from the difference in absorption between samples and standards[13]. Coherent and incoherent scattering were already used in quantitative analysis, whereas the ratio of  $\sigma_R$  elastic to  $\sigma_C$  inelastic depends on the mean atomic number of the sample according to

$$\frac{\sigma_R}{\sigma_C} = (\bar{Z})^{2.4} \quad (1.2)$$

Cesareo[14] described a quantitative analysis method of silver in silver-copper alloys based on coherent and incoherent scattering of  $Am^{241}$  59.61 keV monoenergetic gamma rays. To apply the coherent/incoherent scattering method in the silver-copper alloys, the concentration of silver must be larger than 1%. Although XRF analysis gives the best results with standard samples, the coherent/incoherent scattering method is more adequate for the analysis of ancient samples where the silver content is increased on the surface. The method is independent of the shape of the samples. Nielson[15] used the coherent/incoherent scattering for the calculation of the matrix correction and estimated the quantities of the light elements below  $Z=13$  in the environmental samples by the difference from the scattered x-ray peaks.

• **Coherent, (Rayleigh, elastic, unmodified) Scattering**

In the case of x-ray interaction with a single free electron, when the incident x-ray beam and the scattered has the same energy, the scattering process is called coherent scattering. The differential cross section of the free electron for coherent scattering in the solid angle  $d\Omega$  is given by Thomson's equation

$$\frac{d\sigma_R}{d\Omega} = r_e^2 \frac{(1 + \cos^2 \phi)}{2} \quad (1.3)$$

where  $r_e = e^2/m_0c^2$  is the classical electron radius ( $r_e = 2.818 \times 10^{-15}$  m),  $e$  is the charge of the electron,  $m_0$  is the electron rest mass,  $c$  is the velocity of light and  $\phi$  is the scattering angle. The total coherent scattering by an atom is the sum of the coherent scattering amplitudes from each of the electrons in the atom. Therefore the total cross section for coherent scattering is given by

$$\sigma_R = \pi r_e^2 \int_0^\pi (1 + \cos^2 \phi) \sin \phi d\phi \quad (1.4)$$

The coherent scattering cross section depends on the atomic structure factor,  $F(x,Z)$  which represents the phase difference between the waves scattered by the  $Z$  orbital electrons and is expressed by the following equation

$$F(x,Z) = \int_0^{\infty} \rho(r) 4\pi r \frac{\sin\left(\frac{2\pi}{\lambda} r \cdot 2x\right)}{\frac{2\pi}{\lambda} r \cdot 2x} dr \quad (1.5)$$

$$x = \frac{\sin(\phi/2)}{\lambda} \quad (1.6)$$

where  $\rho(r)$  is the total electron density,  $r$  is the distance from the nucleus. The values of the atomic structure factor  $F(x,Z)$  were calculated theoretically based on models of electron distributions (Hartree-Fock or Thomas-Fermi) for all atoms[16, 17]. Therefore, the total coherent scattering cross section for atom  $Z$  is given by

$$\sigma_R^Z = \pi r_e^2 \int_0^\pi [F(x, Z)]^2 (1 + \cos^2 \phi) \sin \phi d\phi \quad (1.7)$$

The coherent scattering increases as the radiation energy decreases or as the atomic number of the scattering atom increases.

- **Incoherent, (Compton, inelastic, modified) Scattering**

If the energy of the scattered photon has been modified, the scattered x-ray is said to be incoherently or Compton scattered. Compton was the first to show that the energy of x-radiation scattered by a single free electron is changed. The incoherent scattering can be used for matrix absorption correction, particularly for heavy trace element determinations in geological specimens.

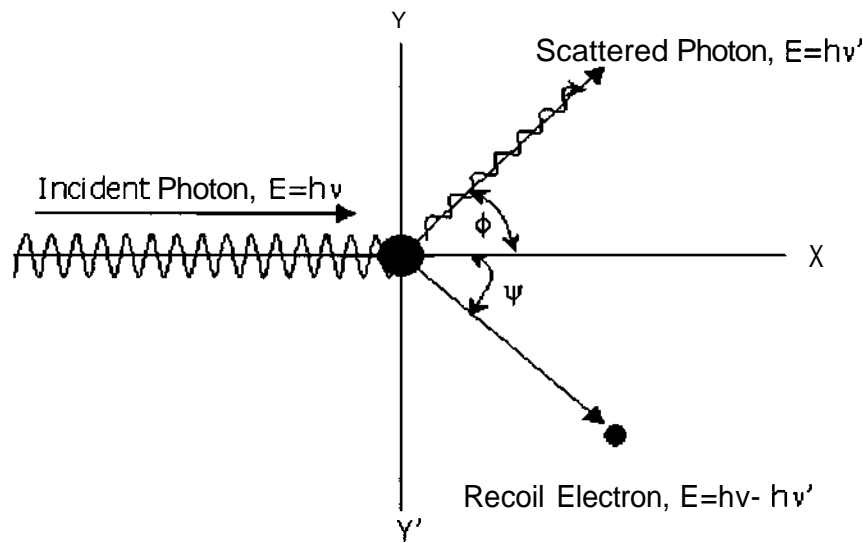


Fig. 1.1 Compton Scattering

Incoherent scattering increases as the energy of radiation increases or as the atomic number of the scattering atom decreases. The energy shift between incoherent and coherent peaks is independent of the scattering substance and of the incident photon energy but it depends on the scattering angle. When the incident photon strikes a free electron as shown in Fig. 1.1, the direction of the electron recoil occurs under an angle  $\psi < \pi/2$  with the primary radiation, while the scattered photon has lost some energy and is deflected under an angle  $\phi < \pi$  with a new frequency  $\nu'$ . Therefore, along the X and Y axes in Fig. 1.1 and according to the conservation of momentum and the conservation of the energy, the following equations are valid

$$\frac{h\nu}{c} = \frac{h\nu'}{c} \cdot \cos \phi + \frac{m_0 V}{\sqrt{1-\beta^2}} \cdot \cos \psi \quad (1.8)$$

$$0 = \frac{h\nu'}{c} \cdot \sin \phi + \frac{m_0 V}{\sqrt{1-\beta^2}} \cdot \sin \psi \quad (1.9)$$

$$h\nu = h\nu' + m_0 c^2 \left( \frac{1}{\sqrt{1-\beta^2}} - 1 \right) \quad (1.10)$$

where  $K$  is the velocity of the recoil electron and  $\beta = \frac{v}{c}$ . By solving equations 1.8-1.10 one can obtain the frequency  $\nu'$  of the scattered photon

$$\nu' = \frac{\nu}{1 + \alpha(1 - \cos \phi)} \quad (1.11)$$

$$\alpha = \frac{h\nu}{m_0 \cdot c^2} \quad (1.12)$$

Equation 1.11 can be rewritten

$$E_{Compton} = \frac{\epsilon}{1 + \alpha(1 - \cos \phi)} \quad (1.13)$$

When the scattering angle  $\phi = 0$  there is no change of the scattered photon energy. In addition, the direction of the recoil electron is obtained from

$$\tan \psi = \frac{1}{(1 + \alpha) \cdot \tan(\phi/2)} \quad (1.14)$$

The cross section of incoherent scattering is the average intensity in any direction. The cross section of incoherent scattering of a free electron in a direction  $\phi$  is given by Klein-Nishina equation

$$\frac{d\sigma_c}{d\Omega} = \frac{1}{2} r_e^2 \left[ \left( \frac{h\nu'}{h\nu} \right)^2 \left( \frac{h\nu}{h\nu'} - \frac{h\nu'}{h\nu} \right) \sin^2 \phi \right] \quad (1.15)$$

Combining equations 1.11, 1.12 and 1.15, equation 1.15 can be rewritten as follows

$$\frac{d\sigma_c}{d\Omega} = \frac{1}{2} r_e^2 \left[ \frac{1 + \cos^2 \phi + \frac{1 - \cos \phi}{1 + \alpha(1 - \cos \phi)}}{1 + \alpha(1 - \cos \phi)} \right] \quad (1.16)$$

where

$$H(\alpha, \phi) = [1 + \alpha(1 - \cos \phi)]^{-2} \left( 1 + \cos^2 \phi + \frac{1 - \cos \phi}{1 + \alpha(1 - \cos \phi)} \right) \quad (1.17)$$

By integrating equation 1.16, the total incoherent cross section over all angles is given by

$$\sigma_c = \pi r_e^2 \int_0^\pi H(\alpha, \phi) \cdot \sin \phi \cdot d\phi \quad (1.18)$$

The atomic cross section depends on the incoherent scattering function  $S(x, Z)$ , that accounts for the phase differences between the waves scattered by electrons in the atom. The incoherent scattering function  $S(x, Z)$  depends on the atomic number  $Z$  and the value of  $x$  which is defined by equation 1.6. The incoherent scattering function  $S(x, Z)$  was calculated theoretically in the mentioned tables[16, 17]. Therefore, the total incoherent cross section is



$$\sigma_c^Z = \pi r_e^2 \int_0^\pi S(x, Z) \cdot H(\alpha, \phi) \cdot \sin \phi \cdot d\phi \quad (1.19)$$

### 1.1.1.2 Photoelectric Effect

The photoelectric cross section is the most important quantity in quantitative analysis methods whereas it represents more than 95% of the attenuation coefficient. Therefore the value of the mass absorption coefficient reflects primarily the photoelectric cross section. The probability of an x-ray photon being absorbed to produce a photoelectron is a function of the photon energy. The photoelectric effect can be described as follows: If an incident photon of energy  $h\nu$  strikes one of the inner electrons in the atom and the photon energy is larger than the binding energy of this electron, the incident photon can be absorbed and its energy is transferred to the electron, which is ejected from its shell. The ejected electron is called photoelectron.

### 1.1.1.3 X-Ray Absorption

The description of x-ray absorption by layers of assorted materials was given by Barkla and Sadler[18, 19]. They quantified the transmission properties with respect to photon incident energy and the atomic number of the material in terms of the mass absorption coefficient  $\mu_{a,b}(E) = \mu_{lin a,b}(E) \rho_b$  in  $\text{cm}^2/\text{g}$ , which is given by the relation

$$\mu_{a,b}(E) = \mu_{ijk,b}(E) = \mu_{lina,b}(E) / \rho_b = (\rho_b \cdot D)^{-1} \cdot \ln(I_0(E)/I(E)) \quad (1.20)$$

where  $D$  is the thickness of the layer in units of cm,  $I_0(E)$  is the intensity of the incident beam,  $E$  is the energy of incident photons,  $I(E)$  is the intensity of the transmitted beam,  $\rho_b$  is the density of the layer in  $(\text{g}/\text{cm}^3)$ ,  $a = ijk$ ,  $i$  is the element,  $j$  is the ionized shell,  $k$  is the deexcited shell,  $b$  is the absorber, and  $\mu_{lina,b}(E)$  is the linear absorption coefficient which is dependent on the sample density  $\rho_b$ . Equation 1.20 can be transformed to

$$I(E)/I_0(E) = \exp(-\mu_{ijk,b}(E) \cdot \rho_b \cdot D) \quad (1.21)$$

This equation is called Beer-Lambert's law[20, 21]. The exponential term of the mass absorption coefficient in equation 1.21 is given by

$$\exp\left(\mu_{a,b}(E) \cdot \frac{m}{F}\right) = \exp(\mu_{a,b}(E) \cdot \rho_b \cdot D) = \exp(\mu_{lina,b}(E) \cdot D) \quad (1.22)$$

where the term  $\frac{m}{F}$  represents the mass per unit area of the specimen. If a thin layer of the specimen is considered, the mass absorption coefficient would write as follows:

$$\mu_{a,b}(E) \cdot d\left(\frac{m}{F}\right) = \mu_{a,b}(E) \cdot \rho_b \cdot dD = \mu_{lina,b}(E) \cdot dD \quad (1.23)$$

When the material is made up of a homogeneous mixture of pure elements, the resultant mass absorption coefficient can be calculated from

$$\mu_{a,b}(E) = \sum_{q=1}^n c_q \cdot \mu_{a,q}(E) \quad (1.24)$$

where  $c_i$  is the concentration of the element in the specimen in weight fractions,  $\mu_{a,i}(E)$  is the mass absorption coefficient of that element. From equation 1.24, the fraction of absorption of element  $i$  can be calculated and represented by

$$\frac{c_i \cdot \mu_{a,i}(E)}{\mu_{a,b}(E)} \quad (1.25)$$

The total concentration over all the elements in the specimen is

$$\sum_{q=1}^n c_q = 1 \quad (1.26)$$

Generally, the calculation of the photon interaction data is performed in terms of cross sections in units of  $\text{cm}^2/\text{g}$  or barns/atom,

$$\mu_{lin}(E) / \rho \text{ (cm}^2/\text{g)} = \mu_{ijk,b}(E) \text{ (cm}^2/\text{g)} = \mu_{ijk,b}(E) \cdot \frac{N_A \cdot 10^{-24}}{A} \text{ (barns/atom)} \quad (1.27)$$

where  $A$  is the atomic weight of the element in g/mole,  $N_A$  is Avogadro's number, ( $N_A = 6.0221367 \times 10^{23}$  atoms/mole). The total mass absorption coefficient can be expressed as the sum over the cross sections for the most probable individual processes by which photons interact with the atom [22]

$$\mu(E) = \tau(E) + \sigma_{coh}(E) + \sigma_{incoh}(E) \quad (1.28)$$

where  $\tau(E)$  is the photoelectric cross section,  $\sigma_{coh}(E)$  and  $\sigma_{incoh}(E)$  are the coherent and incoherent cross sections. The photoelectric cross section  $\tau(E)$  includes the probability for ionizing all the shells in an atom which can be described by the following equation

$$\tau = \tau_K + (\tau_{L1} + \tau_{L2} + \tau_{L3}) + (\tau_{M1} + \tau_{M2} + \tau_{M3} + \tau_{M4} + \tau_{M5}) + \dots \quad (1.29)$$

where each term expresses the photoelectric cross section for a particular subshell of the atom. Fig. 1.2 shows a schematic diagram of the relation between the mass absorption cross section, photoelectric cross section, coherent and incoherent scattering in  $\text{cm}^2/\text{g}$  versus the photon energy in keV for Er-68. According to Fig. 1.2 as the photon energy increases the mass absorption cross section as well as the photoelectric cross section decrease as the probability of a photon ejecting an electron from an atom increases within certain limits. These limits are the sharp discontinuities that can be observed in the curve of Fig. 1.2. They are related to the critical excitation energies of each shell which is called the binding energy of each shell and this sharp discontinuities are called the absorption edges. According to Fig. 1.2, at photon energy 1.3 keV, Q, P, O and N shell can already be ionized and there is no possibility to ionize the M shells. At photon energy 1.5 keV,  $M_4$  and  $M_5$  shells are ionized whereas the critical value of excitation of  $M_4$  and  $M_5$  shells is reached, and consequently, the absorption edges of both  $M_4$  and  $M_5$  are observed at 1.453 keV and 1.409 keV, respectively. In the same manner, at photon energies less than 57.486, (the binding energy of the Er-K shell) all the shells can be ionized except K shell

and at photon energy greater than 57.486, all shells can be ionized with observing all the absorption edges from M<sub>5</sub> shell to K shell as shown in Fig. 1.2.

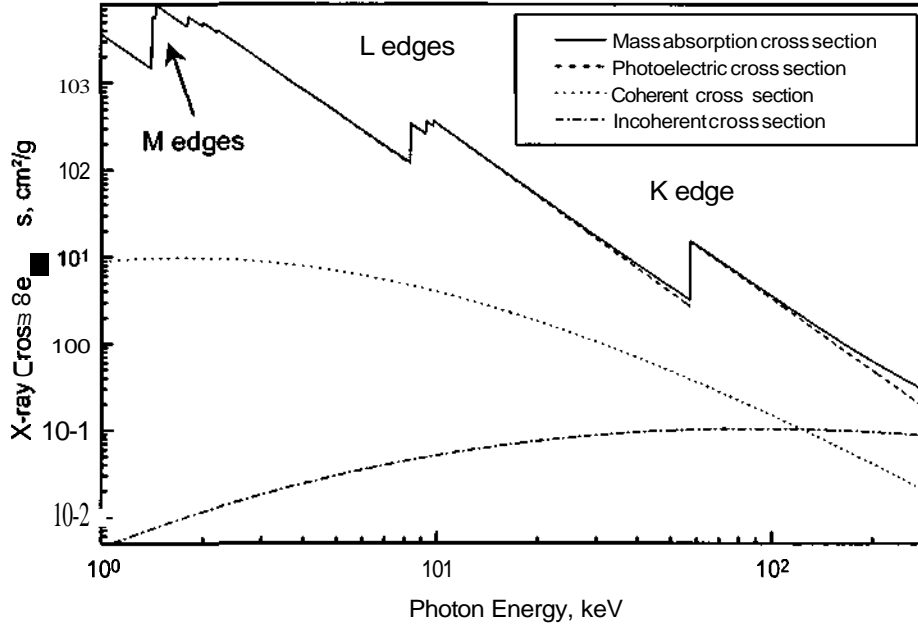


Fig. 1.2 X-ray cross sections of Er versus Photon Energy

### 1.1.2 Fluorescence Yield

The fluorescence yield is one of the major factors which determine the intensities of x-ray spectra. Consequently, it plays a very important role in quantitative analysis using different computational methods. The fluorescence yields were determined experimentally and theoretically[23, 24]

The fluorescence yield  $\omega$  is the ratio of x-ray photons emitted from a given shell and the number of vacancies created in that shells, or the yield of x-ray photons is reduced by the Auger effect. Therefore, the fluorescence yield  $\omega$  denotes the probability of an excited state to deexcite by emission of characteristic X-radiation and it can be defined by

$$\omega = \frac{n_f}{n} \quad (1.30)$$

where,  $n$  is the number of the primary holes that have been induced by the ionization in a given level and  $n_f$  is the number of characteristic photons from that level that effectively leave the atom. The fluorescence yield does not depend on the type of process that led to the excitation of the atom. It is a function of atomic number  $Z$  and the ionized shell whereas the fluorescence yield increases with increasing atomic number as given in Fig. 1.3 according to the fluorescence yield values given by Hubbell[25]. It differs significantly from one shell to another.  $\omega_K$  is much larger than  $\omega_L$  and  $\omega_L$  is much larger than  $\omega_M$ . The values of  $\omega_K$  are known with a higher degree of accuracy than  $\omega_L$  values because the former are related to a one level shell while the latter are weighted averages of three shells  $L_I$ ,  $L_{II}$  and  $L_{III}$ . Processes competing to fluorescence

are the emission of an Auger electron with probability  $a$  and the Coster-Kronig transition with probability  $f$ . The sum of the transition probabilities must equal unity

$$\omega + f + a = 1 \quad (1.31)$$

Hubbell[25] presented a comparison of the fluorescence yield values based on experimental and theoretical models. They extended and modified the fluorescence yield values generated by Bambynek[26], Cohen[27] and Burhop[28] for the elements with atomic number  $3 < Z < 100$ . They used the semi-empirical fitting formula of  $\omega_K$  introduced by Burhop[28]

$$\omega_K = \frac{\left( \sum_{i=0}^3 C_i Z^i \right)^4}{\left( 1 + \sum_{i=0}^3 C_i Z^i \right)^4} \quad (1.32)$$

where  $C_i$  are the fit coefficients that have been reevaluated by Bambynek[26] for  $3 < Z < 100$ . The values of  $C_i$  for  $\omega_K$  are,

$$\left. \begin{aligned} C_0 &= 0.0370 \pm 0.0052 \\ C_1 &= 0.03112 \pm 0.00044 \\ C_2 &= (5.44 \pm 0.11) \times 10^{-5} \\ C_3 &= -(1.250 \pm 0.070) \times 10^{-6} \end{aligned} \right\} \quad (1.33)$$

Equation 1.32 with a different set of fit coefficients can be applied to average L-shell fluorescence yields. The related fit coefficients values of  $C_i$  are

$$\left. \begin{aligned} C_0 &= 0.177650 \\ C_1 &= 0.00298937 \\ C_2 &= 8.91297 \times 10^{-5} \\ C_3 &= -2.67184 \times 10^{-7} \end{aligned} \right\} \quad (1.34)$$

These fit coefficients are valid for  $30 < Z < 96$  for  $\omega_L$ .

Cohen[27] has extended  $\omega_K$  to lower Zs down to  $Z=3$ . Hubbell[25] has proposed a semi-empirical fitting formula of  $\omega_M$  for the range  $19 < Z < 100$  which is given by

$$\omega_M = 1.29 \times 10^{-19} (Z - 13)^4 \quad (1.35)$$

In the present work, the values of fluorescence yields were used from Hubbell[25]. The Z-dependence is plotted in Fig. 1.3.

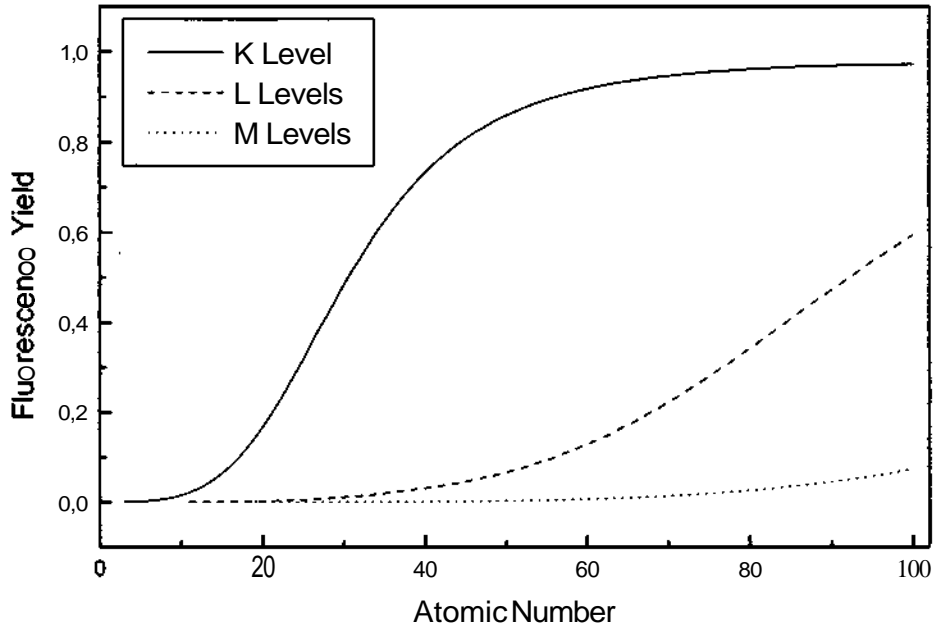


Fig. 1.3 Fluorescence yield versus atomic number

### 1.1.3 Transition Probability

The transition probability  $p_{ijk}$  is defined as the value of the probability that an electron passes from a certain orbital to an empty level. It can be described as the ratio of the intensity of the observed line (or lines) to the sum of the intensities. So, the transition probability of  $K_{\alpha_1,2}$ ,  $K_{\beta_1,2}$ ,  $L_{\alpha_1,2}$  and  $L_{\beta_1,2}$  can be described by the following equations

$$p_{K_{\alpha_1,2}} = \frac{I(K_{\alpha_1} + K_{\alpha_2})}{\sum_n I(K_n)}, \quad p_{K_{\beta_1,2}} = \frac{I(K_{\beta_1} + K_{\beta_2})}{\sum_n I(K_n)} \quad (1.36)$$

where  $n = \alpha_1, \alpha_2, \beta_1, \beta_2, \beta_3, \beta_4$  and  $\beta_5$

$$p_{L_{\alpha_1,2}} = \frac{I(L_{\alpha_1} + L_{\alpha_2})}{\sum_n I(L_n)}, \quad p_{L_{\beta_1,2}} = \frac{I(L_{\beta_1} + L_{\beta_2})}{\sum_n I(L_n)} \quad (1.37)$$

where  $n = \alpha_1, \alpha_2, \beta_1, \beta_2, \beta_3, \beta_4, \beta_5, \beta_6, \beta_7$  and  $\beta_8$

In the present work, the intensities of the individual lines were taken from the tables of Johnson and White [29].

## 1.2 Theoretical Bases of X-Ray Tube Spectra

The theoretical x-ray tube spectrum has a great influence on the computed characteristic fluorescence intensity of the specimen and consequently on the calculations of the quantitative x-ray fluorescence analysis using the fundamental parameter approach. In the present work, the theoretical x-ray tube spectra based on the equidistribution proposed by Love and Scott[30-33] are used.

### 1.2.1 The Continuous X-Radiation, (Bremsstrahlung)

The first description of the continuous x-radiation appears as the result of the progressive deceleration of electrons impinging on an anode without explanation of the minimum wavelength,  $\lambda_0$ [34, 35] which is the most characteristic feature of the continuous radiation. The minimum wavelength,  $\lambda_0$  (related to the maximum electron energy  $E_0$ ), (see equation 2, introduction) is independent on the atomic number of the target material. It means that the energy of any electromagnetic radiation in the emission spectrum can never be higher than the kinetic energy of the electrons striking the target.

Sommerfeld[36] described a new interpretation of the continuous radiation based on the quantum and wave mechanics. He considered the deceleration of the incident electron that enters the field of the nucleus due to the Coulombian force. Therefore, if the incident electron may lose all or any fraction of its energy by interaction with the nuclei of the atoms, this will lead to a continuous radiation of identical x-ray photon energy. Sommerfeld has not taken into account all possible directions and the speed values of the decelerated electrons for all possible values of the energy losses. Kirkpatrick and Wiedmann[37] solved this problem and calculated the total intensity emitted from a thin film in all directions as given in the following equation

$$N = \left( \frac{8\pi}{3} \right) (I_x + I_y + I_z) \quad (1.38)$$

where  $I_x$ ,  $I_y$  and  $I_z$  are the photon emission intensities in the three Cartesian directions. This approximation is not valid for a thick target where the electron collisions occur beneath the surface with a large number of atoms in different directions. Therefore, a lot of new theoretical descriptions were published dealing with the distribution of electrons in terms of depth, direction and energy. Ulrey[38] found a relationship between the total intensity  $I$  of the continuous radiation and the atomic number  $Z$  of the target as well as the applied voltage  $V$

$$I = K.Z.V^2 \quad (1.39)$$

where  $K$  is a constant that includes the electron current  $i$  in the tube. Therefore, an approximately linear increase of the maximum of the spectral responses with the atomic number of the target materials was found at the same tube voltage and currents. So the relative spectral distribution in the continuum is similar from element to element but the absolute intensity is greater for high atomic number.

Kramers[39] combined the classical and quantum concepts and obtained an expression of the spectral distribution of the number  $dN$  of pseudomonochromatic photons with photon energies from  $E$  to  $E + dE$

$$dN = \Omega i \sigma_{K,E} dE = \Omega i \text{const.} Z \left( \frac{E_0}{E} - 1 \right) dE \quad (1.40)$$

where  $\Omega$  is the solid angle of photon flux from point source,  $i$  is the x-ray tube current in the tube,  $\sigma_{KE}$  is Kramers' cross section in units of  $1/s.sr.mA.keV$ ,  $Z$  is the atomic number of the target element,  $E_0$  is the maximum photon energy,  $E$  is the energy of the x-ray photons of the continuous radiation and  $dE$  is the energy interval, respectively. This expression is identical to the empirical relation of Kulenkampff[40]. Therefore equation 1.40 is called Kramers-Kulenkampff's formula. Equation 1.40 is most simple and easy to apply to all cases as it establishes a fundamental relationship between continuous radiation intensity generated in a target, atomic number, incident energy and radiated energy. Due to the neglect of self absorption and back scatter of electrons in the target, the continuous radiation expression given by equation 1.40 is not sufficiently accurate for the present requirements in quantitative analysis using the fundamental parameter approaches. Several modifications of Kramer-Kulenkampff's formula were published.

Rao-Sahib and Wittry[41] calculated the continuous radiation for nineteen thick targets ranging from  $Z=6$  to 92 using Sommerfeld's cross sections and Bethe's retardation law. The absorption in the target and the loss of ionization due to backscatter were considered to correct the continuous radiation. They found their results in better agreement with the experimental responses than Kramers' description. Brunetto and Riveros[42] modified Kramers' law and obtained also a better description of experimental responses. They considered the self absorption, the loss of ionization due to backscatter and the absorption by the exit window of an x-ray tube.

Smith and Reed[43] modified Kramers' equation introducing dimension less exponents  $X$  and  $n$  for a better fitting of experimental data to theory, therefore Kramers' cross section was replaced by

$$\sigma_{SR,E} = \text{const.} Z^n \left( \frac{E_0}{E} - 1 \right)^r \quad (1.41)$$

Several theoretical approaches were published concerning the excitation of the characteristic x-rays by electrons at different depth regarding to the specimen surface followed by absorption of the characteristic x-rays on their paths from the point of origin to the surface.

Castaing and Descamps[44] performed an experimental verification of the theoretical approaches on a specimen with a defined sequence of substrate of element  $a$ , thin layer of tracer element  $b$  overlayer of element  $a$  of variable thicknesses. From the characteristic signal strength of the tracer element  $b$  depending on the overlayer thickness together with the known x-ray absorption in the overlayer follows the depth distribution function (DDF) of the excitation of characteristic x-rays in the element  $a$ . A similar experimental verification of theoretical descriptions of the DDF in the case of the generation of continuous x-radiation is impossible. Therefore the excitation of continuous x-ray radiation by electrons has to be treated in analogy with the excitation of characteristic x-ray radiation, only the absorption edge energy has to be replaced by the variable energy. The best combination of DDF and possible modifications of Kramers' cross section can be determined by comparison of computed spectral responses with measured continuous spectra.

Love and Scott's DDF[30-33] has been found[47, 52] to give a sufficient agreement over wide  $Z$  and  $E_0$  ranges. Thus, in this work, the continuous x-radiation has been described by Smith and Reed's version of Kramers' cross section with  $n-1$  and Love and Scott's DDF. In Love and

Scott's concept, the DDF is assumed to be constant from the surface to depth  $2\overline{\rho z}$  which is given by the following equation

$$\overline{\rho z} = \frac{0.49269 - 1.0987\eta + 0.78557\eta^2}{0.70256 - 1.09865\eta + 1.0046\eta^2 + \ln U_0} \ln U_0 \quad (1.42)$$

with

$$\rho z_m = \frac{1}{Z} \left( 0.787 \times 10^{-5} \sqrt{J} E_0^{3/2} + 0.735 \times 10^{-6} E_0^2 \right) \quad (1.43)$$

$$\eta = E_0^m \left[ 0.1904 - 0.223(\ln Z) + 0.1292(\ln Z)^2 - 0.0149(\ln Z)^3 \right] \quad (1.44)$$

$$m = 0.1382 - (0.9211 \sqrt{Z}) \quad (1.45)$$

$$U_0 = E_0/E \quad (1.46)$$

$$J = 0.0135Z \quad (1.47)$$

where  $p$  is the density in  $\text{g/cm}^3$ ,  $z$  is the linear dimension of depth in  $\text{cm}$ ,  $pz$  is the depth expressed in mass per unit area,  $A$  is the relative atomic weight. The probability  $dp$  for generation of x-ray photons in a depth  $pz$  to  $(pz) + d(\rho z)$  is proportional to  $d(\rho z)$ . With

$$\int_0^{2\overline{\rho z}} dp = k \int_0^{2\overline{\rho z}} d(\rho z) = 1 \quad (1.48)$$

follows the proportionality factor

$$k = \frac{1}{2\overline{\rho z}} \quad \text{and} \quad dp = \frac{d(\rho z)}{2\overline{\rho z}} \quad (1.49)$$

This expression is valid for normal electron incidence with regard to the target surface. An incidence angle ( $p$  with regard to the surface) causes a decrease of the depth  $2\overline{\rho z}$  to  $2\overline{\rho z} \cdot \sin \varphi$ . Therefore, the probability  $dp$  becomes

$$dp = \frac{d(\rho z)}{2\overline{\rho z} \cdot \sin \varphi} \quad (1.50)$$

Considering the photoelectric absorption of photons of energy  $E$  in the target of element  $j$ , a contribution  $dN$  is

$$d^2 N = \Omega \cdot i \cdot \sigma_{SR,E} \cdot dE \cdot dp \cdot e^{-\tau_{E,j} \cdot 2\overline{\rho z} / \sin \varepsilon} \quad (1.51)$$

where  $\tau_{E,j}$  is the mass absorption coefficient for photons of energy  $E$  in element  $j$  in  $\text{cm}^2/\text{g}$  and  $\varepsilon$  is the take-off angle of x-rays with regard to the target surface. By integration of equation 1.51 from  $(pz) = 0$  to  $(pz) = 2\overline{\rho z} \cdot \sin \varphi$ , the pseudomonochromatic contribution  $dN$  becomes

$$dN = \Omega \cdot i \cdot \sigma_{SR,E} \cdot dE \cdot \frac{1 - e^{-\tau_{E,j} \cdot 2\overline{\rho z} \cdot \sin \varphi / \sin \varepsilon}}{\tau_{E,j} \cdot 2\overline{\rho z} \cdot \sin \varphi / \sin \varepsilon} \quad (1.52)$$

or



$$dN = \Omega \cdot i \cdot \text{const} \cdot Z \cdot \left( \frac{E_0}{E} - 1 \right)^x \cdot dE \cdot \frac{1 - \tau_{E,j} \cdot 2\bar{\rho}z \cdot \sin\phi / \sin\varepsilon}{\tau_{E,j} \cdot 2\rho z \cdot \sin\phi \sin\varepsilon} \quad (1.53)$$

In the x-ray tube, the thinner x-ray tube window enhances the soft x-ray output of the tube, which is more efficient to excite the light elements in the sample. Whalen and Turner[45] developed a computer program to calculate the effect of window thickness on light element excitation at three different beryllium window thicknesses. They found that the thinner windows yield considerably more signal than the thicker window. Therefore, the absorption of the beryllium window of the x-ray tube should be considered in equation 1.53. The absorption of the beryllium window is given by the equation,

$$F_{E,Be} = \exp(\tau_{E,Be} \cdot D_{Be} \cdot \rho_{Be}) \quad (1.54)$$

where  $\tau_{E,Be}$  is the photoelectric cross section of beryllium,  $D_{Be}$  is the thickness of the beryllium window and  $\rho_{Be}$  is the density of the beryllium window. In the present work, the thickness of the beryllium window of the KEVEX system is 0.0127 cm. Therefore, equation 1.53 can be rewritten as follows

$$dN = \Omega \cdot i \cdot \text{const} \cdot Z \cdot F_{E,Be} \cdot \left( \frac{E_0}{E} - 1 \right)^x \cdot dE \cdot \frac{1 - \tau_{E,j} \cdot 2\bar{\rho}z \cdot \sin\phi / \sin\varepsilon}{\tau_{E,j} \cdot 2\rho z \cdot \sin\phi \sin\varepsilon} \quad (1.55)$$

Ebel[46] calculated and measured the continuous and characteristic radiation of 22 elements at different energy values in the range from 10 keV to 50 keV. They found a dependence of the exponent  $x$  on the acceleration voltage and on the atomic number of the target element. They applied a unique evaluation of the target absorption factor as assumed by Love and Scott for characteristic radiation of the electron probe micro analysis EPMA. They found from the measured spectral responses that the continuous radiation constant and the exponent  $x$  are

$$\text{const} = 1.36 \times 10^9 \text{ sr}^{-1} \cdot \text{mA}^{-1} \cdot \text{keV}^{-1} \cdot \text{s}^{-1} \quad (1.56)$$

$$x = 1.0314 - 0.0032 \cdot Z + 0.0047 \cdot E_0 \quad (1.57)$$

Schoßmann[47] developed an algorithm for calculating the continuous x-ray tube spectra of pure polished thick metals. These metals are Al, Si, Sc, V, Cr, Mn, Fe, Co, Ni, Cu, Zn, Ga, Ge, As, Y, Zr, Nb, Rh, Pd, Ag, In, Sb, Ce, Tb, Yb, Ta, Re, Pt, Au, and Pb. The development is based again on the eqidistribution proposed by Love and Scott and they compared the results to the responses obtained from algorithms using the absorption correction of Pochou and Pichoir[48], Philibert[49], Sewell[50] and Pella[51]. They used the theoretical description of the white radiation, which is given by

$$\Delta n_E = \sigma_{SR,E} \cdot f \cdot D_E \cdot \Omega \cdot i \cdot t \cdot \Delta E \quad (1.58)$$

where  $\sigma_{SRE}$  is the Kramers cross section of the electron interaction with target atoms which is modified by Smith and Reed[43] by introducing an exponent  $x$ ,  $f$  is the absorption of x-rays of energy  $E$  in the target,  $D_E$  is the detector efficiency of the x-ray detection system within a solid angle  $\Omega$ ,  $i$  is the tube current,  $\Delta E$  is the energy range of a selected portion of the continuous radiation,  $t$  is the time of data accumulation. According to the total number of measured spectral

responses, they obtained a little bit different values of the continuous radiation constant and the exponent  $x$  when compared to 1.56 and 1.57

$$const = 1.35 \times 10^9 \quad sr^{-1} \cdot mA^{-1} \cdot keV \cdot s^{-1} \quad (1.59)$$

$$x = 1.109 - 0.00435 \cdot Z + 0.00175 E_0 \quad (1.60)$$

In this work, the values of the continuous radiation constant and the exponent  $X$  are used according to Schoßmann's data as shown in equations 1.59 and 1.60. According to equation 1.41, when  $n = 1$  and  $x = \setminus$ , the modified cross section  $\sigma_{SR,E}$  is identical with Kramers' cross section,  $\sigma_{KE}$  and the value of the continuous radiation constant can be compared to values in the literature.

## 1.2.2 The Characteristic X-Ray Radiation

As mentioned before, the characteristic x-radiation can be induced either by the impact of accelerated particles (electron, proton, ..etc) or by the impact of high energy radiation from a suitable radioactive source. In Coolidge x-ray tubes, where a cathode electron with sufficient energy strikes the target, it may knock out bound electrons in the inner shells. Consequently, holes are created in these shells. To knock out the bound electrons in the inner shells, the energy of the incident electron or photon must overcome the binding energy of that shell. The distribution of electrons in the ionized atom is then out of equilibrium and within an extremely short time returns to the ground state by transition of electrons from outer shells to inner shells. According to Bohr's theory, an electron of the L or M shell can fall into the K shell, and characteristic  $K_\alpha$  or  $K_\beta$  radiation is emitted. A similar result follows in the case when an electron is knocked out from the L and M shells of the target atom. Therefore, another characteristic x-radiation of  $L_\alpha$ ,  $L_\beta$ ,  $L_\gamma$  and M is emitted. The characteristic radiation appears as superimposed on the continuous x-radiation. The different types of the characteristic x-radiations are illustrated in Fig. 1.4. The electron transitions from the outer to inner shells must obey the selection rules in quantum mechanics ( $\Delta n > 1$ ,  $\Delta l = \pm 1$  and  $\Delta j = \pm 1$  or 0, where,  $n$ ,  $l$ ,  $j$  are principle, angular and total quantum numbers, respectively). In the present target material, (Rh target), if the x-ray tube voltage is larger than the binding energy for Rh K-shell, Rh K-lines are generated.

Wiederschwinger[52], Ebel[46] and Schoßmann[47] employed for the theoretical description of the characteristic signals Love and Scott's depth distribution function. Characteristic count rates  $N_{abc}$  are given by

$$N_{abc} = \Omega \cdot i \cdot const_{bc} \cdot \frac{1}{S_{ab}} \cdot R \cdot \omega_{ab} \cdot p_{abc} \cdot f(\chi_{abc}) \quad (1.61)$$

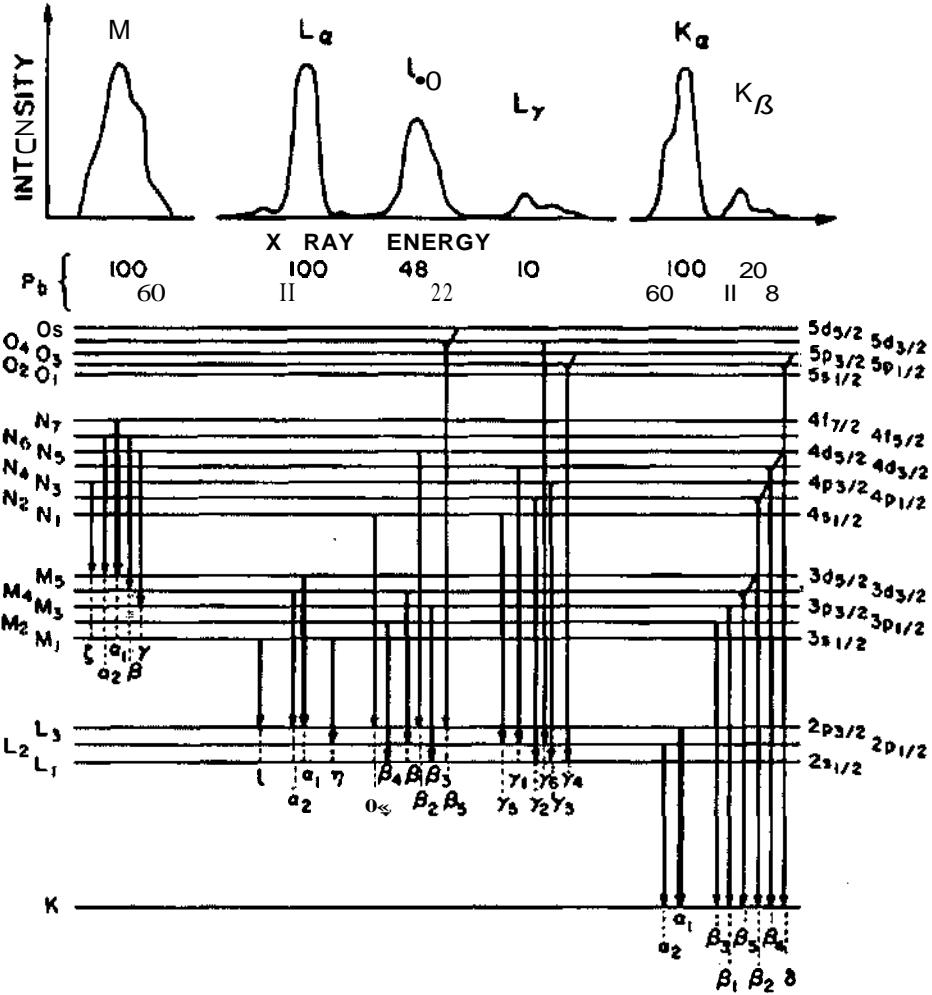


Fig. 1.4 The characteristic x-radiations

where  $a$  defines the element,  $b$  the ionized atomic level and  $c$  is the level from where  $b$  vacancy is filled,  $\omega_{ab}$  is the fluorescence yield,  $p_{abc}$  is the transition probability,  $R$  is the backscattering factor,  $f(\chi_{abc})$  is the absorption term. The  $const_{bc}$  is given in units of  $s^{-1}.sr^{-1}.mA^{-1}$  and has to be determined from measured characteristic spectra. The stopping factor  $\frac{1}{S_{ab}}$  is given by

$$\frac{1}{S_{ab}} = \frac{z_K b_K}{Z} (U_0 \ln U_0 + 1 - U_0) \left[ 1 + 16.05 \sqrt{\frac{J}{E_{ab}}} \frac{\sqrt{U_0 \ln U_0 + 2(1 - \sqrt{U_0})}}{U_0 \ln U_0 + 1 - U_0} \right] \quad (1.62)$$

where  $z_K = 2$ ,  $z_L = 8$ ,  $b_K = 0.35$ ,  $b_L = 0.25$ ,  $U_0 = E_0/E_{ab}$ ,  $J = 0.0135.Z$  with energy  $E_{ab}$  of the absorption edge of the corresponding characteristic radiation.  $z_K$  and  $b_K$  are valid for K-shells and  $z_L$  and  $b_L$  for L-shells. In the case of characteristic radiations the theory is based on the absorbed current, thus the measured total currents have to be corrected for backscattering of electrons. A comparably simple expression for the backscattering factor  $R$  was given by Myklebust[53]:

$$R = 1 - 0.0081517.Z + 3.613 \times 10^{-5}.Z^2 + 0.009583.Z.e^{-U_0} + 0.001141.E_0 \quad (1.63)$$

The absorption of characteristic x-rays in the target is considered by the absorption term  $f(X_{abc})$

$$\chi_{abc} = \tau / \sin \epsilon$$

$$f(\chi_{abc}) = \frac{1 - e^{-\tau \cdot \overline{\rho z} \cdot \sin \phi / \sin \epsilon}}{\tau \cdot \overline{\rho z} \cdot \sin \phi / \sin \epsilon} \quad (1.64)$$

where the depth  $\overline{\rho z}$  is calculated by the expression given for continuous x-radiation (see equation 1.42). Only  $E$  is replaced by  $E_{ab}$  and the photoelectric absorption coefficient  $T$  is valid for the energy  $E_{abc}$  of the characteristic photons in the element  $a$ .

Wiederschwinger[52], Ebel[46] and Schoßmann[47] calculated the numerical values of  $const_{bc}$  from a least squares fit of experimental results of the above given theoretical description:  $const_{K\alpha} = 5 \times 10^{13} \text{ s}^{-1} \cdot \text{sr}^{-1} \cdot \text{mA}^{-1}$ ,  $const_{K\beta} = 5 \times 10^{13} \text{ s}^{-1} \cdot \text{sr}^{-1} \cdot \text{mA}^{-1}$  and  $const_{L\alpha} = 6.9 \times 10^{13} \text{ s}^{-1} \cdot \text{sr}^{-1} \cdot \text{mA}^{-1}$  with standard deviation of 19% for  $K_{\alpha}$  and  $K_{\beta}$  and of 14% for  $L_{\alpha}$  radiation.

### 1.3 Theoretical Bases of the Fundamental Parameter Approach

The fundamental parameter approach provides a theoretical solution to the correction for absorption and secondary fluorescence which is not easy to solve for methods using standards. It is based on the theoretical expression of the x-radiation intensity as a function of the sample concentration, as well as the other fundamental parameters mentioned above. In this work the theoretical primary and secondary fluorescence intensity are treated.

#### 1.3.1 The Primary Fluorescence

Qualitative and quantitative analysis basically depends on the intensity of the characteristic x-radiation from the specimen. The characteristic fluorescence radiation consists of three main contributions, primary, secondary and tertiary fluorescence radiation. In order to describe the theoretical fluorescence intensities, it is necessary to define the experimental and the theoretical parameters. The primary fluorescence is the major contribution to emission in the specimen.

The primary fluorescence of x-rays is defined as the x-rays emitted from atoms of the specimen excited by the incident x-rays only, that means, it results from the direct effect of the incident x-ray beam on the considered element. The photon flux of the incident beam can be expressed as the number of x-ray photons emitted by the excitation source per second per mA, per keV and per solid angle  $\Omega$ . The incident radiation excites the atoms in the specimen resulting in the emission of primary fluorescence in all directions. When the energy of the x-ray photons is higher than the absorption edges, the related characteristic radiation is emitted. This also applies to the characteristic lines of the target when these are present in the primary spectrum. In the theoretical description of the primary fluorescence intensity, the excitation source is considered to be a point source. Fig. 1.5 defines the geometry of the excitation source, the specimen, the detector and the incident and the emitted fluorescence x-ray photon beam. Therefore, the probability of the x-rays originated from the x-ray tube reaching the surface of the specimen in the energy interval  $dE$  is [54]

$$x_E \cdot dE = \frac{A \cdot \cos \alpha}{d^2} \cdot I \quad (1.65)$$

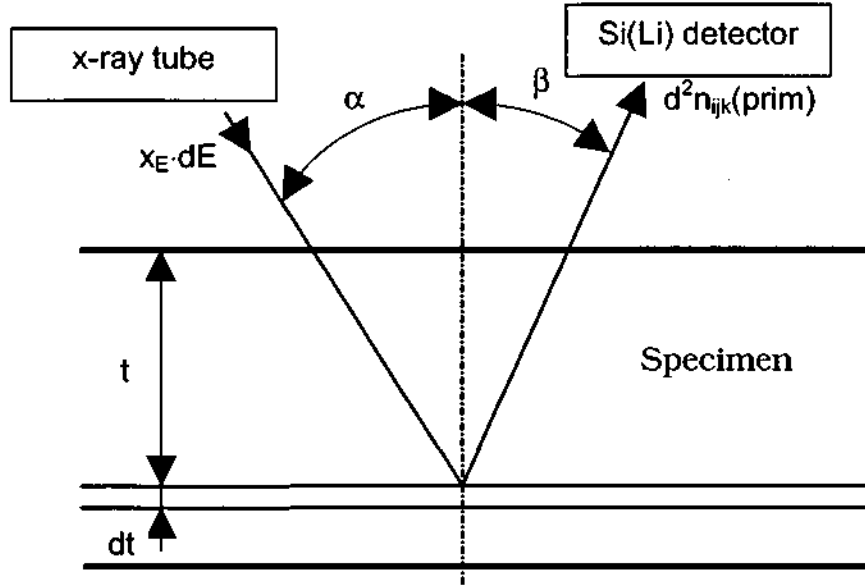


Fig. 1.5 A Schematic diagram of the incident and the fluorescence photon beam

where  $I$  is the current of the x-ray tube,  $A$  is the irradiated area on the surface of the specimen,  $x_E$  is the spectral density distribution, ( $X$  is the incidence angle with regard to the surface normal,  $d$  is the distance from target to the sample, and  $\frac{A \cos \alpha}{d^2}$  is the solid angle of the incident beam. In the same manner, the probability of the spectral intensity reaching a depth  $t$  is

$$x_E \cdot dE \cdot \frac{A \cdot \cos \alpha}{d^2} \cdot I \cdot e^{-\tau_{E,c} \cdot \rho_c \cdot \frac{t}{\cos \alpha}} \quad (1.66)$$

where  $\tau_{E,c}$  is the photoelectric cross section of the specimen including all elements. Hence, the probability that the spectral intensity of the incident beam can be absorbed in a thin layer of volume  $A \cdot dt$  can be expressed by

$$x_E \cdot dE \cdot \frac{A \cdot \cos \alpha}{d^2} \cdot I \cdot e^{-\tau_{E,c} \cdot \rho_c \cdot \frac{t}{\cos \alpha}} \cdot \frac{dt}{\cos \alpha} \cdot \rho_c \cdot \tau_{E,c} \quad (1.67)$$

where  $\tau_{E,c}$  is the total photoelectric cross section

$$\tau_{E,c} = \sum_{i=1}^n c_i \tau_{E,i} \quad (1.68)$$

Suppose equation 1.68 for one element of concentration  $c_i$  and photoelectric cross section  $\tau_{E,i}$ , equation 1.67 becomes

$$x_E \cdot dE \cdot \frac{A \cdot \cos \alpha}{d^2} \cdot I \cdot e^{-\tau_{E,c} \cdot \rho_c \cdot \frac{t}{\cos \alpha}} \cdot \frac{dt}{\cos \alpha} \cdot \rho_c \cdot c_i \cdot \tau_{E,i} \quad (1.69)$$

According to the photoelectric cross section of an element  $i$  in a defined atomic level  $j$ , the absorption edge factor  $M_{ij}$  must be taken into account,

- For quantum energy  $> K$  absorption edges, hence,

$$K \quad M_{iK} = \frac{S_{iK} - 1}{S_{iK}} \quad (1.70)$$

$$L1 \quad M_{iL1} = \frac{1}{S_{iK}} \frac{S_{iL1} - 1}{S_{iL1}} \quad (1.71)$$

$$L2 \quad M_{iL2} = \frac{1}{S_{iK}} \frac{1}{S_{iL1}} \frac{S_{iL2} - 1}{S_{iL2}} \quad (1.72)$$

$$L3 \quad M_{iL3} = \frac{1}{S_{iK}} \frac{1}{S_{iL1}} \frac{1}{S_{iL2}} \frac{S_{iL3} - 1}{S_{iL3}} \quad (1.73)$$

- For quantum energy  $> L_1$  absorption edge to quantum energy  $= K$  absorption edge

$$L1 \quad M_{iL1} = \frac{S_{iL1} - 1}{S_{iL1}} \quad (1.74)$$

$$L2 \quad M_{iL2} = \frac{1}{S_{iL1}} \frac{S_{iL2} - 1}{S_{iL2}} \quad (1.75)$$

$$L3 \quad M_{iL3} = \frac{1}{S_{iL1}} \frac{1}{S_{iL2}} \frac{S_{iL3} - 1}{S_{iL3}} \quad (1.76)$$

where  $S_{iK}, S_{iL1}, S_{iL2}$  and  $S_{iL3}$  are the jump ratios of the K-,  $L_1$ -,  $L_2$ - and  $L_3$ -edges. To obtain the fluorescence beam of x-ray photons, one has to consider some factors such as the fluorescence yield  $\omega_{ij}$  of level  $j$  of element  $i$ , transition probability,  $p_{ijk}$ , the solid angle of the detected fluorescence beam of x-ray photons  $\Omega/4\pi$  and the detector efficiency  $\epsilon_{ijk}$ . Hence equation 1.69 can be rewritten

$$x_E \cdot dE \cdot \frac{A \cdot \cos \alpha}{a^2} \cdot I \cdot e^{-\tau_{E,c} \cdot \frac{\Omega}{4\pi} \cdot \frac{t}{\cos \alpha}} \cdot \frac{dt}{\cos \alpha} \cdot \rho_c \cdot c_i \cdot \tau_{E,i} \cdot M_{ij} \cdot \omega_{ij} \cdot p_{ij} \cdot \frac{\Omega}{4\pi} \cdot e^{-\tau_{ijk} \cdot \rho_c \cdot \frac{t}{\cos \alpha}} \cdot \epsilon_{ijk} \quad (1.77)$$

where  $\beta$  is the take-off angle with regard to the surface normal,  $\tau_{ijk}$  is the photoelectric cross section of the sample which is the sum of the photoelectric cross section of each element in the sample,  $\tau_{ijk}$  multiplied by its concentration,  $c_q$

$$\tau_{ijk,c} = \sum_{q=1}^n c_q \cdot \tau_{ijk,q} \quad (1.78)$$

Hence, the count rate due to primary fluorescence from a thin layer  $dt$  of volume  $A \cdot dt$  is

$$d^2 n_{ijk}(\text{prim}) = x_E \cdot dE \cdot \frac{A \cos \alpha}{a^2} \cdot I \cdot e^{-\tau_{E,c} \cdot \rho_c \cdot \frac{t}{\cos \alpha}} \cdot \frac{dt}{\cos \alpha} \cdot \rho_c \cdot c_i \cdot \tau_{E,i} \cdot M_{ij} \cdot \omega_{ij} \cdot p_{ijk} \cdot \frac{\Omega}{4\pi} \cdot e^{-\tau_{ijk} \cdot \rho_c \cdot \frac{t}{\cos \alpha}} \cdot \epsilon_{ijk} \quad (1.79)$$

It should be noticed that we must take in our consideration the whole sample whereas equation 1.79 is valid for a thin layer of sample with volume  $A \cdot dt$ . So, we integrate from  $t = 0$  to  $t = \infty$ .

$$dn_{ijk}(prim) = x_E \cdot dE \cdot \frac{A \cdot \cos \alpha}{d^2} \cdot I \cdot \frac{1}{\cos \alpha} \cdot c_i \cdot M_{ij} \cdot \omega_{ij} \cdot p_{ijk} \cdot \frac{\Omega}{4\pi} \cdot \epsilon_{ijk} \cdot \frac{\tau_{E,i}}{\cos \alpha + \frac{\tau_{ijk,c}}{\cos \beta}} \quad (1.80)$$

By integration of equation 1.80 from the binding energy of the element  $E_{ij}$  to the maximum energy  $E_0$ , the contribution from primary excitation becomes

$$n_{ijk}(prim) = \frac{A \cdot \cos \alpha}{d^2} \cdot I \cdot \frac{1}{\cos \alpha} \cdot c_i \cdot M_{ij} \cdot \omega_{ij} \cdot p_{ijk} \cdot \frac{\Omega}{4\pi} \cdot \epsilon_{ijk} \cdot \int_{E_{ij}}^{E_0} \frac{x_E \cdot \tau_{E,i}}{\cos \alpha + \frac{\tau_{ijk,c}}{\cos \beta}} \cdot dE \quad (1.81)$$

The dimensions of the different quantities of equation 1.81 are

$\frac{A \cdot \cos \alpha}{d^2}$  (sr),  $I$  (mA),  $\frac{1}{\cos \alpha} \cdot c_i \cdot M_{ij} \cdot \omega_{ij} \cdot p_{ijk} \cdot \frac{\Omega}{4\pi} \cdot \epsilon_{ijk} \cdot x_E$  ( $s^{-1} \text{ mA}^{-1} \text{ keV}^{-1} \text{ sr}^{-1}$ ),  $\tau_{E,i}$ ,  $\tau_{E,c}$ ,  $\tau_{ijk,c}$  ( $\text{cm}^2 \text{ g}^{-1}$ ),  $E_{ij}$  (keV).

From equation 1.81, the quantities  $\frac{A \cdot \cos \alpha}{d^2} \cdot I \cdot \frac{\Omega}{4\pi} \cdot \frac{1}{\cos \alpha}$  can be considered as a constant value.

$$CONST = \frac{A \cdot \cos \alpha}{d^2} \cdot I \cdot \frac{\Omega}{4\pi} \cdot \frac{1}{\cos \alpha} \quad (1.82)$$

So equation 1.81 becomes

$$n_{ijk}(prim) = CONST \cdot c_i \cdot M_{ij} \cdot \omega_{ij} \cdot p_{ijk} \cdot \epsilon_{ijk} \cdot \int_{E_{ij}}^{E_0} \frac{x_E \cdot \tau_{E,i}}{\cos \alpha + \frac{\tau_{ijk,c}}{\cos \beta}} \cdot dE \quad (1.83)$$

where the spectral density distribution  $x_E$  is given by equation 1.53. In the present work, the target material is rhodium, Rh-45. Together with equations 1.82, 1.70, primary excitation by continuous radiation follows from

$$n_{ijk}(prim) = CONST \cdot c_i \cdot \frac{S_{iK} - 1}{S_{iK}} \cdot \omega_{ij} \cdot p_{ijk} \cdot \epsilon_{ijk} \cdot \int_{E_{ij}}^{E_0} \frac{x_E \cdot \tau_{E,i}}{\cos \alpha + \frac{\tau_{ijk,c}}{\cos \beta}} \cdot dE \quad (1.84)$$

where,  $S_{iK}$  is jump ratio of the  $K$  shell. Taking into account the effect of white and characteristic radiation (equations 1.55 and 1.61) on the count rate due to primary excitation follows

$$n_{ijk}^{(prim)} = CONST.c_i \cdot \frac{S_{iK} - 1}{S_{iK}} \cdot \omega_{ij} \cdot P_{ijk} \cdot \tau_{ijk} \cdot \left\{ \int_{E_{i,j}}^{E_j} \frac{x_E \cdot \tau_{E,j}}{\tau_{E,c}} \frac{dE}{\cos \alpha} + \sum_{a=1}^n Const_{hc} \cdot \frac{1}{S_{ab}} \cdot R \cdot \omega_{ab} \cdot P_{abc} \cdot f(x_{abc}) \cdot \frac{\tau_{abc,i}}{\frac{\tau_{abc,c}}{\cos \alpha} + \frac{\tau_{ijk,c}}{\cos \beta}} \right\} \quad (1.85)$$

### 1.3.2 The Secondary Fluorescence

Secondary fluorescence is often associated with an element of higher atomic number than that of the fluorescent element and it can be defined as the x-rays emitted from atoms excited by the primary fluorescent x-rays from coexistent elements. The secondary excitation enhances the intensity of an element in the sample.

For example, if a Cu-Zn binary alloy is exposed to an incident radiation, the primary fluorescence of both Cu and Zn will be emitted. In addition, the secondary fluorescence possibilities are given in Table 1.1. For instance, the primary fluorescence of Zn-K $\beta$  is sufficiently energetic to excite K $\alpha$ , K $\beta$ , L $\alpha$ , L $\beta$  of Cu and L $\alpha$ , L $\beta$  of Zn. On the other hand, the primary fluorescence Zn-K $\alpha$  is not sufficiently energetic to excite Cu-K $\alpha$  or Cu-K $\beta$  because the photon energy of Zn-K $\alpha$  is lower than the absorption edge of the Cu-K shell. Therefore, the characteristic radiation (K $\alpha$ , K $\beta$ , L $\alpha$ , L $\beta$ ) of Cu will be enhanced by including the secondary fluorescence. Also, the primary fluorescence Zn-L lines can not excite the L characteristic radiation of Cu (L $\alpha$  and L $\beta$ ) whereas the photon energy of Zn-L lines is lower than the absorption edge of the Cu-L edges (see Table 1.2 and Figs. 1.6 and 1.7). Therefore, all possibilities of the secondary excitation as illustrated in Table 1.1 must be considered.

Table 1.1 The secondary fluorescence possibilities

Primary Fluorescence	Secondary Fluorescence							
	Cu				Zn			
	K $\alpha$	K $\beta$	L $\alpha$	L $\beta$	K $\alpha$	K $\beta$	L $\alpha$	L $\beta$
Cu-K $\alpha$			X	X			X	X
Cu-K $\beta$			X	X			X	X
Cu-L $\alpha$								
Cu-L $\beta$								
Zn-K $\alpha$			X	X			X	X
Zn-K $\beta$	X	X	X	X			X	X
Zn-L $\alpha$								
Zn-L $\beta$								

Table 1.2 The absorption edges and the characteristic radiations of Cu and Zn

Cu				Zn			
Edge, keV		Line, keV		Edge, keV		Line, keV	
K	8.979	K $\alpha$	8.03	K	9.659	K $\alpha$	8.63
		K $\beta$	8.93			K $\beta$	9.61
L $I$	1.096	L $\alpha$	0.928	L $I$	1.194	L $\alpha$	1.009
L $II$	0.951	L $\beta$	0.948	L $II$	1.044	L $\beta$	1.032
L $III$	0.931			L $III$	1.021		



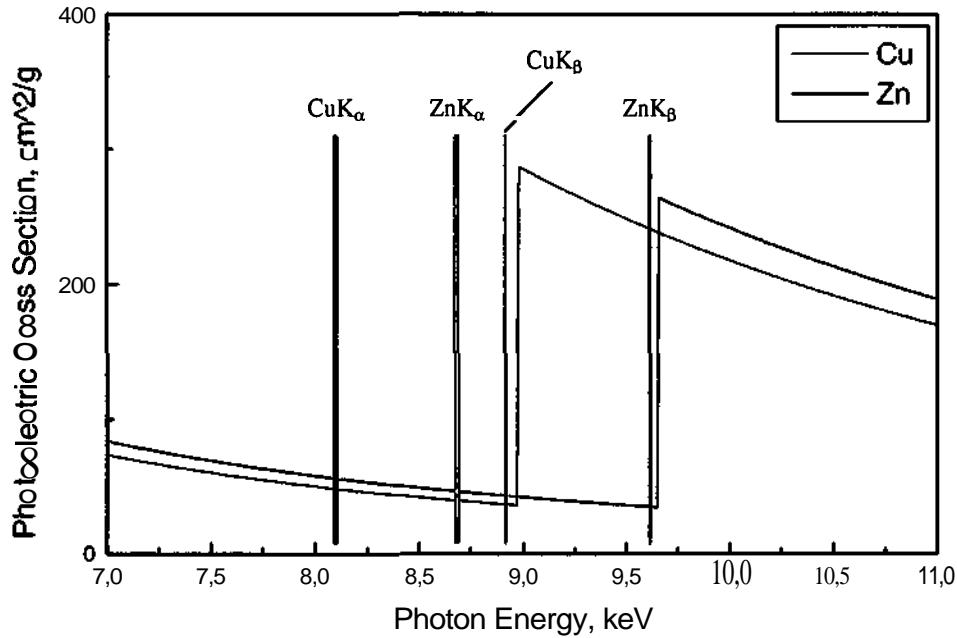


Fig. 1.6 Secondary fluorescence possibilities at K edges of Cu-Zn

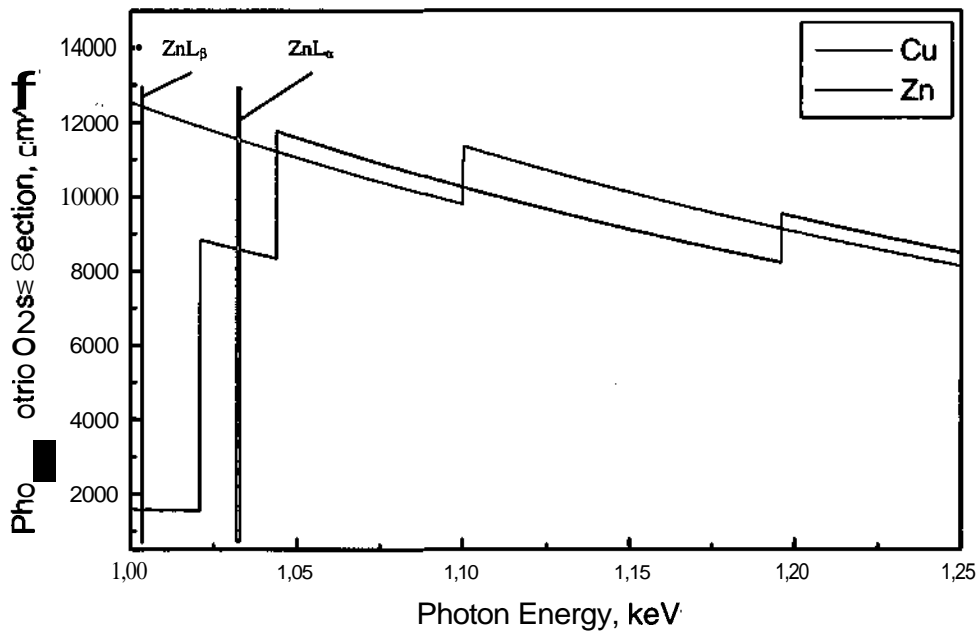


Fig. 1.7 Secondary fluorescence possibilities at L edges of Cu-Zn

The theoretical expression of the secondary fluorescence was first derived by Gillam and Heal[3] assuming monochromatic excitation. The derivation of the secondary excitation can be explained as illustrated in Figs. 1.8 and 1.9. As mentioned before the Zn-K<sub>β</sub> is sufficiently energetic to excite both Cu-K<sub>α</sub> and Cu-K<sub>β</sub> in the Cu-Zn binary alloys. The incident beam is partly absorbed at depth  $\xi$  by an elementary thickness  $d\xi$  with volume  $A \cdot d\xi$ . So, the characteristic fluorescence radiation excites different elements in this volume, producing a primary fluorescence

of all the elements in the specimen (Cu and Zn in this case). The fluorescence radiation of Zn-K<sub>β</sub> (xyz x=Zn, y=K, z=M<sub>23</sub>+N<sub>23</sub>) excites Cu-K<sub>α</sub>, (ijk i=Cu, j=K, k=L<sub>23</sub>), therefore the secondary excitation will enhance the primary excitation of Cu-K<sub>α</sub>. In the volume  $\mathcal{A}.d\xi$  as described in Fig. 1.8, the amount of x-radiation which reaches this volume will be absorbed between the angles  $\gamma$  to  $\gamma+d\gamma$  and can be described as follows

$$\frac{2.r.\sin\gamma.\pi.r.d\gamma}{4.\pi.r^2} = \frac{\sin\gamma.d\gamma}{2} \quad (1.86)$$

The x-radiation will be attenuated till it reaches the distance  $r$  as shown in Fig. 1.8, whereas

$$r = \frac{t - \xi}{\cos\gamma} \quad \text{and} \quad dr = \frac{dt}{\cos\gamma} \quad (1.87)$$

According to Fig. 1.8 and at the elementary depth  $dr$ , the primary radiation will be absorbed. As shown in Fig. 1.9 and by integration of the different parameters ( $\xi$  changes from 0 to  $t$  and  $t$  changes from 0 to  $\infty$ ,  $\gamma$  changes from 0 to  $\pi/2$  and  $E$  from  $E_1$  to  $E_0$ ), the count rate due to secondary excitation can be expressed by

$$d^4 n_{ijk}(\text{sec.}, xyz)_1 = x_E . dE . \frac{A \cos\alpha}{d^2} . I . e^{-\tau_{E,c} \cdot \frac{\xi}{\cos\alpha}} . \rho_c . c_x . \tau_{E,x} . M_{xy} . p_{xy} . \omega_{xy} \cdot \frac{\sin\gamma.d\gamma}{2} . e^{-\tau_{xyz,c} \cdot \rho_c \cdot \frac{t-\xi}{\cos\gamma}} . \frac{dt}{\cos\gamma} . c_i . \rho_c . \tau_{xyz,i} . M_{ij} . \omega_{ij} . p_{ijk} . \frac{\Omega}{4.\pi} . e^{-\tau_{ijk,c} \cdot \rho_c \cdot \frac{r}{\cos\beta}} . \epsilon_{ijk} \quad (1.88)$$

With the count rate of the primary excitation equation 1.88 becomes

$$d^4 n_{ijk}(\text{sec.}, xyz)_1 = \frac{1}{2} . CONST . B_{ijk} . B_{xyz} . c_i . c_x . \tau_{E,x} . \tau_{xyz,i} . \epsilon_{ijk} . \rho_c^2 . x_E . \frac{\sin\gamma}{\cos\gamma} . e^{\left(\frac{\tau_{ijk,c}}{\cos\beta} + \frac{\tau_{xyz,c}}{\cos\gamma}\right) \rho_c \cdot t} . e^{-\left(\frac{\tau_{E,c}}{\cos\alpha} + \frac{\tau_{xyz,c}}{\cos\gamma}\right) \rho_c \cdot \xi} . dE . d\gamma . dt . d\xi \quad (1.89)$$

where

$$\begin{aligned} B_{ijk} &= M_{ij} . \omega_{ij} . p_{ijk} \\ B_{xyz} &= M_{xy} . \omega_{xy} . p_{xyz} \end{aligned} \quad (1.90)$$

On the other hand, according to Fig. 1.9, we find

$$r = \frac{\xi - t}{\cos\gamma} \quad \text{and} \quad dr = \frac{-dt}{\cos\gamma} \quad (1.91)$$

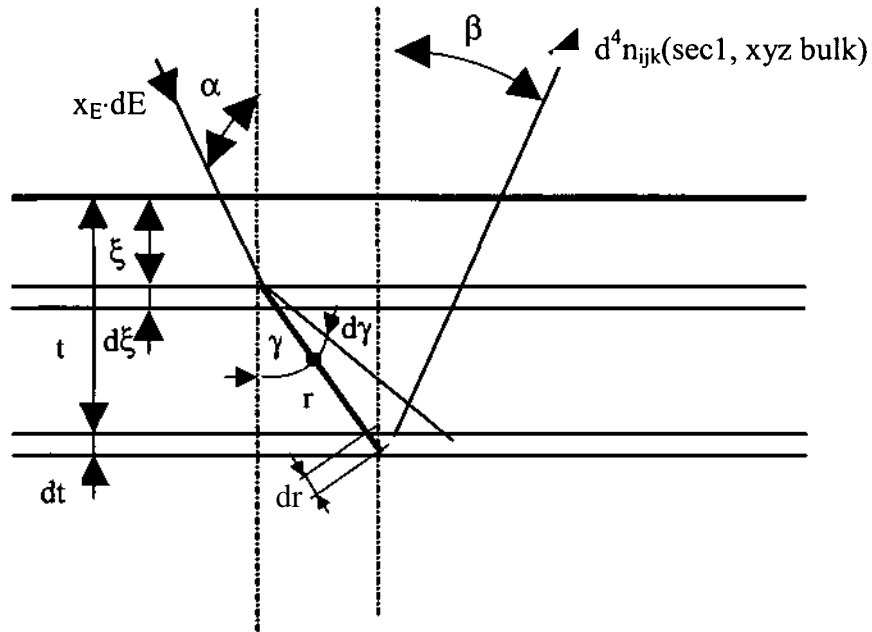


Fig. 1.8 A Schematic diagram of incident and fluorescence photon beams, (case 1)

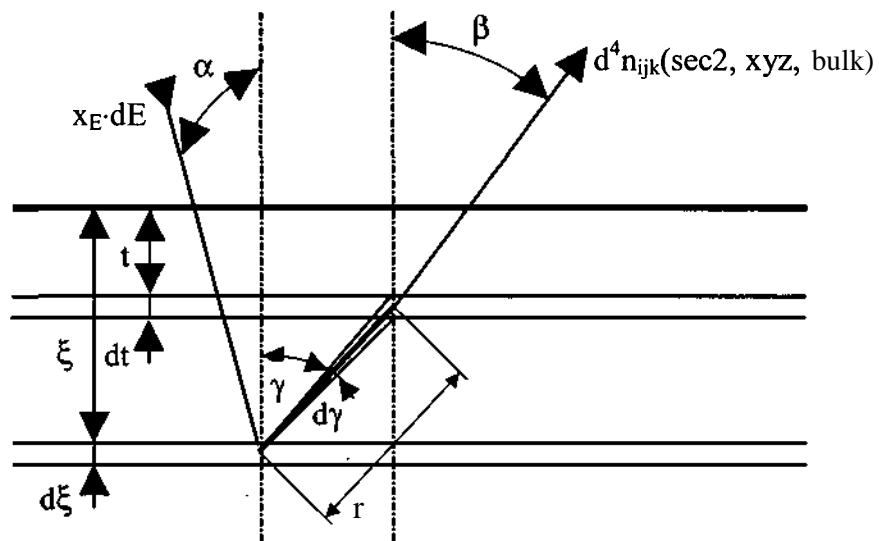


Fig. 1.9 A Schematic diagram of incident and fluorescence photon beams (case 2)

Then the count rate of the secondary excitation in this case can be expressed by

$$d^4 n_{ijk}(\text{sec.}, xyz)_2 = 1 \cdot \text{CONST} \cdot B_{ijk} \cdot B_{xyz} \cdot c_i \cdot c_x \cdot \tau_{E,x} \cdot \tau_{xyz,i} \cdot \epsilon_{ijk} \cdot \rho_c^2 \cdot x_E \cdot \frac{\sin \gamma}{\cos \gamma} \cdot e^{\left(\frac{\tau_{ijk,c}}{\cos \beta} + \frac{\tau_{xyz,c}}{\cos \gamma}\right) \rho_c \cdot t} \cdot e^{-\left(\frac{\tau_{E,c}}{\cos \alpha} + \frac{\tau_{xyz,c}}{\cos \gamma}\right) \rho_c \cdot \xi} \cdot dE \cdot d\gamma \cdot dt \cdot d\xi \quad (1.92)$$

By using an integration of the different parameters ( $\xi$  changes from  $t$  to  $0$  and  $t$  changes from  $0^\circ$  to  $0$ ,  $\gamma$  changes from  $0$  to  $\pi/2$  and  $E$  from  $E_{xy}$  to  $E_0$ ), we obtain the count rate of the secondary excitation in this case. From equations 1.89 and 1.92, the total secondary excitation is equal to the sum [ $n_{ijk}(\text{sec.}, xyz) = n_{ijk}(\text{sec.}, xyz)_1 + n_{ijk}(\text{sec.}, xyz)_2$ ]

$$n_{ijk}(\text{sec.}, xyz) = \int_{E=E_{xy}}^1 \text{CONST} \cdot B_{ijk} \cdot B_{xyz} \cdot c_i \cdot c_x \cdot \tau_{xyz,i} \cdot \epsilon_{ijk} \cdot \left[ \frac{x_E \cdot \tau_{E,x}}{\tau_{E,c} + \frac{\tau_{ijk,c}}{\cos \alpha}} \cdot \left\{ \frac{\cos \beta}{\tau_{ijk,c}} \cdot \ln \left( 1 + \frac{1}{\cos \beta} \cdot \frac{\tau_{ijk,c}}{\tau_{xyz,c}} \right) + \frac{\cos \alpha}{\tau_{E,c}} \cdot \ln \left( 1 + \frac{1}{\cos \alpha} \cdot \frac{\tau_{E,c}}{\tau_{xyz,c}} \right) \right\} \right] \cdot dE \quad (1.93)$$

Taking into account the effect of white and characteristics radiation on the count rate of secondary excitation from equations 1.55 and 1.61, the count rate of the secondary excitation becomes,

$$n_{ijk}(\text{sec.}, xyz) = \frac{1}{2} \cdot \text{CONST} \cdot B_{ijk} \cdot B_{xyz} \cdot c_i \cdot c_x \cdot \tau_{xyz,i} \cdot \epsilon_{ijk} \cdot \int_{E=E_{xy}}^{E_0} \frac{x_E \cdot \tau_{E,x}}{\tau_{E,c} + \frac{\tau_{ijk,c}}{\cos \alpha}} \cdot \left\{ \frac{\cos \beta}{\tau_{ijk,c}} \cdot \ln \left( 1 + \frac{1}{\cos \beta} \cdot \frac{\tau_{ijk,c}}{\tau_{xyz,c}} \right) + \frac{\cos \alpha}{\tau_{E,c}} \cdot \ln \left( 1 + \frac{1}{\cos \alpha} \cdot \frac{\tau_{E,c}}{\tau_{xyz,c}} \right) \right\} \cdot dE + \frac{1}{2} \cdot \frac{A \cdot \cos \alpha}{d^2} \cdot I \cdot \frac{1}{\cos \alpha} \cdot \frac{\text{fl}}{4\pi} \cdot M_{ij} \cdot \omega_{ij} \cdot P_{ijk} \cdot M_{xy} \cdot \omega_{xy} \cdot P_{xyz} \cdot c_i \cdot c_x \cdot \tau_{xyz,i} \cdot \epsilon_{ijk} \cdot \sum_{a=1}^n \text{const}_{bc} \cdot \frac{1}{S_{ab}} \cdot R_{ab} \cdot \omega_{ab} \cdot P_{abc} \cdot f(x_{abc}) \cdot \frac{\tau_{abc,x}}{\tau_{abc,c} + \frac{\tau_{ijk,c}}{\cos \beta}} \cdot \left\{ \frac{\cos \beta}{\tau_{ijk,c}} \cdot \ln \left( 1 + \frac{1}{\cos \beta} \cdot \frac{\tau_{ijk,c}}{\tau_{xyz,c}} \right) + \frac{\cos \alpha}{\tau_{abc,c}} \cdot \ln \left( 1 + \frac{1}{\cos \alpha} \cdot \frac{\tau_{abc,c}}{\tau_{xyz,c}} \right) \right\} \quad (1.94)$$

The total count rate is the sum of the contribution from primary and secondary excitation.

$$n_{ijk}(\text{theoretical}) = n_{ijk}(\text{prim}) + n_{ijk}(\text{sec.}, xyz) \quad (1.95)$$

### 1.3.3 The Tertiary Fluorescence

The tertiary fluorescence is often associated with the secondary fluorescence of an element which has a photon energy higher than that of the fluorescent element and it can be defined as the x-ray emitted from atoms excited by secondary fluorescent x-rays from coexistent elements. The tertiary excitation rarely enhances the intensity of an element in the sample. At the same time, the calculation complexity of the tertiary fluorescence is more complicated than the primary and the secondary fluorescence calculation. Fig. 1.10 illustrates the effective percentage

of the contributions from primary, secondary and tertiary excitation and the calculation complexity. Therefore, tertiary fluorescence is not considered in this work.

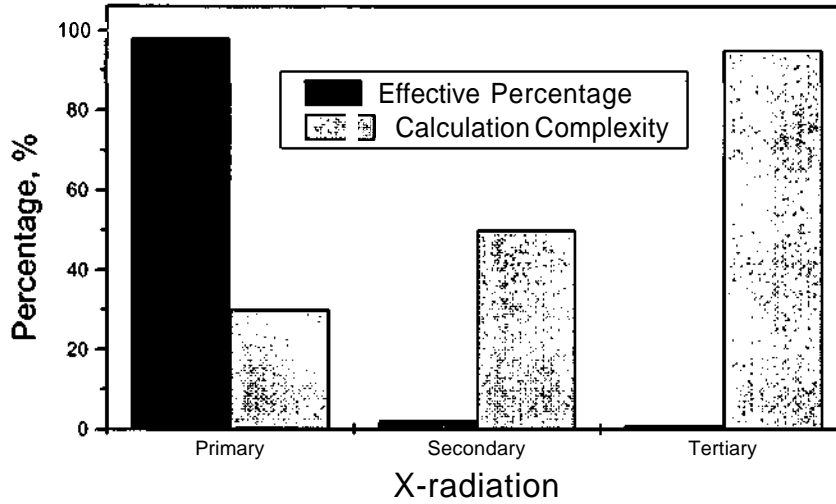


Fig. 1.10 Primary, secondary and tertiary fluorescence complexity.

### 1.3.4 Iteration Procedure

To calculate the concentrations of the  $n$  elements in any type of specimen, the total concentration of all elements in the specimen must be equal 1, that means

$$\sum_{i=1}^n c_i = 1 \quad (1.96)$$

A starting value of the concentration ( $c_i$ ) of any element in the specimen is calculated from the measured signals of fluorescence radiations by

$$c_i(1, \text{calculated}) = \frac{n_k(\text{experimental})}{\sum_{q=1}^n n_{qjk}(\text{experimental})} \quad (1.97)$$

where  $n_{ijk}$  is the experimental count rate of a specific element and  $\sum_{q=1}^n n_{qjk}$  is the total experimental count rate of all elements in the specimen. The correction factor of the concentration of each element,  $k_i$  is the ratio between the experimental count rate of the fluorescence beam of x-ray photons and the theoretical as given by equation 1.95,

$$k_i = \frac{n_{ijk}(\text{experimental})}{n_{ijk}(\text{theoretical})} \quad (1.98)$$

Then the second approximation of the concentration of each element in the specimen can be calculated according

$$c_i(2, \text{calculated}) = \frac{k_i \cdot c_i(1, \text{calculated})}{\sum_{q=1}^n k_q \cdot c_q} \quad (1.99)$$

The concentration of these elements would be improved by this iteration procedure using the correction factor until,  $c_i(m-1, \text{calculated}) = c_i(m, \text{calculated})$ . The final concentration of the element can be calculated in weight percents or in atomic percents

Concentration in weight percent

$$c_i(\text{weight}\%) = 100 \cdot \frac{c_i(\text{At}\%) \cdot A_i}{\sum_{q=1}^n c_q(\text{At}\%) \cdot A_q} \quad (1.100)$$

Concentration in atomic percent

$$c_i(\text{At}\%) = 100 \cdot \frac{\frac{c_i(\text{weight}\%) \cdot A_i}{A_i}}{\sum_{q=1}^n \frac{c_q(\text{weight}\%) \cdot A_q}{A_q}} \quad (1.101)$$

where  $A_i$  and  $A_q$  are the atomic weight of element  $i$  and atomic weights of each element  $q$  in the specimen, respectively.

#### 1.4 Si(Li) Detector

In the present work, a Lithium drifted silicon (Si(Li)) detector was used. Nowadays, it can be used in a wide variety of applications including x-ray fluorescence, x-ray microanalysis, particle induced x-ray emission, x-ray diffraction and Mössbauer spectroscopy. The mechanism by which x-rays are detected in a Si(Li) detector is similar to that of the gas filled proportional counters, but certain differences arise from the fact that the detection medium is solid. The use of Si(Li) detectors is of great advantage, its dimensions are much smaller than the equivalent gas filled detectors and best energy resolution is achievable. Also, Si(Li) detectors have an efficiency which can be varied to match the requirements of the application.

A Si(Li) detector[55] is manufactured from high-purity single crystal of p-type silicon. However, p-type silicon of sufficiently high purity is difficult to fabricate. Most Si crystals contain extrinsic holes, caused by impurities, which lead to a significant "leakage" of current at the required bias voltage. In order to compensate for these extrinsic holes, lithium (an n-type dopant), is diffused into the material at 350 - 450°C from the rear contact under a voltage applied between the front and rear detector contact. The lithium atoms compensate the extrinsic charge-carriers in the p-type silicon and provide a wide "intrinsic" region of high resistance. A high concentration of Li near the rear contact creates an n-type region, over which a layer of gold is deposited by evaporation to fabricate a non rectifying contact to the n-type region. In the non rectifying contact the output signal is obtained via a connection to the back n-type layer.

In the front of the detector (where the x-ray photons enter) a Schottky barrier contact is applied to produce a p-i-n diode. This consists of a 0.02  $\mu\text{m}$  gold layer followed by 0.1  $\mu\text{m}$  thick silicon dead layer. The dead layer is the region where the electrical resistivity is too low to allow

full collection of electron-hole pairs that have been released by the absorption of an x-ray photon. So, the photons interacting with the detector in the dead layer are measured with abnormally low pulse height or they are not measured at all. This problem is most significant for very low energy x-rays which have a high probability of being absorbed in the dead layer. In front of the Schottky barrier contact, there is a window. The window is usually a beryllium foil with thickness in the range 8 to 12  $\mu\text{m}$ . The Be window must be vacuum tight and strong enough to withstand atmospheric pressure on the outside. If the beryllium window is removed, the detector can record x-rays of energies below 1 keV, but there is a risk of surface contamination leading to a degradation of performance. Fig. 1.11 shows the sensitive volume of the Si(Li) detector and the x-ray interaction which ranges from 4 -16 mm in diameter and 3-5 mm in thickness depending on the application.

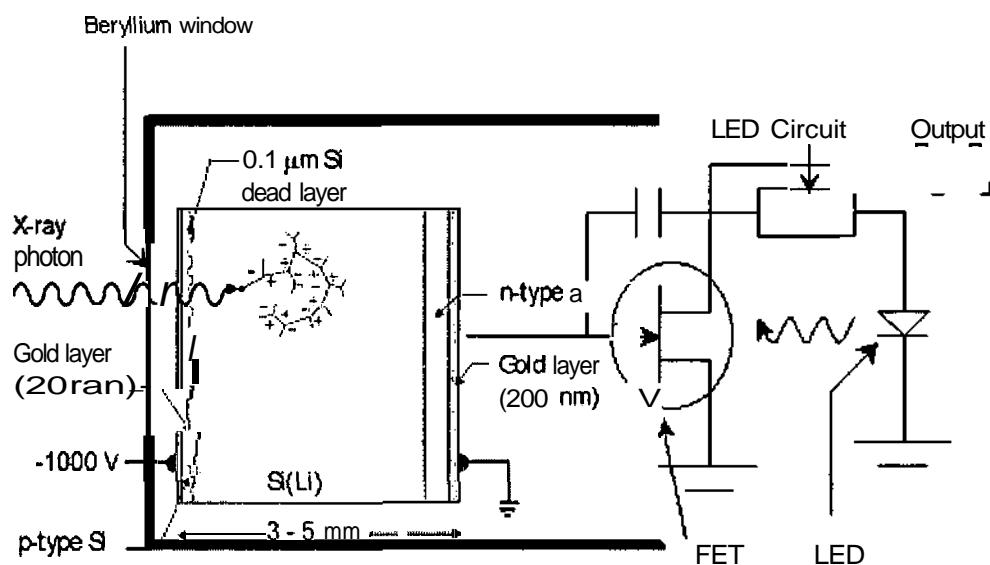


Fig. 1.11 Schematic diagram of the sensitive volume of the Si(Li) detector.

#### 1.4.1 Detector Efficiency

The detection and the measurements of the characteristic x-rays depend on the detector efficiency. The detector efficiency differs from one detector to another as a function of the atomic number of the semiconductor and the thickness of the depletion layer in the detector. The most significant development in x-ray intensity measurements used in energy dispersive spectrometry are solid state detectors, as Si(Li) or Ge(Li). The major advantages of the solid state detectors are

- energy conversion is very efficient,
- resolution is excellent, the spectral lines can be resolved,
- detector is free from pulse-height drift and broadening at intensities up to 10000 cps,
- small size of the detectors permits use near to the specimen.

As mentioned above, the Si(Li) detector consists of a silicon single crystal semiconductor having a compensated intrinsic (i-type) region sandwiched between p-positive and negative regions. The compensated region is formed by diffusion of Lithium into p-type silicon. The p-type layer on the detector is an inactive or dead layer. There is no contribution to the detection process. When an x-ray photon enters the detector diode and passes through the active semiconductor volume, a cloud of ionization is generated as electron-hole pairs. The number of electron-hole pairs created equals the total electric charge released, which is proportional to the energy of the

detected photon. This charge is swept from the detector diode by high voltage applied. The preamplifier is responsible for collecting this charge on a feedback capacitor to produce an output pulse which is proportional to the original x-ray photon energy. The relation between the total charge of electron-hole pairs  $Q$  and the x-ray photon energy  $E_x$  is

$$Q = \frac{E_x}{3.8} \times 1.6 \times 10^{-19} \quad C \quad (1.102)$$

The value 3.8 refers to the effective ionisation potential required to produce a single electron-hole pair. Charge sensitive preamplification is needed to integrate the total collected charge into a current pulse. For this function a field effect transistor (FET) is used and this has to be maintained also at liquid nitrogen temperature to reduce noise level. The current pulse is subsequently amplified and converted to a potential pulse by additional preamplifier stages.

The most important physical features of the detector are its area and thickness. Geometric efficiency increases, but the resolution decreases with increasing area. Absorption efficiency increases with thickness. The smaller diameter detectors yield better energy resolution at low energy, and the thicker detectors have a higher detection efficiency at energies above about 20 keV. In the present work, Si(Li) solid state detector was used in EDXRF-KEVEX 0700. The detector efficiency was calculated

#### 1.4.1.1 Detector Efficiency of EDXRF-KEVEX 0700

In the Energy Dispersive X-ray Fluorescence Spectrometer, (EDXRF-KEVEX 0700), the system works under atmospheric pressure and the detector is also maintained at liquid nitrogen temperature. Several practical x-ray detector forms are designed to improve charge collection and resolution. The Si(Li) detector with the EDXRF-KEVEX 0700 consists of Beryllium window of thickness  $d_{Be} = 0.002$  cm, gold layer of thickness  $d_{Au} = 0.000002$  cm, inactive silicon layer of thickness  $d_{Si} = 0.00001$  cm and finally active silicon layer of thickness  $d_{Si} = 0.3$  cm. The detector efficiency was calculated according to the detector efficiency from Fiori[56],

$$\epsilon_{ijk} = e^{-\mu_{E,Be} \cdot \rho_{Be} \cdot d_{Be}} \cdot e^{-\mu_{E,Au} \cdot \rho_{Au} \cdot d_{Au}} \cdot (1 - e^{-\mu_{E,Si} \cdot \rho_{Si} \cdot d_{Si}}) \cdot (1 - e^{-\mu_{E,Si} \cdot \rho_{Si} \cdot d_{Si}}) \quad (1.103)$$

where  $\mu_{E,Be}$ ,  $\mu_{E,Au}$ ,  $\mu_{E,Si}$  are the mass absorption coefficients in  $\text{cm}^2/\text{g}$  of beryllium, gold and silicon at photons of energy  $E(\text{keV})$  respectively,  $\rho_{Be}$ ,  $\rho_{Au}$ ,  $\rho_{Si}$  are the densities of beryllium, gold, silicon in  $(\text{g}/\text{cm}^3)$  respectively. Fig. 1.12 shows the calculated detector efficiency depending on the photon energy in keV. According to Fig. 1.12, the detector is more sensitive in the photon energy range from 5-25 keV.



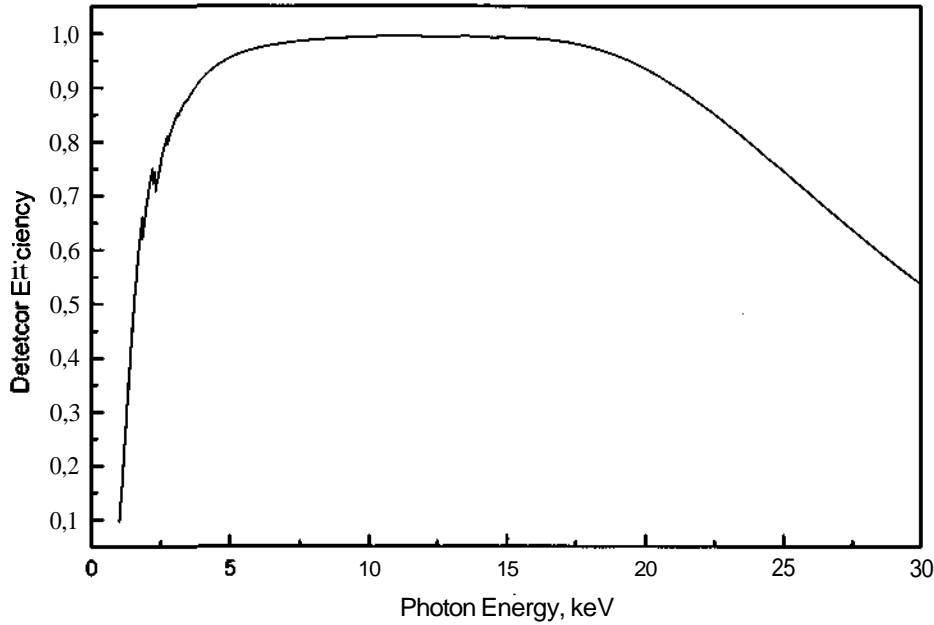


Fig. 1.12 Calculated detector efficiency in the Kevex 0700 instrument.

#### 1.4.1.2 Detector Efficiency of EPMA

In the Electron Probe Micro Analyser (EPMA), the system worked under vacuum and the detector must be maintained at liquid nitrogen temperature to reduce noise when a potential is applied across the detector. In EPMA the detector is slightly different from the mentioned EDXRF-Kevex 0700 detector. The detector efficiency of the EPMA detector is given by a new expression

$$\varepsilon_{ijk} = \left(1 - e^{(-\mu_{E,Si} \cdot \rho_{Si} \cdot d_{Si})}\right) e^{(-\mu_{E,Si} \cdot \rho_{Si} \cdot d_{Si})} \cdot e^{(-\mu_{E,Ni} \cdot \rho_{Ni} \cdot d_{Ni})} \cdot e^{(-\mu_{E,Al} \cdot \rho_{Al} \cdot d_{Al})} \cdot e^{(-\mu_{E,Polymer} \cdot \rho_{Polymer} \cdot d_{Polymer})} \cdot (0.9 + 0.2 \cdot e^{(-\mu_{E,Si} \cdot \rho_{Si} \cdot d_{grid})}) \quad (1.104)$$

where

$$\mu_{E,Polymer} = 0.0262 \cdot \mu_{E,H} + 0.6911 \cdot \mu_{E,C} + 0.0733 \cdot \mu_{E,N} + 0.2094 \cdot \mu_{E,O} \quad (1.105)$$

The polymer layer is made up of four elements with a defined concentration: hydrogen with concentration 2.62 wt%, carbon with concentration 69.11 wt%, nitrogen with concentration 7.33 wt% and oxygen with concentration 20.94 wt%. The concentration of the elements in the polymer and the detailed structure of the EPMA detector were supplied by the detector manufacturer.  $\mu_{E,H}$ ,  $\mu_{E,C}$ ,  $\mu_{E,N}$ ,  $\mu_{E,O}$ ,  $\mu_{E,Al}$ ,  $\mu_{E,Ni}$  and  $\mu_{E,Polymer}$  are the mass absorption coefficients in  $\text{cm}^2/\text{g}$  of photons of energy  $E$  of hydrogen, carbon, nitrogen, oxygen aluminum, nickel and polymer respectively,  $\rho_{Al}$ ,  $\rho_{Ni}$ ,  $\rho_{Polymer}$  are the densities of aluminum, nickel and polymer layer in the detector window in  $\text{g}/\text{cm}^3$ ,  $d_{Si} = 0.335 \text{ cm}$  is the thickness of the active silicon layer,  $d_{Si} = 8.5 \times 10^{-7} \text{ cm}$  is the thickness of the inactive silicon layer,  $d_{Ni} = 8 \times 10^{-7} \text{ cm}$  is the thickness of the nickel layer,  $d_{pol} = 6 \times 10^{-7} \text{ cm}$  is the thickness of the polymer layer,  $d_{Al} = 8 \times 10^{-6} \text{ cm}$  is the thickness of the aluminum layer, and finally  $d_{grid} = 0.038 \text{ cm}$  is the

thickness of the Si grid in the detector window. The silicon grid is made of only 20% of silicon in the grid and the rest, 80% has no photoelectric absorption. Figure 1.13 shows the calculated detector efficiency of the EPMA detector.

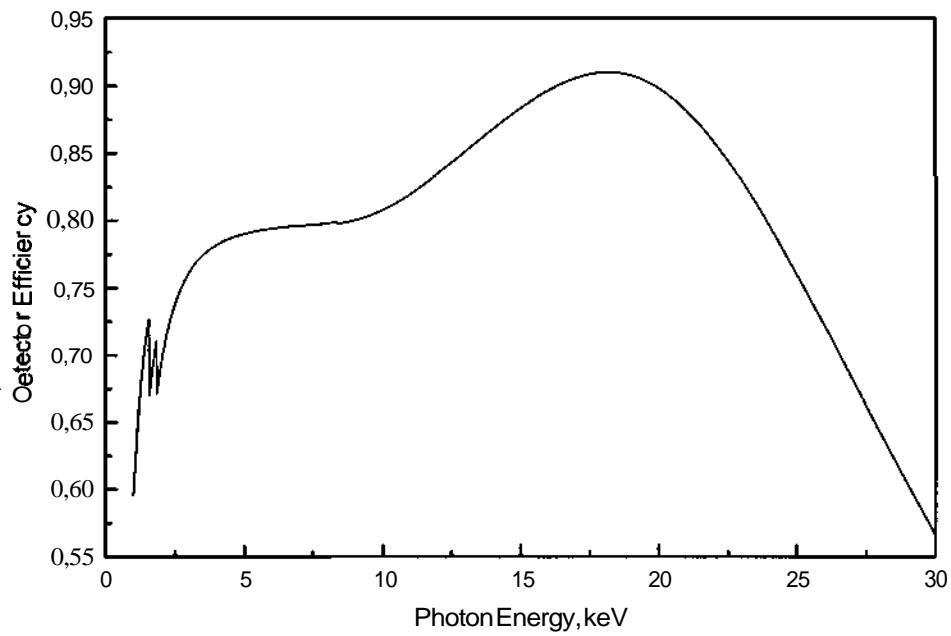


Fig. 1.13 Calculated EPMA detector efficiency

## CHAPTER 2

### QUANTITATIVE ANALYSIS USING FUNDAMENTAL PARAMETER APPROACH

This work has been performed by using an energy dispersive x-ray fluorescence spectrometer (EDXRF). In the present work, the EDXRF-KEVEX 0700 was used which is a technique for simultaneous qualitative and quantitative analysis for all the elements with atomic number higher than 10. The medium and heavy elements can easily be analysed in an air environment in the sample chamber, but for analysing light elements, the samples must be analysed under vacuum. Edward EDM6 Vacuum Pump is supplied with the EDXRF-KEVEX 0700 which is capable of pumping 108 litres per minutes. When the sample is excited by a suitable excitation source, the characteristic radiations of the elements composing the sample are emitted and can be measured by the detection system. Therefore, these procedures allow to qualitatively and quantitatively determine the relative concentration of the elements in the sample. The photon energy of the excitation source must be sufficiently energetic to eject the electrons from the appropriate atomic levels of the elements in the specimen under investigation. The minimum energy required to excite the characteristic x-rays in specific shell is the binding energy in that shell. The major requirements of an excitation source are that it should be stable, efficient and sufficiently energetic to excite the elements of interest. Also, the count rates for each analyte line as well as the peak to background ratio must be considered.

There are two different excitation modes in EDXRF-KEVEX 0700, direct excitation mode and secondary target excitation mode. In the direct excitation mode, the sample is directly excited with the radiation generated by the x-ray tube. This mode offers the advantages of the high intensity source and a large distribution of x-ray energies for the efficient excitation of a wide range of elements. The main disadvantage of this mode is that the x-ray continuum is scattered from the sample and appears as a background in the x-ray energy spectrum. This mode is recommended for obtaining a qualitative survey of the elements present in a sample but it is not recommended for analysing low concentration elements. In the secondary target excitation mode, the output of the x-ray tube strikes a secondary target which then emits x-rays of energies that are characteristic of its material. The sample is thus excited by an essentially monoenergetic beam of x-ray photons. Secondary target excitation mode offers low background and excellent analysis flexibility such as the excitation energy which can be selected by choosing an appropriate secondary target. Also, in the secondary target excitation mode, the matrix effect procedures are effective and simple. On the other hand the main disadvantages of the secondary target excitation mode are that the intensity of the excitation beam is reduced due to a combination of geometric losses, secondary target, conversion efficiency and filter losses. In addition, the quantitative analysis using the fundamental parameter methods becomes more complicated in the secondary target excitation mode whereas the combination geometry becomes more complex than in the direct excitation mode. In the present work, the direct excitation mode has been used in all the experiments. Fig. 2.1 shows a schematic diagram of the EDXRF-KEVEX 0700 in the direct excitation mode.

#### 2.1 X-Ray Tube Spectra

A Coolidge tube was used in this work with a tungsten filament in a sealed glass tube evacuated to less than  $10^{-5}$  mm Hg. When the filament is heated by passing a current through it, it emits electrons. The emitted electrons are accelerated toward the target to produce x-rays.

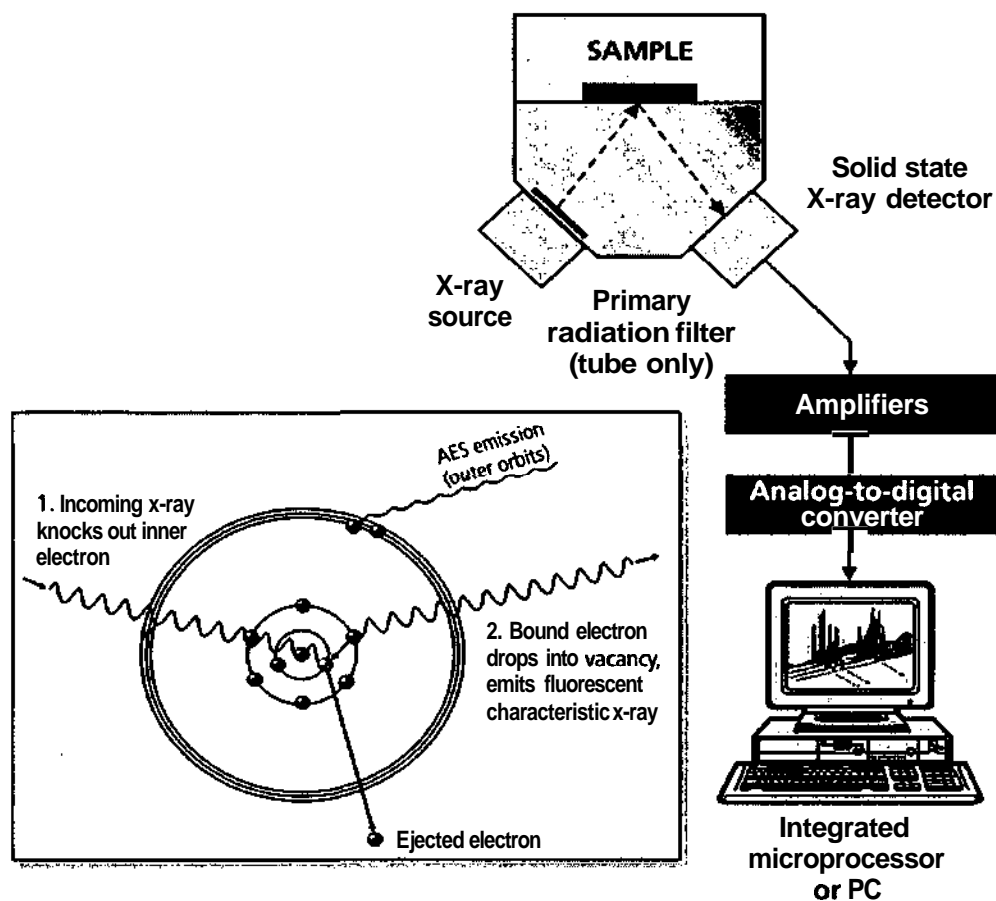


Fig. 2.1 A Schematic diagram of the EDXRF, direct excitation mode.

The x-ray tube in the present work has a grounded anode with side window, hermetically sealed, dielectric liquid filled head and shielded against radiation leakage. In addition, it is cooled by recycling liquid coolant through the copper rod. The anode material is Rhodium provided as standard, and the side window is Beryllium of thickness 0.0127 cm. The range of the target current is from 0 to 2 mA. The tube voltage is in the range from 0 to 60 kV and the maximum power dissipation at target is 120 W. The present x-ray tube is shielded by using a metal shielding in order to emit radiation of less than 0.5 mR/hr through sides and back of package at 1 inch from its surface. The filament emits electrons which are focused by a cup and accelerated by the high voltage between the filament assembly and the target, which represents the positive electrode, (anode). When high energy electrons strike the Rhodium target, x-rays are produced which pass through the Beryllium window. Less than 1% of the electron energy is converted into x-rays, the remainder is transformed into heat. Consequently, a spectrum of a continuous x-ray superposed with a few characteristic spectral lines of the target element is produced. The distribution of the x-ray tube spectra is essential in the x-ray fluorescence analysis using fundamental parameters and it depends on the target element and it differs from one target to another.

### 2.1.1 Comparison Between Theoretical and Experimental Continuous X-Ray Spectra

A comparison between theoretical and experimental continuous x-radiation was carried out at high voltage of 30 kV. The experimental x-ray tube spectra were measured directly at the defined conditions of the beam geometry in the present x-ray tube. The theoretical x-ray tube spectra are based on the mentioned derivation in chapter 1. For comparison between theoretical and experimental x-ray tube spectra the different conditions and parameters such as solid angle, detector efficiency, etc.. must be taken into account on the two approaches. That means that the

theoretical x-ray tube spectra were calculated for the same conditions of the experimental x-ray tube spectra. These conditions are,

- The energy of impinging electrons,  $E_0 = 30 \text{ keV}$
- The solid angle of the x-ray tube,  $\Omega = 0.0036674 \text{ sr}$
- The x-ray tube current  $I = 423 \times 10^{-9} \text{ mA}$
- The incidence angle of electrons on the target,  $\varphi = 45^\circ$
- The take off angle of tube x-rays from the target with regard to the plane surface  $\xi = 45^\circ$
- T is the measuring time.  $T = 1000 \text{ s}$

A comparison between experimental and theoretical x-ray tube spectra at 30 keV is shown in Fig. 2.2. The theoretical x-ray tube spectra is derived from the universal equations (equations 1.55 & 1.61, chapter 1) and the experimental x-ray tube spectra is from measurements with EPMA.

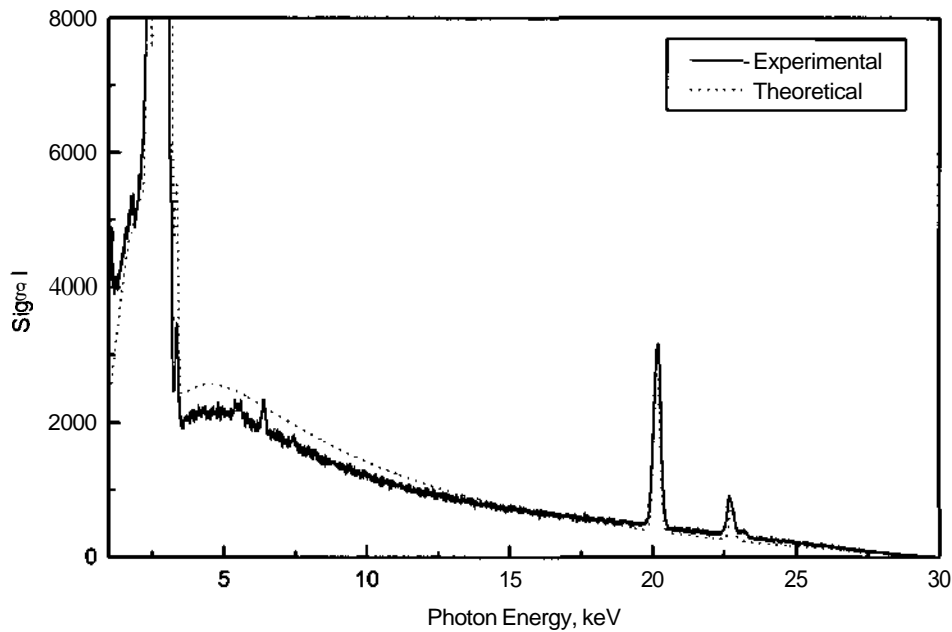


Fig. 2.2 Experimental and theoretical x-ray tube spectra at electron energy 30 keV, including Rh  $K_\alpha$  and  $K_\beta$ -radiation, ( $\varphi = 45^\circ$ ,  $\xi = 45^\circ$ )

The characteristic radiation ( $K_\alpha$  and  $K_\beta$ ) of the Rh target were measured and calculated theoretically (according to equation 1.61). The characteristic  $K_\alpha$ - and  $K_\beta$ -radiations of the Rh target as shown in Fig. 2.2 determined. The background radiations on right and left side of the K-lines were subtracted from the count rate of the K lines of the target according to the following equation,

$$I_{Chr} = \bar{I}_{Chr} - \left( \frac{B_R + B_L}{2} \right) \times N \quad (2.1)$$

where,  $I_{Chr}$  is the net count rate of the K-lines,  $\bar{I}_{Chr}$  count rate of the K-lines including the background,  $B_R$  is the background on the right hand side,  $B_L$  is the background on the left hand side,  $N$  is the number of channels in the K-lines range in the multichannel analyzer. Table 2.1

shows a comparison between the experimental and theoretical results. The comparison between theoretical and experimental characteristic radiation was performed at photon energy 30 keV at the same conditions as mentioned above. The mentioned analytical algorithms are used directly in the comparison of the continuous radiation as well as the characteristic radiation. According to table 2.1, the minimum difference between the experimental and the theoretical characteristic  $K_{\alpha}$  radiation is 13.84%. On the other hand the maximum difference between the experimental and the theoretical characteristic  $K_{\beta}$  radiation is 20.82%. Therefore, the measured x-ray spectra is still more convenient for the quantitative analysis using fundamental parameter methods.

Table 2.1 Comparison of characteristic radiations of Rh target  
(theoretical and experimental results)

	Rh-1( $\varphi = 45^{\circ}$ , $\epsilon = 45^{\circ}$ )	
	$K_{\alpha}$ , cps	$K_{\beta}$ , cps
Experimental	83514	17126
Theoretical	71956	13560
Differences	13.84%	20.82%

## 2.2 Solid Angle

In the normal case, when the incidence angle of the fluorescence radiation with regard to the specimen surface is  $90^{\circ}$ , the specimens were irradiated directly without extra sample holders. In this case, the solid angle  $\Omega$  is given by

$$\Omega = \left( \frac{\text{irradiated area}}{d^2} \right) = \frac{\pi \bar{r}^2}{\bar{d}^2} = \frac{\pi r^2}{d^2} = 0.004007133 \text{ sr} \quad (2.2)$$

where  $\bar{r}$  is the radius of the smallest aperture in the slider in front of the x-ray tube (the present slider has four apertures with different diameters 1.5, 2, 2.5 and 3 mm),  $r$  is the radius of irradiated area in the specimen ( $r = 1.642857$  mm),  $\bar{d}$  is the distance source to the circular aperture, ( $\bar{d} = 21$  mm),  $d$  is the distance source to the surface of the specimen, ( $d = 46$  mm). In this case, we assume that the x-rays from the tube are assumed as spot source. According to the instrument geometry, the incidence angle of the tube radiation, ( $\alpha$ ) is equal  $70^{\circ}$ . In this case the irradiated area appears as an ellipse with axes 3.3 mm and 9.6 mm. In special cases, a specific kind of sample holder (stop) has been used whereas the diameter of the specimen is smaller than the diameter of the original sample holder. Therefore, when the stop is in front of the specimen, the solid angle will change according to the diameter of the stop as well as the incidence angle of the tube radiation, ( $\alpha=70^{\circ}$ ) as shown in Fig. 2.3.

In the present work, three Al stops were prepared with three different diameters, 2, 5 and 10 mm. In each case, the solid angle is defined according to the irradiated area which will be restricted by the diameter of the stop. It is given by the following equation:

$$\Omega = \left( \frac{\text{irradiated area}}{d^2} \right) \times \sin(20) \quad (2.3)$$

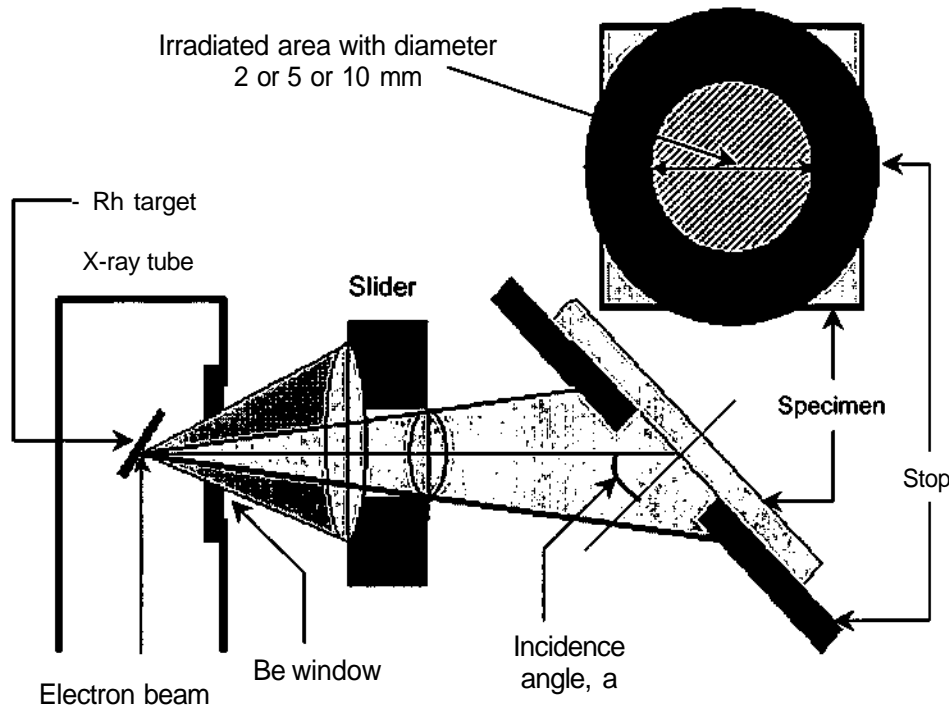


Fig. 2.3 Irradiated area with Al stop with diameter 5 mm and ellipse diameters 3.3 mm and 9.6 mm.

where the angle between the incident radiation and the surface of the specimen is  $20^\circ$ . In this case we have three different solid angles called  $\Omega_2$ ,  $\Omega_5$ ,  $\Omega_{10}$ . Fig. 2.3 shows a schematic diagram when the Al or Ti stop diameter is equal 2 or 5 or 10 mm and the ellipse axes will change according to the diameter of the stop. As mentioned before the irradiated area is not defined very well. If we consider that there is instead of a spot source an area bombarded by electrons resulting from a great number of spot sources, the kradiated area in this case will be larger than the value mentioned above whereas each spot makes a specific kradiated area. For this reasons, we assume that the kradiated area will be varied according to these number of spot sources.

Table 2.2 gives the solid angle in case of Al stop with diameter 2, 5 and 10 mm as well as the solid angle without stop ( $\Omega_{rel}$ ) by using pure copper specimen. In this case we assume that the kradiated ellipse will increase according to the increase of the slider diameter as shown in table 2.2. The solid angle values in table 2.2. must be normalized whereas the slider diameter does not change. The normalization of the solid angle,  $\bar{\Omega}$  is according to equation,

$$\bar{\Omega} = \Omega \times \left( \frac{\pi \times r^2}{\pi \times \bar{r}^2} \right) \quad (2.4)$$

where  $\Omega$  is the solid angle according to table 2.2,  $r$  is the diameter of the slider in front of the x-ray tube window,  $\bar{r}$  is the assumed diameter of the same slider. Table 2.3 shows the normalized solid angle which will be taken into account in the future applications. Fig. 2.4 shows the relation between the count rates of pure copper specimen, ( $K_\alpha$ -radiation) versus the different solid angles, ( $\Omega_2$ ,  $\Omega_5$ ,  $\Omega_{10}$  and  $\Omega_{rel}$ ). In this case the solid angle changes as the diameter of the Al stop changes. According to Fig. 2.4, as the solid angle increases the count rates of the copper K $\alpha$ -radiation increases too. This refers to the increase of the kradiated area on the specimen. Also, as

the diameter of the Al stop increases, the count rate of the different elements increase and consequently the correction factor becomes more significant.

Table 2.2. Solid angles without stop(Ref.) and with different diameters of Al stop

Slider Diam.	Ellipse Diameters	$\Omega_{2, sr}$	$\Omega_{5, sr}$	$\Omega_{10, sr}$	$\Omega_{ref, sr}$
1.5	3.3, 9.6	.0005078	.002667	.004007	.0040071
2	4.4, 12.81	.0005078	.003014	.007112	.0071238
2.5	5.48, 16.01	.0005078	.003174	.008858	.0111309
3	6.57, 19.21	.0005078	.003174	.010619	.0160285

Table 2.3. Normalised values of solid angles without stop(Ref.) and with different diameters of Al stop

	Count rate	Solid angle, sr			
		Ellipse 3.3&9.9	Ellipse 4.4&12.81	Ellipse 5.48&16.01	Ellipse 6.57&19.21
$\Omega_2$	148.4	0.0005078	0.0002856	0.0001828	0.0001269
$\Omega_5$	831.9	0.002667	0.001697	0.001143	0.000793
$\Omega_{10}$	2736	0.004007	0.004001	0.003189	0.002655
$\Omega_{ref}$	3997	0.0040071	0.0040071	0.0040071	0.0040071

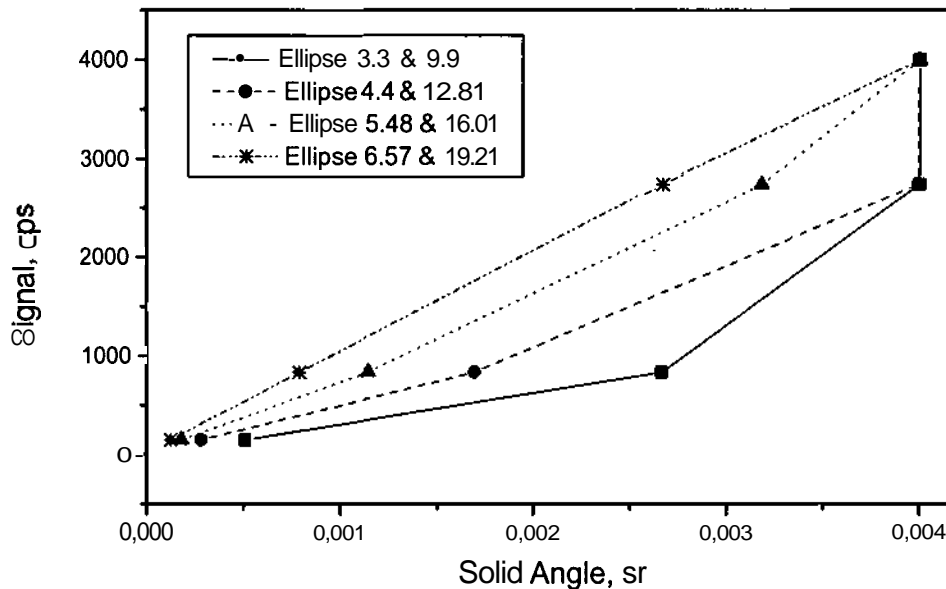


Fig. 2.4, Relation between the solid angle and the count rate of pure copper specimen



### 2.3 Correction Factor

According to the theoretical description in chapter 1, we can easily define the correction factor  $k_i$ . It is the ratio between the experimental count rate to the calculated count rate of the element  $i$  in the specimen. So the correction factor  $k_i$  can be defined according to the following equation

$$k_i = \frac{n_{ijk} \text{ (Measured)}}{n_{ijk} \text{ (Calculated)}} \quad (2.5)$$

The calculated count rate was calculated theoretically according to the previous description of the primary and secondary excitation equations. A value of  $k_i=1$  indicates perfect correlation of the calculated and measured count rate, whereas a value of  $k_i$  greater than or less than 1 indicates the correction factor has to be explained. As mentioned above, to obtain good results of the correction factor, all the different fundamental parameters must be well defined. According to the geometrical shape of some specimens, it is not possible to measure all of the specimens directly on the EDXRF-KEVEX 0700 because the area of some specimens is smaller than the sample holder area of the EDXRF-KEVEX 0700. Therefore, all of these specimens were measured with a specific holder of Ti and/or Al of specific diameter as mentioned above. A slider of diameter 1.5 mm was used in front of the x-ray tube. The main function of the x-ray slider is to reduce the x-ray intensity that reaches the specimen.

As given in table 2.3, there are four different solid angles in case of Al stop with diameter 5 mm. The correction factor was calculated by using these four different values of solid angle at 5 mm for a set of sixteen pure element specimens as shown in table 2.4. The correction factor calculation was estimated by using both the theoretical and the experimental x-ray tube spectra. Fig. 2.5 shows a relation between the correction factor and the atomic number at different solid angle. The correction factor increases as the axes of the irradiated ellipse increase. At irradiated ellipse 6.57 & 19.21 mm axes, the correction factor is approximately 0.1. This value is comparable with the correction factor without stop. There is a good agreement between the correction factor calculated by experimental and theoretical x-ray tube spectra at low and intermediate Z elements. A remarkable difference was observed at elements with  $Z>35$ .

Fig. 2.6 shows a comparison between the correction factors in both Al and Ti stop. According to Fig. 2.6, it was found that there is no difference between the two correction factors in both Al and Ti stop. Fig. 2.7 shows an example of the spectrum of pure Pd specimen with the spectrum of the Ti stop which is listed in table 2.5. The Ti stop spectrum was subtracted from the pure element spectra. The lower values of the correction factors in case of Al and Si refer to the lower detector efficiency in this range. It was found that there is no difference in the intensity of the pure elements in both Al and Ti stop.

Table 2.4 The Correction factor of pure element specimens using Al stop with diameter 5 mm (with different irradiation ellipse)

Element	Correction factor, Ellipse 3.3& 9.6		Correction factor, Ellipse 4.4& 12.81		Correction factor, Ellipse 5.4& 16.01		Correction factor, Ellipse 6.6& 19.21	
	Theo.	Exp.	Theo.	Exp.	Theo.	Exp.	Theo.	Exp.
AM3	,004	,003	,006	,005	,009	,007	,013	,010
Si-14	,006	,005	,009	,007	,015	,011	,021	,016
Sc-21	,016	,014	,025	,022	,037	,033	,053	,047
Ti-22	,017	,015	,026	,024	,039	,035	,057	,051
V-23	,017	,015	,026	,024	,039	,035	,056	,050
Cr-24	,016	,015	,026	,024	,038	,035	,055	,050
Mn-25	,017	,015	,027	,024	,039	,036	,057	,052
Fe-26	,017	,016	,027	,025	,040	,037	,058	,054
Co-27	,018	,017	,028	,026	,042	,039	,060	,057
Ni-28	,017	,017	,027	,026	,040	,039	,058	,056
Cu-29	,018	,017	,028	,027	,041	,039	,059	,057
Zn-30	,017	,017	,027	,027	,040	,039	,058	,057
Ge-32	,017	,018	,027	,028	,039	,041	,057	,059
Mo-42	,015	,019	,024	,030	,035	,045	,050	,065
Pd-46	,014	,018	,021	,028	,032	,041	,046	,059
Ag-47	,016	,019	,025	,030	,036	,045	,053	,065

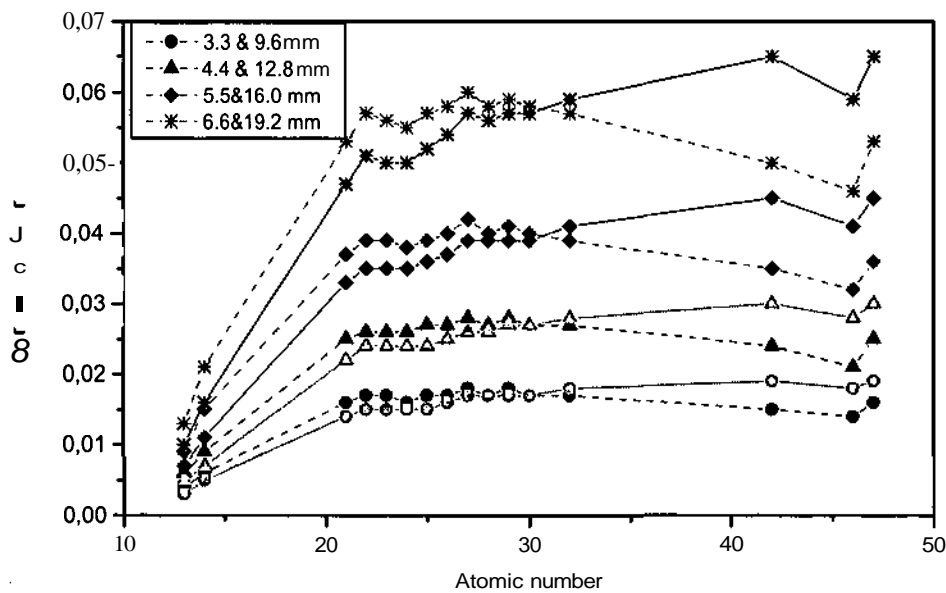


Fig. 2.5 Relation between the atomic number of and the correction factor at Al stop with 5 mm diameter (with different irradiated areas), \_\_\_\_\_ experimental spectra, \_\_\_\_\_ theoretical spectral

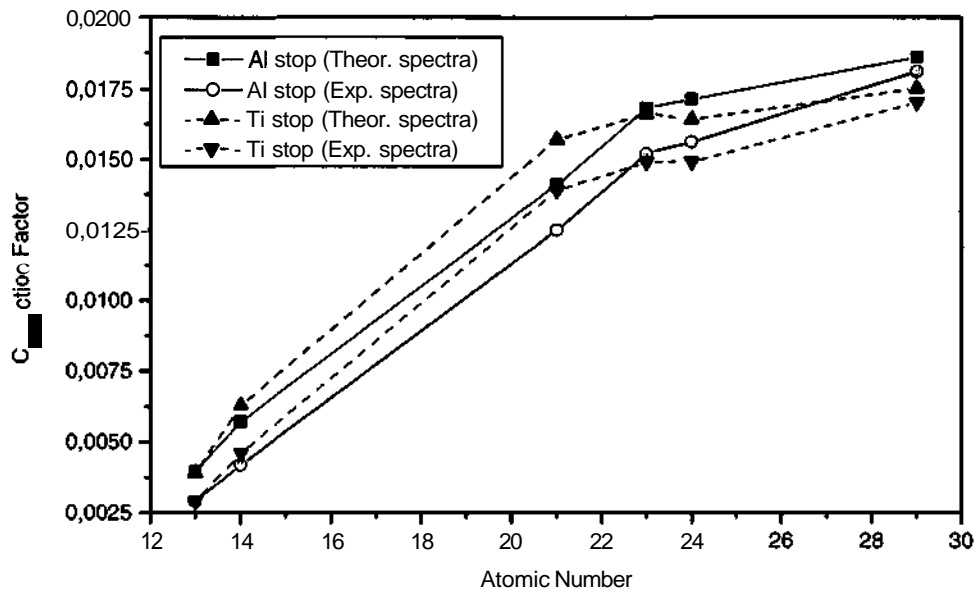


Fig. 2.6 The relation between the correction factor and atomic number in case of Al and Ti stop.

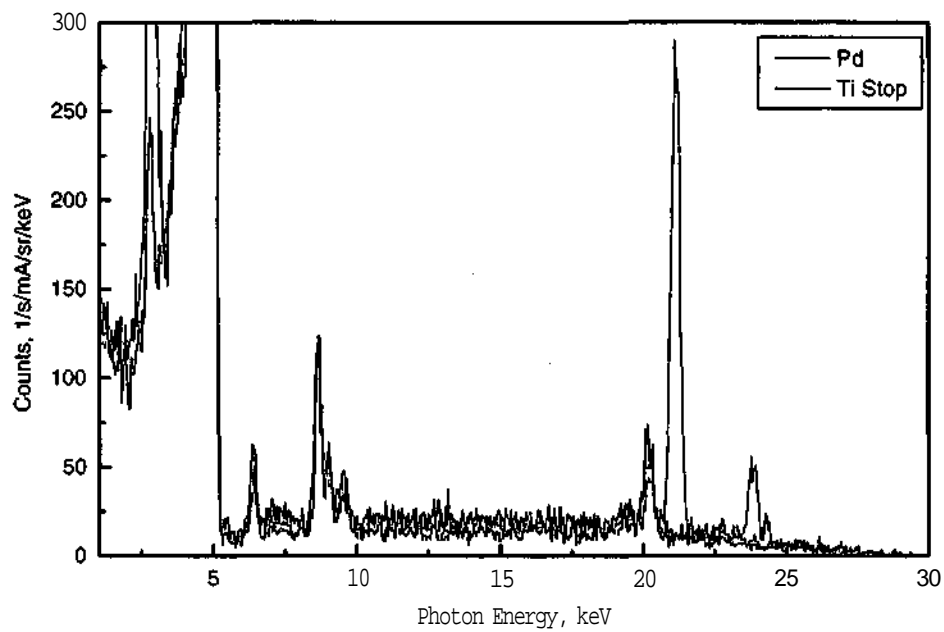


Fig. 2.7 The spectrum of Pd with Ti stop at 30 kV, 0.01 mA, incidence angle = 70°, take-off angle = 45°.

## 2.4 Quantitative Analysis of Binary Alloys Using Fundamental Parameter Approach

In the present work, three different types of binary alloys have been investigated. These are Cu-Zn, Au-Ni and Al-Cu binary alloys. The calculated intensity of each elements in these binary alloys basically depends on the calculated primary and secondary fluorescence intensities given in equations 1.85 and 1.94, (See chapter 1). In the present quantitative analysis processing, fluorescence yields  $\omega_{ij}$  have been taken from Hubbell[25], transition probabilities  $p_{ij}$  from Johnson and White[29] and the photoelectric cross sections as well as the scattering cross sections from McMaster[75].

### 2.4.1 Cu-Zn Binary Alloy

Fig. 2.8 shows the theoretical fluorescent x-ray intensities of copper and zinc versus the copper concentration in weight fractions. According to theoretical calculations of the calibration curves of Cu and Zn given in Fig. 2.8, the copper fluorescent x-ray intensity is affected by the Zinc x-ray intensity, whereas the Zinc fluorescent x-ray intensities are approximately not affected. In the present quantitative calculations, the EDXRF-KEVEX 0700 has been used at the following operating conditions

- The incidence angle of electrons with regard to the target surface is  $70^\circ$ .
- The take off angle of x-rays with regard to the target is  $45^\circ$ .
- The tube current is 0.01 mA
- X-ray tube voltage is 20 kV
- The energy interval is 0.01 keV
- The solid angle of the x-ray detection is 0.0040071 sr

According to equations 1.85 and 1.94, the final concentration of Cu and Zn have been calculated using the iteration procedures. The final concentrations of Cu and Zn are listed in Table 2.5

Table 2.5 Results of the concentrations of Cu-Zn binary alloy

<i>Element</i>	<i>Concentration, Weight fraction</i>
Cu	59,7124
Zn	40,2876

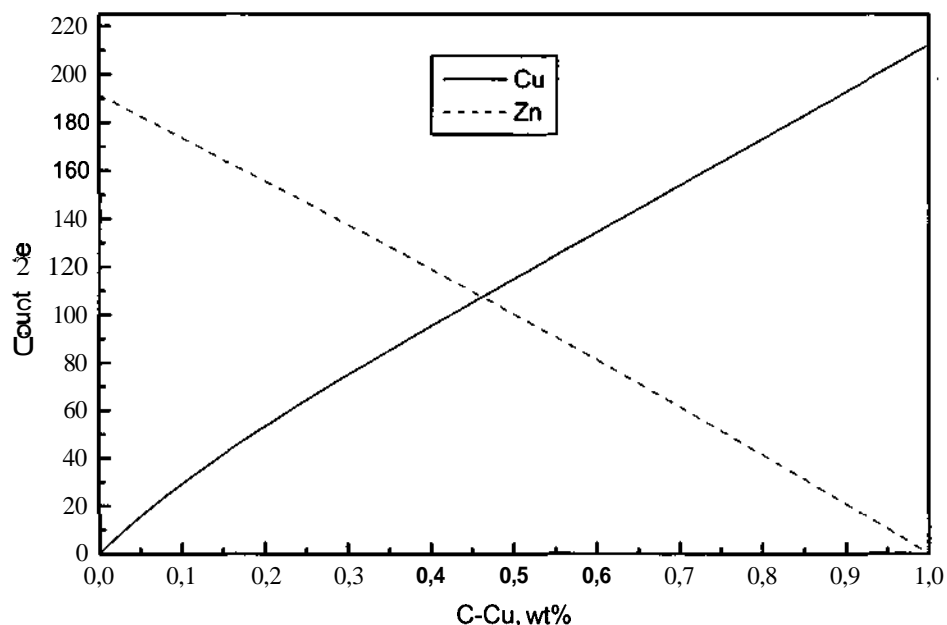


Fig. 2.8 The fluorescent x-ray intensities of copper and zinc versus the weight fraction of copper.

#### 2.4.2 Au-Ni Binary Alloys

In the case of Au-Ni binary alloys, a series of nine samples with different concentrations of Au and Ni are taken into consideration. The concentration of these samples are well known as given from the supplier. Fig. 2.9 shows the fluorescent x-ray intensities of gold and nickel versus the concentration of gold in weight fractions. According to Fig. 2.9, the theoretical calculations of the calibration curves of Au and Ni show that the nickel fluorescent x-ray intensity is affected by the gold x-ray intensity, whereas the gold fluorescent x-ray intensities are approximately not affected. The EDXRF-KEVEX 0700 has been used at the same operating conditions mentioned in the Cu-Zn binary alloy and the final concentrations of Au and Ni have been calculated. The final concentrations of Au and Ni are listed in table 2.6. A comparison study between x-ray fluorescence spectrometry software (XRF, Version 2.1, S. R. Afshar[124]), the present algorithm and EPMA as well as the concentration from the supplier was carried out as shown in table 2.6. Fig. 2.10 shows an example of the Au-Ni spectrum. According to the results in table 2.6, it can be said that there is a reasonable agreement between the three different methods.

Table 2.6 shows the comparison of results

S.N	Present work		XRF software		EPMA		Supplier	
	<i>Au</i>	<i>Ni</i>	<i>Au</i>	<i>Ni</i>	<i>Au</i>	<i>Ni</i>	<i>Au</i>	<i>Ni</i>
1	91,39	08,61	90,60	9,40	90,85	09,15	90	10
2	72,76	27,23	71,10	29,90	71,50	28,50	70	30
3	22,08	77,90	21,40	78,60	24,53	75,47	20	80
4	11,90	88,10	11,50	88,50	13,40	86,60	10	90
5	69,67	30,30	68,00	32,00	62,27	37,73	60	40
6	83,20	16,70	82,00	18,00	80,79	19,21	80	20
7	44,70	55,29	42,80	57,20	43,94	56,06	40	60
8	54,30	45,69	52,70	47,30	55,38	44,62	50	50
9	33,90	66,01	32,90	67,10	34,85	65,15	30	70

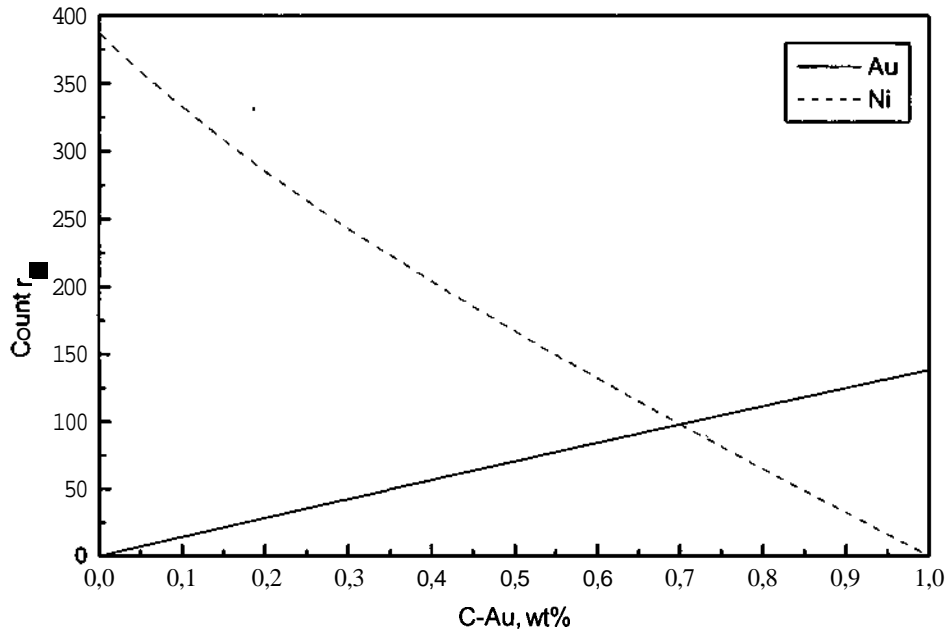


Fig. 2.9 The fluorescent x-ray intensities of gold and nickel versus the weight fraction of gold

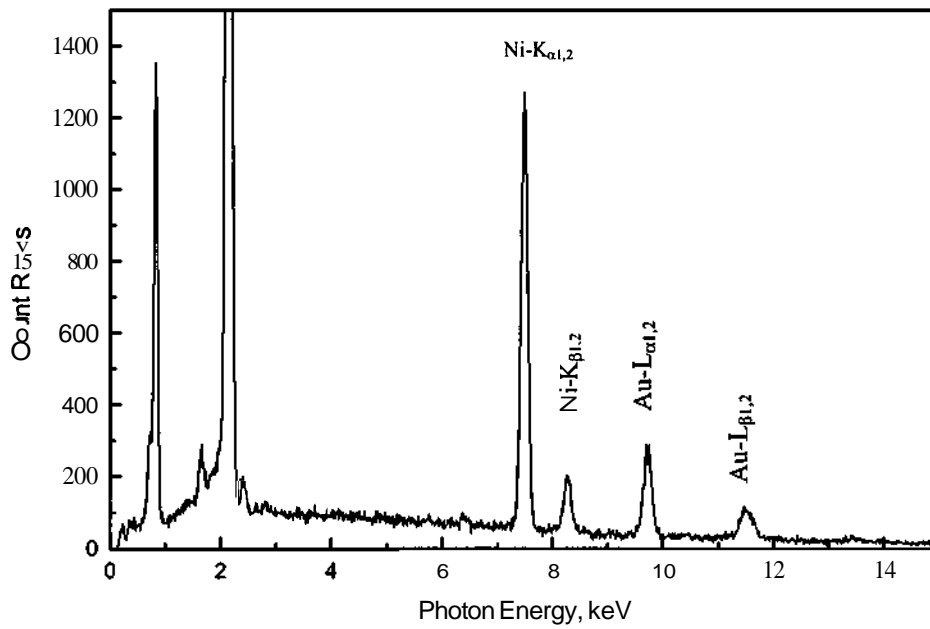


Fig. 2.10 Example of the spectrum form EPMA.

### 2.4.3 Al-Cu Binary Alloy

The detector efficiency of the EDXRF-KEVEX 0700 is very poor at the lower photon energy range, therefore, some troubles arise in the measurements of the Aluminum  $K_{\alpha}$ -radiation which lies at 1.486 keV. To overcome this problem, Al and Cu pure elements as well as the Al-Cu alloy under investigation were prepared. Afterwards, all the specimens were irradiated directly using the main sample holder of EDXRF-KEVEX 0700 without any interference with the characteristic radiations from the additional stop holder. Therefore, the solid angle equals 0.004007133 sr. Figs. 2.11-2.13 show the characteristic radiations of these samples. According to Figs. 2.11-2.13, the characteristic radiations of these pure elements were measured and the correction factors were calculated. Table 2.7. gives the count rates of these pure elements as well as the correction factors. If the measured count rates equal to the calculated count rates, the correction factor will be one. In this case, the count rate of the pure elements can be calculated according to equations 1.85 and 1.94. According to table 2.7, the deviation of the correction factor comes from the imprecise definition of the used different parameters such as solid angle of both x-ray irradiated area and detector, the thickness of Be-window of both x-ray tube and detector, the ice on the Si-crystal detector due to the using of liquid nitrogen and the contamination on x-ray tube target, tube window, and detector window.

Table 2.7 Correction factor of the pure elements

Element	$K_{\alpha}$ -radiation	Measured Count rates	Correction factor	Calculated count rates
Al	1.486	50.71	0.01064	4764.85
Cu	8.04	1313.05	0.06276	20920.87

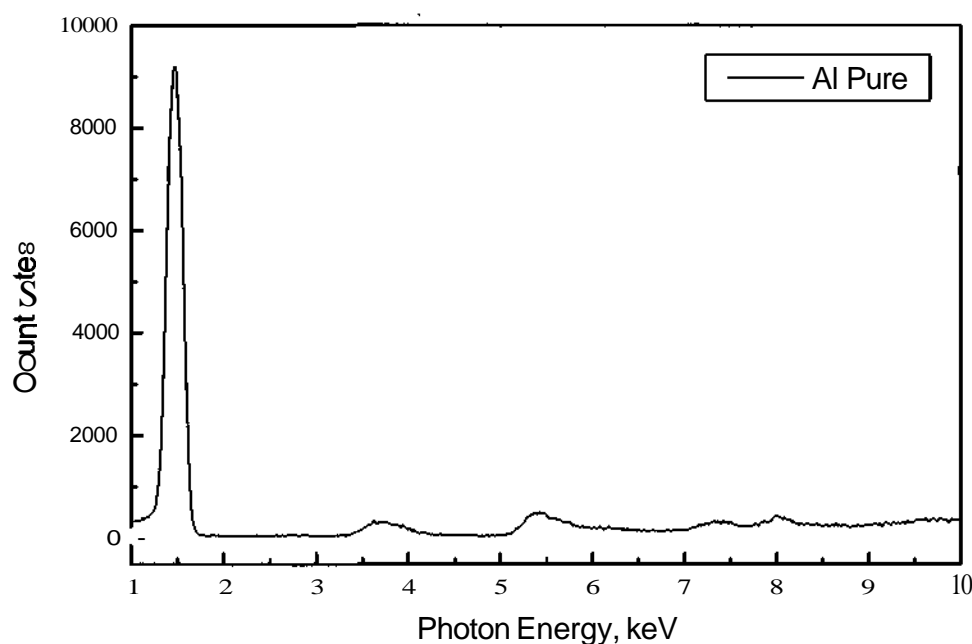


Fig. 2.11  $K_{\alpha}$ -radiation of pure aluminium, applied voltage =20 kV, current = 0.01 mA, vacuum < 1 mbar, measuring time =1800 s.

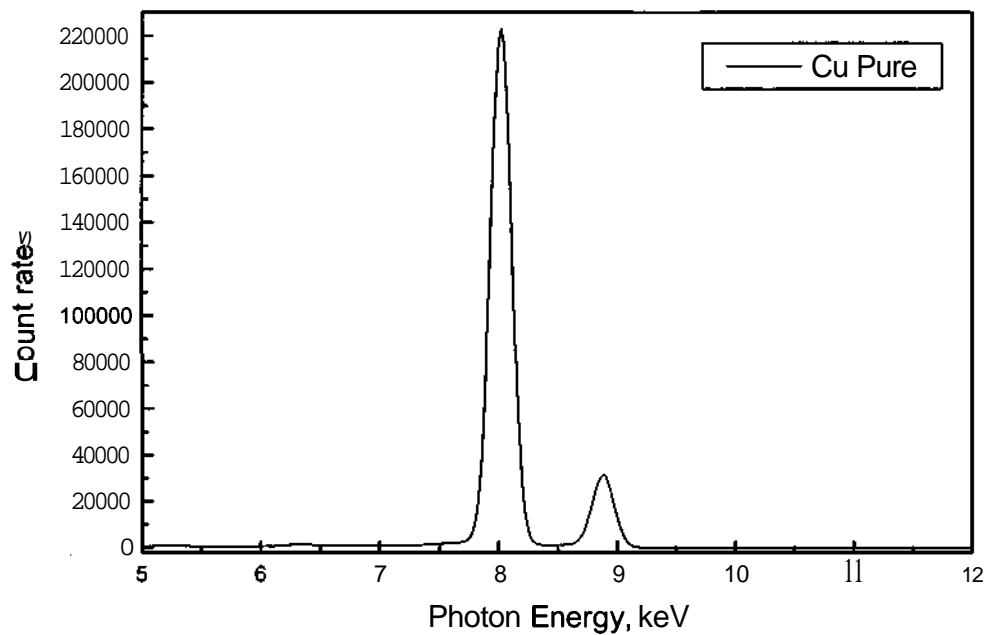


Fig. 2.12  $K_{\alpha}$  and  $K_{\beta}$  radiation of pure copper, applied voltage =20 kV, current=0.01 mA, vacuum < 1 mbar, measuring time =1800 s.

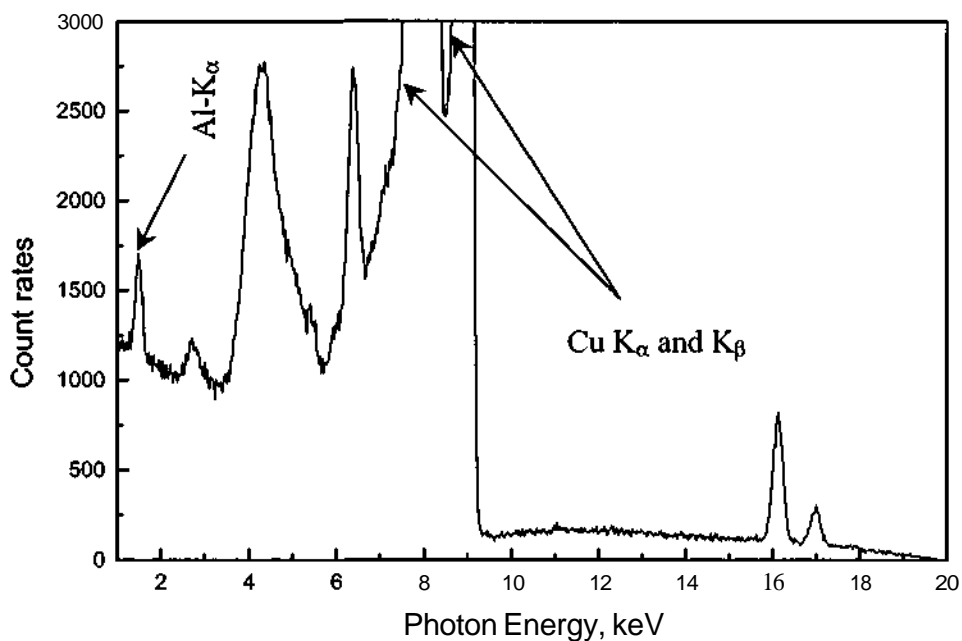


Fig. 2.13. Al-Cu alloy spectra by using EDXRF, voltage = 20 kV, current = 0.01 mA, vacuum < 1 mbar, measuring time = 1hour



### 2.4.3.1 Quantitative Analysis Results

Quantitative analysis using the present fundamental parameters procedure was carried out for Al-Cu alloy by two independent techniques, the EPMA and the EDXRF. As mentioned above, the sensitivity of EDXRF-KEVEX 0700 is very low in the low Z elements and lower photon energy as well. So, the aluminum signal appears very weak and can not be distinguish from the background radiation. To overcome this problem, the measuring time was increased to 1 hour and the EDXRF-KEVEX 0700 instrument was operated under vacuum less than 1 mbar. In this case, the aluminum signal can be distinguished from the background radiation as shown in Fig. 2.13. Quantitative analysis by using measured count rates directly gives wrong concentrations as shown in table 2.8. Therefore, the count rates of aluminium and copper were recalculated according to the following equations,

$$(Al - \text{count rates})_{\text{Calculated}} = \frac{(Al - \text{count rates})_{\text{Measured}}}{(K - \text{factor})_{Al - \text{pure}}} = \frac{1.363}{0.01064} = 128.1 \quad (2.6)$$

$$(Cu - \text{count rates})_{\text{Calculated}} = \frac{(Al - \text{count rates})_{\text{Measured}}}{(K - \text{factor})_{Cu - \text{pure}}} = \frac{1320.16}{0.06276} = 21035.12 \quad (2.7)$$

According to these count rates of aluminium and copper, the concentration of aluminium and copper has been computed as shown in table 2.9 by using equations 1.85 and 1.94.

Table 2.8 Quantitative analysis of Al-Cu alloy by using EDXRFS, KEVEX 0700, (wrong results).

Element	K <sub>α</sub> -radiation	Measured Count rates	Correction factor	Concentration, Wt%
Al	1.486	1.363	0.074	1.44
Cu	8.04	1320.16	0.074	98.56

Table 2.9 Quantitative analysis of Al-Cu alloy by using EDXRFS, KEVEX 0700, (correct results).

Element	K <sub>α</sub> -radiation	Calculated count rates	Normalized correction factor	Concentration, Wt%
Al	1.486	128.10	1.2	7.98
Cu	8.04	21035.12	1.2	92.02

Table 2.10 Comparison between the Quantitative analysis of Al-Cu alloy by using XRFA and EPMA

Element	EDXRFS		EPMA	
	Intensity, calculated	Concentration, wt%	Intensity	Concentration, wt%
Al	128.10	7.98	15.39	8.33
Cu	21035.12	92.02	298.69	91.67

On the other hand the calculated count rates shown in table 2.9 give the right concentrations. According to table 2.9, the correction factors of the Al and Cu in Al-Cu alloy are greater than 1. This is referred to the poor statistics of the aluminium signal as shown in Fig.

2.13. Fig. 2.14 shows the complete  $K_{\alpha}$ - and  $K_{\beta}$ -radiations of the Cu signal with a different scale. In this case the  $K_{\alpha}$ -radiation of aluminium disappears. The same quantitative analysis was performed by another independent technique which is EMPA. The EPMA quantitative analysis was carried out without standard material and it is worked under vacuum. At low photon energy, the detector efficiency of EPMA is more effective than the detector efficiency of the EDXRFS-KEVEX 0700, therefore,  $K_{\alpha}$ -radiation of aluminium can be measured easily in the EPMA. Table 2.10 shows a comparison between the quantitative analysis by using the two independent techniques. According to the results from table 2.10, there is a good agreement between the two techniques.

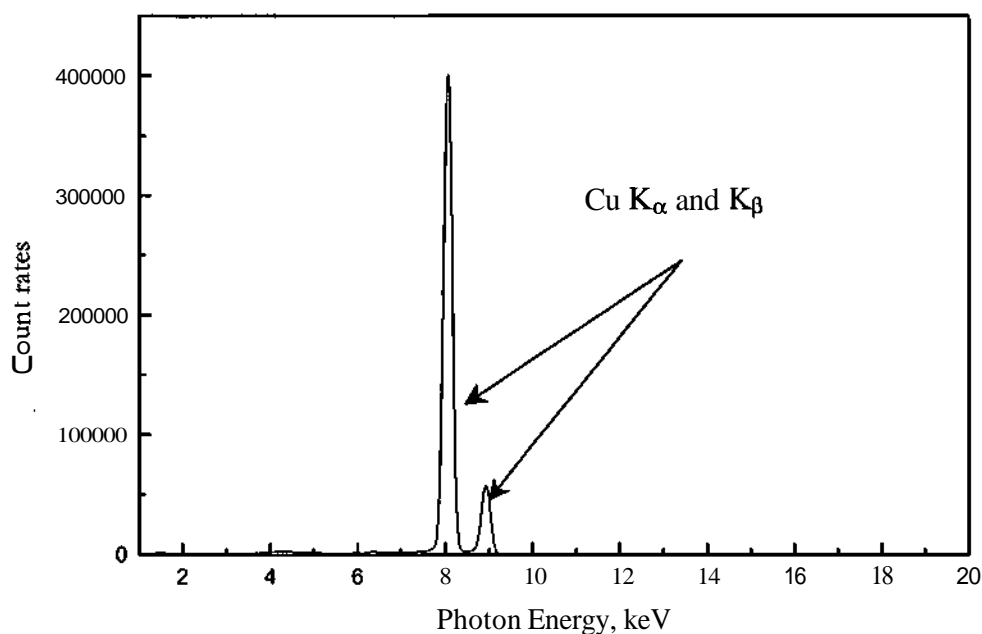


Fig. 2.14 Al-Cu alloy spectra by using EDXRFS, voltage = 20 kV, current = 0.01 mA, vacuum < 1 mbar, measuring time = 1 hour, (different scale).

## 2.5 The Effect of X-Ray Tube Voltage Variation on the Results of Quantitative Analysis of a Ternary Alloy Cu-Zn-Pb

In the present work, a Rh target was used. At a low x-ray tube voltage, there occurs no excitation of characteristic Rh K-radiation. As the tube voltage is increased, more and more of the target spectra is effective and the Rh fluorescence intensity rises rapidly. Generally, the tube should be operated at 3 to 10 times the voltage corresponding to E edge of the element in the target. If the x-ray tube voltage of the target is greater than the ionization potential for Rh K-shell, Rh K lines will be generated.

The continuous spectra distribution as well as the characteristic spectra of the target have a great influence on the characteristic fluorescence intensity. So, the spectral distribution as well as the characteristic spectra of the target are important whereas it determines how well the characteristic radiation will be excited in the specimen. The x-ray spectrum of the x-ray tubes depends on several parameters such as:

- The target material, the target element must have suitable thermal and mechanical properties. Tungsten is the most common target material. It has a very high melting point and reasonable thermal conductivity and is of high atomic number, ( $Z=74$ ). At the same time the W target causes some problems like the direct interference of W L lines with the characteristic K or L

lines of various elements in the specimen. Many different target materials were used such as Pt, Mo, Ag, Cu, Fe, Cr and Rh targets. In the present work, Rh target was used.

- Beryllium window thickness, the tube window thickness is important especially for exciting low atomic number elements. For example, sulfur is excited about 250 times more effectively by a 0.0254 cm Be window tube than by the Be thickness 0.1016 cm. This is according to the absorption of the effective portion of the primary spectrum by Be. In the present work, the thickness of Be is equal 0.005 0.0127 cm.
- The focal spot, when the focal spot is off center, closer to the window, the x-ray intensity is increased.
- The incidence angle of electrons onto the anode.
- The photons take-off angle from the anode.
- The operating voltage.
- The contamination and impurities of the anode and of the window material.

There is no x-ray tube which provides an optimum for all analytical purposes, but each kind of x-ray tube is suitable for a special sample according to the elements of interest.

For the quantitative analysis, an accurate data must be obtained. The conversion of the intensity to concentration is performed by fundamental parameter method using three main steps:

- The preparation of a specimen from the sample submitted for analysis
- The excitation of a suitable emission line from each element to be analyzed and the measurement of its intensity.
- The conversion of the measured intensity into elemental concentration by fundamental parameter method.

According to the previous theoretical descriptions, (chapter 1), the calculated counting intensity of the primary and secondary beam of x-ray photons is given by equations 1.85 and 1.94. In the present work, a quantitative analysis of a ternary alloy, ( Cu-Zn-Pb) was carried out by employing fundamental parameters approach. For this purpose the mentioned equations of the primary and secondary excitation were used. The initial count rates of Cu, Zn and Pb were measured from EDXRFS-KEVEX 0700 at the following operating conditions

- The incidence angle of electrons with regard to the target surface is  $70^\circ$ .
- The take off angle of x-ray with regard to the target is  $45^\circ$ .
- The tube current is 0.01 mA
- X-ray tube voltage is variable from 20 kV-30 kV
- The energy interval is 0.01 keV
- The solid angle of the x-ray detection is 0.0040071 sr.

The count rate of the three elements was measured at different x-ray tube voltages from 20 to 30 kV. It can be observed that, the count rate of the three elements is increased as x-ray voltage increases as shown in Fig. 2.15. The concentration of the three elements was calculated as shown in Table 2.11. It can be observed that the concentration of copper is varies from 57.14% to 57.92% as shown in Fig. 2.16, Zn is varies between 39.19% to 39.55% as shown in Fig. 2.17 and Pb is between 2.63% to 3.5% as shown in Fig. 2.18.

Table 2.11 the concentration of the ternary alloys at different x-ray tube voltages

Voltage, kV	Count rate, cpm			Concentration, %		
	Cu	Zn	Pb	Cu	Zn	Pb
20	835.1	536.2	6.55	57.14	39.36	3.5
21	960.8	619.1	7.30	57.67	39.19	2.13
22	1084	716.3	9.45	57.27	39.42	3.31
23	1219	812.9	10.08	57.52	39.49	2.98
24	1358	910.0	11.08	57.77	39.42	2.81
25	1494	1005.0	12.87	57.91	39.26	2.83
26	1649	1129.0	14.27	57.76	39.51	2.73
27	1818	1256.0	15.83	57.81	39.55	2.64
28	2007	1394.0	18.13	57.87	39.47	2.65
29	2175	1517.0	20.68	57.92	39.36	2.71
30	2365	1669.0	22.38	57.86	39.52	2.63

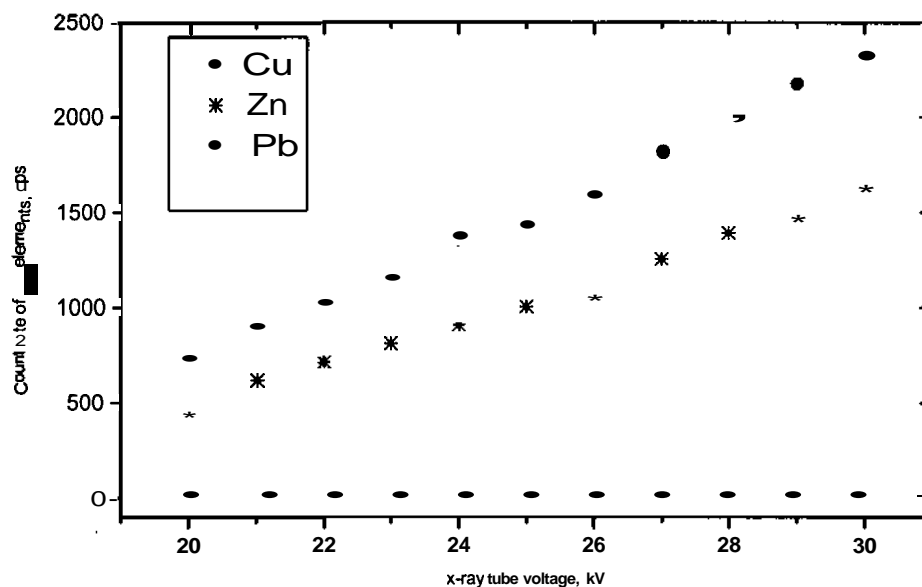


Fig. 2.15 Relation between count rate of the elements and x-ray tube voltage.

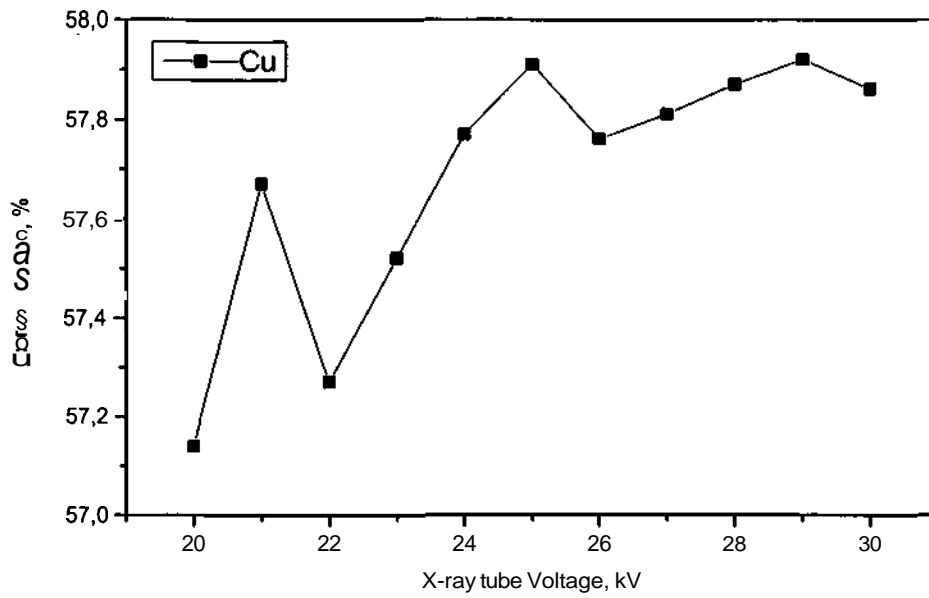


Fig. 2.16 Relation between the Cu-concentration and the x-ray tube voltage

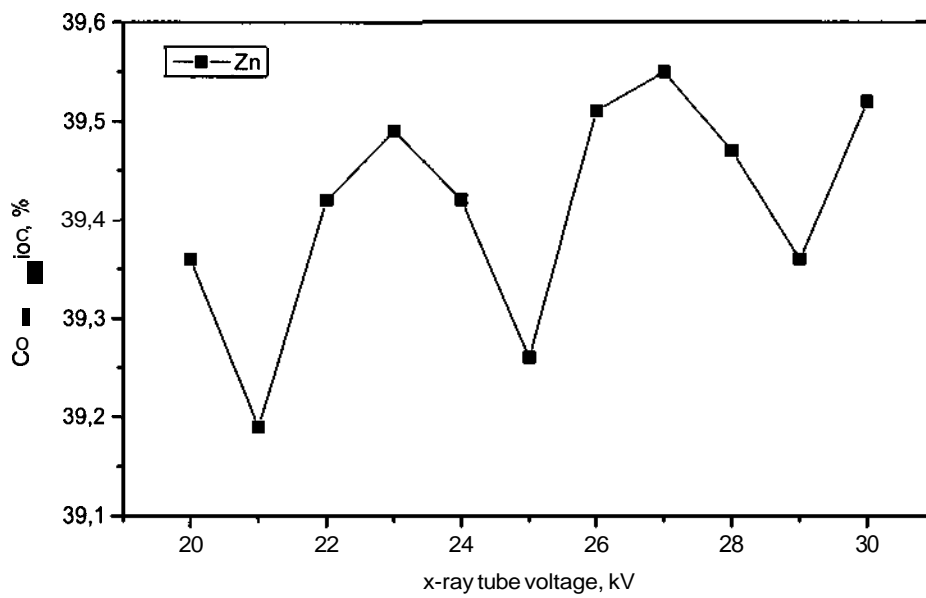


Fig. 2.17 Relation between the Zn-concentration and x-ray tube voltage.

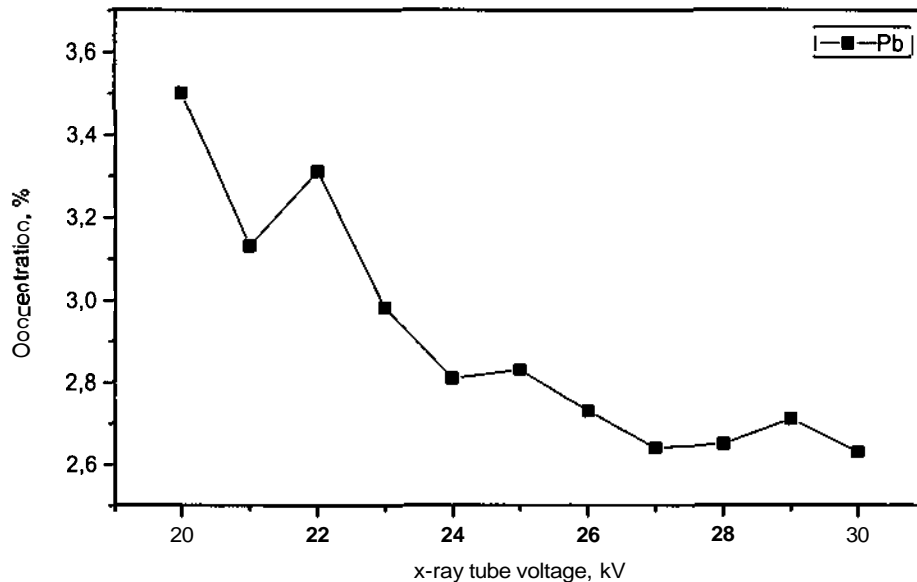


Fig. 2.18 Relation between the Pb-concentration and x-ray tube voltage.

## 2.6 Cu-Zn-Pb Quantitative Analysis Using Theoretical and Experimental X-ray Spectra

According to the previous descriptions, the equations of primary and secondary excitation, quantitative analysis of ternary alloys, (Cu-Zn-Pb) was carried out employing fundamental parameters approach.

In the quantitative analysis using experimental x-ray spectra, the values of the x-ray tube spectra were experimentally measured and stored in a data file. On the other side, in the theoretical quantitative analysis, the x-ray tube spectra were calculated according to the previous theoretical descriptions of the x-ray tube spectra given in chapter 1 and stored also in a data file. Both experimental and theoretical x-ray tube spectra were re-evaluated at the same optimal conditions, such as the detector efficiency, incidence and take off angles, current....etc.

The count rate of the elements in the ternary alloys was measured by EDXRFS-KEVEX 0700, at the following operating conditions,

- The incidence angle of electrons with regard to the target surface is  $70^\circ$ .
- The take off angle of x-ray with regard to the target is  $45^\circ$ .
- The tube current is 0.01 mA
- X-ray tube voltage is 30 kV
- The energy interval is 0.01 keV
- The solid angle of the x-ray detection is 0.0040071 sr.

The flow chart mentioned below describes the procedures of the calculations of the comparisons between theoretical and experimental quantitative analysis of ternary alloy. According to Table.2.12 there is a good agreement between the quantitative analysis of the brass using the theoretical and experimental x-ray spectra. This means the theoretical evaluation

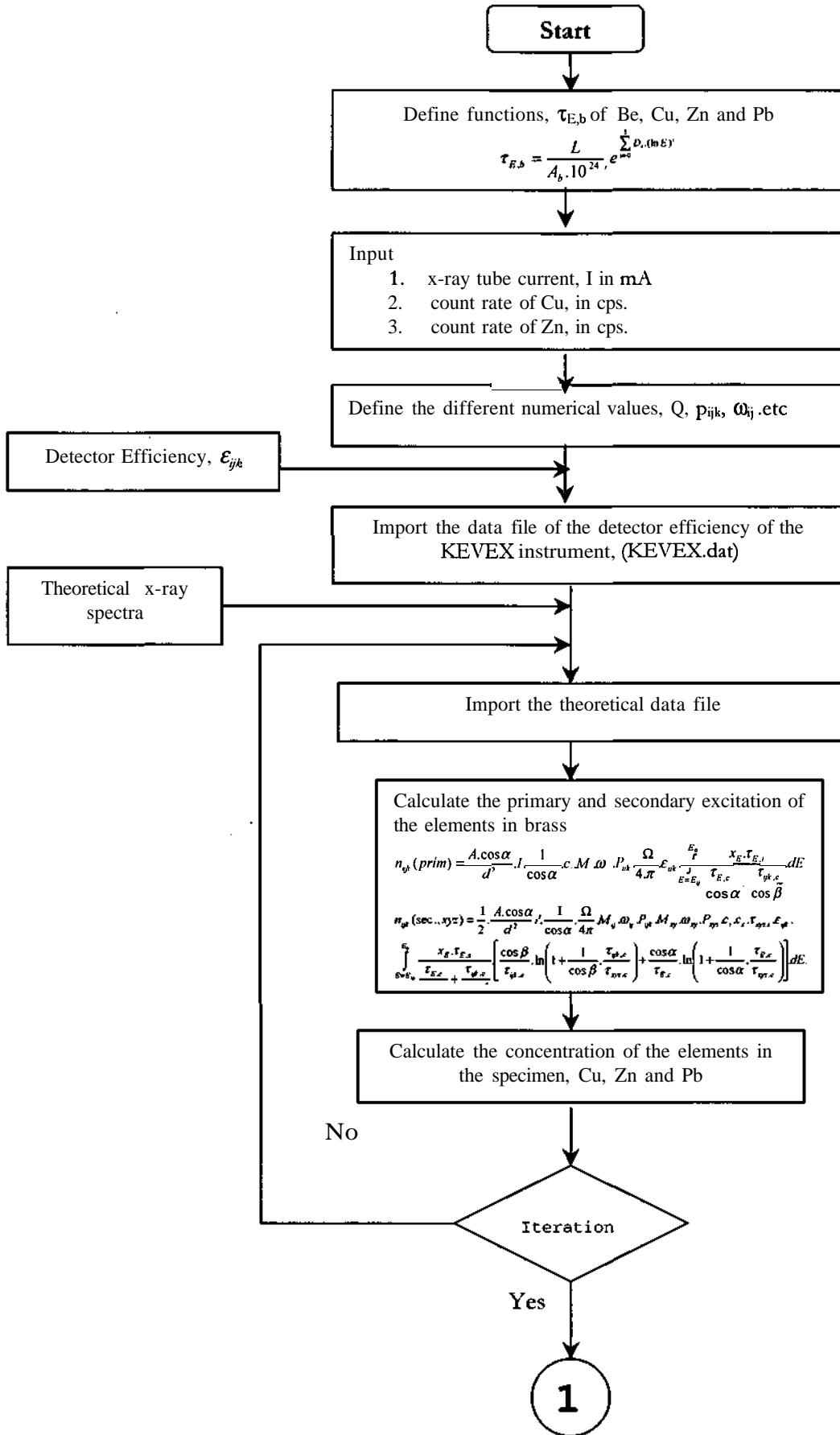
analysis approach is a powerful method. Table 2.13 gives the different k-factors in the quantitative analysis of the brass.

Table 2.12 comparison between computed quantitative analysis of ternary alloy

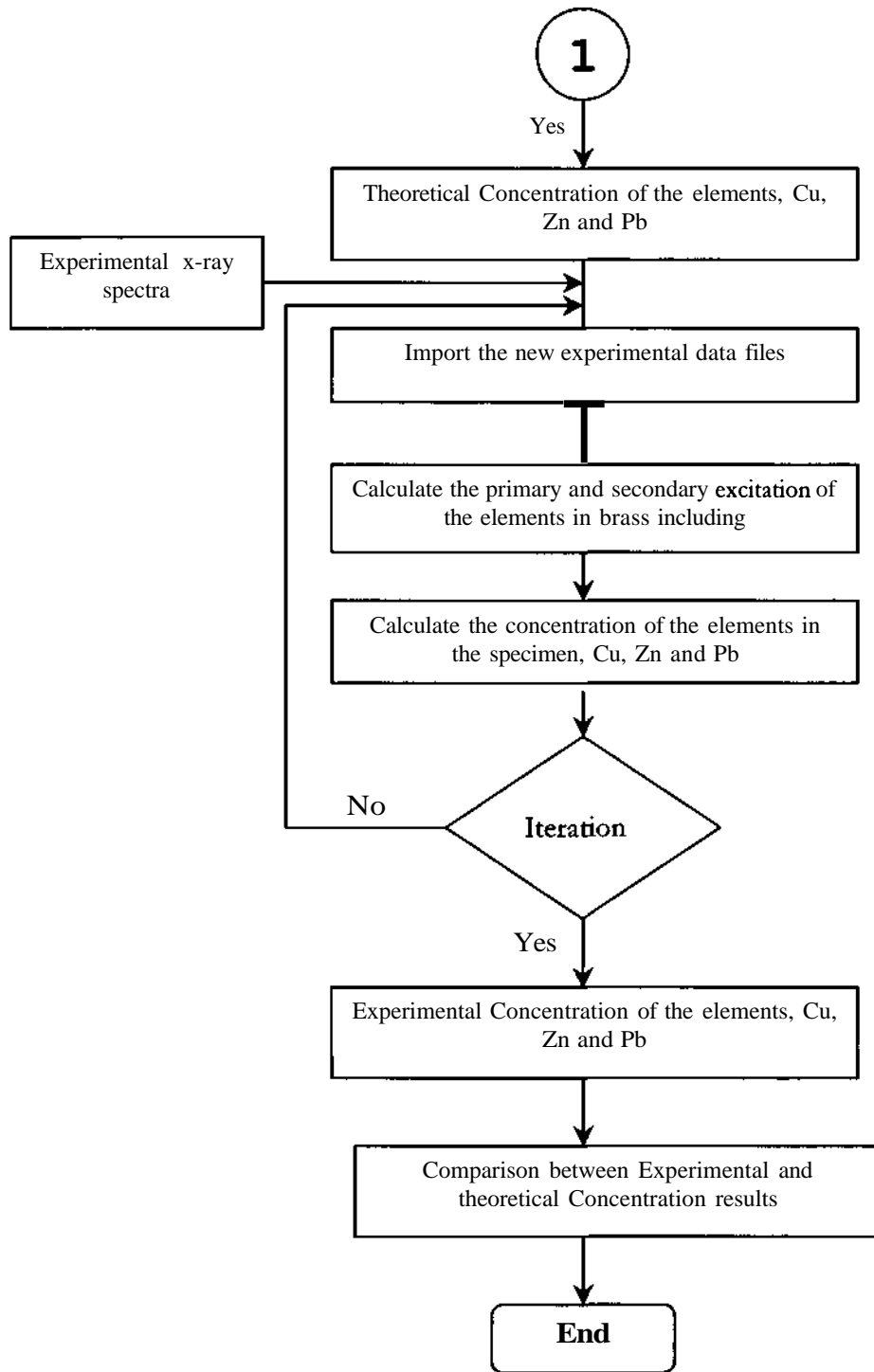
Elements	Count rate,	Computed Concentration (Love & Scott), Wt%	Computed Concentration, (Exp. Data file), Wt%
<b>Cu</b>	<b>2365</b>	<b>58.53</b>	<b>57.78</b>
<b>Zn</b>	<b>1669</b>	<b>38.86</b>	<b>39.38</b>
<b>Pb</b>	<b>22.38</b>	<b>2.61</b>	<b>2.84</b>

Table 2.13 comparison between The computed K-factor

Elements	Computed K-factor (Love & Scott)	Computed K- factor (Exp. Data file)
Cu	,088	,086
Zn	,088	,086
Pb	,088	,086







Flow chart 1. Quantitative analysis

## CHAPTER 3

# UNCERTAINTIES IN THE DATABASES OF X-RAY CROSS SECTIONS

The databases of the x-ray cross sections are required in the theoretical calculations of x-ray tube spectra, the detector efficiency and the fundamental parameter approach.

One of the main reasons for the errors in quantitative analysis by fundamental parameter methods comes from the uncertainties of fundamental parameter values. The main effective parameters are the values of the total photoelectric cross sections, the position of the absorption edges and the related jump ratio of each edge. For this work, most of the published experimental and theoretical databases for x-ray cross sections were studied, corrected, completed and re-evaluated. Numerous errors and exceptions were found in some of these databases and all of these errors and missing data were corrected. These corrections improve the quality of the quantitative analysis by fundamental parameter methods.

### 3.1 The Experimental Database

The National Institute of Standards and Technology (NIST) and the Photon and Charged Particles Data Center (PCPDC) reviewed[96] the database of the experimental x-ray absorption in the photon energy range from 10 eV to 13.5 GeV. The database was extracted from the accumulated work in the period from 1907 to 1986 and was converted to a machine-readable form.

Saloman[57] presented this collection of the experimental data of elements from hydrogen to uranium in the energy range from 0.1 to 100 keV. The collection included approximately 20000 data points abstracted from 512 independent literature sources, unpublished reports and private communication. There are about 2500 data points for energies 0.1-1 keV, 5300 data points for energies 1-10 keV, and 5600 data points for energies 10-100 keV. They compared experimental data of x-ray mass absorption coefficients to theoretical values calculated by using the relativistic Hartree-Slater model[58] as well as the semiempirical data of Henke[59], which cover the energy range 0.03-10 keV. In the photon energy range 0.1-1 keV, Saloman[57] found that the semiempirical database of Henke[59] are in reasonable agreement with the experimental data, however good experimental data are lacking for many elements. Also, in the photon energy range 1-10 keV the semiempirical values of Henke[59] and the theoretical values of the relativistic Hartree-Slater model[58] are in a good agreement with the experimental data particularly for elements with atomic number less than 55. Above  $Z=55$ , there are 10%-20% differences between theoretical values of the relativistic Hartree-Slater model[58] and the semiempirical values of Henke[59]. The comparison for the range 10-100 keV generally shows excellent agreement between the theoretical values of the relativistic Hartree-Slater model[58] and the experimental data for atomic numbers higher than 3 (except Si where 5%-10% discrepancies above 30 keV exist). Saloman[57] mentioned that, the experimental values for atoms with  $Z$  less than 4 are questionable because of the sensitivity of the experiments to impurities in the samples due to the very low cross sections of these elements.

Schäfer[60] developed an interactive graphics database that includes all the data points of Saloman[57]. From this database he prepared eighty machine-readable files for eighty elements including all the available data points from Saloman[57]. Each file consists of the photon energy in eV and the related values of the mass attenuation coefficients in barns/atom.

In 1996 Hubbell[61] developed an additional database of NIST/PCPDC by accumulating the data published in the period from 1981 to 1995. He converted the units of the photon

energies to eV and the unit of the mass absorption coefficients to barns/atom. He estimated the uncertainty of the collected database by calculating the differences between independent measurements for the same elements and energies by different authors under different experimental conditions. He found that, the uncertainties range is from  $\pm 0.2\%$  to  $\pm 50\%$ .

Unacceptable data points were found in the course of the present investigation in the experimental data of Saloman[57] for the element *Te* as well as in the experimental data of Hubbell[61] for elements *Na*, *Fe*, *Y*, *W*, and *Pb*. In addition, errors and missing data points were found in Schäfer's machine readable files for elements *Li*, *B*, *N*, *Al*, *Si*, *Kr*, *Nb*, *Pd*, *Cd*, *Sn*, *Sb*, *I*, *Pb*, and *U*. Therefore, the unacceptable data points in both Saloman and Hubbell were cancelled. Also, in Schäfer's machine-readable data files, the errors were corrected and the missing data points were added. Table 3.1 describes these errors in each of these databases. In order to see the mentioned unacceptable data points, Figs. 3.1-3.3 illustrate the relation between the mass absorption cross sections versus the photon energy for the elements *Sn*, *W* and *Te*.

In this work, the experimental data of Saloman (Schäfer's machine readable files) and Hubbell were blended together as well as the available recent measurements of the x-ray mass absorption coefficients[62-68]. A new set of machine-readable data files was developed to include all the available measurements of the x-ray mass absorption coefficients. According to the final version of the experimental data files, there are fifteen elements missing in the interesting photon energy range (1-150 keV) where there exist no experimental data. The missing elements are *Tc*, *Ru*, *Cs*, *Pm*, *Eu*, *Os*, *Po*, *At*, *Rn*, *Fr*, *Ra*, *Ac*, *Pa*, *Np*, and *Pu*. Due to the last version of the experimental data files, Fig. 3.4 describes the experimental and theoretical values depending on McMaster's data of x-ray mass absorption coefficients of *Xe* versus the photon energy. There is a good agreement between the experimental data and the calculated data of McMaster. Remarkable differences between the experimental and the McMaster data at low photon energy range are due to the fact that the McMaster data are valid only in the range of 1 keV to 1 MeV and increasing errors close to 1 keV have to be expected.

Table 3.1 Erroneous data points in the empirical database

Schäfer Data File [60]				
Element	Wrong Data Points		Missing Data Points	
	E, eV	$\mu$ , barns/atom	E, eV	$\mu$ , barns/atom
B-5			84990	2.601
Li-3	5047	4.55	8047	4.55
N-7	5048	170	8048	170
	15190	9.014	25190	9.014
Al-13	6340	2010	8040	2010
Si-14	1487	46400		
Kr-36	2970	475000	2097	475000
Nb-41			14 data points, from Hon, and Heinrich[69]	
Pd-46	8094	27560	8904	27560
Cd-48	0	273		
	7027	271000	4027	271000
Sn-50	9630	78060	6930	78060
Sn-50	125 data points, from Nordfors and Noreland[70]			
Sb-51			125 data points, from Nordfors and Noreland[70]	
I-53	27200	5500	37200	5500
Pb-82	0	1857		
U-92	2188	2056000	1188	2056000
Hubbell Database [61]				
Element	Wrong Data Points		References	
	E, eV	$\mu$ , barns/atom		
Na-11	1075	2500000	Tuilier [71]	
Fe-26	4000	239500	Del Grande [72]	
	22600	1.641+3	Quanruzzaman [73]	
Y-39	18620	1215	Wang Dachun [74]	
W-74	22600	2937	Quanruzzaman [73]	
Pb-82	5415	2.140=05	Del Grande [72]	
Saloman Database [57]				
Element	Wrong Data Points		References	
	E, eV	$\mu$ , barns/atom		
Te-52	4342	7200	Nordfors and Noreland[70]	

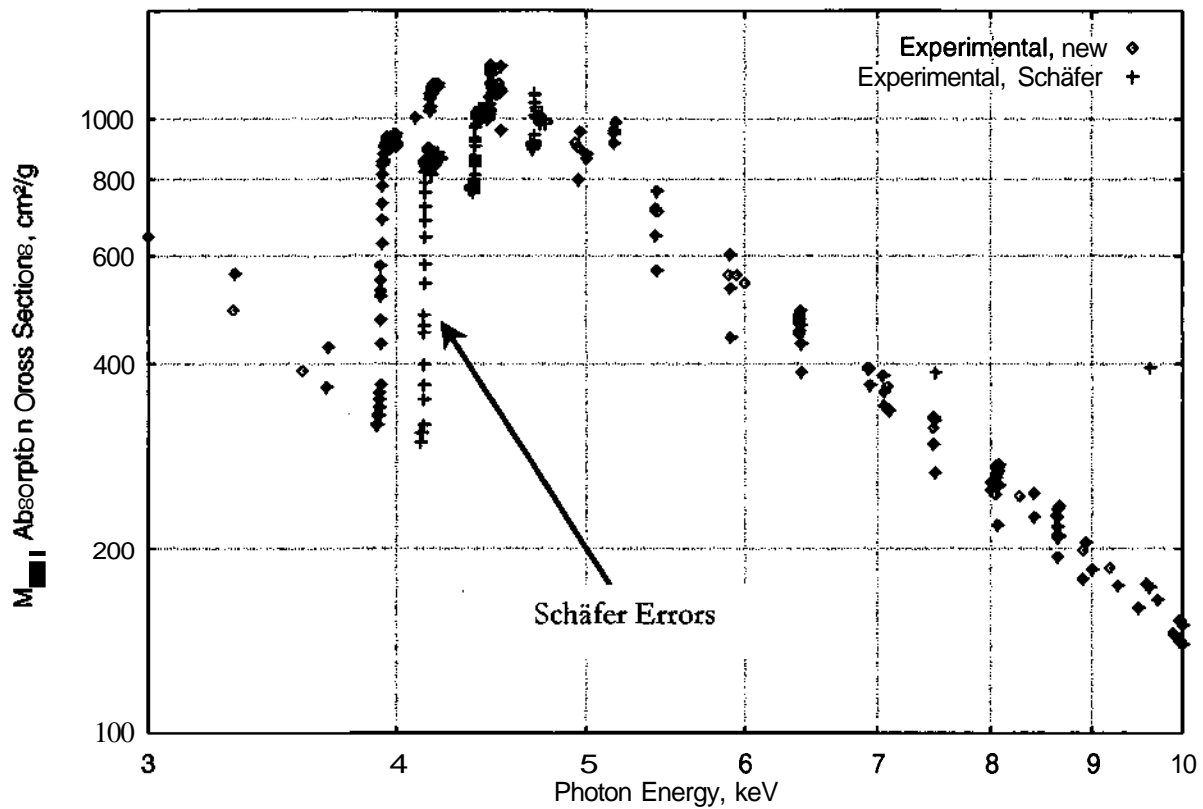


Fig. 3.1 Mass absorption cross section of Sn-50 versus the photon energy.

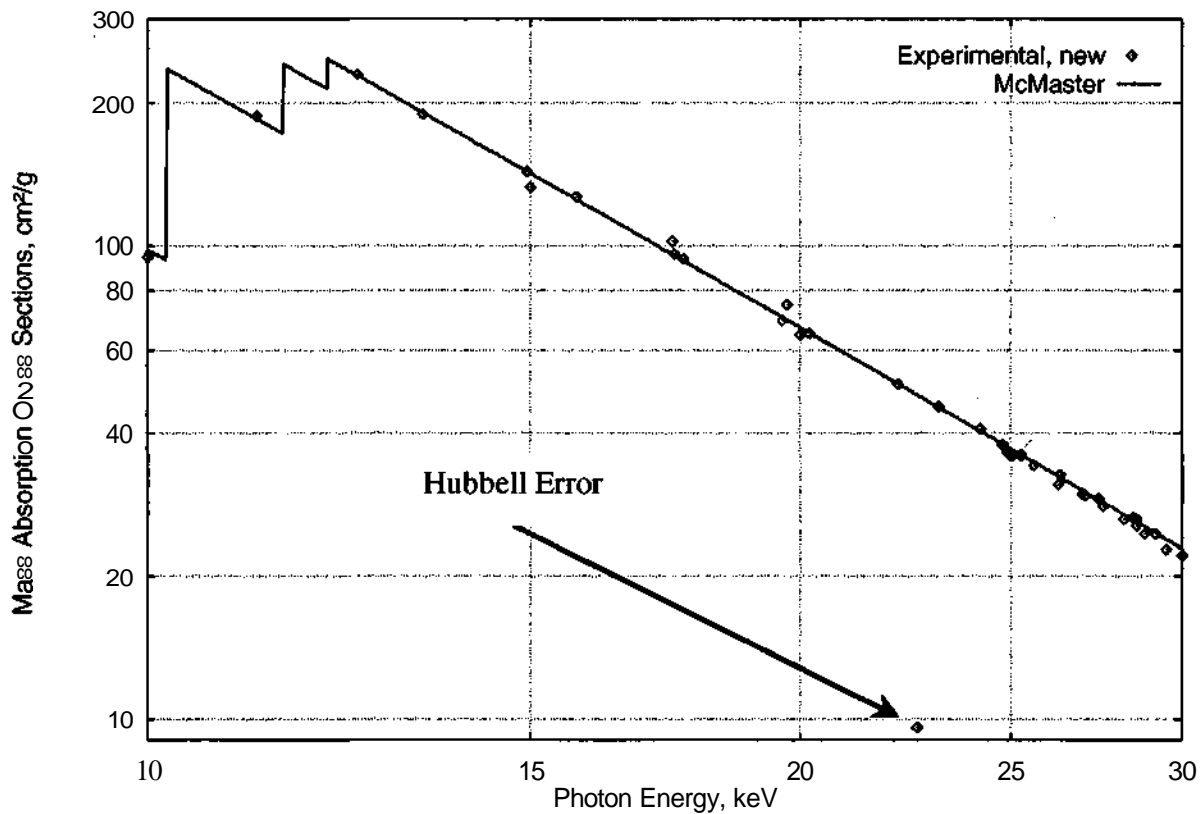


Fig. 3.2 Mass absorption cross section of W-74 versus the photon energy.

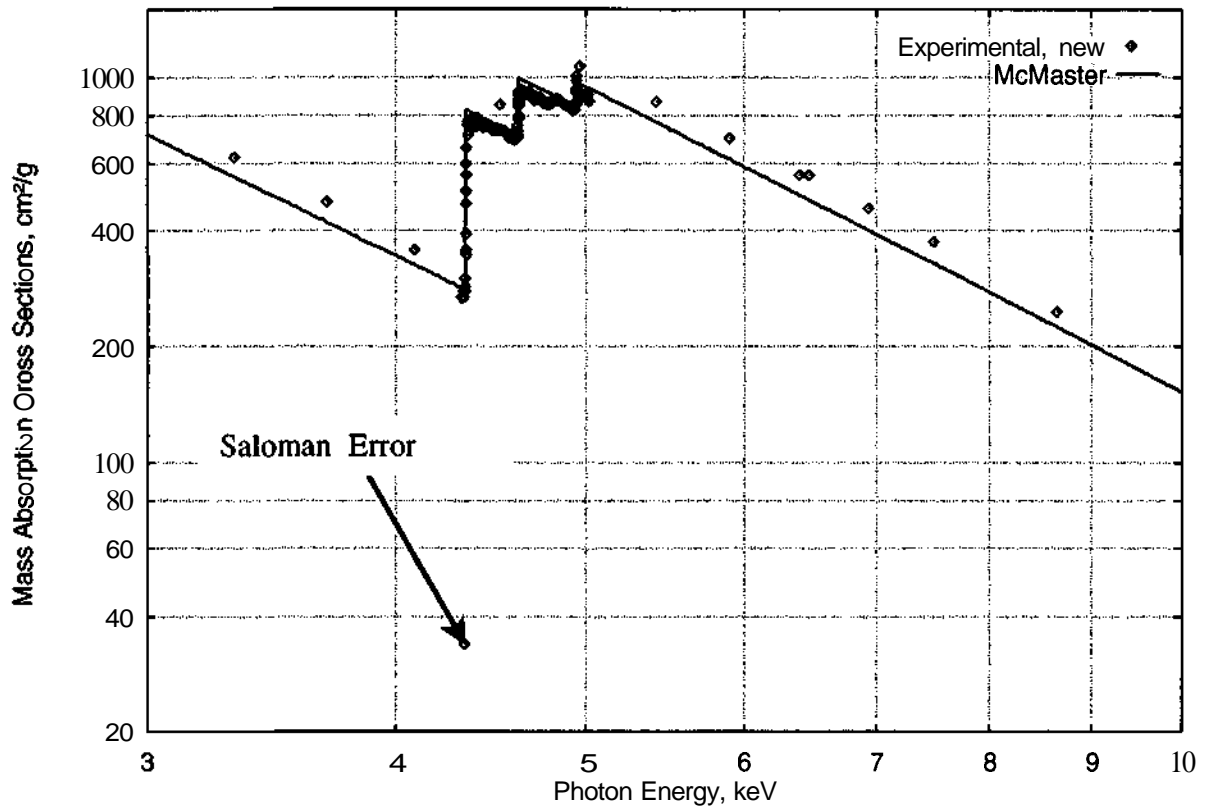


Fig. 3.3 Mass absorption cross section of Te-52 versus the photon energy.

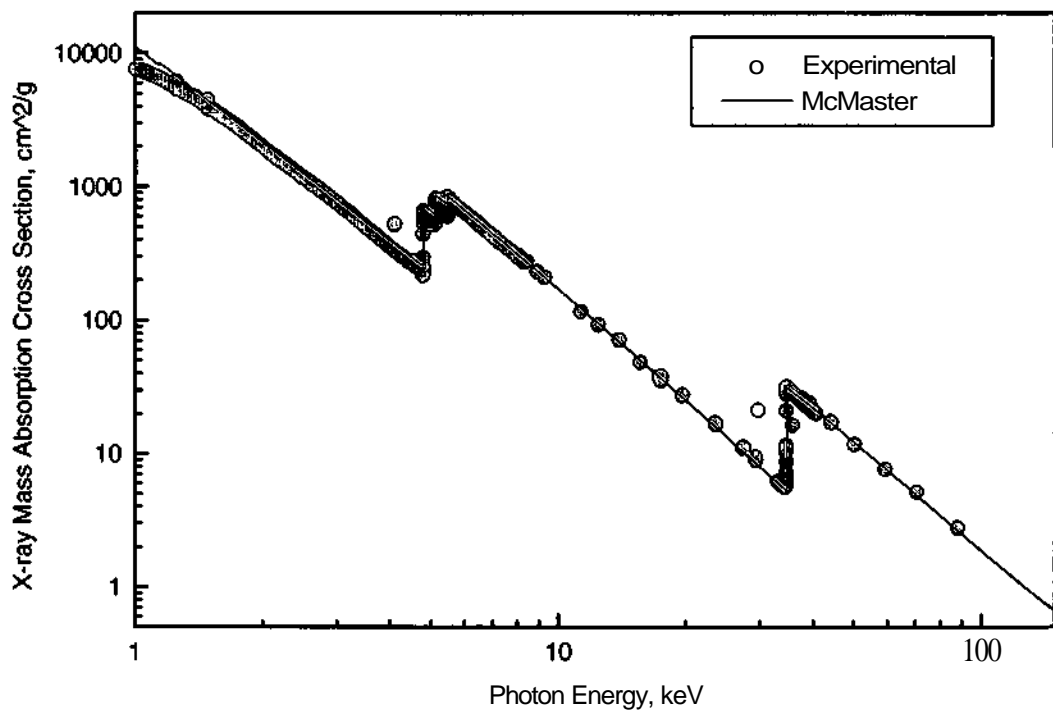


Fig. 3.4 X-ray mass absorption cross section of Xe-54 versus the photon energy.

### 3.2 McMaster Database

A great number of scientific investigations is based on the compilation of x-ray cross sections given by McMaster[75]. McMaster described the compilation of x-ray cross sections in the range of 1 keV to 1 MeV. They used the form factors of Cromer and Mann[76] to compute the incoherent scattering cross sections for 35 elements. The remaining elements were obtained from a sliding polynomial fit across  $Z$  for each energy. In the same way, they used the form factors for Cromer and Waber[77] to calculate the coherent scattering cross sections. Also, they derived the high energy photoelectric cross sections from Schmickley and Pratt[78]. To derive the experimental photoelectric cross section, they subtracted the computed scattering cross section from the experimental total absorption cross section.

For each element, McMaster described.

- The cross sections in barns/atom and  $\text{cm}^2/\text{g}$ .
- The cross sections of the  $K_{\alpha_1}$ ,  $K_{\beta_1}$ ,  $L_{\alpha_1}$ ,  $L_{\beta_1}$  in barns/atom and  $\text{cm}^2/\text{g}$ .
- Atomic weight, density and atomic density in  $\text{g}/\text{mole}$ ,  $\text{g}/\text{cm}^3$ ,  $10^{24} \text{ atoms}/\text{cm}^3$ , respectively.
- The conversion factor  $C$  is used to convert from barns/atom to  $\text{cm}^2/\text{g}$  by the following formula

$$\sigma(\text{barns/atom}) = C \cdot \sigma(\text{cm}^2/\text{g})$$

$$C = \frac{A(\text{g/mole})}{N(\text{atom/mole})} \times 10^{24} \quad (3.1)$$

where  $A$  is the atomic weight and  $N$  is Avogadro's number.

- The K and L edges as well as the related edge jumps
- The fit coefficients of the scattering and the photoelectric cross sections. These coefficients can be used to generate the values in the compilation tables according to equation

$$\left. \begin{aligned} \ln \tau(E) &= \sum_{i=0}^3 A_i (\ln E)^i \\ \ln \sigma_{coh}(E) &= \sum_{i=0}^3 B_i (\ln E)^i \\ \ln \sigma_{incoh}(E) &= \sum_{i=0}^3 C_i (\ln E)^i \\ \mu(E) &= \tau(E) + \sigma_{coh}(E) + \sigma_{incoh}(E) \end{aligned} \right\} \quad (3.2)$$

where  $\mu(E)$  is the mass absorption coefficient for the three kinds of interactions which can occur in the specimen, (the total photoelectric absorption  $T(E)$  , the total coherent scattering coefficient  $\sigma_{coh}(E)$  and the total incoherent scattering coefficient  $\sigma_{incoh}(E)$  ) and  $E$  is the photon energy in keV and  $A_i, B_i, C_i$  are the fit coefficients.

According to the given data of the McMaster database, there are seven elements missing. These elements are  $Po$ ,  $At$ ,  $Fr$ ,  $Ra$ ,  $Ac$ ,  $Pa$ , and  $Np$ . Also, the positions of both N and M absorption edges are not given as well as the related jump ratio of each absorption edge. In the present investigation, the position of both M and N absorption edges are included as well as the related jump ratio of each absorption edge. In this case, the correct values of photoelectric cross sections in M and N ranges will be obtained.

### 3.2.1 Errors in the McMaster database

There are four essential criticisms on the McMaster tables. These are:

- **The Missing elements**

As mentioned above, seven elements are missing in the McMaster database. In the present work, these seven elements were added to McMaster database by using the photoelectric cross sections from Scofield's database[79], the coherent and incoherent scattering cross sections from Elam[80] and the absorption edge positions from Bearden[81]. The edge jumps of these elements were calculated in the same way as the calculation of M-edges and the related jump ratio in the McMaster database, which is described below.

Brennan and Cowan[82] developed a FORTRAN program, which calculates photoabsorption cross sections and atomic scattering factors for materials of arbitrary, uniform composition or for arbitrary layered materials. Depending on McMaster's database, Brennan and Cowan[82] developed a new set of coherent and incoherent scattering cross sections including the missing seven elements in McMaster database. But, in the present investigation the coherent and incoherent database of Elam was used for the missing elements because it is more recent than Brennan and Cowan's database.

- **The fit coefficients of the N range:**

According to the given data in the McMaster database, the N-fit coefficients and the M-fit coefficients for the elements from Z=61 (Neodymium) to Z=69 (Thulium) are identical. It was found that the N-fit coefficients of these elements are completely wrong in the McMaster database. Therefore, the fit coefficients of the total photoelectric cross sections are calculated according to equation 3.2. In the N-range, a least squares fit using a linear dependence was used to recalculate the N-fit coefficients of these elements. The least squares fit using a linear response was used because of the small number of available data points in this range. For instance, Dysprosium, Dy-66, M-edges are given in Fig. 3.5. According to Fig. 3.5 the fit coefficients  $A_0$  and  $A_1$  of the N range can be easily calculated at two different photon energies,  $E_1$ ,  $E_2$  by using equation 3.2

$$\ln \tau_{E,ijk} = A_0 + A_1 \cdot \ln E_1 \quad (3-3)$$

$$\ln \tau_{E,ijk} = A_0 + A_1 \cdot \ln E_2 \quad (3.4)$$

Hence, the fit coefficients of the N-range,  $A_0$ , and  $A_1$  were calculated for the elements from Neodymium to Thulium. The N-fit coefficients of these elements are given in Table 3.2.



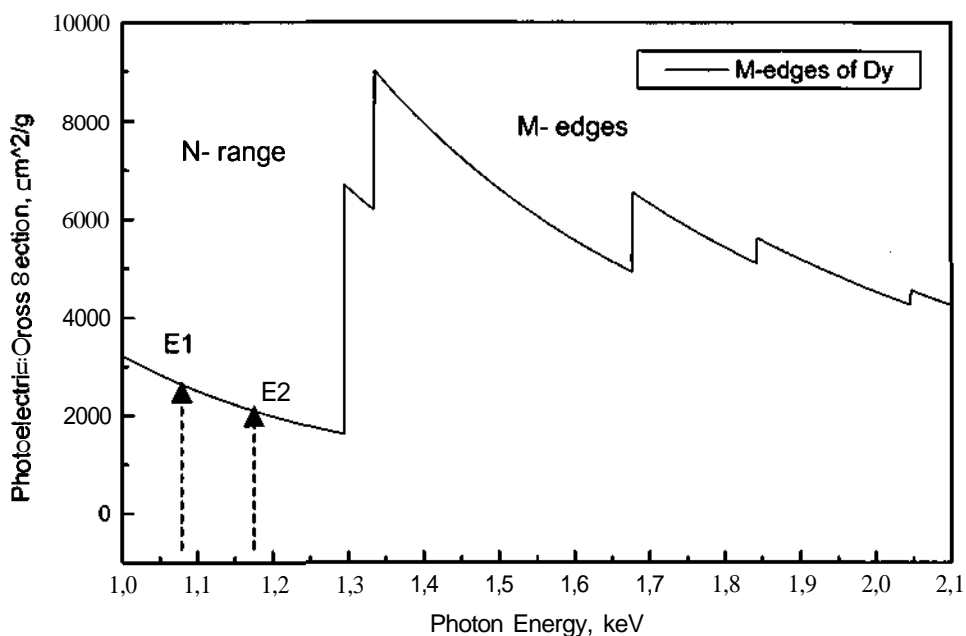


Fig. 3.5 Relation between photoelectric cross section and photon energy at N and M ranges of Dysprosium.

Table 3.2 New fit coefficients in the N-range

Element	McMaster Values		Corrected Values	
	$A_0$	$A_1$	$A_0$	$A_1$
Pm-61	15.5131	-2.59623	13.3455069	-2.5957691
Sm-62	15.6006	-2.61328	13.4108451	-2.6139213
Eu-63	15.7063	-2.63481	13.4826916	-2.6344478
Gd-64	15.7159	-2.60843	13.5452754	-2.6085396
Tb-65	15.8415	-2.64040	13.6154730	-2.6406124
Dy-66	15.9225	-2.65289	13.6771676	-2.6529813
Ho-67	16.0140	-2.67903	13.7440146	-2.6795252
Er-68	16.0672	-2.67587	13.8333505	-2.6744841
Tm-69	16.1269	-2.67886	13.8915452	-2.6796450

The new fit coefficients were used to modify the computer algorithm for the calculation of the mass absorption cross section in the N-range of the McMaster database. In this case, the calculated mass absorption cross section is identical with the numerical values in McMaster tables. There is another possibility to get the same photoelectric cross section as in the McMaster tables. In this case the fit coefficients of M-edges were used in the N-edge range and the jump ratio of the  $M_5$ -edge was used for calculation of the photoelectric cross section in the N-range. In the present investigation, the new fit coefficients of the N-edges are recommended and used for the calculation of x-ray cross sections.

- **M-edges and the related Jump ratio:**

The positions of M-edge energies are not defined in the McMaster tables excluding the  $M_1$ -edge which is already given. Therefore, in the present work, the M-edges and the related jump ratios were calculated for the elements from Te-52 to Pu-94. The other M-edges are below 1 keV and it is out of interest.

The M-edge energies of these elements have been extracted from the numerical values of photoelectric cross sections versus photon energy in the original McMaster tables. The jump ratio  $S_{iM}$  of any of the M-edges can be calculated by the following equation

$$S_{iM} = \frac{\tau_{E_{edge}-0.001, i}}{\tau_{(E_{edge}-0.001)_{McMaster}, i}} \quad (3.5)$$

where,  $i$  is the element,  $\tau_{E_{edge}-0.001}$  is the calculated photoelectric cross section without the related edge which is not tabulated in McMaster's data base,  $\tau_{(E_{edge}-0.001)_{McMaster}, i}$  is the tabulated photoelectric cross sections in McMaster's data base that added the rekted M edge.

For instance, in the calculation of the jump ratio of the  $M_1$ -edge of Uranium which lies at  $E_{edge} = 5.549$  keV, the photoelectric cross section was calculated at energy  $E = 5.548$  keV as a part of the  $L_3$ -edge. That means, the  $M_1$ -edge was not considered. Also, the photoelectric cross section at photon energy  $E = 5.548$  keV is tabulated in McMaster's database (In this case the  $M_1$  edge was included) as illustrated in Fig. 3.6. Similarly, the same method was applied to all the other elements to calculate the energy of all M-edges as well as the related jump ratios. Table 3.3 shows the calculated M-edge energies as well as its jump ratios for these elements. Fig. 3.6 illustrates the  $M_1$ -edge of Uranium. According to Fig. 3.6, it is easy to calculate the jump ratio for each edge. According to Table 3.3 the proper values of the photoelectric cross section can be easily described in McMaster's tables. The M edges of the missing seven elements were taken from Bearden[81].

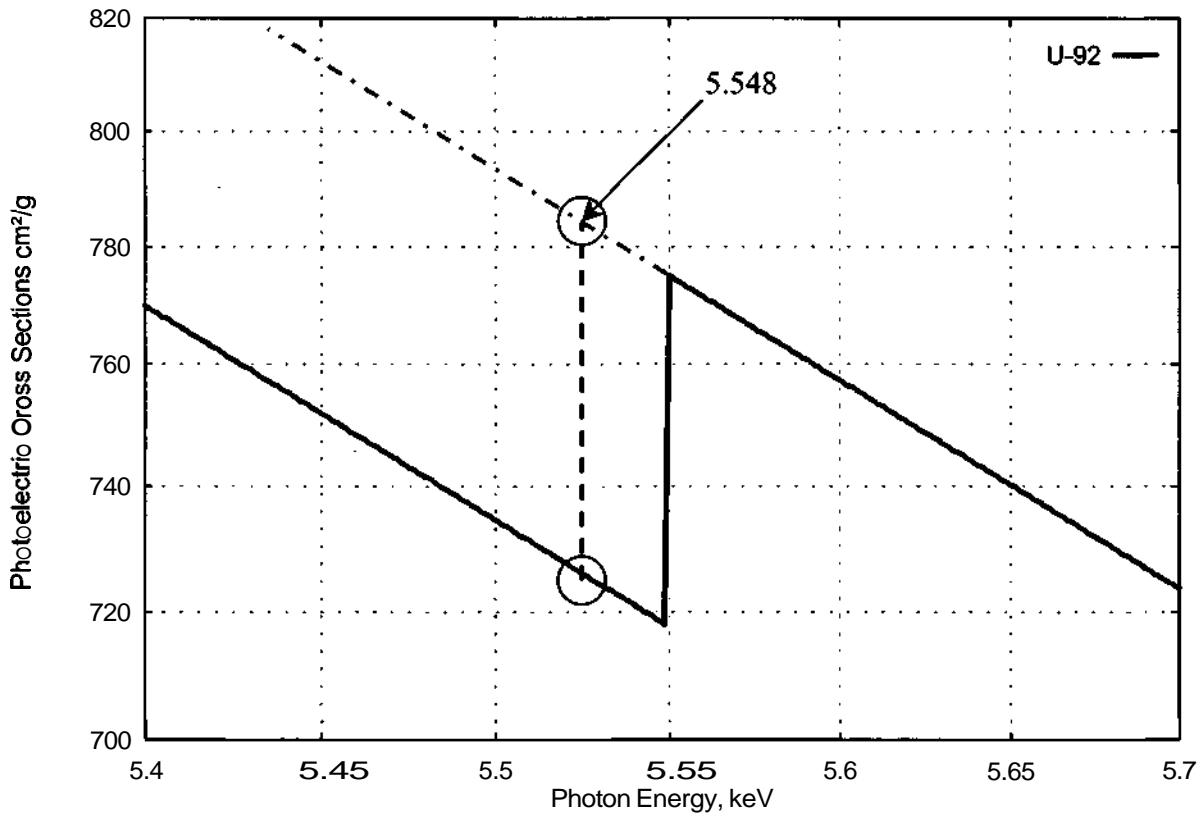


Fig. 3.6  $M_1$ -edge of Uranium

Table 3.3 M-edge energies and the calculated jump ratios

El.	M1		M2		M3		M4		M5	
	E edge	Jump	E edge	Jump	E edge	Jump	E edge	Jump	E edge	Jump
Te-52	1.006	1.05024								
I-53	1.072	1.05017								
Xe-54	1.143	1.05015								
Cs-55	1.218	1.0499	1.071	1.09479	1.002	1.27885				
Ba-56	1.293	1.05991	1.131	1.08496	1.061	1.28692				
La-57	1.363	1.05989	1.205	1.09436	1.125	1.29310				
Ce-58	1.434	1.06001	1.276	1.09430	1.186	1.30166				
Pr-59	1.508	1.05997	1.337	1.09422	1.237	1.31048				
Nd-60	1.575	1.05975	1.404	1.10378	1.294	1.31624	1.004	1.48061		
Pm-61	1.651	1.05999	1.472	1.10379	1.357	1.31609	1.056	1.48054	1.030	3.83116
Sm-62	1.729	1.06026	1.542	1.10374	1.421	1.32467	1.108	1.47112	1.082	3.91855
Eu-63	1.800	1.05999	1.613	1.11313	1.481	1.31375	1.158	1.47728	1.128	4.03492
Gd-64	1.882	1.07022	1.690	1.10278	1.544	1.32187	1.221	1.46812	1.181	3.82659
Tb-65	1.967	1.06997	1.768	1.10282	1.611	1.40689	1.280	1.37947	1.240	4.04456
Dy-66	2.046	1.07016	1.843	1.10288	1.677	1.33029	1.335	1.45865	1.295	4.12349
Ho-67	2.127	1.06981	1.922	1.10277	1.739	1.33908	1.390	1.44944	1.345	4.22569
Er-68	2.212	1.07029	2.006	1.11197	1.811	1.33616	1.455	1.44029	1.41	4.07484
Tm-69	2.307	1.06992	2.093	1.11264	1.888	1.33564	1.515	1.44040	1.471	4.08397
Yb-70	2.398	1.07008	2.171	1.12163	1.951	1.33305	1.578	1.43139	1.528	3.75938
Lu-71	2.492	1.07989	2.265	1.11103	2.026	1.33352	1.639	1.43117	1.589	3.65885
Hf-72	2.602	1.07992	2.364	1.12038	2.110	1.33037	1.718	1.42252	1.662	3.56745
Ta-73	2.703	1.08002	2.469	1.12031	2.194	1.33033	1.793	1.42244	1.735	3.45350
W-74	2.818	1.07998	2.575	1.12966	2.281	1.32798	1.871	1.41341	1.809	3.04366
Re-75	2.931	1.08008	2.681	1.12942	2.367	1.32811	1.949	1.41324	1.883	3.05549
Os-76	3.050	1.08018	2.792	1.12958	2.457	1.32759	2.031	1.41384	1.960	2.82413
Ir-77	3.172	1.08038	2.909	1.12916	2.550	1.33656	2.116	1.40491	2.041	3.21391
Pt-78	3.297	1.08037	3.026	1.12918	2.645	1.33613	2.202	1.39898	2.122	3.39742
Au-79	3.425	1.07991	3.149	1.12959	2.743	1.27887	2.291	1.77622	2.206	2.26338
Hg-80	3.562	1.07977	3.280	1.12955	2.847	1.34488	2.385	1.39001	2.295	2.76505
Tl-81	3.7	1.08006	3.416	1.12953	2.956	1.34383	2.485	1.39044	2.389	2.66957
Pb-82	3.850	1.07984	3.554	1.12980	3.066	1.34397	2.586	1.39035	2.484	2.67025
Bi-83	3.999	1.07973	3.696	1.12972	3.177	1.35319	2.687	1.38129	2.579	2.55513
Po-84*	4.149	1.04381	3.854	1.06142	3.302	1.15902	2.798	1.46209	2.683	2.7223
At-85*	4.317	1.04385	4.008	1.06112	3.426	1.15777	2.909	1.47142	2.787	2.75904
Rn-86	4.478	1.07971	4.158	1.13021	3.534	1.35222	3.014	1.37583	2.886	2.33229
Fr-87*	4.652	1.04305	4.327	1.06209	3.663	1.15888	3.136	1.4734	2.999	2.6832
Ra-88*	4.822	1.04341	4.489	1.06189	3.792	1.16249	3.248	1.45091	3.105	2.5835
Ac-89*	5.002	1.04349	4.656	1.06178	3.909	1.16467	3.370	1.43912	3.219	2.5187
Th-90	5.182	1.08013	4.831	1.13892	4.046	1.34911	3.491	1.36146	3.332	1.91464
Pa-91*	5.367	1.04297	5.001	1.06178	4.174	1.16699	3.611	1.42905	3.442	2.45427
U-92	5.549	1.07993	5.181	1.13891	4.304	1.34964	3.728	1.36148	3.552	2.11519
Np-93*	5.722	1.04356	5.366	1.06027	4.435	1.16537	3.85	1.41616	3.664	2.45087
Pu-94	5.914	1.07999	5.54	1.13889	4.555	1.34962	3.969	1.35539	3.774	1.90128

\*The seven missing elements were added to the McMaster database by using the photoelectric cross sections of Scofield's database[79], coherent and incoherent scattering cross sections are from Elam[80].

- **Missing N edges**

In the McMaster database, the  $N_1$ -edge of some elements is given and the other N-edges are missing. At photon energies less than the  $N_1$ -edge, the tabulated values of the x-ray cross sections in McMaster's database are completely wrong. To include the missing N-edges and correct the x-ray cross sections in the N-range, Bearden's values [81] were used. It was found that the edges of Bearden were used in Memar's[83] calculation of the Scofield photoelectric cross sections instead of Scofield's values. Also, it was found that the N-edge energies of Bearden are approximately the same as the Siegbahn values[84]. Therefore, the N-edge energies of Bearden were added to the McMaster database and the related jump ratios were calculated (as jump ratios calculation in M edges) in order to correct photoelectric cross sections in the N range.

Figs. 3.7, 3.8 and 3.9 show a comparison between the photoelectric cross section versus photon energy given by McMaster and McMaster with the N-edge energies of Bearden (Shaltout's version). The comparison was performed for just three elements *Rn*, *Th*, and *U*. There are still seven elements missing in the McMaster database. The photoelectric cross sections of these seven missing elements were taken as mentioned above from the Scofield database using the edge energies of Bearden's[81] and the coherent and incoherent scattering cross sections of Elam[80]. Table 3.4 gives the N edge energies and the related jump ratios, which are used in the present work. According to Figs. 3.7, 3.8, 3.9, it becomes clear that the N-edges are completely missing in the McMaster tables, excepted the  $N_1$ -edge and there is a good modification of McMaster's database by adding Bearden's N-edge energies(Shaltout's version). In the present investigation these new considerations on N-edge energies were taken into account in the calculation of the x-ray cross sections of McMaster's database. This will improve the numerical values of the x-ray cross sections in the N-ranges to get more accurate results for the different theoretical quantitative analysis methods.

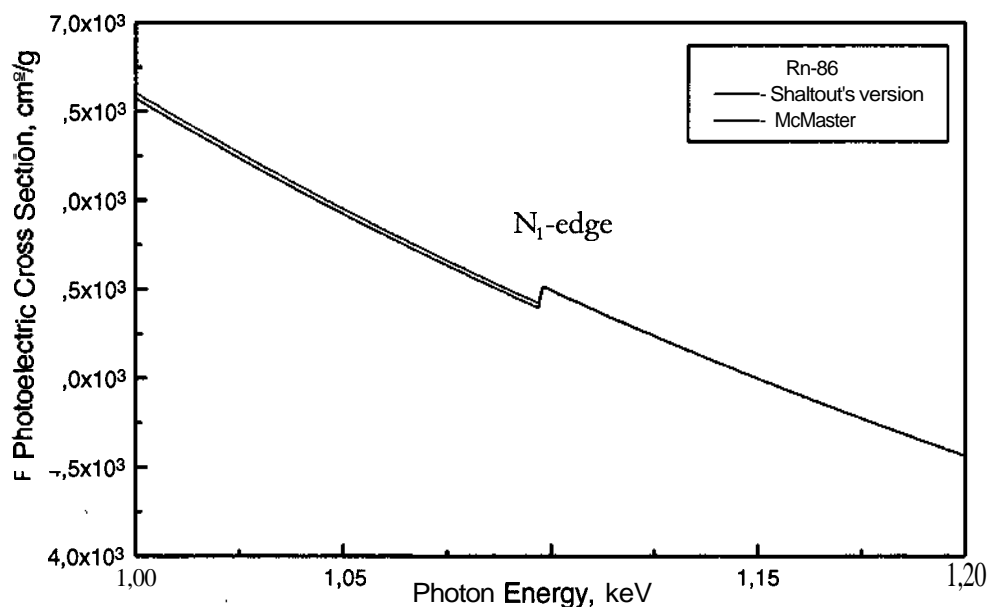


Fig. 3.7.  $N_1$ - edge of Rn

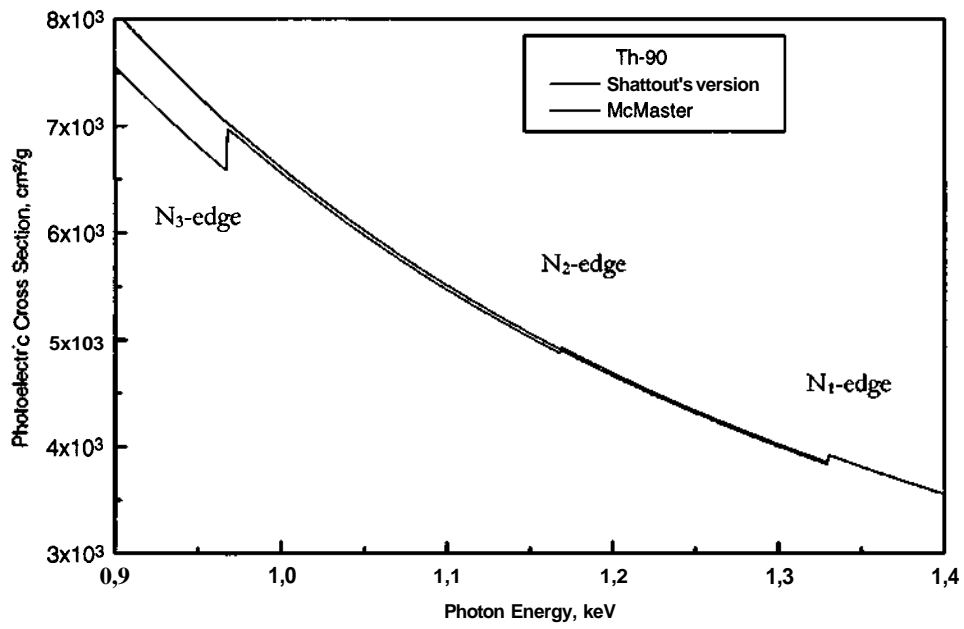


Fig. 3.8  $N_1$ -,  $N_2$ - and  $N_3$ -edges of Th

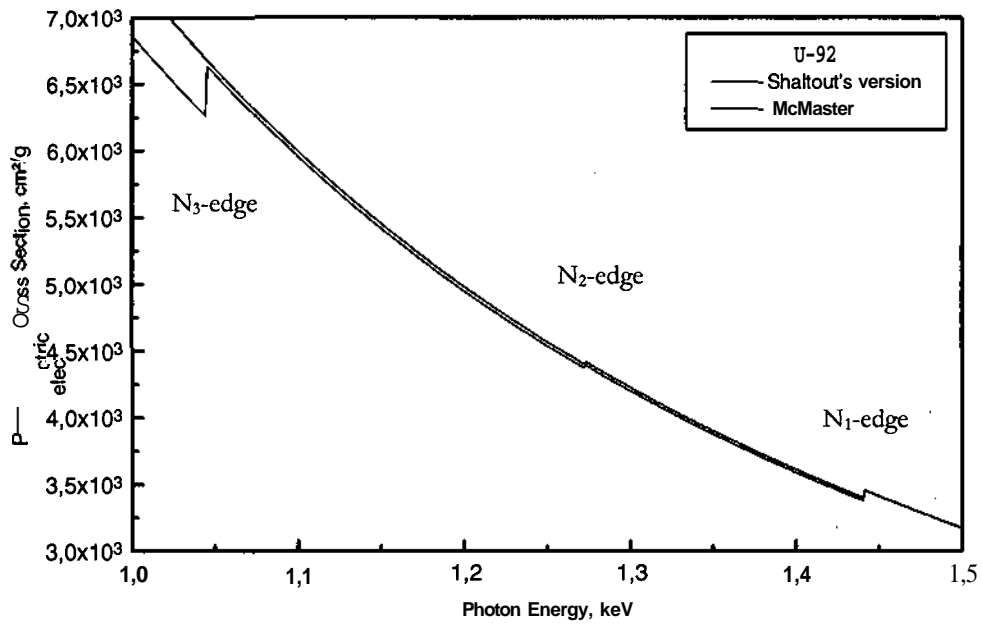


Fig. 3.9.  $N_1$ -,  $N_2$ - and  $N_3$ - edges of U

Table 3.4. N-edge energies and the calculated jump ratios.

Element	N <sub>1</sub>		N <sub>2</sub>		N <sub>3</sub>	
	E edge	Jump	E-edge	Jump	E-edge	Jump
At-85*	1.042	1.02139				
Rn-86	1.097	1.021205				
Fr-87*	1.153	1.021108				
Ra-88*	1.2084	1.02065	1.0576	1.01431		
Ac-89*	1.269	1.02046	1.08	1.01361		
Th-90	1.3295	1.020254	1.1682	1.01425		
Pa-91*	1.3871	1.01988	1.2243	1.0141	1.0067	1.06377
U-92	1.4408	1.019498	1.2726	1.01384	1.0449	1.06414
Np-93*	1.501	1.018778	1.328	1.01326	1.087	1.06263
Pu-94	1.558	1.018965	1.377	1.01298	1.12	1.06234

\* The missing elements in McMaster database.

### 3.2.2 Edge Energies and the Related Jump Ratios

The jump ratio was given in equation 3.5. Figs. 3.10 shows a relation between the edge energies of the L<sub>1</sub> shell of most elements in the periodic tables (from two different sources, McMaster and Bearden) versus the atomic number of these elements. It can be seen that the edge energies of the L<sub>1</sub> shell in both McMaster and Bearden is approximately identical.

Figs. 3.11 shows a relation between the relative error of the L<sub>1</sub>-edges energies ( $RD\%_S = \left( \frac{E_{Edge, Bearden} - E_{Edge, McMaster}}{E_{Edge, Bearden}} \right) \times 100$ ) versus the atomic number of these elements. It can be seen that the relative error is approximately zero at elements with Z higher than 25. For the elements of Z lower than 25, a remarkable difference is found.

All the different edge energies and the related jump ratios basically depend on McMaster database except the M- and N-edges mentioned above. On the other hand, Fig. 3.12 shows a comparison between the jump ratio of the K-edge of both McMaster and Veigele versus the atomic number of the elements, (the jump ratio values of Veigele were taken from Mantler's database[85]). According to Fig. 3.12, it can be seen that, the difference between the two different sources is high for low atomic number and there is a good agreement between them for elements of atomic number higher than 17. Fig. 3.13 shows the relation between the relative deviation of the jump ratio of both McMaster and Veigele,  $RD\%_S$  versus the atomic number

$$RD\%_S = \left( \frac{S_{McMaster} - S_{Veigele}}{S_{Veigele}} \right) \times 100 \quad (3.6)$$

where,  $S_{McMaster}$  and  $S_{Veigele}$  are the jump ratio of the K edge in both McMaster and Veigele respectively. It can be seen that, for the elements of atomic number higher than 17, the relative deviation is equal or less than 10%. The disagreements between McMaster and Veigele for elements of atomic number lower than 11 refer to the values of the K-edge energies of less than 1 keV.

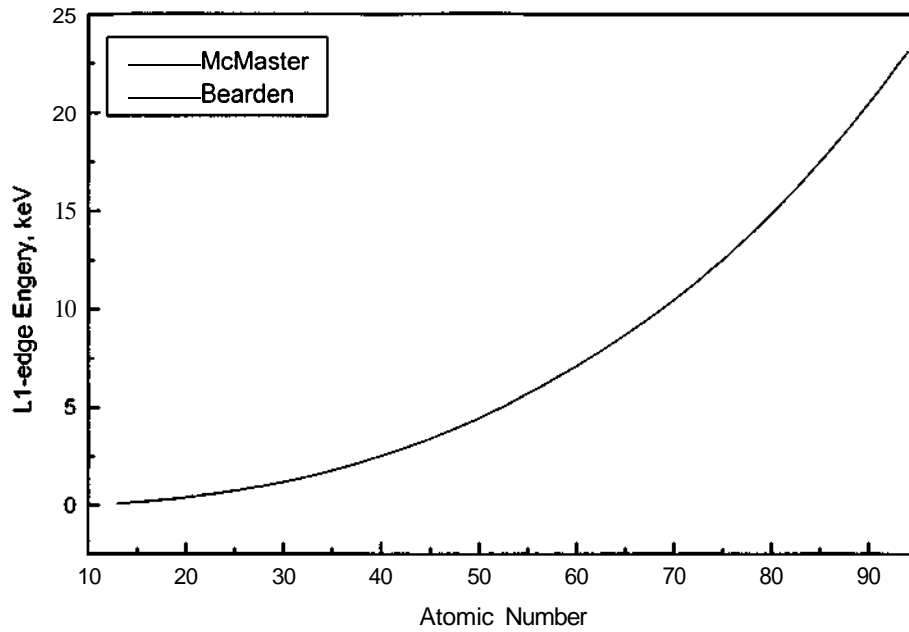


Fig. 3.10 Relation between the K edge energy versus atomic number

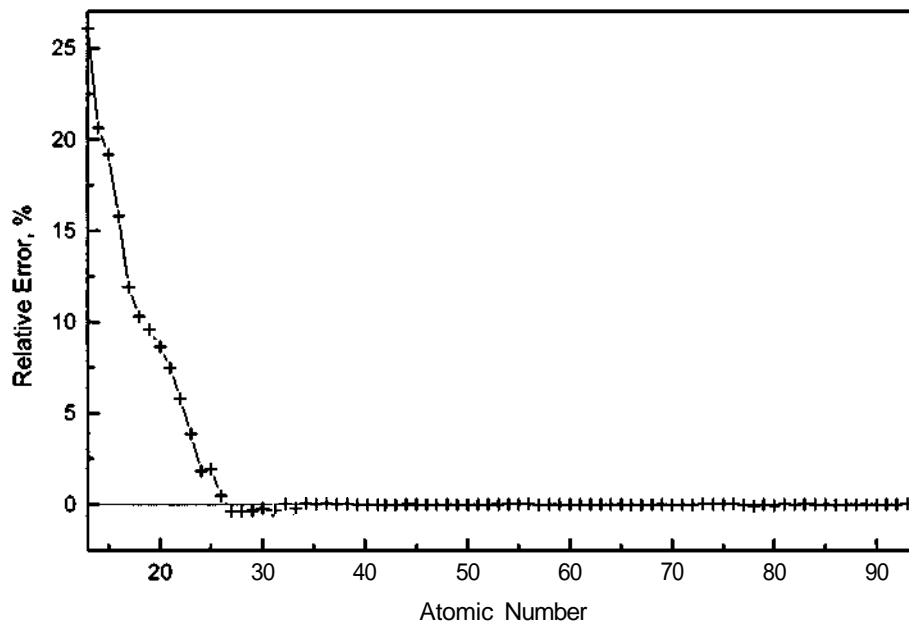


Fig. 3.11 Relative error of L<sub>1</sub>-edges versus atomic number.

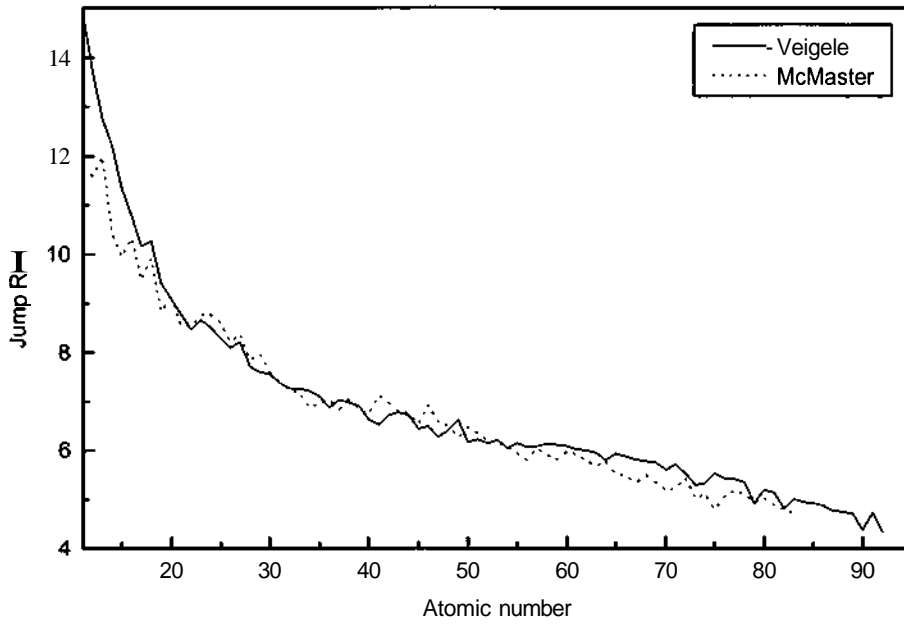


Fig. 3.12 Relation between the jump ratio of K edges and atomic number.

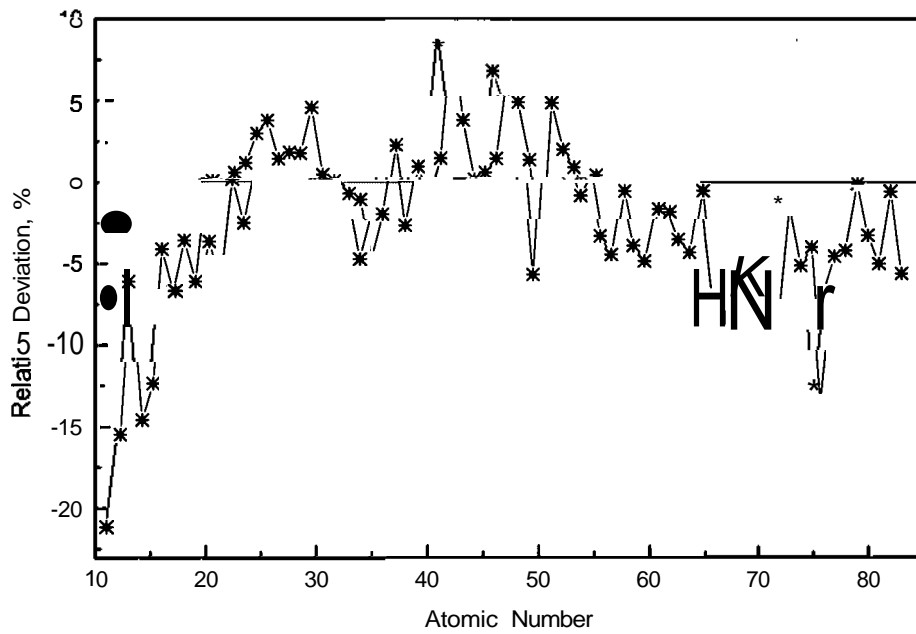


Fig. 3.13 Relation between the relative deviation,  $RD\%_s$  of the jump ratios and atomic number from McMaster and Veigele.



### 3.2.3 Shaltout's Corrected Version of McMaster's database

For further application in quantitative analysis an algorithm is used for the calculation of the photoelectric, coherent, incoherent and mass absorption cross sections versus the photon energy of McMaster's database including the corrected values of the mentioned critical errors. This algorithm is valid for the elements from  $Z=1-94$  at photon energies of 1-1000 keV. In the algorithm, the requested element can be selected and a data file and a plot of the x-ray cross sections versus the photon energy of this element can be easily obtained. The algorithm is called "MODMCM.BAS".

### 3.2.4 Previous Description of McMaster Database, (MUCAL Program)

The International XAFS (X-ray Absorption Fine Structure) Society (IXS), presented[86] an algorithm called "MUCAL" that calculates x-ray absorption cross sections using the McMaster database in both FORTRAN and C language. The MUCAL algorithm was written by Pathikrit Bandyopadhyay at the University of Notre Dame, USA and the latest revision of the MUCAL algorithm is from 1995. The European Synchrotron Radiation Facility, ESRF[87] presents the McMaster database depending on the MUCAL algorithm. The description of the McMaster database in both IXS and ESRF are completely identical because both of them depend on the MUCAL program. The previous descriptions of IXS and ESRF did not take into account the critical consideration mentioned above. In addition, there are big differences between the original McMaster database and both IXS and ESRF descriptions especially in the M and N ranges. In order to see the differences between the previous and the present description of McMaster, Figs. 3.14 and 3.15 give a comparison between the mass absorption cross sections versus the photon energy of Pu-94 in three different descriptions of McMaster. The three descriptions are the original source of McMaster, my corrected version of McMaster and in the MUCAL description of McMaster. According to Figs. 3.14 and 3.15, the M-and N-range description in the MUCAL program ignored both M-and N-edges and therefore is completely wrong. Also, the original McMaster database did not take into account the N-edges except the  $N_1$ -edge as described before. The corrected version of McMaster's database takes into account all these considerations. Thus, in the present investigation McMaster database means my corrected version of McMaster.

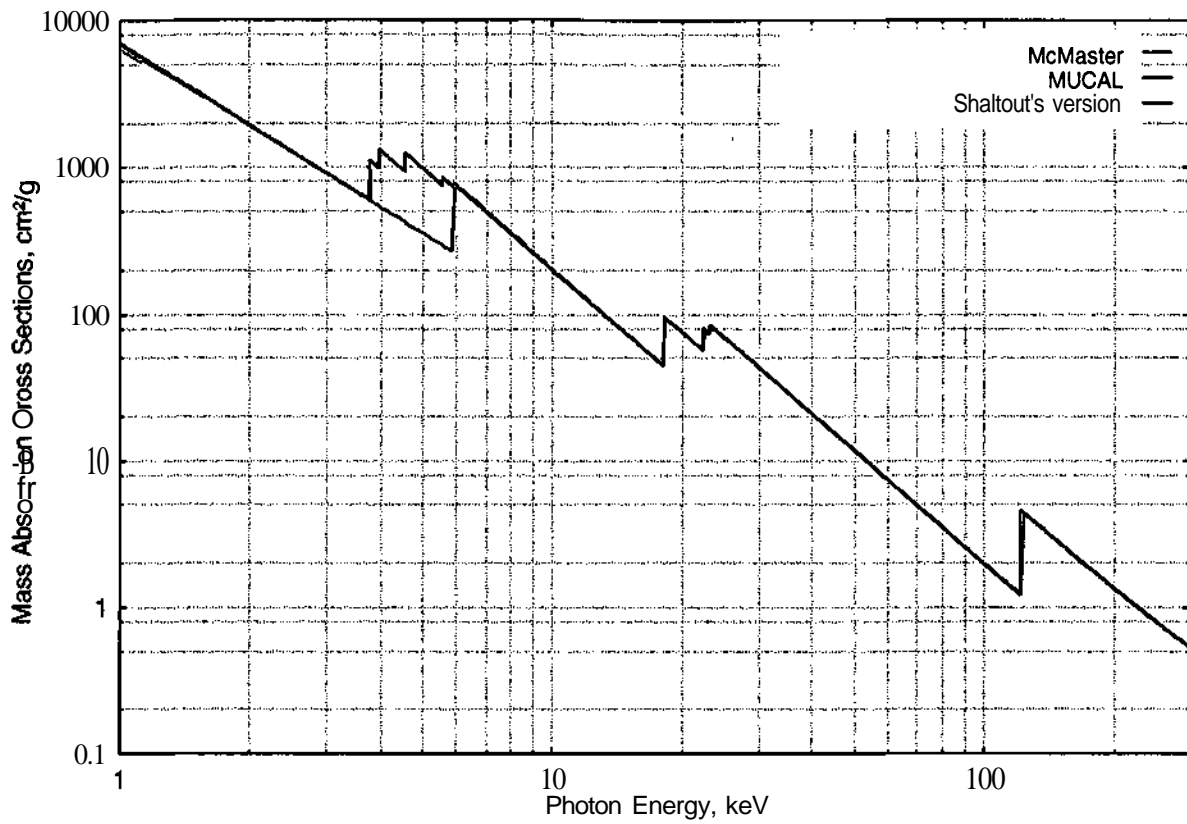


Fig. 3.14 Relation between the mass absorption coefficient of Pu-94 and the photon energy.

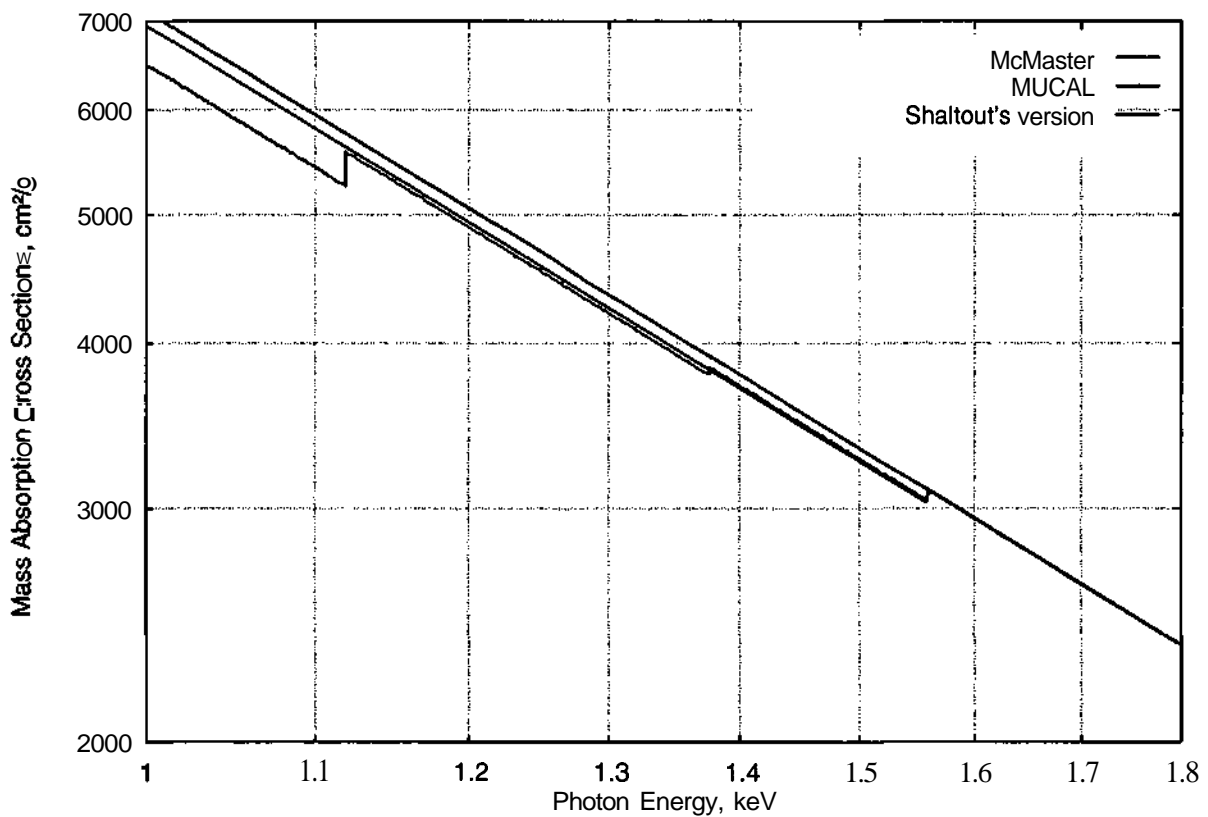


Fig. 3.15 Relation between the mass absorption coefficient of Pu-94 and the photon energy.

### 3.3 Scofield's Database

The knowledge of the total photoelectric cross sections as well as the photoelectric cross sections of each subshell is essential for many applications such as the total electron yield, x-ray photoelectron spectrometry, x-ray fluorescence analysis and electron probe micro analysis.

Henke[88], Del Grande[89, 90], Deslattes[91], Hubbell[92, 93], Saloman[94] and Storm[95] gave the total cross sections and attenuation coefficients as well as partial cross sections for different processes such as incoherent scattering, coherent scattering, photoelectric absorption, pair and triplet production for the elements at different photon energy ranges. The majority of these databases are for neutral, isolated atoms of each element and the others are for compounds and mixtures. Although, the photoelectric cross section in different photon energy ranges is required in a variety of applications, for the present work, the photoelectric cross sections from 1 keV to 300 keV were absolutely the most interesting in the mentioned applications. Hubbell's[96], Kissel and Pratt's[97] and Cullen's[98-101] tables depend on Scofield's database.

Therefore, the present investigation deals also with Scofield's database for the theoretical calculation of photoionization cross sections from 1 keV to 1500 keV. As mentioned that Scofield extended his calculation down to 0.1 keV[96], but these data were not published. The theoretical calculations of Scofield do not include coherent or incoherent scattering. The purpose of the present investigation is to examine and present accurate values for total photoelectric cross sections as well as the photoelectric cross sections of the subshells. For this purpose, a least squares fitting was used to calculate the fit coefficients of each subshell for each element from atomic number  $Z=1$  (hydrogen) to 94 (plutonium). A set of fit coefficients is used to recalculate Scofield's tabulated photoelectric cross sections at photon energies from 1 to 300 keV.

#### 3.3.1 Description of Scofield's Database

Scofield's database contains calculated values of the photoionization cross sections for elements of atomic number from  $Z=1$  (hydrogen) to  $Z=102$  (Nobelium) and for a set of photon energies from 1 keV to 1500 keV. The total cross sections, the cross sections for the ionization from K, L, M, and the sum of the other shells as well as the individual subshells are given.

For elements with atomic numbers from 2 to 54, Scofield presented correction factors for individual atomic subshells, by which the photoelectric cross sections can be renormalized. So that they correspond more to a relativistic Hartree-Fock model rather than the Hartree-Slater model used in the original calculation. This renormalization is most significant for the outer atomic shells; the total cross section is lowered by no more than 10 percent at energies above 1 keV but Scofield has not actually applied this renormalization to the cross sections given in his tables. For each element Scofield's database includes

- Atomic number
- The number of the electron states
- Values of cross sections of photon energies at a given number.
- A complete description of the electron levels ( $1s^{1/2}$ ,  $2s^{1/2}$ ,  $2p^{1/2}$ , etc...). The x-ray levels are defined as those states that occur as initial and/or final states in x-ray transitions. The x-ray level notation is used for many electron systems. The electron configurations are recommended[102] and it already was used in Scofield's database.
- The number of electrons in each subshell (called NE in Scofield's tables)
- The absorption edges of each subshell, in keV (called E (KEV)). According to Scofield's database, the absorption edges of Bearden were used instead of Scofield's values.

- The square of the ratio of wave function near the origin for an electron with the same set of quantum numbers in a coulomb potential with the same nuclear charge (called NORM, "normalization").
- The atomic number of the interesting element is written again with the following expression "PHOTELECTRIC CROSS SECTIONS (BARNs)". Then, the photon energies and the total cross section as well as the cross sections for the ionization of K, L, M and the sum of the other subshells are given.
- The photon energies are repeated again and the individual cross sections of the subshells are given until the last subshell of that element. The atomic number of the element is mentioned again in each set of individual subshell data.

According to the present approximation of Scofield's database, neither the absorption edge nor the normalization values were used as well as the number of electrons in each subshell. The number of individual subshells differs from one element to the other. Table 3.5. shows an example of the construction of Scofield's tables for the element iron, Z=26. According to the theoretical calculation of Scofield for photon energies much higher than the binding energy of an electron, the photoelectric cross section is proportional to the square of the bound state wave function at the nucleus (at least in the potential model). Scofield calculated the average over the photon polarization and direction. Thus correlations with the photons, polarization or direction were not treated. Scofield considered in his calculations that the electrons in the initial and final state are treated as moving independently in the same central potential. According to Scofield's tables the final expression for the cross section is given by the equation

$$\sigma = \frac{4\pi\alpha (h)^2}{h\omega (m.c)^2} \sum_a \frac{N_a \cdot E_b}{P_n} \cdot \sum_{k_b} (2J_b + 1) \cdot \sum_L \frac{(2L+1)}{L(L+1)} \times [X(k_a, k_b, L) \cdot R_e^2 + X(k_a, -k_b, L) \cdot R_M^2] \quad (3.7)$$

where

$\hbar\omega$  is the photon energy

$E_b$  &  $P_n$  is the final electron energy and momentum.

$a$  &  $b$  are the single particle states of the electron being removed.

$$R_e = \int \frac{dr}{kr} (F_b G_a - G_b F_a) L(L+1) j_L(kr) + (k_b - k_a) (F_b G_a + G_b F_a) \left( r \frac{d}{dr} + 1 \right) j(kr) \quad (3.8)$$

$$R_M = (k_a + k_b) \int dr j_L(kr) (F_b G_a + G_b F_a) \quad (3.9)$$

$$X = (2\ell_a + 1)(2\ell_b + 1) \begin{pmatrix} \ell_a & \ell_b & L \\ 0 & 0 & 0 \end{pmatrix}^2 \begin{pmatrix} L & \ell_b & \ell_a \\ & j_b & j_a \end{pmatrix}^2 \quad (3.10)$$

Scofield used the central potential, which is identical to the variation of the Hartree potential. The calculation of the central potential is carried out in a logarithmic mesh in  $r$  and starts with a Thomas-Fermi potential. Scofield computed the matrix elements by integration in a linear mesh in  $r$ . For photon energies of the same order of magnitude as the electron binding energy, the bound-state wave function is calculated. For the energies much higher than the binding energy, the bound-state wave function is not needed out of the exponentially decaying region. Also, according to Scofield's calculation the total cross section is given as an infinite sum over the multipoles of the radiation field and a sum over the angular momenta of the continuum states. Also, in the computation of Scofield a number of terms required for a given accuracy were determined by experiments. Scofield obtained an accuracy of at least 0.1% in calculating the total cross section but this accuracy is not correct for the individual subshell contributions. Scofield checked the subshell cross sections for the elements of atomic number Z=4, 50 and 92 and for photon energies of 10, 100, and 1000 keV by varying the other parameters in his program. He

found that the estimated percentage errors for the subshell cross section is greater than 0.1%. Scofield mentioned that the large inaccuracies in the *d* and *f* subshell cross sections at 1000 keV for  $Z=92$  are due to an insufficient number of multipoles being included, but these errors have a negligible effect on the total cross sections. The photoelectric cross sections includes the probability for ionizing all the shells in an atom, (see equation 1.29). If the energy of the incoming photon is less than that required to ionize a particular shell, then the term for that shell will be zero. According to Scofield's database, Fig. 3.16 gives the relation between the photoelectric cross section and photon energy of each subshell of Cr. As can be seen from Fig. 3.16, there is no possibility to ionize the K shell below the binding energy of Cr K-shell, which is equal 5.989 keV. When the incoming photon energy is higher than the binding energy of the Cr K-shell, then the ionization of that shell becomes possible as given by Fig. 3.16.

Table 3.5. Sample of data structure of Scofield tables.

Z= 26	10 STATES			28 ENERGYS		
STATE	NE	E(KEV)	NORM			
1 S 1/2	2.00	7.0834	.96864			
2 S 1/2	2.00	.8430	.71326			
2 P 1/2	2.00	.7336	.57899			
.....	.....	.....	.....			
.....	.....	.....	.....			
3 D 5/2	3.60	.0127	.04234			
4 S 1/2	2.00	.0075	.05516			
Z= 26	PHOTOELECTRIC CROSS SECTIONS(BARNSS)					
ENERGY(KEV)	TOTAL	K-SHELL	L-SHELL	M-SHELL	ALL OTHER	
1.00E+00	8.4208E+05	.0e+00	7.4923E+05	9.1400E+04	1.4494E+03	
1.50E+00	3.1484E+05	.0e+00	2.7971E+05	3.4473E+04	6.6498E+02	
2.00E+00	1.5045E+05	.0e+00	1.3329E+05	1.6796E+04	3.7300E+02	
3.00E+00	5.1398E+04	.0e+00	4.5335E+04	5.9037E+03	1.5924E+02	
.....	.....	.....	.....	.....	.....	
.....	.....	.....	.....	.....	.....	
1.00E+03	3.2594E-2	2.9356E-02	2.8030E-03	4.0821E-04	2.6313E-05	
1.50E+03	1.5211E-2	1.3704E-02	1.3049E-03	1.9008E-04	1.2399E-05	
Z= 26	1 S 1/2	2 S 1/2	2 P 1/2	2 P 3/2	3 S 1/2	3 P 1/2
1.00E+00	.0e+00	1.1698E+05	2.14E+05	4.1803E+05	2.1475E+04	2.0474E+04
1.50E+00	.0e+00	6.1302E+04	7.45E+04	1.4391E+05	9.9829E+03	7.5869E+03
2.00E+00	.0e+00	3.6465E+04	3.32E+04	6.3649E+04	5.6310E+03	3.5604E+03
3.00E+00	.0e+00	1.6348E+04	9.99E+03	1.8998E+04	2.4169E+03	1.1465E+03
.....	.....	.....	.....	.....	.....	.....
.....	.....	.....	.....	.....	.....	.....
1.00E+03	2.9356E-02	2.7165E-03	3.2726E-05	5.3725E-05	3.9607E-04	4.6034E-06
1.50E+03	1.3704E-02	1.2670E-03	1.3732E-05	2.4226E-05	1.8474E-04	1.9218E-06
Z= 26	3 P 3/2	3 D 3/2	3 D 5/2	4 S 1/2		
1.00E+00	3.9857E+04	3.8858E+03	5.7077E+03	1.4494E+03		
1.50E+00	1.4643E+04	9.1699E+02	1.3430E+03	6.6498E+02		
2.00E+00	6.8300E+03	3.1465E+02	4.5981E+02	3.7300E+02		
3.00E+00	2.1799E+03	6.5287E+01	9.5061E+01	1.5924E+02		
.....	.....	.....	.....	.....		
.....	.....	.....	.....	.....		
1.00E+03	7.5357E-06	2.2771E-09	4.1768E-09	2.6313E-05		
1.50E+03	3.4206E-06	8.5377E-10	1.8247E-09	1.2399E-05		

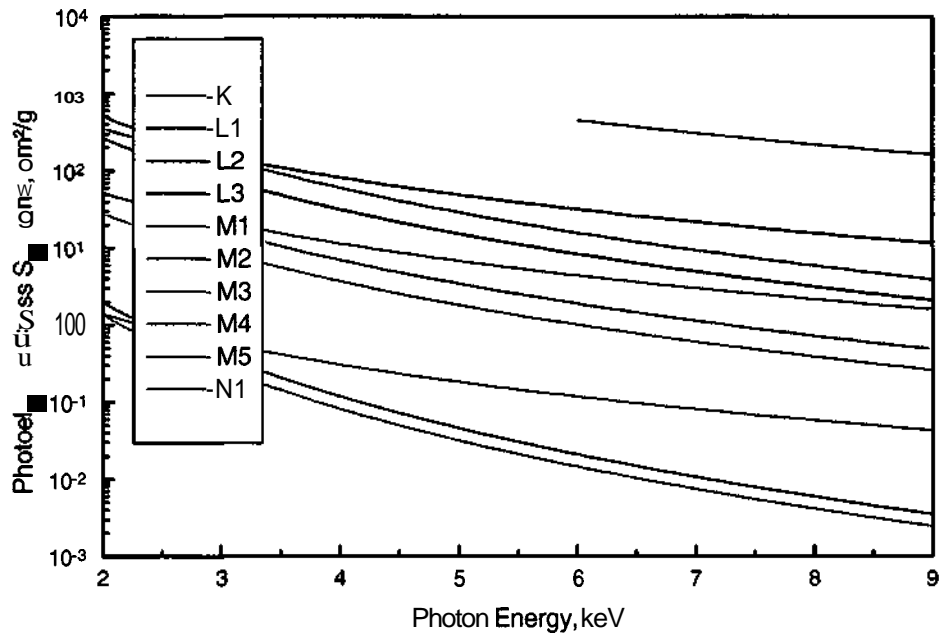


Fig. 3.16 The relation between the photoelectric cross sections of the individual subshells of Chromium versus the photon energy

### 3.3.2 Criticisms

For some elements in the original tables of Scofield, the first values of the data points of the individual photoelectric cross sections of the subshells are less than the next values. In addition, the elements (At-85, Fr-87) have comparably higher first values than the remaining values, particularly in the range of  $M_4$  and  $M_5$  edges. Figs. 3.17 and 3.18 give examples. Fig. 3.17 shows the relation between the photon energy versus the photoelectric cross sections of At-85 for  $M_4$  and  $M_5$  edges. As shown in Fig. 3.17 the first values of both  $M_4$  and  $M_5$  edges are comparably higher than the expected values of extrapolation. Fig. 3.18 shows the relation between the photon energy versus the individual photoelectric cross section of Au-79 for  $M_3$ ,  $M_4$  and  $M_5$  edges. As shown in Fig. 3.18 the first values of both  $M_4$  and  $M_5$  edges are comparably lower than the expected values of extrapolation, whereas the response of  $M_3$  is completely homogeneous. In the normal case, the first value is the greatest of the series of subshell values, as shown in Fig. 3.18 in case of Au- $M_3$ . According to Figs. 3.17 and 3.18, the first values both of  $M_4$  edge and  $M_5$  edge and some sequence of in  $L_2$  and  $L_3$  are questionable. On the other hand, the other edges are completely correct.

Therefore, in the present work, these few data points were excluded from the individual least square fitting of photoelectric cross sections. Table 3.6 shows a list of elements and the subshells that have questionable data points.

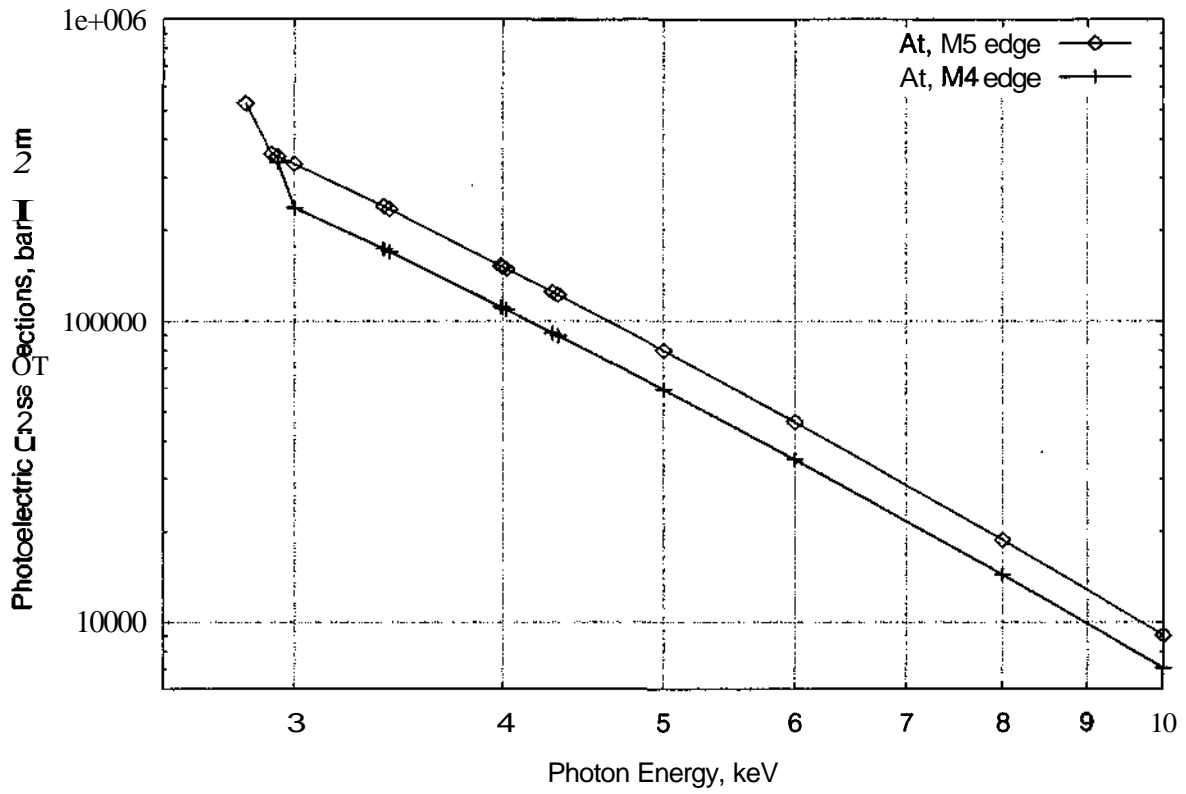


Fig. 3.17 Relation between the individual photoelectric cross section versus the photon energy of both M<sub>4</sub> and M<sub>5</sub> subshells of At.

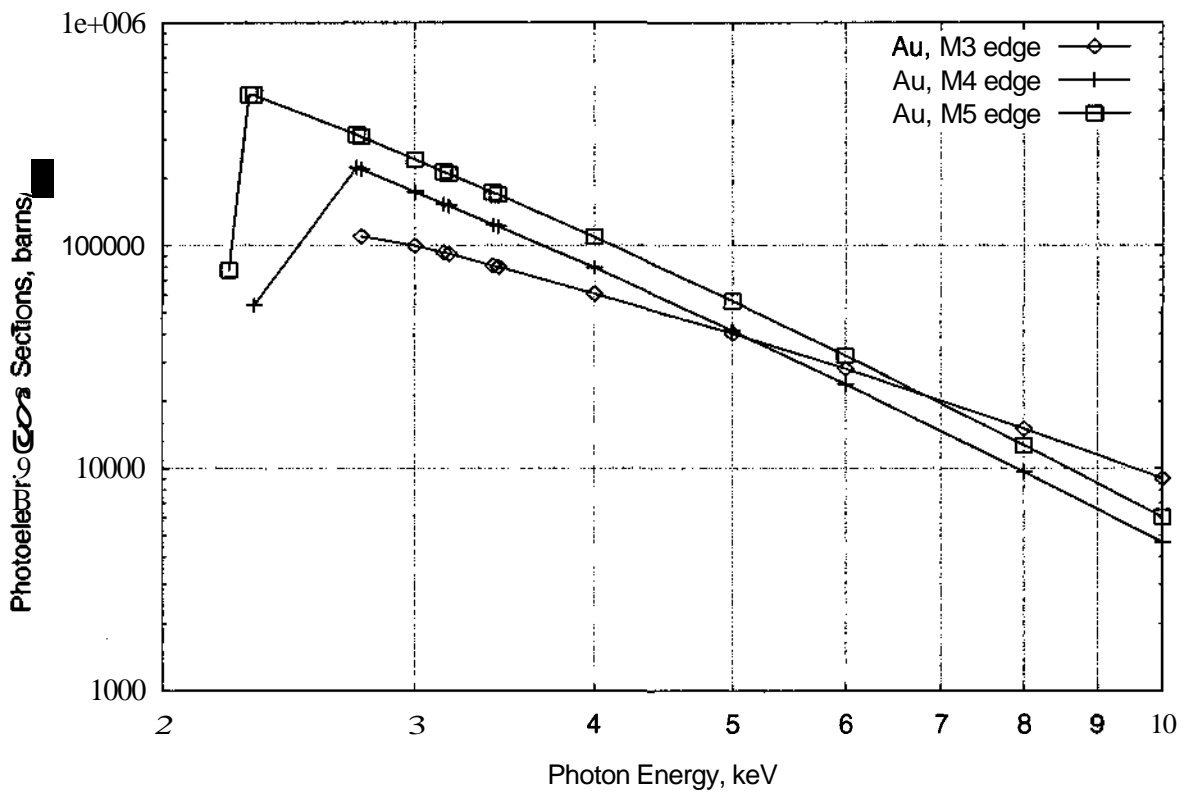


Fig. 3.18 Relation between the individual photoelectric cross section versus the photon energy of both M<sub>3</sub>, M<sub>4</sub> and M<sub>5</sub> subshells of Au.

Table 3.6 Excluded data points in Scofield's data

Element	Edge		Edge	
	Edge	The number of the excluded data points	Edge	The number of the excluded data points
Zn-30	L <sub>2</sub>	1	L <sub>3</sub>	2
Ga-31	L <sub>2</sub>	1	L <sub>3</sub>	1
Ge-32	—	—	L <sub>3</sub>	2
Nd-60	M <sub>4</sub>	1	—	—
Pm-61	M <sub>4</sub>	1	M <sub>5</sub>	2
Sm-62	M <sub>4</sub>	1	M <sub>5</sub>	2
Eu-63	M <sub>4</sub>	1	M <sub>5</sub>	2
Gd-64	M <sub>4</sub>	1	M <sub>5</sub>	2
Tb-65	M <sub>4</sub>	1	M <sub>5</sub>	2
Dy-66	M <sub>4</sub>	1	M <sub>5</sub>	2
Ho-67	M <sub>4</sub>	1	M <sub>5</sub>	2
Er-68	M <sub>4</sub>	1	M <sub>5</sub>	2
Tm-69	M <sub>4</sub>	1	M <sub>5</sub>	3
Yb-70	M <sub>4</sub>	1	M <sub>5</sub>	2
Lu-71	M <sub>4</sub>	1	M <sub>5</sub>	2
Hf-72	M <sub>4</sub>	1	M <sub>5</sub>	2
Ta-73	M <sub>4</sub>	1	M <sub>5</sub>	2
W-74	M <sub>4</sub>	1	M <sub>5</sub>	2
Re-75	M <sub>4</sub>	1	M <sub>5</sub>	2
Os-76	M <sub>4</sub>	1	M <sub>5</sub>	2
Ir-77	M <sub>4</sub>	1	M <sub>5</sub>	2
Pt-78	M <sub>4</sub>	1	M <sub>5</sub>	2
Au-79	M <sub>4</sub>	1	M <sub>5</sub>	1
Hg-80	M <sub>4</sub>	1	M <sub>5</sub>	1
Tl-81	M <sub>4</sub>	1	M <sub>5</sub>	1
Pb-82	M <sub>4</sub>	1	M <sub>5</sub>	1
Bi-83	—	—	M <sub>5</sub>	1
At-85	M <sub>4</sub>	1	M <sub>5</sub>	1
Fr-87	M <sub>4</sub>	1	M <sub>5</sub>	1

### 3.3.3 Least Squares Fitting of Scofield Data

The main aim of the least squares fitting of Scofield data is to get a set of fit coefficients comparable to McMaster's tables. This set of fit coefficients will be used to calculate the total photoelectric cross sections as well as the individual photoelectric cross sections at appropriate photon energy values and energy intervals whereas the total and the photoelectric subshell cross section is one of the main fundamental parameters used in the quantitative analysis using the fundamental parameter approach. Before the least squares fitting of Scofield data, all the excluded points in the different subshell, which are listed in Table 3.6, were cancelled. Memar[83] calculated the fit coefficients of the elements from  $Z=1$  (hydrogen) to  $Z=92$  (uranium) depending on the theoretical photoionization cross section of Scofield. Memar's calculation is valid till 30 keV as a maximum photon energy. So it is not possible to use Memar's fit coefficients for photon energies higher than 30 keV.



In the present investigation, an algorithm is used for the calculation of the fit coefficients for the elements of atomic number  $Z=1$  (hydrogen) to  $Z=94$  (plutonium) by using the least squares fitting. The least square fitting of Scofield's data was performed using a fifth order parabola. The algorithm is called "SCOFTT.BAS" and it is given in chapter 4. The present algorithm enables to read all the information in Scofield's database and calculates the fit coefficients in barns/atom using second, third, fourth and fifth order parabola of the individual subshells. Ninety four data files were produced by using the present algorithm under the name LSF\_XX.DAT (xx means the element). Table 3.7 gives Aluminum as an example for the data files.

Table 3.7 An example of Aluminum Al-13 fit coefficient data file.

Conv=	44.78
K edge	1.5596
a(0)=	12.876542958013030
a(1)=	-1.709076365664478
a(2)=	-0.677451198672250
a(3)=	0.193660111345145
a(4)=	-0.031253016560903
a(5)=	0.002045332968881
L1 edge	0.1177
a(0)=	10.120903169238660
a(1)=	-2.139853621533601
a(2)=	-0.234534781994972
a(3)=	0.028312547430417
a(4)=	-0.003805948436999
a(5)=	0.000343419933539
L2 edge	0.0731
a(0)=	9.086644728276591
a(1)=	-3.147990869334202
a(2)=	-0.175340502047214
a(3)=	-0.000912888551776
a(4)=	0.002394966585441
a(5)=	0.000007734125351
L3 edge	0.0731
a(0)=	9.763365456829177
a(1)=	-3.149498018421944
a(2)=	-0.185881932917000
a(3)=	0.005927682824480
a(4)=	0.000335960226294
a(5)=	0.000185162354014
M1 edge	0.0
a(0)=	7.485376175567705
a(1)=	-2.170470214362852
a(2)=	-0.206871381539542
a(3)=	0.018376658902399
a(4)=	-0.002164305525239
a(5)=	0.000240254912950
M2 edge	0.0
a(0)=	3.980467103780270
a(1)=	-3.075421897566031
a(2)=	-0.207329046963373
a(3)=	0.008027544223220
a(4)=	0.000991480822013
a(5)=	0.000095782892545
M3 edge	0.0
a(0)=	4.657686383791889
a(1)=	-3.076922018735227
a(2)=	-0.220762686003341
a(3)=	0.016323628147637
a(4)=	-0.001317918364826
a(5)=	0.000289433480657

The data file of Aluminum contains the conversion factor to convert from barns/atom to  $\text{cm}^2/\text{g}$ , the edge energies in keV and the new fit coefficients of each subshell respectively. The other elements from atomic number  $Z=95$  (americium) to  $Z=102$  (Nobelium) are not of interest. Ebel[103] developed the mentioned data files (LSF\_XX.DAT) and produced another set of data files called XX.MU (XX means the element) which are more useful. Cross sections are given in  $\text{cm}^2/\text{g}$ . The coherent and incoherent scattering are not included in Scofield's database. Therefore, in order to calculate the mass absorption cross sections from Scofield's data, coherent and incoherent scattering were provided from Elam's database[80]. As given in Table 3.8, for each element, the data file contains

- Element Symbol, atomic number and atomic weight.
- The fit coefficients using fifth order parabola of the coherent and incoherent cross sections which are calculated from Elam database[80].
- The fit coefficients using fifth order parabola of the individual subshells and the sum of K, L, M and N shells as well as the edge energies and the related jump ratios.

Table 3.8 An example of Aluminum Al-13 fit coefficient of Ebel[103] data files.

Al	Z	A	rho			
13	26.97		2.7020E+00			
Al	coherent and incoherent lsf-coefficients					
	8.12846D-01	-2.77190D-01	9.52812D-02	-1.74117D-01	3.52346D-02	-2.28175D-03
	-4.23404D+00	1.41843D+00	-4.04661D-01	1.11095D-01	-2.17371D-02	1.56199D-03
Al	edge-energies edge-jumps and Isf-coefficients					
K	1.55960	11.04798				
	9.07478E+00	-1.70908E+00	-6.77451E-01	1.93660E-01	-3.12530E-02	2.04533E-03
L1	0.1177	1.00000				
	6.31914E+00	-2.13985E+00	-2.34535E-01	2.83125E-02	-3.80595E-03	3.43419E-04
L2	0.0731	1.00000				
	5.28488E+00	-3.14799E+00	-1.75341E-01	-9.12888E-04	2.39497E-03	7.73400E-06
L3	0.0731	1.00000				
	5.96160E+00	-3.14950E+00	-1.85882E-01	5.92768E-03	3.35960E-04	1.85162E-04
M1	0.0000	1.00000				
	3.68361E+00	-2.17047E+00	-2.06871E-01	1.83767E-02	-2.16430E-03	2.40254E-04
M2	0.0000	1.00000				
	1.78705E-01	-3.07542E+00	-2.07329E-01	8.02754E-03	9.91480E-04	9.57820E-05
M3	0.0000	1.00000				
	8.55925E-01	-3.07692E+00	-2.20763E-01	1.63236E-02	-1.31792E-03	2.89433E-04
global data						
Al	Isf-coefficients of K- L- M- and N-range					
	9.19448E+00	-1.78566E+00	-6.27948E-01	1.77936E-01	-2.88295E-02	1.90100E-03
	7.07665E+00	-2.64277E+00	-8.10773E-02	3.18226E-03	-1.15238E-03	5.33374E-04
	0.00000E+00	0.00000E+00	0.00000E+00	0.00000E+00	0.00000E+00	0.00000E+00
	0.00000E+00	0.00000E+00	0.00000E+00	0.00000E+00	0.00000E+00	0.00000E+00

In the present investigation, the new data files[103] are used to obtain Scofield's x-ray cross sections (Scofield approximation). Figs. 3.19, 3.20, 3.21 show relative deviation from the original Scofield's data at fifth order parabola at maximum photon energy range 1 - 300 keV respectively. Figs. 3.19, 3.20, 3.21 were performed for *Mn*, *Eu* and *Bi* for the total subshells. According to Figs. 3.19, 3.20, 3.21, the fifth order parabola was used because it produced the minimum relative error when compared to the fourth, third order parabola. Therefore, the present fit coefficients are valid in the range from 1 keV to 300 keV and the new fit coefficients can be used afterwards in our quantitative analysis programs. To see the difference between the present fit coefficients and the original data of Scofield. Figs. 3.22 and 3.23 show the relation between the photon energy and the individual photoelectric cross section of the  $L_1$  and  $L_2$  subshells of gold. These Figs. have been performed by using the present fit coefficients ( called "approximation") and the original data point of Scofield. According to Figs. 3.22 and 3.23, it is shown that, the new fit coefficients give completely identical T-values with the original data of Scofield in the photon energy range from 1 to 300 keV.

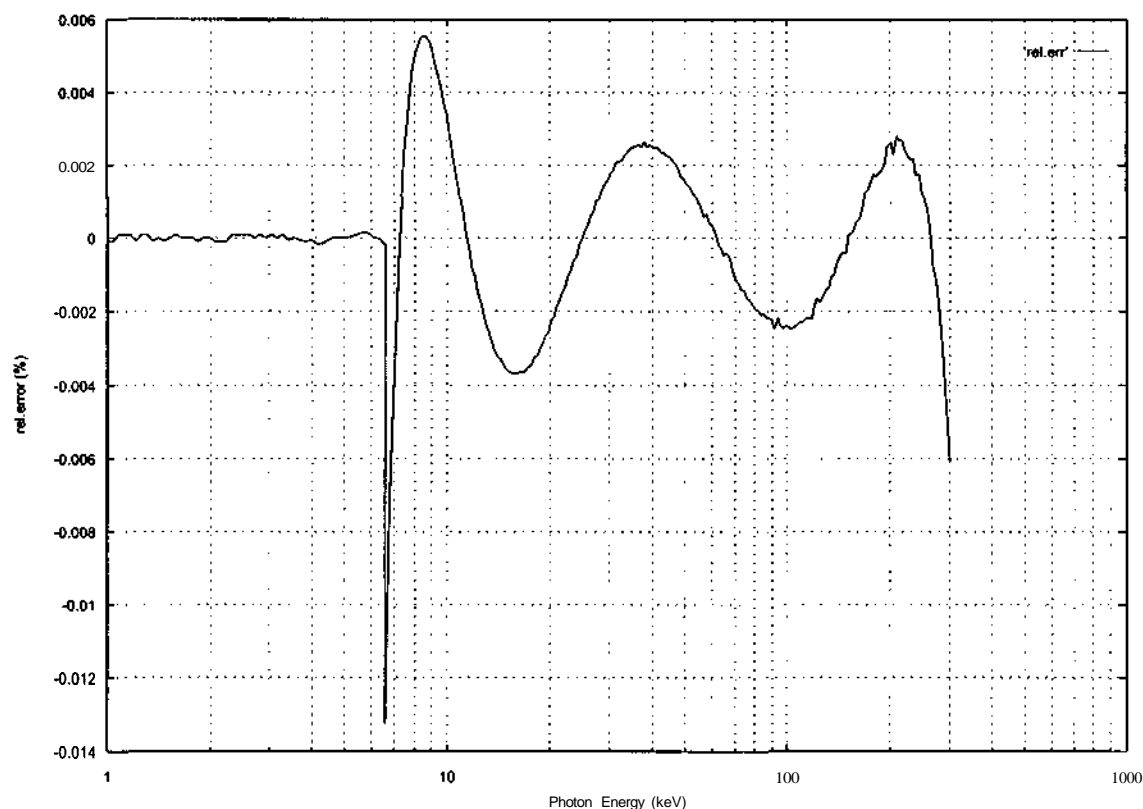


Fig. 3.19. Relation between the relative deviation of Mn versus photon energy.

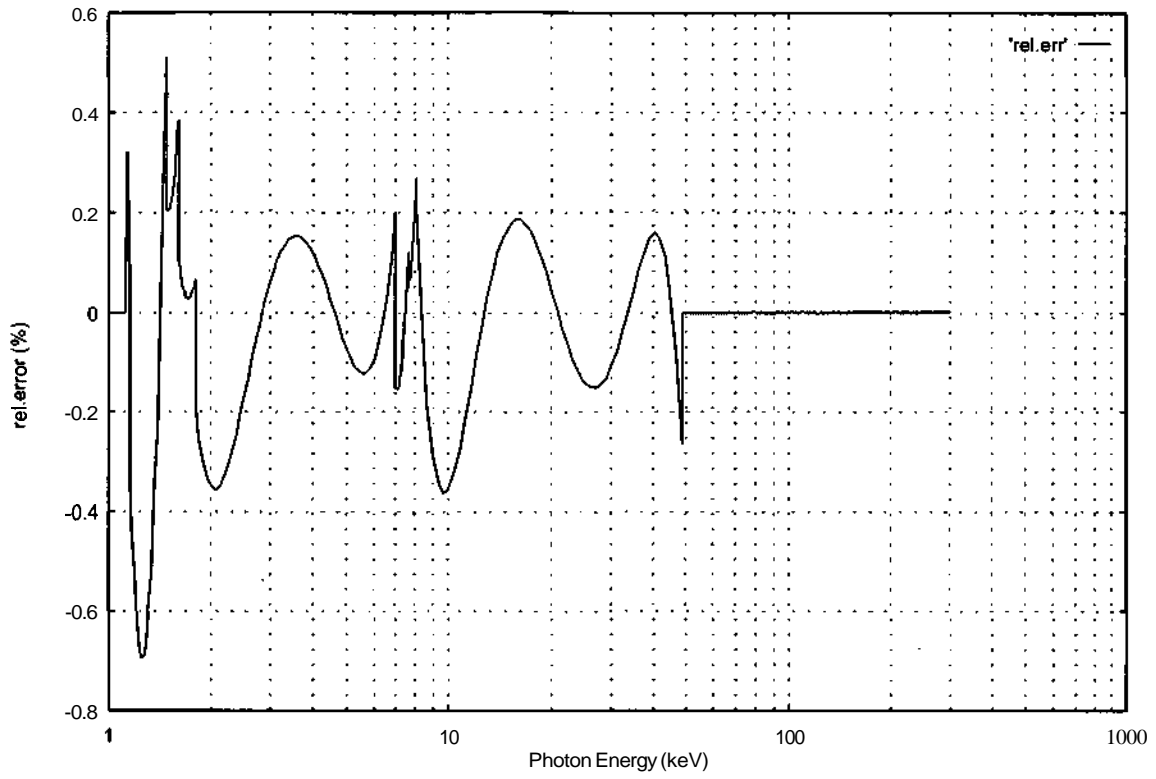


Fig. 3.20 Relation between the relative deviation of Eu versus photon energy.

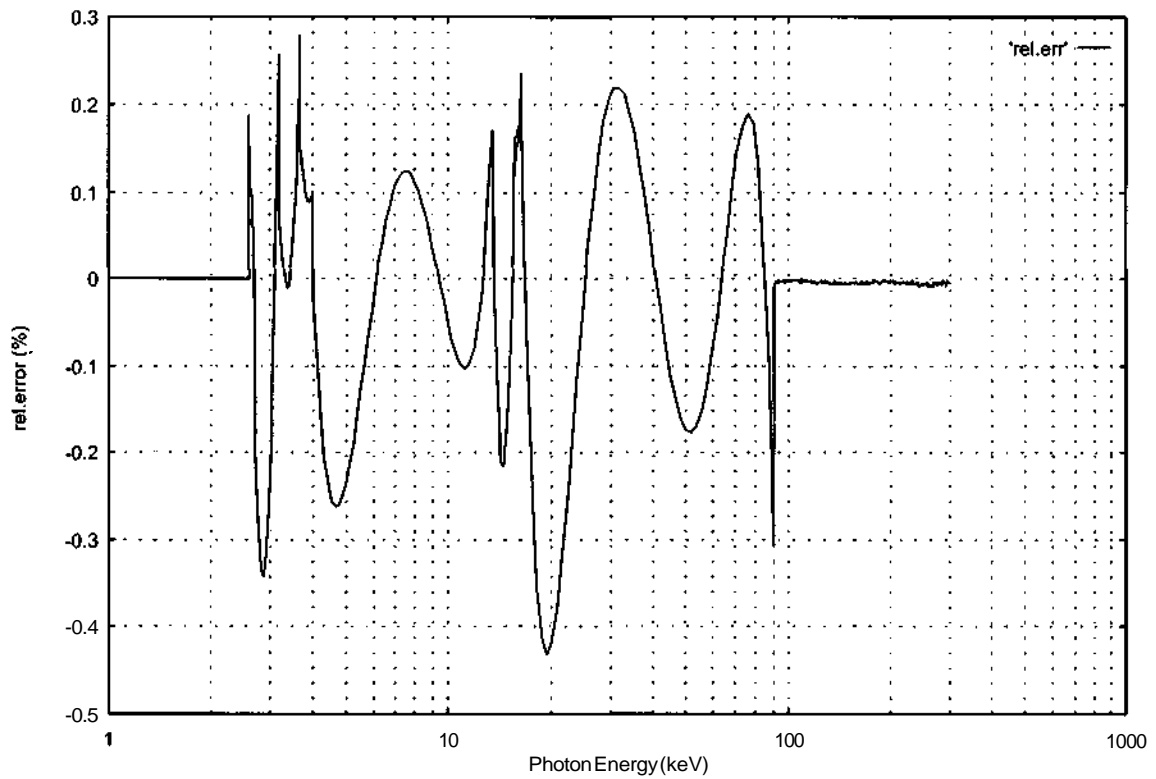


Fig. 3.21. Relation between the relative deviation of Bi versus photon energy.

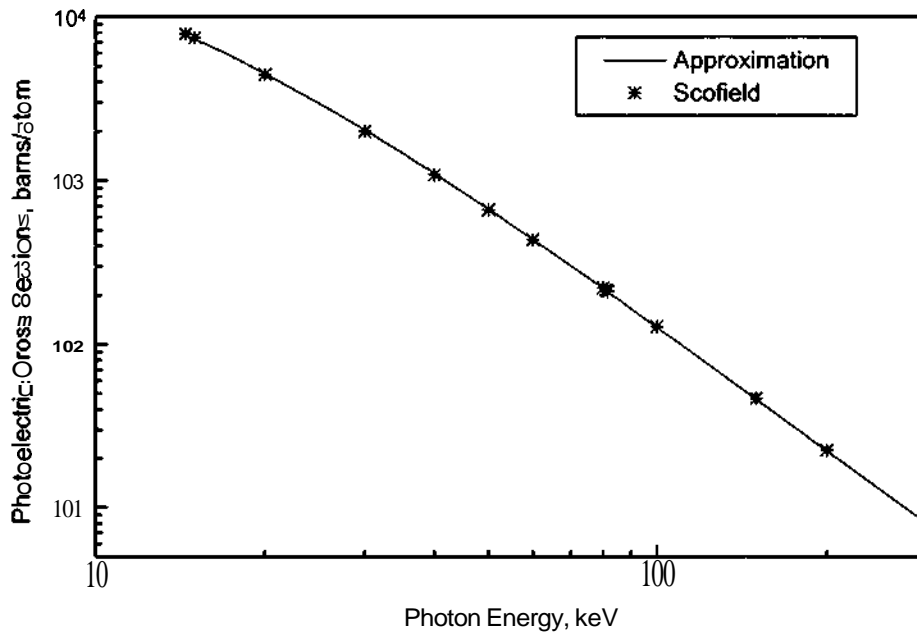


Fig. 3.22 Comparison between T-values from the new fit coefficients and the original data points of Scofield, Au-L<sub>1</sub>.

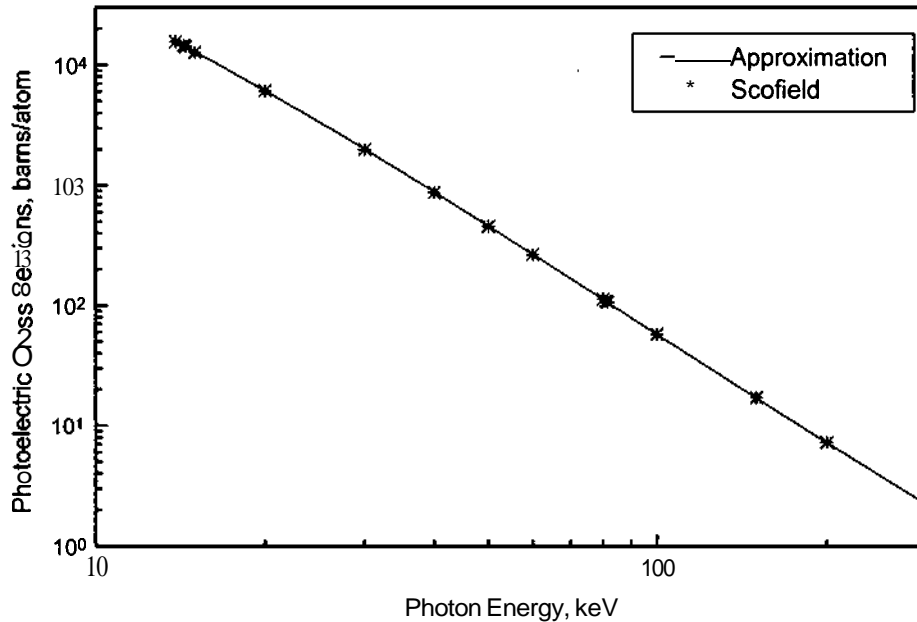


Fig. 3.23 Comparison between T-values from the new fit coefficients and the original data points of Scofield, Au-L<sub>2</sub>.

According to the present approximation[103] a computer algorithm was used for the calculation of photoelectric cross sections, coherent scattering, incoherent scattering and the mass absorption coefficient. Fig. 3.24 compares the photoelectric cross section of the original Scofield data and the present approximation of Scofield using the least squares fit for Gd. A

remarkable difference appears at the  $M_4$  and  $M_5$  edges. Also, a slight difference appears in the edge positions whereas Bearden's values were used in the present approximation of Scofield's data rather than the mentioned values in the original Scofield's database. On the other hand, Fig. 3.25 describes a relation between the different cross sections versus the photon energy depending on Scofield's database and Elam's scattering data.

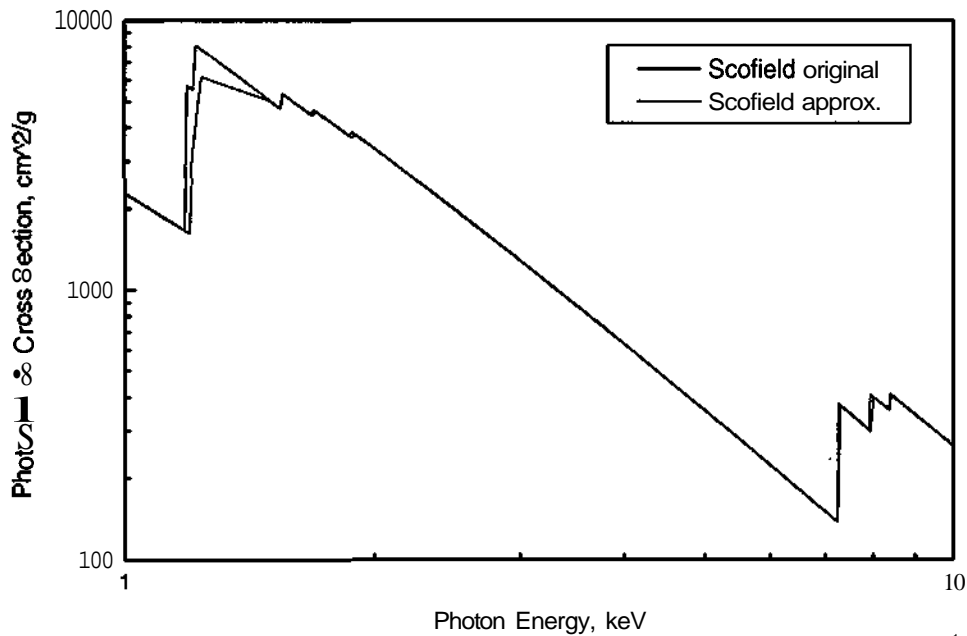


Fig. 3.24 Comparison between the photoelectric cross section of the original and the present approximation of Scofield's data for Gd.

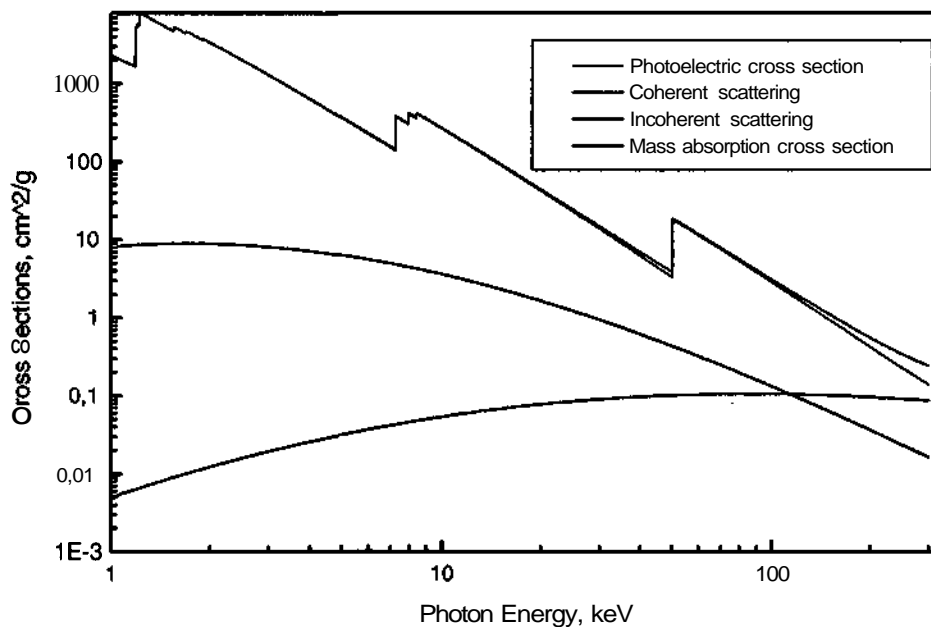


Fig. 3.25 Relation between cross sections versus the photon energy depending on Ebel's[103] approximation of Scofield's database for Gd.

### 3.3.4 Comparison Between Edge Energy Values of Scofield and Bearden

The theoretical results of Scofield are strictly valid only for free atoms. For molecules and solids there are differences, particularly near absorption edges. Also, the binding energy values of x-ray levels (edge energies) of Scofield are not recommended, because it depends on theoretical calculations of Scofield. In the present work, the experimental binding energy values of x-ray levels of Bearden[81] were used since Bearden's values are from experimental measurements. To see the difference between the binding energy values of x-ray levels in both Scofield and Bearden, Fig. 3.26 gives a comparison between the binding energy of the x-ray level values for the individual shells from K to O<sub>5</sub> for Pu. The energies of the x-ray levels from Q<sub>1</sub> level to Q<sub>6</sub> level are not included. Fig. 3.27 shows the relation between the relative deviation between Bearden and Scofield  $RD\%_E$  versus the binding energy values of Pu.

$$RD\%_E = \frac{E_{\text{Bearden}} - E_{\text{Scofield}}}{E_{\text{Scofield}}} \times 100 \quad (3.11)$$

It was shown that the relative deviation,  $RD\%_E$  increases in the higher x-ray levels, ( $RD\%_E \approx 5\%$ ). In the lower x-ray levels the relative deviation is relatively small. (less than 1%).

It was found that the edge energy values of Bearden are not complete. Therefore, the missing values of the edge energies were taken from Siegbahn[84] and Cardona and Ley[104]. Table 3.9 gives the values of the edge energy from Siegbahn[84] and Cardona and Ley[104] instead of the missing values in Bearden's tables. Also, it was found that there are some edge energy values not included in all of the sources such as La N<sub>6</sub> and N<sub>7</sub>.

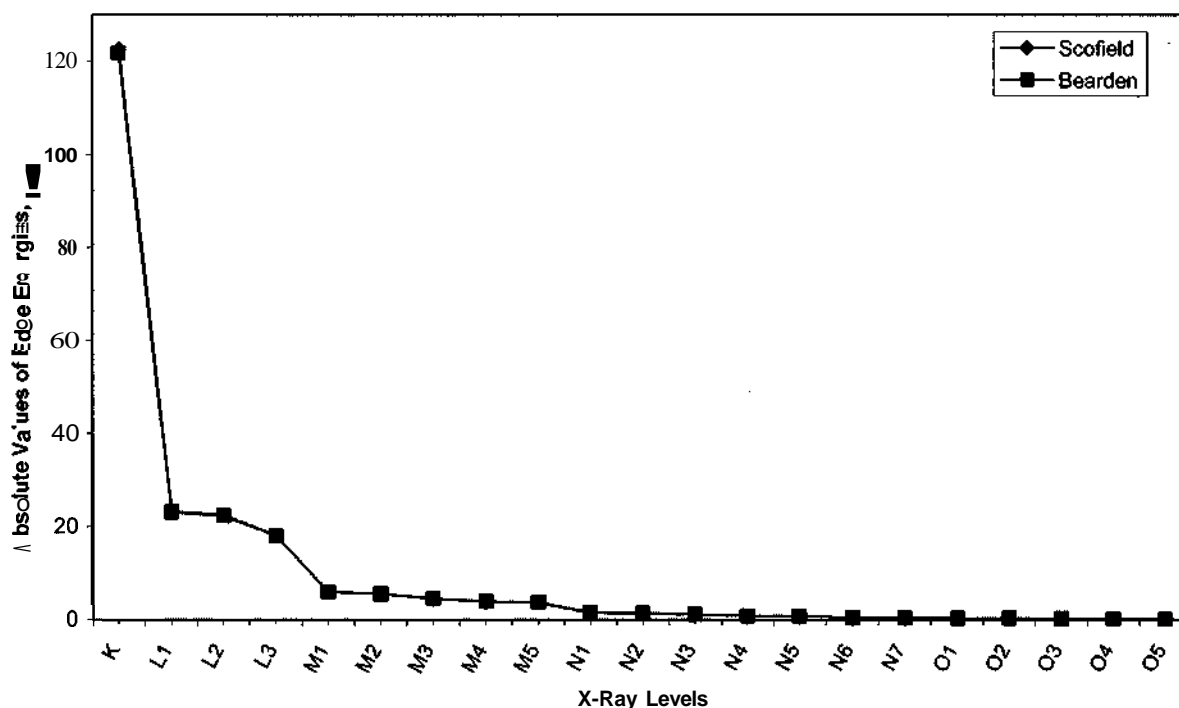


Fig. 3.26 Comparison between the x-ray levels values in Scofield and Bearden for Plutonium.

Table 3.9 The missing edge energy values in Bearden's tables .

El.	X-ray Level	Edge Energy, keV	EL	X-ray Level	Edge Energy, keV
Kr	M1	0.2928	At*	O3	0.115
Tc	M1	0.544	At*	O4, O5	0.040
Xe*	M1	1.1487	At**	P1	0.018
Xe*	M4	0.689	At**	P2, P3	0.008
Xe*	N1	213.2	Rn*	N5	0.541
Xe*	N4	69.5	Rn*	N6, N7	0.238
Xe*	N5	67.5	Rn*	O1	0.214
Xe*	O1	23.3	Rn*	O2	0.164
Xe*	O2	13.4	Rn*	O3	0.127
Xe*	O3	12.13	Rn*	O4, O5	0.048
Pm**	M1	1.650	Rn**	P1	0.026
Pm**	N1	0.331	Rn**	P2, P3	0.011
Pm**	N6, N7	0.004	Fr*	N6, N7	0.268
Pm**	O1	0.038	Fr*	O1	0.234
Pm**	O2, O3	0.022	Fr*	O2	0.182
Bi**	P1	0.008	Fr*	O3	0.140
Po*	N6, N7	0.184	Fr*	O4, O5	0.058
Po*	O1	0.177	Fr*	P1	0.034
Po*	O2	0.132	Fr*	P2, P3	0.015
Po*	O3	0.104	Ac*	N5	0.639
Po**	P1	0.012	Ac*	N6, N7	0.319
Po**	P2, P3	0.005	Ac*	O1	0.272
At*	N5	0.507	Ac*	O2	0.215
At*	N6, N7	0.210	Ac*	O3	0.167
At*	O1	0.195	Ac*	O4, O5	0.08
At*	O2	0.148	Np**	O1	0.338

\* Cardona and Ley[104].

\*\* Siegbahn84]



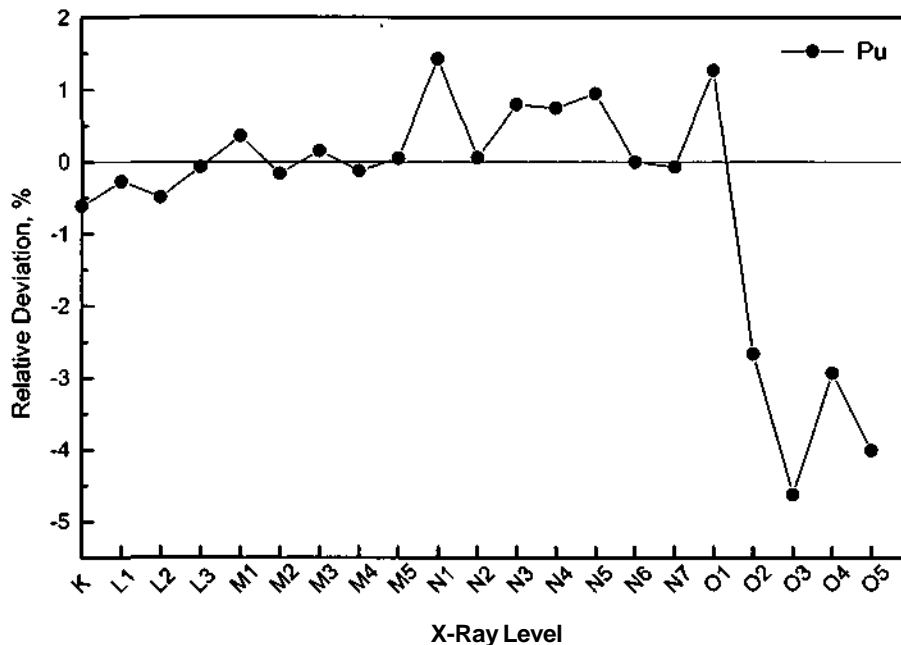


Fig. 3.27 The relative deviation between the binding energy of the x-ray levels of Bearden and Scofield

### 3.4 XCOM Database

In 1987 Berger and Hubbell[105] created the XCOM database of the cross sections and attenuation coefficients for the elements (from atomic number  $Z=1$ , (Hydrogen) to  $Z=100$ , (Fermium)), compounds and mixtures at photon energies between 1 keV to 100 GeV. The XCOM database includes the coherent scattering cross section, incoherent scattering cross section, photoelectric cross section and the pair production cross section (in nuclear and electron fields). They obtained the incoherent scattering cross sections[106] from a combination of the Klein-Nishina formula and nonrelativistic Hartree-Fock incoherent scattering functions including radiative and double Compton-scattering corrections. In addition they added the coherent scattering cross sections[107] from a combination of the Thompson formula and relativistic Hartree-Fock atomic form factors. Also, they obtained the photoelectric cross sections from the present database of Scofield[79]. As mentioned above, Scofield's database extends only up to 1.5 MeV. At higher energies, where the photoelectric cross section is quite small, Berger and Hubbell used a semi-empirical formula[108, 109] in order to link Scofield's values at 1.5 MeV to the asymptotic high-energy limit. Berger and Hubbell omitted the renormalization of the Scofield cross sections in the database for the XCOM database whereas some reviews[110] indicate that on the whole, agreement with experiment is better when the renormalization is not done. They interpolated the combined photoelectric absorption cross section for all shells with use of log-log cubic-spline fits, but only at energies above the K-shell absorption edge. Below this energy, interpolation is applied to the logarithm of the photoelectric absorption cross section for each separate shell and fitted as a linear function of the logarithm of the photon energy. They used separate fitting for each shell to avoid the error that would be introduced by interpolating across absorption edges.

They obtained the cross sections for pair production from Hubbell[93] which are based on complicated combinations of formulas from Bethe-Heitler theory with various other theoretical models to take into account screening, Coulomb, and radiative corrections. Different

combinations were used in the near-threshold, intermediate and high-energy regions to obtain the best possible agreement with experimental cross sections. In this work the cross sections of the pair production are not of interest.

According to XCOM database, Berger and Hubbell developed the XCOM software package and the final version of the XCOM program (version 3.1) is available in the NIST web page[111] which contains the data files of each element, FORTRAN-77 source code, and compiled executables. In the present work, version 3.1 of XCOM database was used. The XCOM program provides total cross sections and attenuation coefficients as well as partial cross sections for the following processes: incoherent scattering, coherent scattering, photoelectric absorption, and pair production in the field of the atomic nucleus and in the field of the atomic electrons. For compounds, the quantities tabulated are partial and total mass interaction coefficients, which are equal to the product of the corresponding cross sections times the number of target molecules per unit mass of the material. Berger and Hubbell mentioned that the main limitations of the XCOM database is the cross sections for elements pertain to isolated neutral atoms, and do not take into account molecular and solid-state effects which modify the cross sections, especially in the vicinity of absorption edges. Fig. 3.28 illustrates the different cross sections of XCOM database versus the photon energy. To see the difference between XCOM database and Scofield's database, Fig. 3.29 compares between the XCOM database, original Scofield's database and the present approximation of the Scofield's database for Gd. According Fig. 3.29, both XCOM database and original Scofield's database are not well described in the  $M_4$  and  $M_5$  edges. On the other side, such problems were already solved as mentioned above in the present approximation of Scofield's database. In addition, although XCOM database depends basically on the Scofield's database, there are some differences between them in  $M_4$  and  $M_5$  edges. The difference between the three curves as illustrated in Fig. 3.29 in the  $M_4$  and  $M_5$  edges originated from that, the Bearden's experimental values of the absorption edges were used in the present approximation which are completely different from Scofield's theoretical values as well as the absorption edge values used in XCOM database. These differences are not observed in both K and L edges.

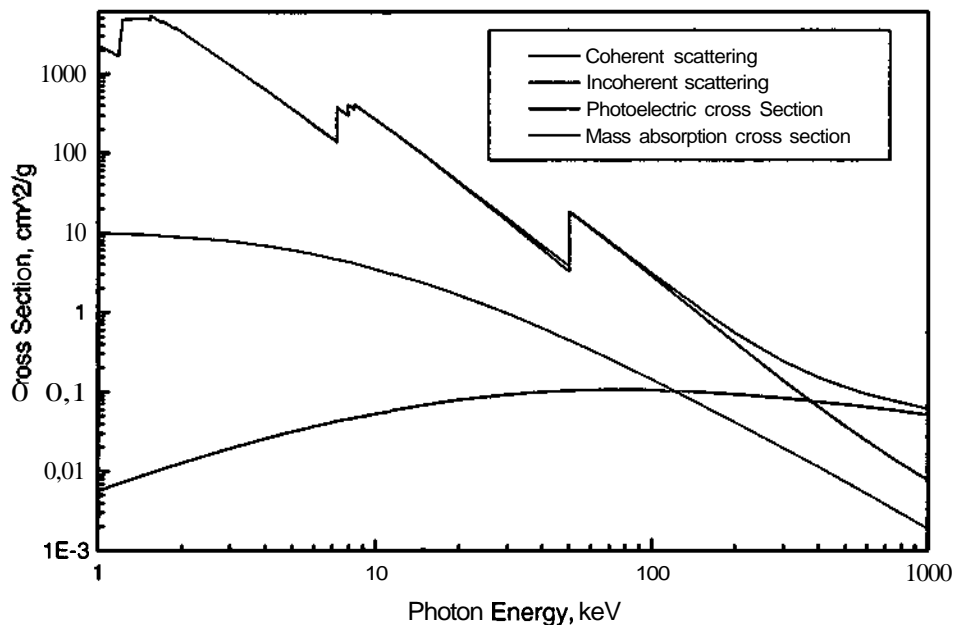


Fig. 3.28 Relation between x-ray cross sections versus the photon energy according to XCOM database for Gd.

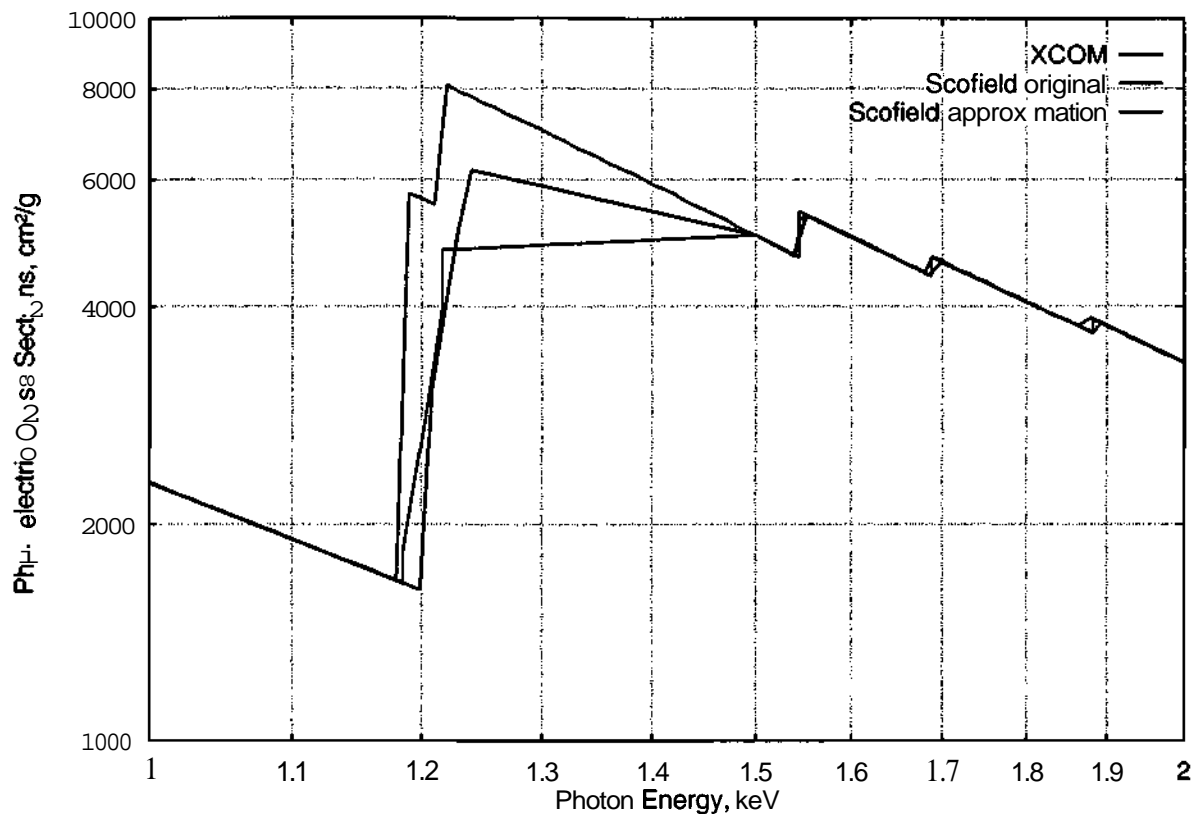


Fig. 3.29 Relation between photoelectric absorption coefficients versus photon energy, for Gd depending on Scofield's database.

### 3.5 Elam's Database

Elam[80] modified the XCOM database without any corrections in  $M_4$  and  $M_5$  edges. He found the following minor errors,

- The  $L_1$  edge entered as  $L_3$  edge in the three data files of In, Sn, and Sb
- In the data file of the element Re, the correct value of the  $M_5$  edge is 1883 eV.
- The edge energies of the data files of the elements Mo, Fr, Ra, Ac, and U are not entered with enough precision to match the energies in the list of edges in the beginning of the file.

Therefore Elam[80] produced a new database from the XCOM database including full information about element symbol, atomic number, atomic weight, density, edge symbol, edge energy, fluorescence yield, jump ratio, transition probability from each subshell, and the total transition probability. In Elam's database, the values of the energies are in eV and the values of cross sections are in  $\text{cm}^2/\text{g}$  and both of them were given in logarithmic scale. A computer algorithm has been developed for Elam's database which can be used afterward in the theoretical quantitative analysis. This computer algorithm can be used to obtain the cross sections of coherent, incoherent, photoelectric and total mass absorption by using the spline interpolation of log values via Numerical Recipes spline evaluation routine "SPLINT"[112]. According to Elam's database, Fig. 3.30 illustrates the relation between the x-ray cross sections versus the photon energies for Gd. To see the difference between XCOM and Elam's database, Fig. 3.31 shows a comparison between the photoelectric cross section of Gd using Scofield's fit of the present approximation, Scofield's original, XCOM, and Elam's databases. As shown in Fig. 3.31, it becomes clear that, Elam's database is the same as XCOM's database with the exception of the mentioned minor errors. According to Fig. 3.31, the edge energies used in Elam's database are slightly different from that mentioned in XCOM's database. Therefore, a small difference between XCOM's and Elam's databases appears near the edges.

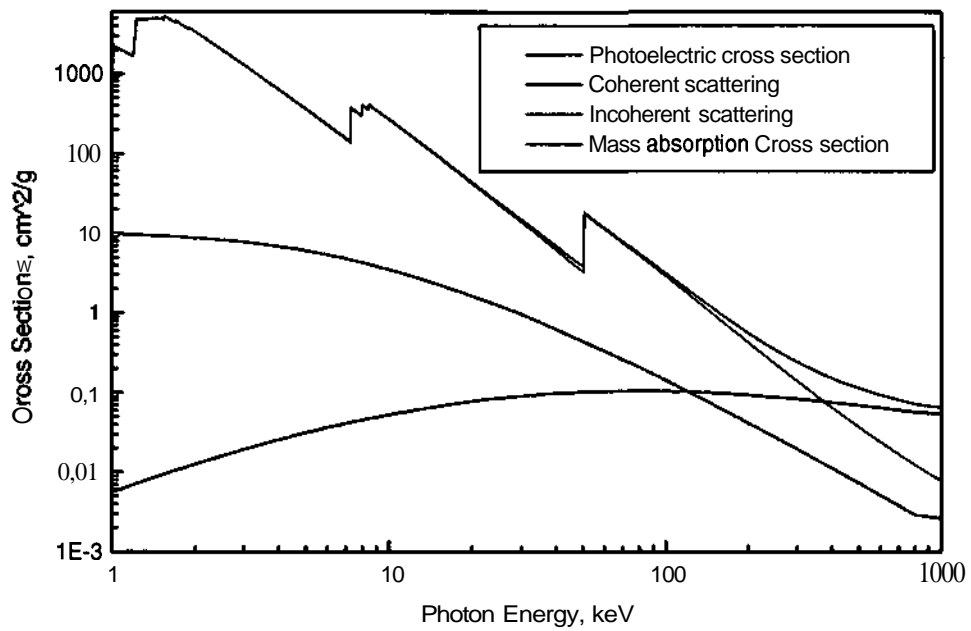


Fig. 3.30 Relation between cross sections versus photon energy for Gd depending on Elam's database.

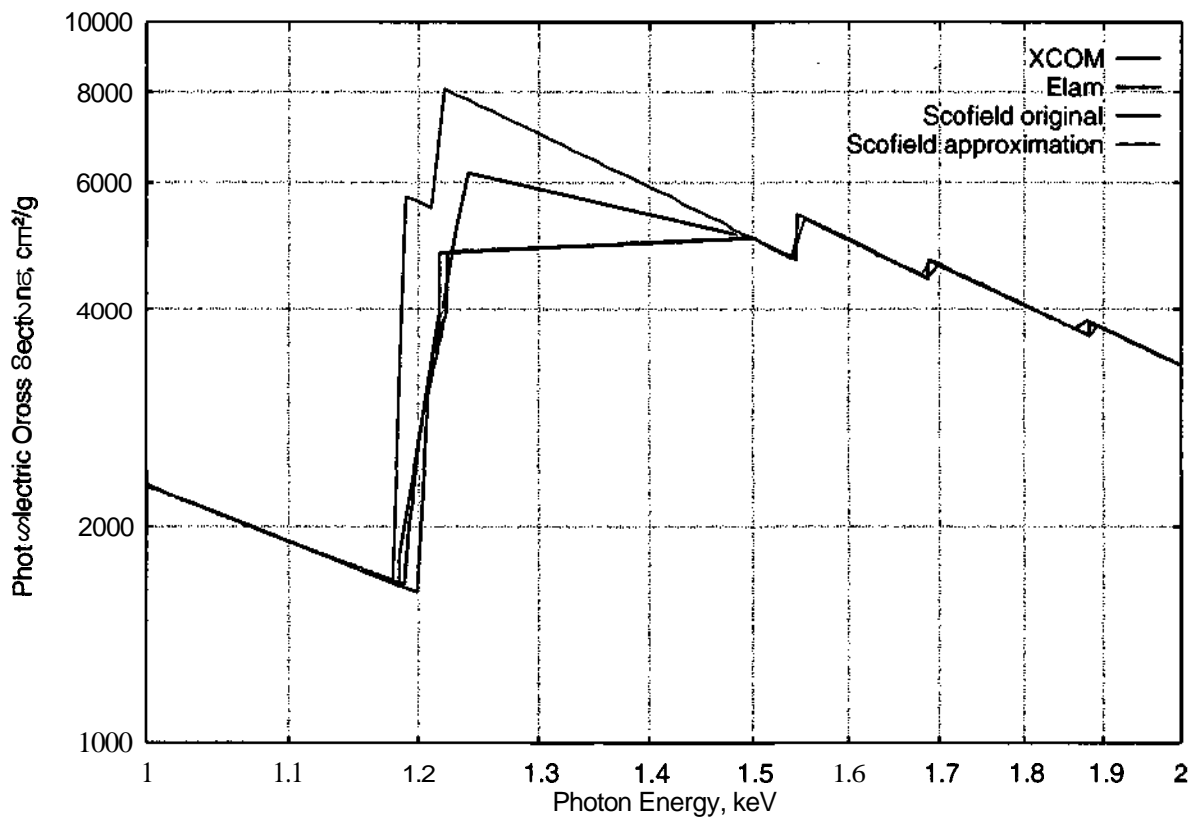


Fig. 3.31 Relation between photoelectric absorption coefficients versus photon energy, for Gd depending on Scofield's database.

### 3.6 Cullen's Database

In 1997, Cullen distributed the evaluated nuclear and atomic database of LLNL, (Lawrence Livermore National Laboratory, Livermore, USA) in a machine-independent character file formats whereas these data are requested in multiple applications as mentioned above. All these data files are available for downloading in the LLNL's homepage[113]. These databases consist of

- The Evaluated Atomic Data Library EADL[114, 115], which includes data to describe the relaxation of ionized atoms back to neutrality, during which photons (fluorescence x-rays) and electrons (Auger and Coster-Kronig) are emitted. It is assumed that the relaxation of an ionized atom is independent of how the atom was ionized, so that this data may be used to describe the relaxation of atoms that were ionized due to either photoionization or electroionization.
- The Evaluated Photon Data Library EPDL[116] that includes data to describe the transport of photons, as well as the initial generation of secondary particles, such as the primary electron emitted due to photoionization or Compton scattering, as well as the electron/positron pair emitted due to pair production.
- The Evaluated Electron interaction Data Library EEDL[117] that includes data to describe the transport of electrons, as well as the initial generation of secondary particles, such as the primary photon due to bremsstrahlung, as well as the primary electron due to inelastic scattering and electronionization.
- The Evaluated Excitation Data Library, EXDL which includes data to describe photoexcitation lines.

All these databases span atomic numbers between  $Z=1$  (hydrogen) and 100 (fermium). Additionally, both EEDL and EPDL databases cover the incident particle energy range from 10 eV to 100 GeV. Also in 1997 Cullen upgraded the old version of the EPDL database (EPDL89)[98] and replaced it by a new database, (EPDL97) which includes data down to 1 eV and all of the most recently available theoretical and experimental data. In the present work the terminology EPDL refers to EPDL97[116] data which has been calculated to higher precision and includes more data points to allow more accurate interpolation between tabulated data points. As the previous databases EPDL data is only applicable to cold, neutral, isolated atoms and no data are provided for compounds or mixture. That means that Cullen didn't consider atoms in environments which can have significant effect on the cross sections near the absorption edges of inner shell electrons and completely alter the cross sections near the edges of the outer shells.

According to the present application of the quantitative analysis using the fundamental parameter method, only the EPDL database was used in the present work and the other databases are not of interest. In EPDL database, the unit of photon energy is MeV and the unit of the cross section is barns/atom. The EPDL database consists of integrated cross section and the related average energy of the following reactions,

- Coherent scattering  
The coherent scattering cross sections are based on the combination of Thomson scattering, form factors, and anomalous scattering factors, which were numerically integrated to define the cross section. The form factors were obtained from Hubbell's calculation[17, 107, 118] of nonrelativistic, relativistic and modified relativistic form factors. On the other hand, Cullen computed the anomalous scattering factors using the relativistic dispersion relation of Pratt [119] from 1 eV to 10 MeV were not considered. The anomalous scattering factors at photon energy higher than 10 MeV, because it has less effect on the coherent cross section. Also the anomalous scattering factors cause very large decreases in the coherent scattering cross

section near absorption edges which improve the accuracy of the coherent scattering cross section.

- Incoherent scattering

The incoherent scattering cross sections are based on the combination of Compton scattering described by the Klein-Nishina formula and Hubbell's scattering function[17, 107, 118].

- Photoelectric cross section of the subshell

Cullen defined the cross sections for all subshells from the edge energy to 100 GeV by combination between the Kissel's data using Scofield's subshell cross sections from the edge energy up to 1 MeV and Hubbell's total photoionization cross sections from 1 keV to 100 GeV.

- Total photoelectric cross section

The total photoelectric cross section is the sum of the subshells cross sections mentioned above.

- PaK production cross section

PaK production cross sections were taken from Hubbell[93] from their threshold at 1.022 MeV up to 100 GeV.

- Triple production cross section

The triple production cross sections are also taken from Hubbell[93] which are included from their threshold at 2.044 MeV up to 100 GeV.

Cullen has already illustrated the formats and the definitions of the EPDL parameters as guidelines which are valuable to understand and to use these data in any kind of programming language. Although EPDL data has been extended down to 1 eV, Cullen mentioned that there are large uncertainties in the current data at low energies. Fig. 3.32 shows the relation between the cross sections of photoelectric, coherent and incoherent versus the photon energy for Gd from Cullen's database, (EPDL). The anomalous scattering factors cause very large decreases in the coherent scattering cross section near absorption edges which are described in Fig. 3.32. Also, to see the differences between Cullen's database and the other discussed databases, (present approximation, Scofield, XCOM and Elam), Fig. 3.33 shows a comparison between the photoelectric cross section of Gd using all of these databases. As shown in Fig. 3.33, it becomes clear that, Cullen's database basically depends on the photoelectric cross sections of the subshells of Scofield. In addition, according to Cullen's processing of his database, the M edges are well described, especially  $M_4$  and  $M_5$  edges as shown in Fig. 3.33 which is not described in Scofield's database.

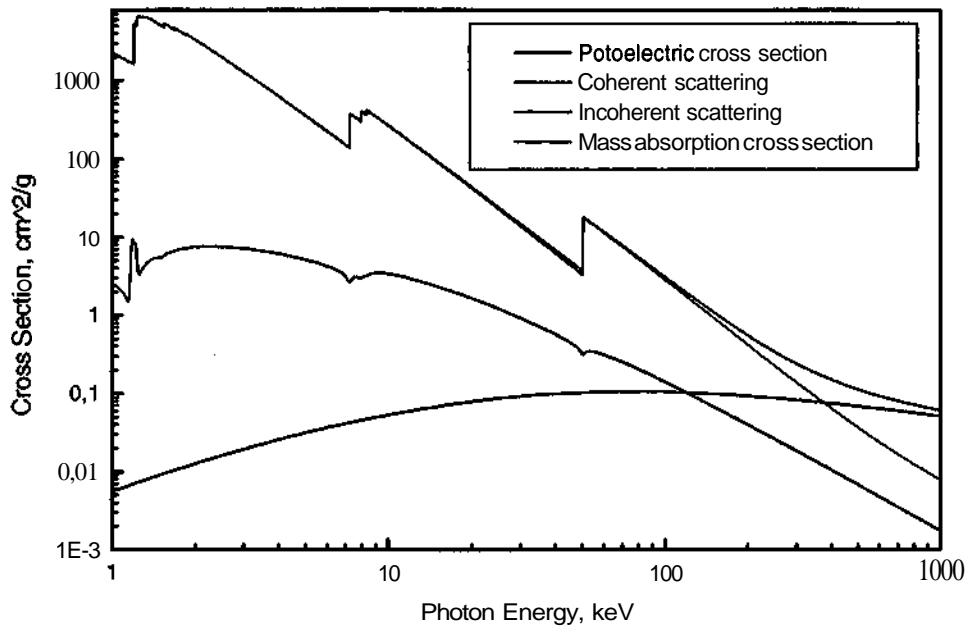


Fig. 3.32 Relation between the cross sections of Gd versus photon energy, depending on Cullen's database.

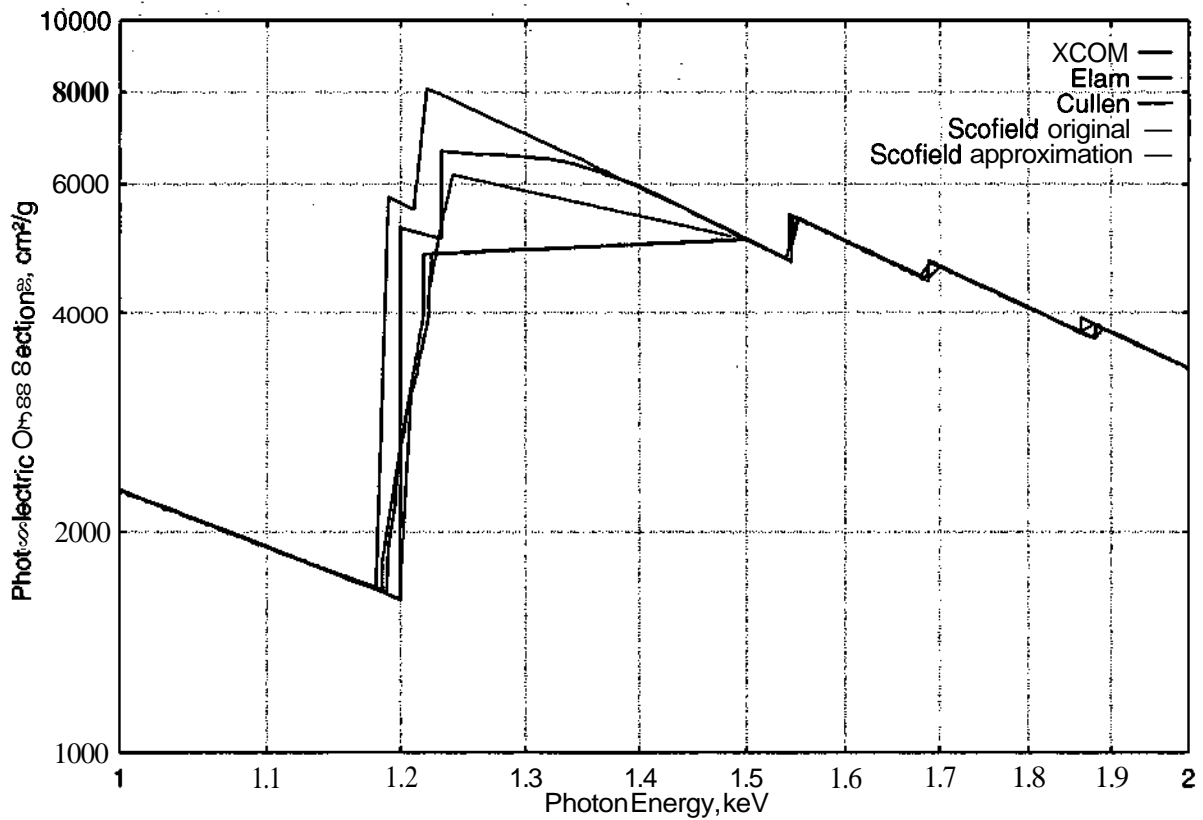


Fig. 3.33 Relation between photoelectric cross section versus photon energy, for Gd.

### 3.6.1 EPICSHOW program

EPICSHOW[120] is a mouse driven interactive graphics program with LLNL's databases that is designed to run on UNIX, IBM, and MAC computers. All data included in this program are based on Cullen's evaluated nuclear and atomic database of LLNL. The EPICSHOW program is written in standard Fortran that can be run on any computer. The main screen layout of EPICSHOW is divided into two parts, the lower part is used to display data and the upper part is used to identify the version of the code and to display options. It is easy to display a kind of data library by selecting it from the upper part of the program's screen layout. Fig. 3.34 illustrates a screen layout of EPICSHOW programs for Gd.

There are some differences between the EPDL database and the abstracted data from the EPICSHOW program, especially in the coherent scattering cross sections and in M-edges. Therefore, the abstracted data from EPICSHOW program is intended only for viewing and estimating data and it is not intended for use in applications. To describe the differences between the EPDL database and the abstracted data from EPICSHOW, Fig. 3.35 shows a comparison between both of them for Gd. Therefore, the abstracted data from EPICSHOW does not consider the  $M_4$  and  $M_5$  edges as in EPDL data.

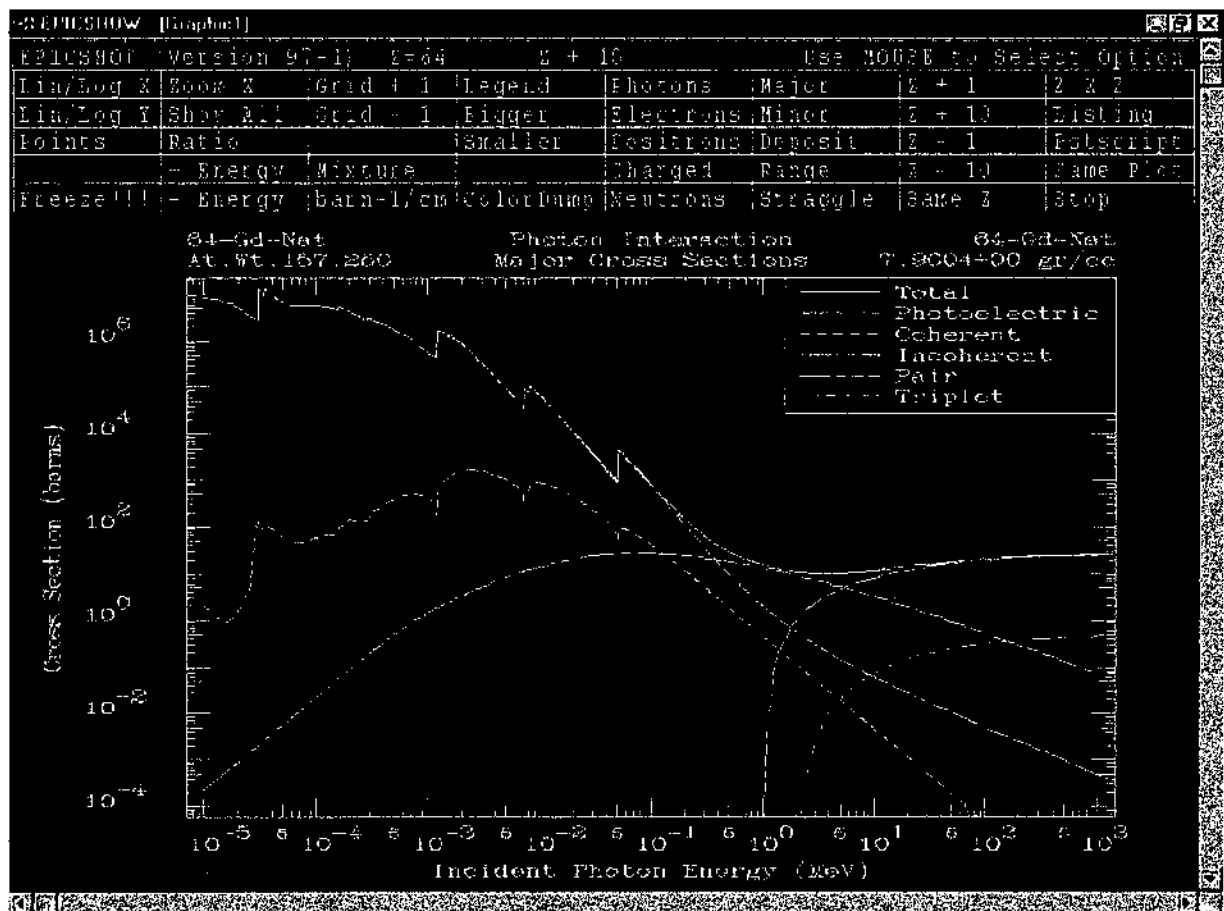
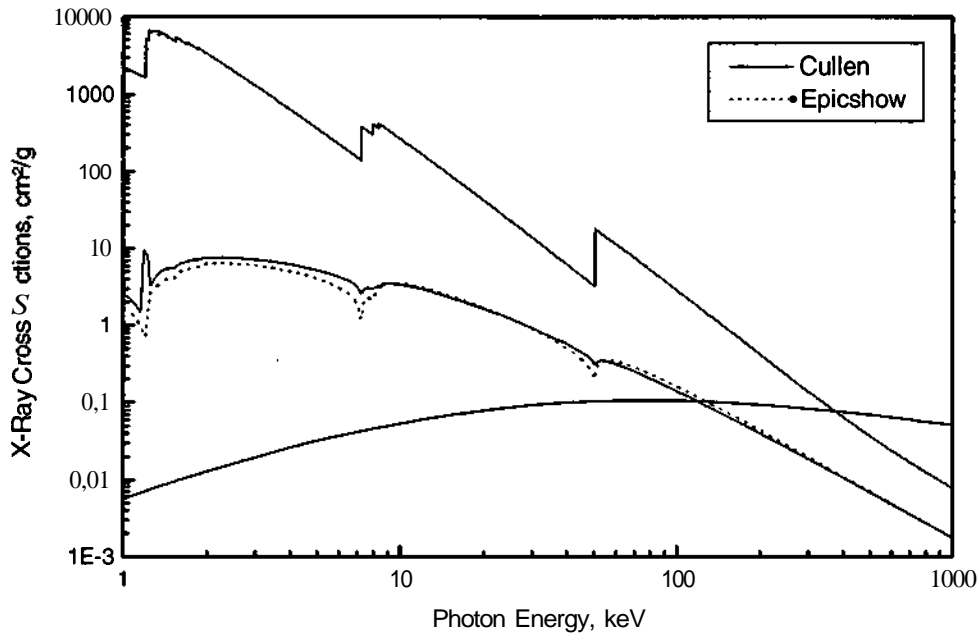
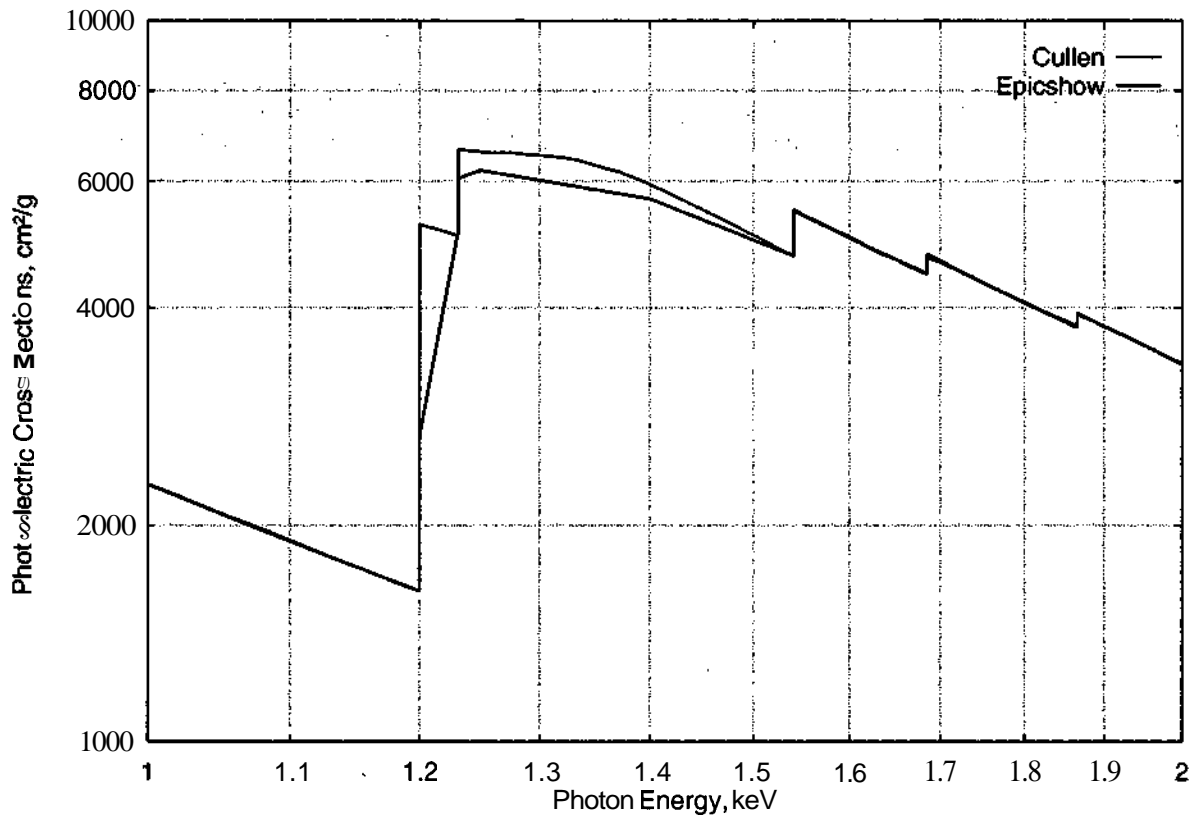


Fig. 3.34 Screen layout of EPICSHOW programs for Gd.





(a)



(b)

Fig. 3.35 Comparison between EPDL data and the abstracted data from EPICSHOW, a- whole scale, b- M edges scale.

### 3.7 Henke's Database

Henke[88] provided tables of photoabsorption, scattering, transmission and reflection data for photon energies from 50 eV to 30 keV and for elements with atomic numbers between  $Z=1$  (hydrogen) to 92 (Uranium). This database is a synthesis of a large body of experimental measurements and theoretical calculations. For many elements there are little or no published data and in such cases Henke relied on theoretical calculations and interpolations over  $Z$ . Therefore, further experimental measurements are needed in order to improve the accuracy of the database of Henke[88].

In the low-energy regions, the primary interactions of x-rays with matter are photoabsorption and coherent scattering. Incoherent scattering is significant only for light elements at higher energies ( $> 10$  keV). These processes may be described accurately outside the absorption edge regions using the complex atomic scattering factors  $f$

$$f = f_1 + i.f_2 \quad (3.12)$$

The atomic scattering factor  $f$  is defined as the factor by which one must multiply the amplitude scattered by a single free electron to yield the total amplitude coherently scattered by the particular atom. Henke[88] applied Kramers-Kronig semiclassical dispersion equation (including the small relativistic correction and the form factor correction for scattering at higher photon energies) whereas Cromers and Liberman have shown that the relativistic quantum theory of the x-ray dispersion does yield the initial Kramers-Kronig equation. Therefore,

$$f_1 = Z^* + C \int_0^\infty \frac{\epsilon^2 \cdot \mu(\epsilon) \cdot d\epsilon}{E^2 - \epsilon^2} \quad (3.13)$$

$$f_2 = \frac{\pi}{Z} \cdot C \cdot E \cdot \mu(E) \quad (3.14)$$

where  $C$  is constant which is equal

$$C = \frac{1}{\pi r_0 \cdot h \cdot c} = 0.91111 \text{ (ev} \cdot \text{A}^{\circ 2})^{-1} \quad (3.15)$$

$r_0$  is the classical electron radius,

$$r_0 = \frac{e^2}{m \cdot c^2} = 2.817940285 \times 10^{-13} \text{ cm} \quad (3.16)$$

$$Z^* = Z - (Z/82.5)^{2.37} \quad (3.17)$$

$\mu(E)$  is the photoelectric cross section at photon energy  $E$ . The factor  $f_1$  can not be defined as an atomic scattering factor for photon energies near the absorption edges because the anomalous dispersion integral term becomes very large and negative at the ionization thresholds. The intensity of the incoherent scattering is the sum of the intensities from individual atoms considering that each will scatter independently without any reinforcement of the total intensity in a particular direction. They developed a formula for estimating the incoherent scattering intensity of a solid and gas which is given by the equation,

$$\sigma_{inc} = 2\pi r_0^2 \int_0^{\pi/2} d\theta (\sin 2\theta) (1 + \cos^2 2\theta) \times (Z - f_0^2 / Z) \quad (3.18)$$

where  $2\theta$  is the scattering angle,  $\theta$  is the exit angle.

According to the dependence of the atomic scattering factors on the available experimental measurements of photoabsorption cross sections, they used the experimental photoabsorption data from both the INSPEC abstracted files and the experimental database of Saloman[57] in the region 10-10000 eV. The INSPEC is a major bibliographic index for journal articles and conference papers in computing, physics and control, electronic and electrical engineering. For energies higher than 10 keV, they used the synthesized photoabsorption cross sections of Biggs and Lighthill[121]. The basic assumption of Henke is that condensed matter may be modeled as a collection of non-interacting atoms. This assumption is in general a good one for energies sufficiently far from absorption thresholds. In the threshold regions, the specific chemical state is important and direct experimental measurements must be made. The photoelectric cross section,  $\mu(E)$  at the incident photon energy  $E$  may be readily obtained from the values of  $f_2$  from equation 3.14 therefore, the photoelectric cross section,  $\mu(E)$  in barns/atom is given by

$$\mu(E) = 2 \times r_0 \times \frac{12.398 \times 10^{-8}}{E} \times 10^{24} \times f_2 \quad (3.19)$$

$$\mu(E) = \frac{2 \times 2.817940285 \times 10^{-13} \times 12.398 \times 10^{-5} \times 10^{24}}{E} \times f_2 \quad (3.20)$$

$$\mu(E) = \frac{69.87364730686 \times 10^3}{E} \times f_2 \quad (3.21)$$

where  $r_0$  is the classical electron radius which is already defined in equation 3.16, and  $E$  is the incident photon energy in keV. Both coherent and incoherent scattering are not described in Henke's database by using the available data of the scattering factors  $f_1$  and  $f_2$ . In order to calculate the mass absorption cross sections depending on Henke's database, both coherent and incoherent scattering were provided from Elam's database[80]. According to the database of Henke including the scattering cross section of Elam as well as the experimental database, Fig. 3.36 illustrates the relation between the different interaction cross sections and the photon energy for Gd. Although Henke's database depends basically on both the theoretical and the experimental measurements, the description of the absorption edges is not accurately described particularly in the M-edges as shown in Fig. 3.36. In addition, some absorption edges are missing in Henke's databases. These absorption edges are given in Table 3.10.

Table 3.10 The missing absorption edges in Henke's database.

Element	Missing edge	Element	Missing edge	Element	Missing edge
Cu	L <sub>1</sub>	Ce	M <sub>1</sub> , M <sub>2</sub> , M <sub>3</sub>	Hf	M <sub>4</sub>
Zn	L <sub>1</sub> , L <sub>2</sub>	Pr	M <sub>1</sub> , M <sub>2</sub> , M <sub>3</sub>	Ta	M <sub>4</sub> , M <sub>5</sub>
Ga	L <sub>2</sub>	Nd	M <sub>1</sub> , M <sub>2</sub> , M <sub>3</sub>	Au	M <sub>1</sub> , M <sub>2</sub> , M <sub>3</sub> , M <sub>4</sub> , M <sub>5</sub>
Ge	L <sub>1</sub> , L <sub>2</sub>	Pm	M <sub>1</sub> , M <sub>2</sub> , M <sub>3</sub> , M <sub>4</sub> , M <sub>5</sub>	At	N <sub>1</sub>
As	L <sub>2</sub>	Sm	M <sub>1</sub> , M <sub>2</sub> , M <sub>3</sub> , M <sub>4</sub>	Rn	N <sub>1</sub>
Se	L <sub>2</sub>	Eu	M <sub>3</sub> , M <sub>4</sub>	Fr	N <sub>1</sub>
Br	L <sub>2</sub>	Gd	M <sub>2</sub> , M <sub>4</sub>	Ra	N <sub>1</sub> , N <sub>2</sub>
Kr	L <sub>2</sub>	Tb	M <sub>4</sub>	Ac	N <sub>1</sub> , N <sub>2</sub>
Te	M <sub>1</sub>	Dy	M <sub>4</sub>	Th	N <sub>1</sub> , N <sub>2</sub>
Xe	M <sub>1</sub>	Ho	M <sub>4</sub>	Pa	N <sub>1</sub> , N <sub>2</sub> , N <sub>3</sub>
Cs	M <sub>1</sub> , M <sub>2</sub>	Er	M <sub>4</sub>	U	N <sub>1</sub> , N <sub>2</sub> , N <sub>3</sub>
Ba	M <sub>1</sub> , M <sub>2</sub> , M <sub>3</sub>	Tm	M <sub>1</sub> , M <sub>4</sub>		
La	M <sub>1</sub> , M <sub>2</sub> , M <sub>3</sub>	Lu	M <sub>1</sub>		

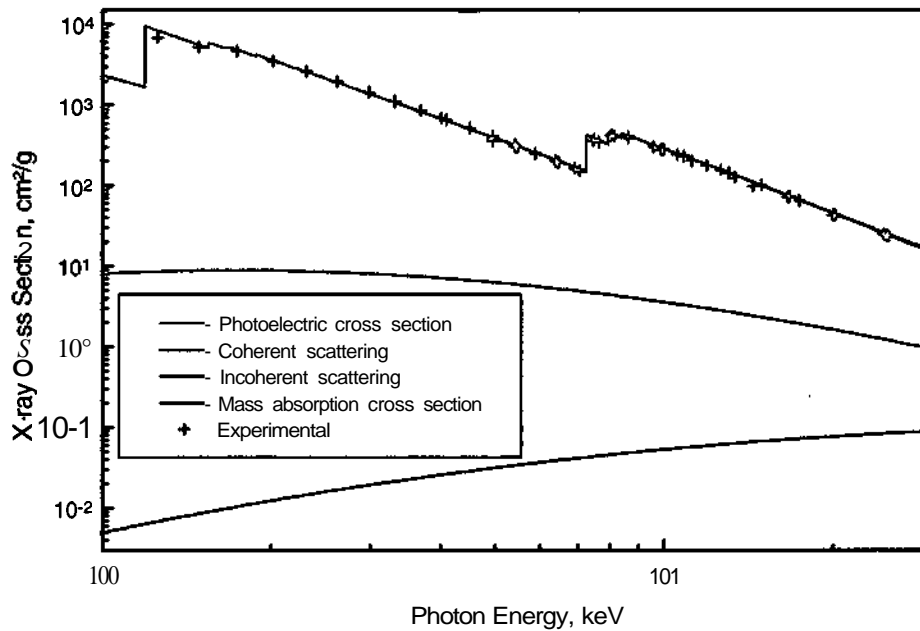


Fig. 3.36 Relation between the cross sections and the photon energy for Gd .

### 3.8 Sasaki's Database

Sasaki[122] calculated the anomalous scattering factors  $f'$ ,  $f''$  for the elements from atomic number  $Z=3$  to 83 plus  $Z=92$  by using the relativistic treatment described by Cromer and Liberman in the energy range from 4.29 keV (2.89 Å) to 123.98 keV (0.1 Å). In addition, he calculated  $f'$ ,  $f''$  values at photon energies near the K,  $L_1$ ,  $L_2$  and  $L_3$  absorption edges using Bearden's[81] tables of the absorption edge values. Sasaki has measured the anomalous scattering factors by using the x-ray spectra produced by synchrotron radiation from storage rings because only a synchrotron radiation source can provide a powerful flux at energy close to the absorption edges. The atomic scattering factors are represented by a complex number,

$$f = f_0 + f' + if'' \quad (3.22)$$

where  $f_0$ ,  $f'$ , and  $f''$  are the Thomson scattering, and the real and imaginary parts of the anomalous dispersion factors, respectively. The  $f'$  values were calculated without the Jensen's correction term on the magnetic scattering. As shown in Scofield's and Henke's databases, both coherent and incoherent scattering can not be described in Sasaki's database by using the available data of the atomic scattering factor. Therefore, in order to calculate the mass absorption cross section depending on Sasaki's database, both coherent and incoherent scattering were provided from Elam's database[80]. Fig. 3.37 shows the relation between the different cross sections and the photon energy for Gd of Sasaki and the experimental databases. The minimum photon energy in Sasaki's database is 4.29 keV, therefore, the M-edges for the elements from atomic number  $Z=3$  to 83 are not described. Only  $M_1$ -,  $M_2$ - and  $M_3$ -edges of Uranium were described. Although both K- and L-edges are well defined in Sasaki database as given in Fig. 3.37, there are remarkable deviations in sharpness of the K edge for the elements U, Bi, Pb, Tl, Hg and Au.

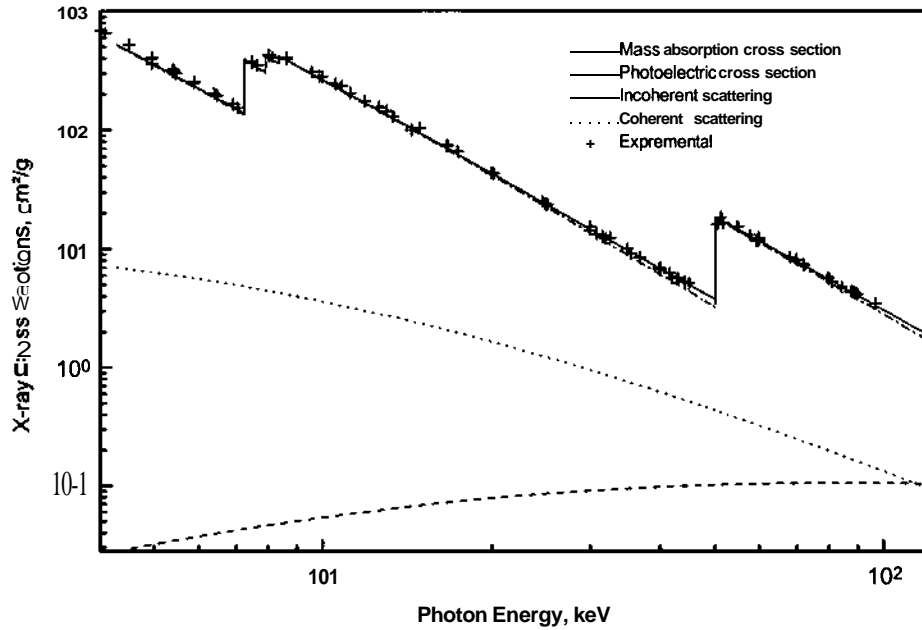


Fig. 3.37 Relation between the cross sections and the photon energy for Gd according to Sasaki and the experimental databases.

### 3.9 Chantler's Database

Chantler[123] described and computed the primary interaction of x-rays with isolated atoms from  $Z=1$  to  $Z=92$  in the energy range from 1 eV to 1 MeV within a self consistent Dirac-Hartree Fock framework. Chantler's calculations basically depend on theoretical calculations regarding previous tabulations. In Chantler's database, the following values are tabulated as a function of energy and wavelength, the theoretical scattering factors,  $f_1$  and  $f_2$ , the sum of the scattering cross sections (coherent and incoherent), the photoelectric cross sections of the atom, the mass absorption cross sections of the atom and the photoelectric cross sections of the K shell respectively. At the top of each table the absorption edge energies were provided.

Both photoabsorption and coherent (Rayleigh) scattering are described by the structure factor  $F$  of the material in condensed or gas phase. The structure factor for a given reflection is a sum over the atoms in the appropriate lattice of the x-ray scattering factors  $f_j$  of the  $j^{\text{th}}$  atom

$$F(hkl) = \sum_j f_j e^{-M_j} e^{2\pi i(hx_j + ky_j + lz_j)} \quad (3.23)$$

where  $M_j$  is the thermal parameter for the given temperature,  $hkl$  refers to Miller indices of the location of the atoms in the unit cell  $x_j, y_j, z_j$ .

The database of Chantler allows a sufficiently fine grid with accurate atomic edge structure. The required values of the mass absorption coefficients can be obtained directly by using the linear interpolation of the tabulated values. Another way to obtain the specific values of the mass absorption coefficient is by using equation 3.14 as performed in both Sasaki's and Henke's databases. Chantler compared his results with the results of Henke and the comparisons

indicates a good agreement over much of the energy range for many elements. According to the given database of Chander, he performed a significant improvement at energies about 30-60 keV, near absorption edges.

Fig. 3.38 describes the tabulated values of Chander for Gd versus the photon energy and compares it with the experimental data. As shown in Fig. 3.38 the M edges includes some fluctuations and consequently the description of M edges need more developments. Also, minor errors are wrong exponents in K-edge energies of elements from Z=31 to 86.

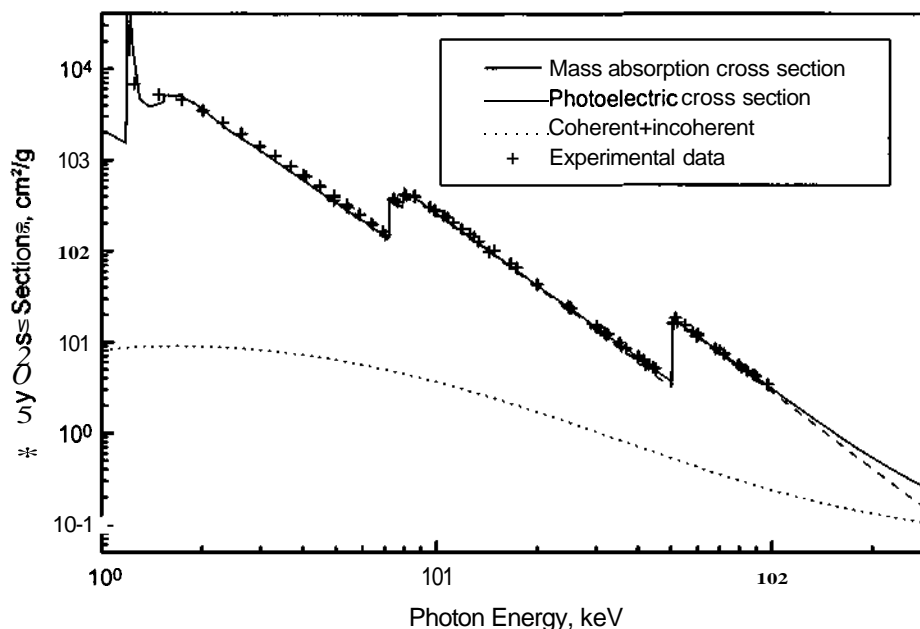


Fig. 3.38 Relation between the cross sections versus photon energy of Gd.

### 3.10 Comparisons between the Available Databases

A computer algorithm has been developed to compare between the eleven databases (Experimental, McMaster, MUCAL, Scofield original, Scofield approximation, XCOM, Elam, Cullen, Henke, Sasaki and Chander databases). All the databases are approximately identical in the photon energy higher than K absorption edges, excluding some elements in Chander's and Sasaki's databases whereas there is a remarkable difference comparing with the other databases. In some elements, the description of the M-edges in Chander, MUCAL, Scofield original, Elam, XCOM, and Henke are questionable especially in  $M_4$ - and  $M_5$ -edge ranges. Although the M-edge energies of Chander's database are defined well but there is a considerable fluctuation from  $M_3$  to  $M_5$  edge at most of the elements. On the other side, the M edges in McMaster, Scofield approximation and Cullen are well defined according to the present investigation mentioned above for Scofield and McMaster. The K, L, M and N absorption edges of Cullen, Scofield, Chander and MUCAL are different from the values in the other databases. In addition a few absorption edges are missing in Henke database. More details about the comparisons between the different data bases are given in the following published paper[103].

### 3.11 Published paper

#### Numerical Description of Photoelectric Absorption Coefficients for Fundamental Parameter Programs

Horst Ebel, Robert Svagera and Maria F. Ebel  
Institut für Festkörperphysik, Vienna University of Technology (Austria)  
Abdallah Shaltout  
National Research Center, Spectroscopy Dept., Dokki, Cairo (Egypt)  
John H. Hubbell  
11830 Rocking Horse Road, Rockville, Maryland 20852 (USA)

##### 3.11.1 Abstract

After a systematic analysis of different databases and a comparison to empirical data we decided to describe photoelectric absorption coefficients, coherent and incoherent scattering coefficients and mass attenuation coefficients in the energy range from 1 to 300keV for elements from  $Z=1$  to 94 by a modified version of Scofield's tables in combination with scattering coefficients from Elam. Modifications include check and correction of edge positions, description of  $M_4$ - and  $M_5$ -ranges of elements from promethium upwards by sawtooth responses and reduction of data by introduction of least squares fits of fifth order to Scofield's and Elam's numerical data. Our database was developed especially for application in fundamental parameter programs for quantitative x-ray analysis (XRFA, EPMA, XPS and TEY).

##### 3.11.2 Introduction

Fundamental parameter programs for quantitative x-ray analysis compare computed and measured signals in order to determine compositions of the investigated specimens. Two of the fundamental parameters are photoelectric and mass attenuation coefficients of the elements. A great number of numerical values of these quantities are given in literature and internet. To get an overview of the actual state an extended search has to be performed. One of the recent papers on this subject was published in 1999 by Hubbell[22]. Besides completeness of such a collection and critical considerations on their features with regard to fundamental parameter algorithms the availability of digitized data for computer programs is an essential criterion.

There exist numerous theoretical or semi-empirical descriptions of photoelectric absorption coefficients versus photon energy with atomic number as parameter but, for comparison of theory and experiment mass attenuation coefficients have to be calculated from photoelectric absorption and scattering coefficients.

It has to be mentioned that fluorescence yields, transition probabilities, Coster-Kronig transition probabilities, photon energies of characteristic radiations, asymmetry parameters of electron emission, inelastic and elastic mean free paths and escape probabilities of electrons released by x-rays are not within the scope of the present paper.

Another feature of the data sets is information necessary for the specific type of fundamental parameter algorithm.

**XRFA:** Edge energies define the integration intervals and absorption edge jumps the absorption in specific shells and subshells of the atoms.

**EPMA:** A situation similar to XRFA arises, considering secondary excitation of characteristic radiations by electron excited characteristic and white radiations of the specimen.

**XPS:** Subshell cross-sections give the number of electrons per photon and kinetic electron energies determine the probability of electron escape without inelastic scattering.

**TEY:** By measuring the x-ray induced total electron yield the knowledge of subshell absorption in combination with the corresponding edge positions allows to quantify the effective number of electrons per photon and from the start energies of the electrons their escape probability.

Whereas in XPS the energy range of photons is restricted by the available x-ray sources of standard equipment to only a few keV, an extension to approximately 50keV becomes necessary for EPMA and TEY and XRFA with high voltage systems up to 200kV or isotope excitation asks for maximum photon energies of 200keV and even more. An argument for a low energy cut-off is the increasing uncertainty of data with decreasing photon energies. For this reason we decided to describe photoelectric absorption and scattering coefficients in an energy range from 1keV up to 300keV. Cross-sections are given in units of  $\text{cm}^2/\text{g}$ .

### 3.11.3 Comparison of different databases

We start by looking at the classical McMaster tables[75]. Elements from  $Z=1$  to  $Z=83$  and elements  $Z=86, 90, 92$  and  $94$  are contained and photon energies cover the range from 1keV to 1MeV. Essential data are conversion from  $b/a$  to  $\text{cm}^2/\text{g}$ , K- and L-edge positions and corresponding jumps, third order least squares fit coefficients of photoelectric absorption in K-, second order fit coefficients in L-, and first order coefficients in M- and N-range and third order least squares fit coefficients of coherent and incoherent scattering coefficients. Least squares fit coefficients of N-range of elements  $Z=61$  to  $Z=69$  are not correct. No detailed information on position and jumps of M-edges of elements  $Z>51$  and N-edges of elements  $Z>85$  is given.

Shaltout completed the McMaster tables by adding the missing elements  $Z=84, 85, 87, 88, 89, 91$  and  $93$ . For this purpose, photoelectric cross-sections have been taken from Scofield's tables[79] and coherent, as well as incoherent scattering cross-sections from Elam's tables[80]. Furthermore, Shaltout corrected the mentioned wrong values of least squares fit coefficients and added missing M- and N-edge data.

The most essential database of photoelectric cross-sections is contained in Scofield's tables. Elements from  $Z=1$  to  $102$  and photon energies from 1keV to 1.5MeV are covered. Shell- and subshell coefficients can be quantified by interpolation of tabulated numerical values. For mass attenuation coefficients coherent and incoherent scattering coefficients have to be taken from other tables. The responses of photoelectric absorption versus photon energy differ from other databases especially in the region of M-edges.

Berger and Hubbell[105] published a database (XCOM) for personal computers. It contains photon energies from 1keV to 100GeV, atomic numbers from 1 to 94 and edge positions, jumps, scattering coefficients, but no shell and subshell cross-sections.



Sasaki's tables[122] are similar to Berger and Hubbell and include elements from  $Z=4$  to 83 and in addition to it,  $Z=92$ . Photon energies extend from 4.29keV to 123.98keV. Interpolation of tabulated values is required.

Data from Henke's tables[88] are valid for elements from  $Z=1$  to 92 and photon energies from 50eV up to 30keV. Photoelectric and scattering coefficients are available. Interpolation of tabulated values is required.

In 1995 Chantler[123] published a database where elements from  $Z=1$  to 92 and photon energies from 1 to 10eV and from 0.4 to 1MeV are within the scope. Additionally to photoelectric and scattering coefficients the photoelectric absorption in the K-shell is also contained. Minor errors are wrong exponents in K-edge energies of elements from  $Z=31$  to 86. Interpolation of tabulated values is required.

The most recent databases are those from Cullen et al[116] (1997) and Elam et al[80] (2001). The first one starts at 1eV and ends at 100GeV for atomic numbers from  $Z=1$  to 100, whereas the second one covers photon energies from 100eV to 1MeV and atomic numbers from  $Z=1$  to 98. A very good agreement between both tables and Scofield's numerical data exists in the range of photon energies from 1 to 300keV. Again M-edges are exceptions. Interpolation of tabulated values is required. Elam's database includes edge positions, jumps, fluorescence yields, transition probabilities, Coster Kronig transition probabilities, photon energies of characteristic radiations and coherent and incoherent scattering coefficients.

Experimental values of mass attenuation coefficients have been collected by Saloman et al[57] and Hubbell[61]. Both papers represent more or less the complete state of experimental results up to 1996. In the meanwhile Ertugrul et al[64], Kerur et al[66], Karabulut et al[65], Angelone et al[63], Chantier et al[68], Mallikarjuna et al[62] and Suzuki and Saito[67] published further experimental values.

Schäfer[60] digitized the tables of Saloman et al[57] and Shaltout digitized Hubbell's[61] data collection and the results from references 62 to 68 from 1keV upwards, to allow a convenient comparison of theoretical and experimental photoelectric absorption coefficients. An additional contribution to this subject was a careful comparison of coherent and incoherent scattering coefficients versus photon energy and atomic number. The result can be summarized by the statement that the agreement of scattering coefficients from different sources does not influence our considerations on photoelectric absorption coefficients.

Figs. 3.39 to 3.45 contain computed responses of mass attenuation coefficients from different databases and experimental data. Elements with increasing atomic number were chosen arbitrarily. The only criterion was the existence of either no edge between 1keV and 300keV (C), or the  $L_3$ - and K-edge (Cu), or the K- and L-edges (Ag), or finally, the K-, L- and M-edges (Au). Magnifications of some interesting features are given in Figs.3.41, 3.43 and 3.45.

In Fig. 3.39 carbon represents mass attenuation coefficients of an element with its K-edge at a photon energy of less than 1keV. The nine computed responses of  $\mu/\rho$  can only be distinguished after magnification. The statistical scatter of measured values is within  $\pm 10\%$ .

Copper (Fig.3.40) has its K-edge at 8.979keV and the  $L_3$ -edge at 1.096keV. A comparably more pronounced scatter of experimental data of up to  $\pm 20\%$  can be observed at photon energies from 1 to 5keV. Fig.3.41 is a magnification of the K-edge. Curves of computed values of  $\mu/\rho$  show differences up to 4% and the K-edge positions vary from 8.95 to 9.03 keV. The scatter of measured data is  $+10\%$  and  $-5\%$  with regard to the computed responses of the different authors.

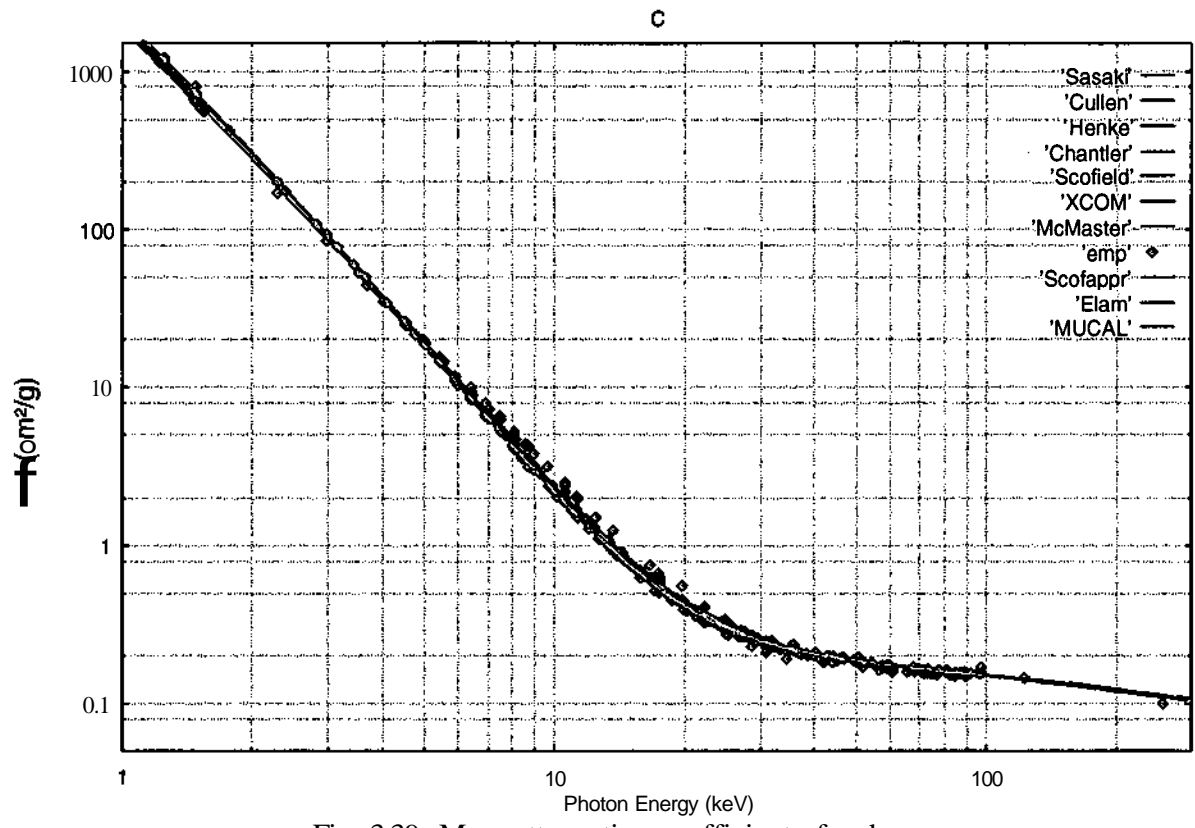


Fig. 3.39 Mass attenuation coefficient of carbon.

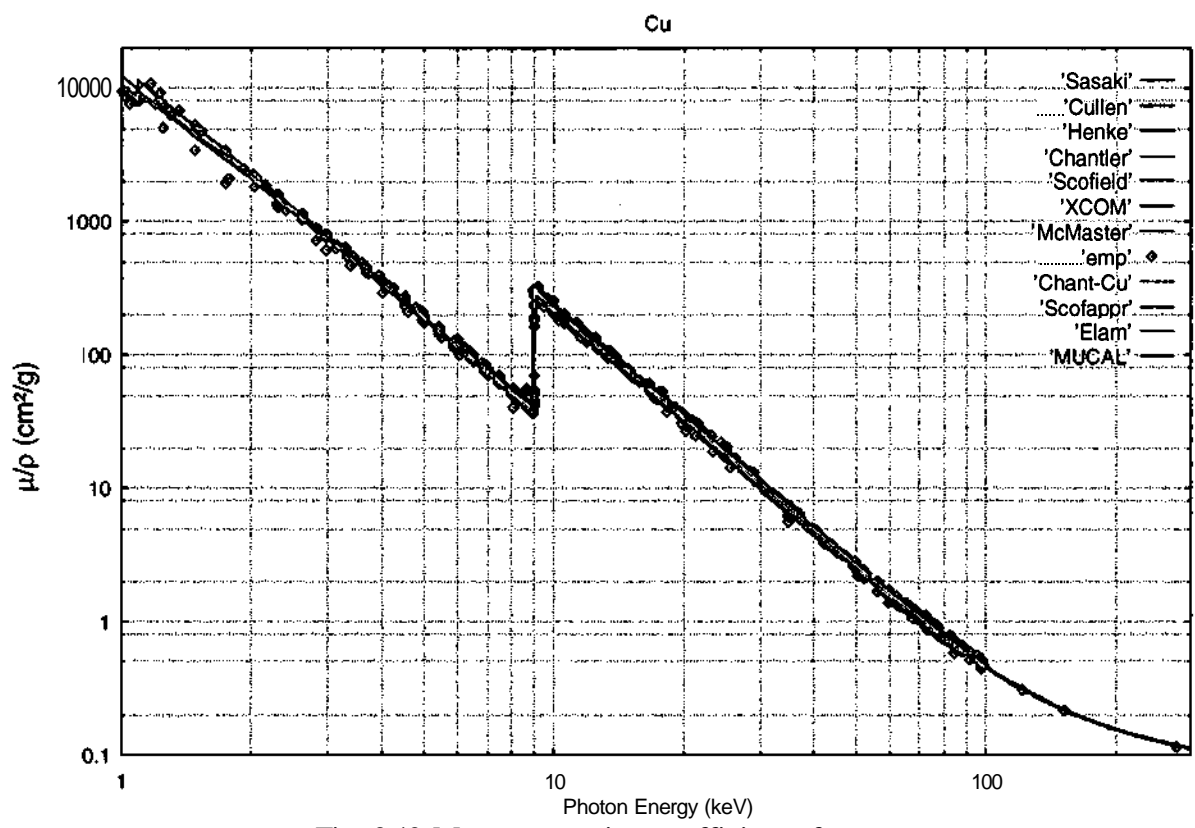


Fig. 3.40 Mass attenuation coefficient of copper.

The measured response of „Chant-Cu" is represented by a "thick" curve. "Chant-Cu" is the result of an extremely careful synchrotron investigation which was performed by Chantier et al[68]. The oscillations are from absorption edge fine structures (EXAFS, XANES). As copper is embedded in another matrix, the shape, position and amplitude of the oscillations change. Since absorption edge structures have to be expected from other edges, elements and matrices also, a general description of photoelectric absorption close to absorption edges becomes questionable.

Silver (Fig.3.42) has its K and L-edges above 1keV. Fig.3.43 is a magnification of the L-edge range. A well pronounced deviation between theory and experiment can be recognized, whereas the computed responses differ only within a few percent. A possible explanation of the finite slopes of measured values at the L-edges could be the bandwidth of the x-ray monochromators in the experiments.

K-, L- and M-edges of gold appear at photon energies greater than 1keV (Fig.3.44). An essential feature in the M-edge region are the remarkable differences between the responses from various databases. Fig.3.45 is a magnification of the M-edge range.

From Figs.3.39 to 3.45 we conclude that above  $M_1$ -,  $L_1$ - and K-edges and below  $M_5$ -,  $L_3$ - and K-edges most of the computed responses of mass attenuation coefficients do not differ too much and are in reasonable agreement with measured values. The situation changes, considering the measured Cu K-edge response of Chantier et al[68] with a deviation of nearly 10% from computed responses due to the superposition of the absorption edge fine structure. Some of the L-edges show systematic deviations between computed responses and measured values. In case of M-edges there exists practically no agreement between the data from different databases.

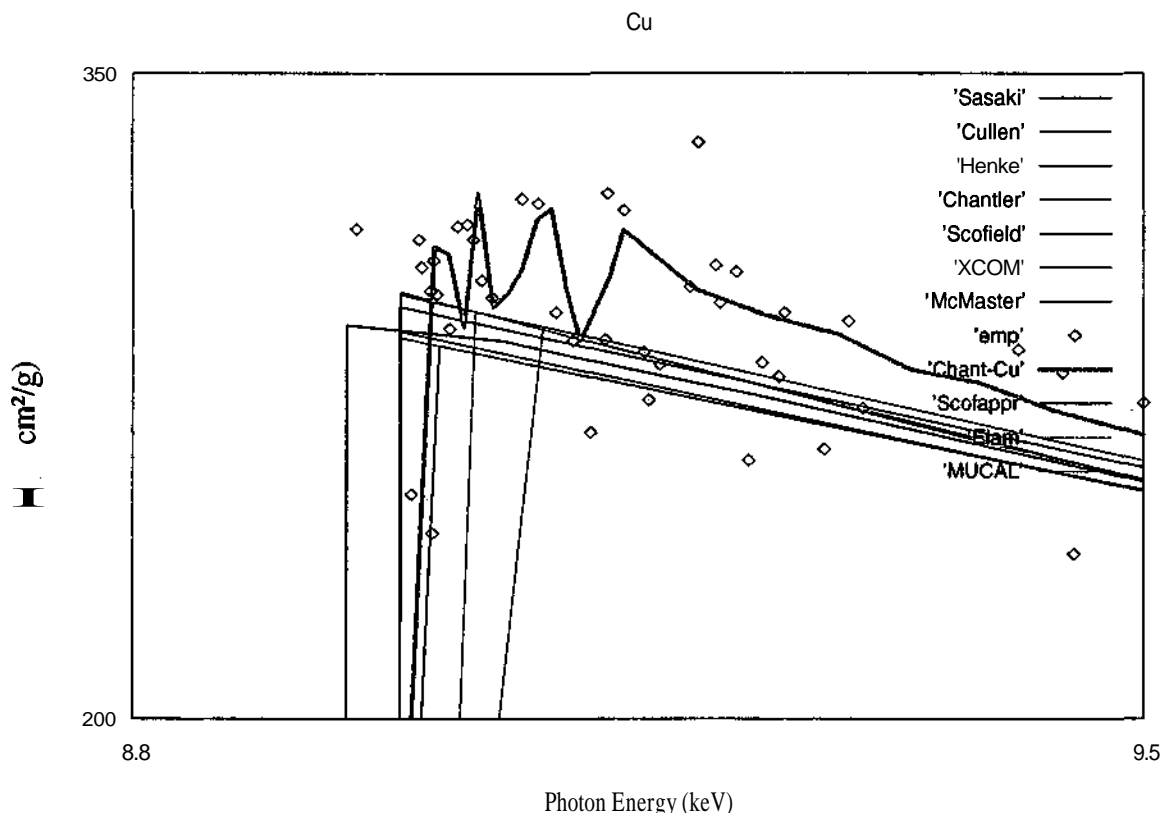


Fig. 3.41 Magnification of the K-edge range of copper.

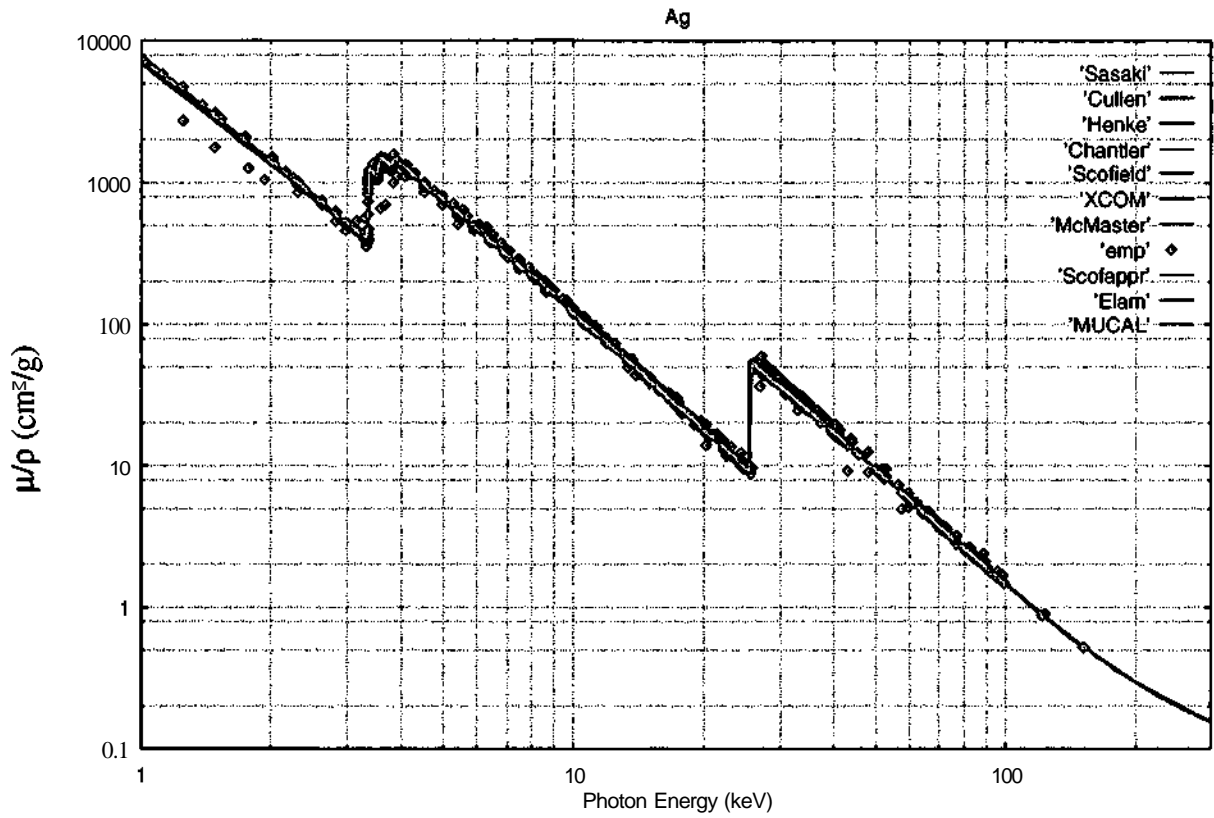


Fig. 3.42 Mass attenuation coefficient of silver.

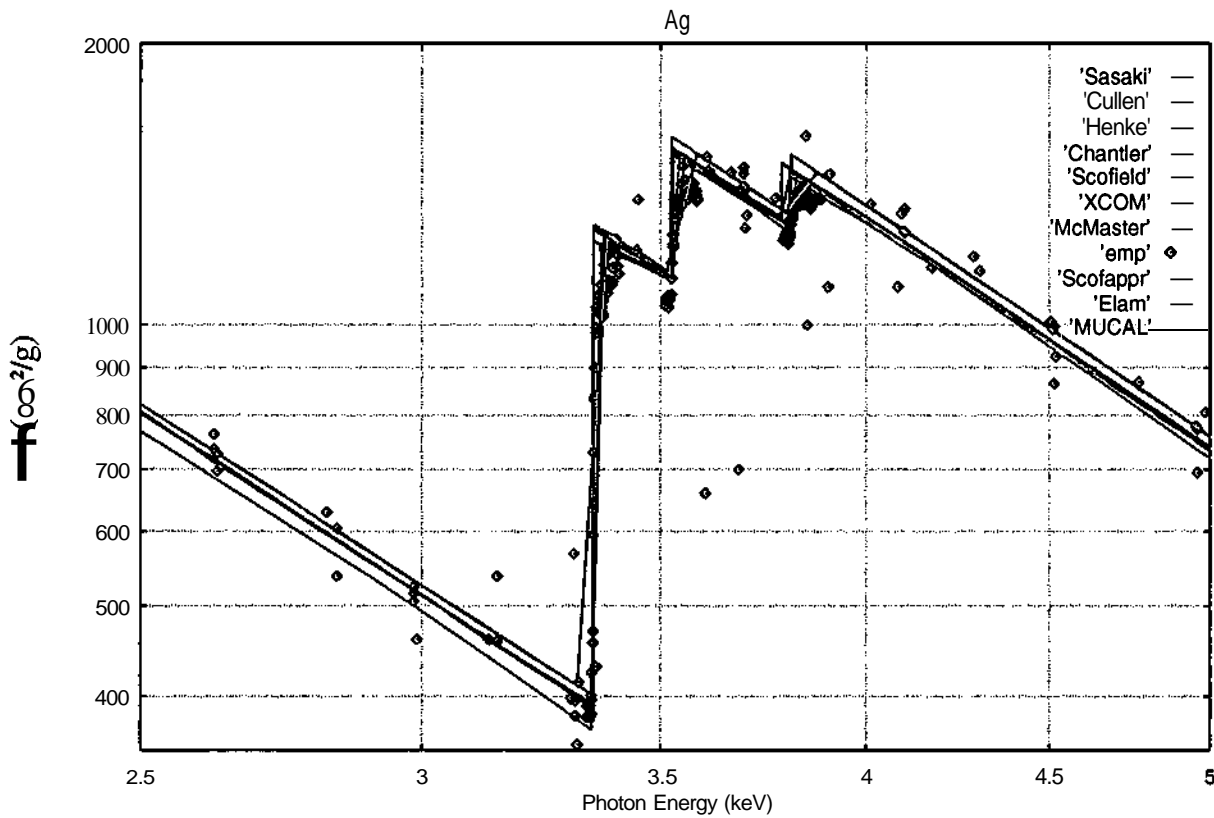


Fig. 3.43 Magnification of the L edge range of silver.

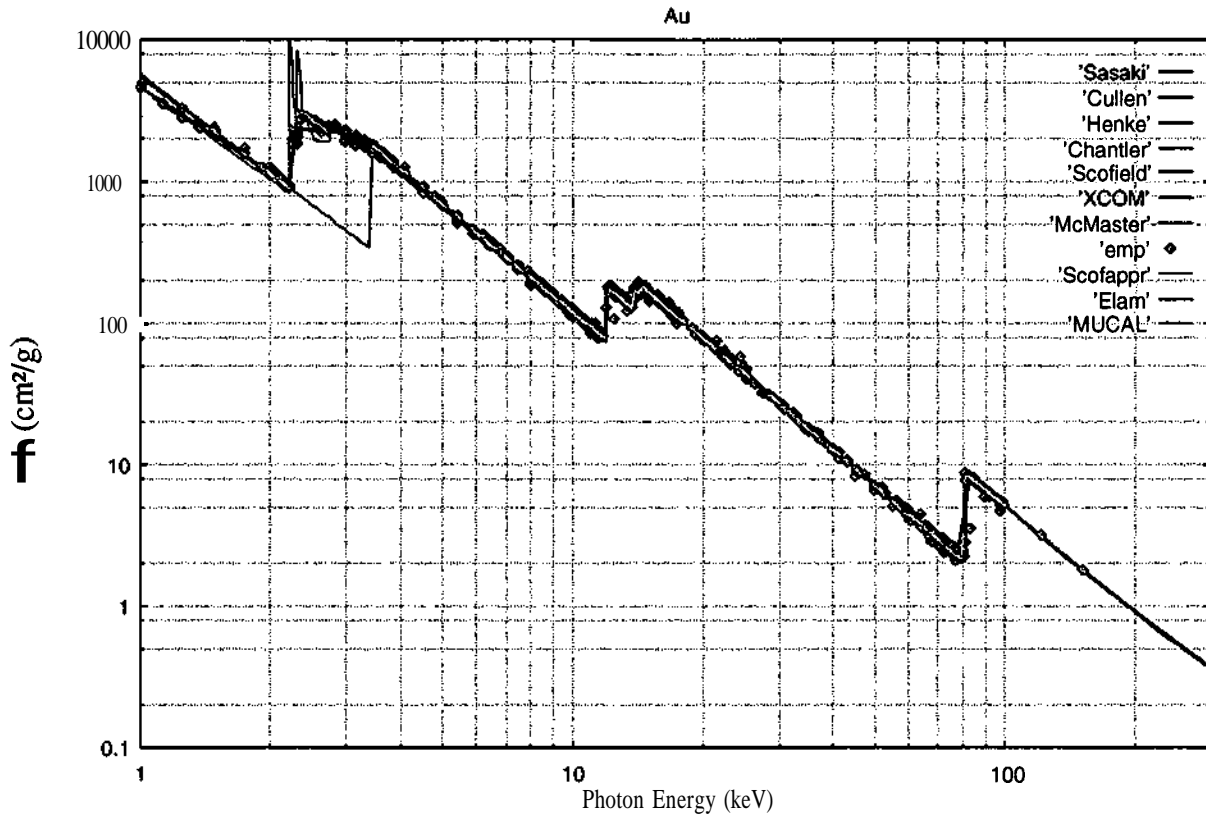


Fig. 3.44 Mass attenuation coefficient of gold.

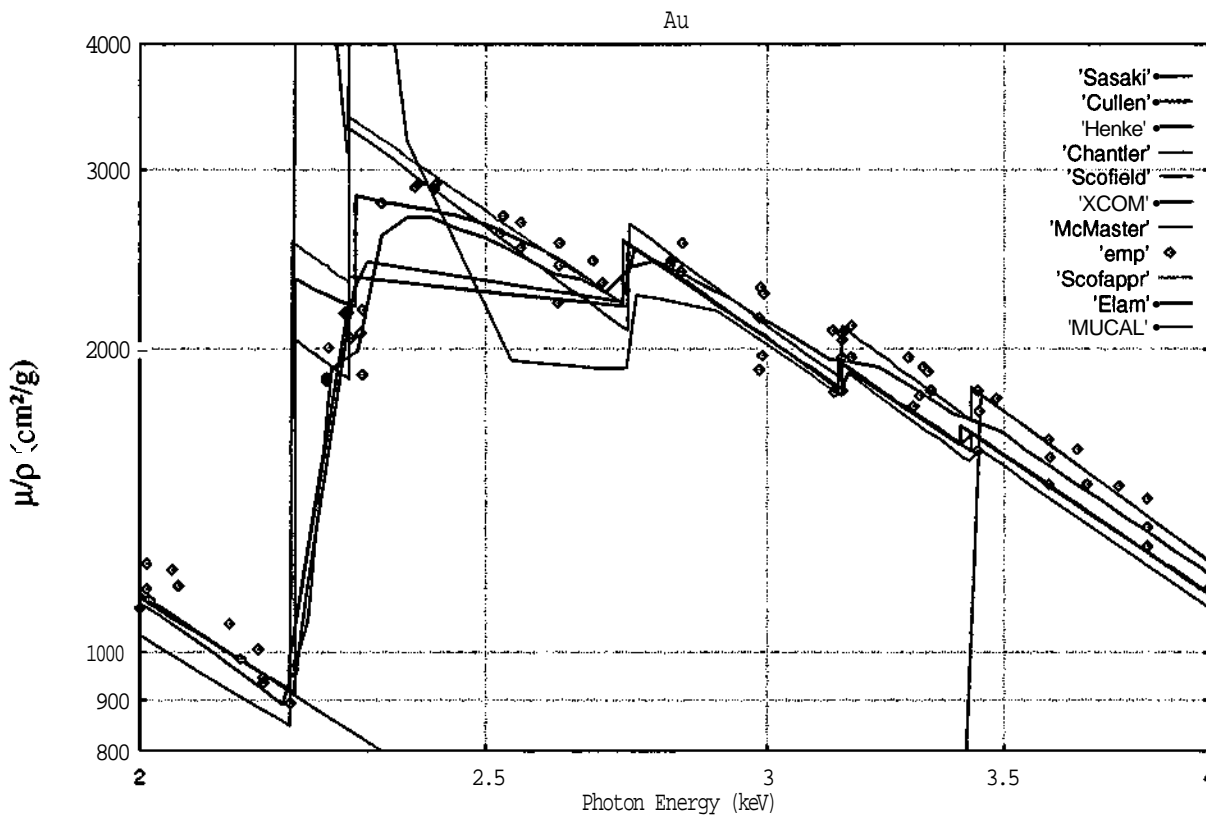


Fig. 3.45 Magnification of the M edge range of gold.

Considering this experience one has to ask for the specifications of a database for fundamental parameter applications. In case of absorption of x-rays of known photon energies mass attenuation or total photoelectric absorption coefficients are essential. With the exception of photon energies close to the absorption edges most of the considered databases can be used for this application. But, there arises another problem. In standard XRFA programs the photoelectric absorption  $\tau_K$  in the K-shell for computation of characteristic K-radiations is obtained from total photoelectric absorption coefficients  $T$  by the use of absorption edge jumps  $S_K$ .

$$\tau_K = \tau \cdot \frac{S_K - 1}{S_K} \tag{3.24}$$

In Fig.3.46 Scofield's K-shell cross-sections of copper are compared with values computed from McMaster's tables by means of absorption edge jumps. An excellent agreement of the responses seems to confirm the validity of the concept of absorption edge jumps. Therefore, the next step is dedicated to L-shell cross-sections by L-edge jumps for computation of characteristic L-radiations. The corresponding equation for the  $L_3$ -jump is

$$\tau_{L_3} = \tau \cdot \frac{S_{L_3} - 1}{S_{L_3}} \tag{3.25}$$

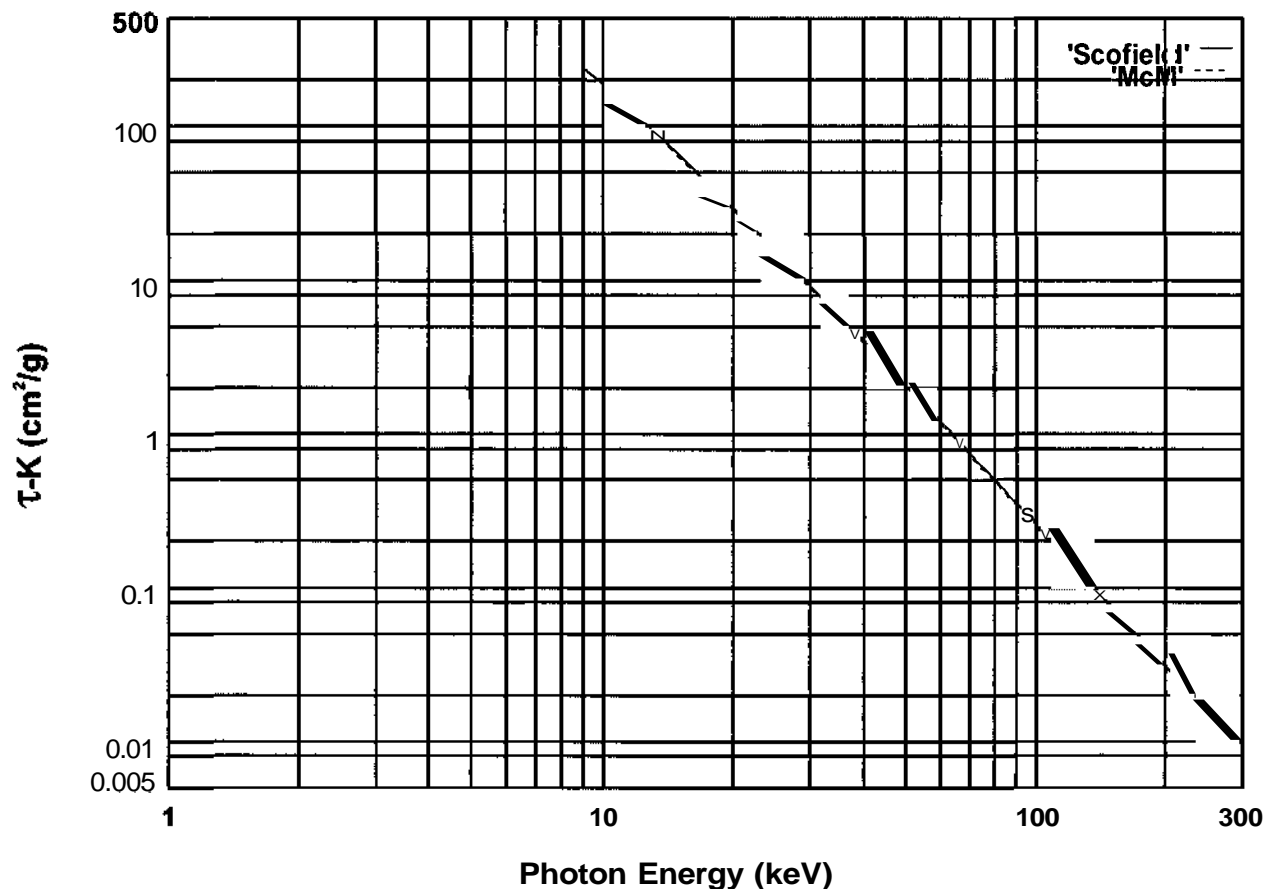


Fig. 3.46 Photoelectric absorption in the K shell of copper from McMaster's and from Scofield's tables.

This expression has to be divided by the jump of  $L_2$  above the  $L_2$ -edge, and furthermore by the jumps of  $L_1$  above the  $L_1$ -edge and K above the K-edge. Thus, in the K-range

$$\tau_{L_3} = \tau \cdot \frac{1}{S_K} \cdot \frac{1}{S_{L_1}} \cdot \frac{1}{S_{L_2}} \cdot \frac{S_{L_3} - 1}{S_{L_2}} \quad (3.26)$$

describes the photoelectric absorption in the  $L_3$ -subshell at photon energies higher than the K-edge energy. A similar procedure gives the values for the other two L-subshells. Fig. 3.47 compares the  $L_3$  subshell cross-section of gold as computed from McMaster's and Scofield's tables. Gold is a prominent candidate for quantitative analysis by characteristic L-radiations. The cross-section  $\sigma_{L\alpha}$  of the strongest Au  $L_\alpha$ -radiations includes also the Coster-Kronig transition probabilities  $f_j$  the photoelectric shell- and subshell coefficients of K,  $L_1$ ,  $L_2$  and  $L_3$ .

$$\sigma_{L\alpha} = \left[ \tau_{L_3} + \tau_K \cdot p_{KL_3} + (\tau_{L_2} + \tau_K \cdot p_{KL_2}) \cdot f_{23} + (\tau_{L_1} + \tau_K \cdot p_{KL_1}) \cdot (f_{15} + f_{12} \cdot f_{23}) \right] \cdot \omega_3 \cdot F_{3\alpha} \quad (3.27)$$

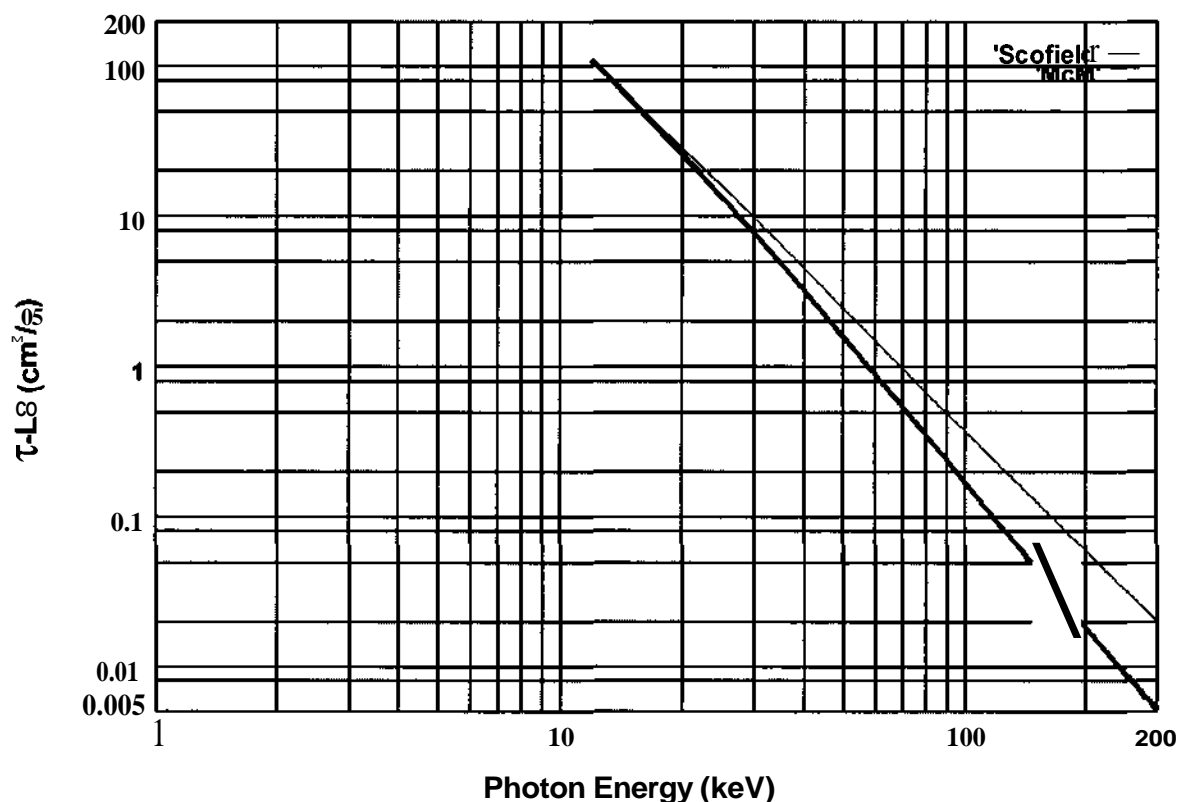


Fig. 3.47 Photoelectric absorption in the  $L_3$  shell of gold from McMaster's and from Scofield's tables.

Fig. 3.48 gives the relative error of  $ff_M$  from the absorption edge jump concept with regard to Scofield's concept of subshell cross-sections. Transition probabilities, fluorescence yield and Coster-Kronig transition probabilities are from Elam's tables. The pronounced difference especially in the photon energy range between  $L_1$  and K makes the concept of absorption edges only a rough approximation in case of L-subshells. Consequently, there remain only Scofield's data from the complete set of databases for application in XRFA.

From the similarity of the fundamental parameter approaches the considerations are also valid for EPMA. On the other hand, the methods of x-ray excited electron emission (TEY and XPS) ask just for subshell cross-sections and can be applied principally only with Scofield's tables. From

these considerations we propose a combination of Scofield's data for cross-sections and Elam's tables for data like edge positions, characteristic energies, transition probabilities, Coster-Kronig transition probabilities and fluorescence yields in case of XRFA and EPMA. In quantitative XPS Reilman's tables[125] are used for asymmetry parameters and Tanuma, Powell and Penn's tables[126, 127, 128] for inelastic mean free paths of electrons. Finally, Ebel's tables[129] give escape probabilities of electrons for application in quantitative TEY.

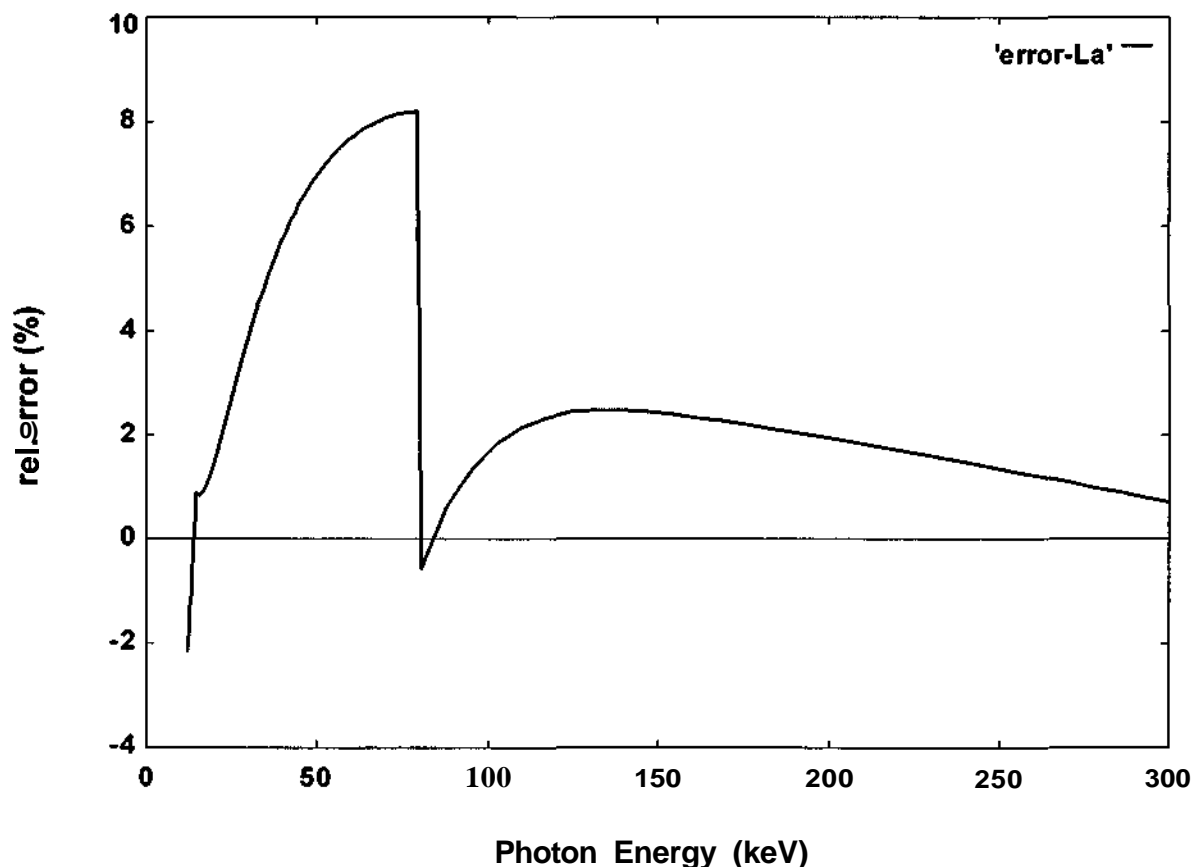


Fig. 3.48 Relative error of the  $L_{\alpha}$  cross-section  $\sigma_{L\alpha}$  of gold

$$rel.error(\%) = \frac{\sigma_{L\alpha,McM} - \sigma_{L\alpha,Scof}}{\sigma_{L\alpha,Scof}} \cdot 100$$

### 3.11.4 Modification of Scofield's database

We describe Scofield's numerical values of shell- and subshell cross-sections by least squares fit polynomials of fifth order. Maximum deviations are less than 0.1%. In some cases (compare  $M_4$ - and  $M_5$ -edges of gold in Fig.3.49 Scofield's values of the subshell cross-sections show close to the edges a pronounced drop towards smaller values at decreasing photon energies instead of a sawtooth behaviour. A comparison with the corresponding Fig.3.45 of the complete database and an additional systematic analysis of the M-edge structures of elements from neodym to plutonium led to the conclusion that the existing theoretical models and experimental data ask for further investigations. Therefore, for an application in fundamental parameter programs of x-ray analysis we recommend a sawtooth response at the  $M_4$ - and  $M_5$ -edges calculated by extrapolation of Scofield's subshell cross-sections. A further modification of Scofield's data arises from a careful check of edge positions. Responses which have been computed by means of this database are indicated by "Scofappr".



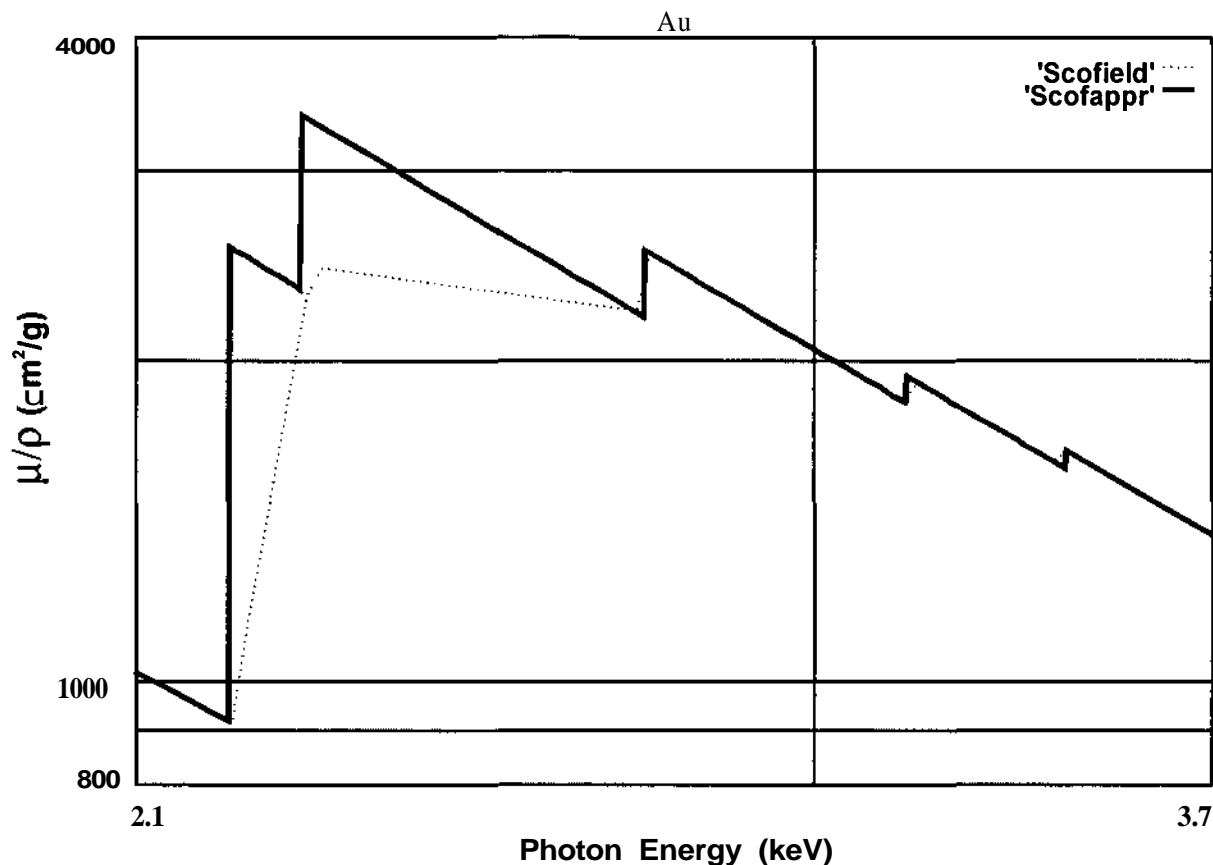


Fig. 3.49 Comparison of our description of Scofield's data (Scofappr) with the original values (Scofield) in the M edge range of gold.

The structure of a datafile is demonstrated by the computer printout of copper. Table 3.11 gives the datafile. Numerical values of the lsf-coefficients are given in single precision. With different values  $E$  (in keV) of the photon energy we compute the following quantities for fundamental parameter programs and start with the determination of the coherent and the incoherent scattering coefficients. All cross-sections are given in units of  $\text{cm}^2/\text{g}$ .

$$\sigma_{coh} Ip = \exp[1.61076 - 0.00786082 \cdot \ln(E) - 0.120265 \cdot (\ln(E))^2 - 0.0847087 \cdot (\ln(E))^3 + ..] \quad (3.28)$$

$$\sigma_{to} Ip = \exp[-5.1247 + 1.52359 \cdot \ln(E) - 1.48407 \cdot (\ln(E))^2 - 1.82812 \cdot (\ln(E))^3 + ..] \quad (3.29)$$

The next step is an arbitrarily chosen photoelectric absorption in the  $L_3$ -subshell ( $\text{Cu}2p_{3/2}$ ) for an application in XPS or TEY

$$\tau_{L_3} Ip = \exp[8.69516 - 2.45156 \cdot \ln(E) - 0.287522 \cdot (\ln(E))^2 + 0.0375707 \cdot (\ln(E))^3 + ..] \quad (3.30)$$

with kinetic energy  $E_{kin}$  of the photoelectron

$$E_{kin} = E - IE_{L_3} \quad (3.31)$$

$E_{L_3} = 0.9311 \text{ keV}$  is the  $L_3$  edge energy or binding energy of  $\text{Cu}2p_{3/2}$  electrons. The total photoelectric absorption coefficient is obtained from the "global data". For photon energies  $E$  above the K-edge energy the K-range fit has to be used

$$\tau / \rho = \exp[5.99849 + 4.41377 \cdot \ln(E) - 3.57877 \cdot (\ln(E))^2 + 0.910946 \cdot (\ln(E))^3 + \dots] \quad (3.32)$$

and for photon energies below the K-edge energy the L-range fit

$$Tl_p = \exp[9.36846 - 2.3652 \cdot \ln(E) - 0.0728571 \cdot (\ln(E))^2 - 0.112747 \cdot (\ln(E))^3 + \dots] \quad (3.33)$$

At photon energies between  $1 \text{ keV}$  and  $L_1$  the numerical value has to be divided by the  $L_1$  edge jump  $1.1279$ . Computed values of coherent and incoherent scattering coefficients, of the photoelectric absorption coefficient in the  $L_3$ -subshell, of the kinetic energy of  $\text{Cu}2p_{3/2}$  photoelectrons and of the total photoelectric absorption coefficient together with the mass attenuation coefficient of copper are given in Table 3.12.

For high  $Z$  elements where the  $M_5$ -edge energy exceeds  $1 \text{ keV}$  the scheme is as follows: From  $1 \text{ keV}$  to  $M_5$  we use the N-range fit, from  $M_5$  to  $L_3$  the M-range fit and from  $L_3$  to K the L-range fit. Jumps are considered by dividing by the corresponding edge jump values. Thus, for example at a photon energy between  $M_4$  and  $M_3$  we use the M-range fit and divide by the jumps of  $M_1$ ,  $M_2$  and  $M_3$ .

In case of copper the edges  $L_2$ ,  $L_3$ ,  $M_1$  to  $M_5$  and  $N_1$  are at edge energies of less than  $1 \text{ keV}$  and the corresponding edge jumps are not employed.

As a final remark we would like to mention that in all of our data files edge energies or binding energies of shells and subshells have been taken from Bearden's tables[81] and from Cardona's tables[104].

Data files are available at <http://www.ifp.tuwien.ac.at/forschung/horst.ebel>.

Table 3.11 Datafile of copper for computation of coherent and incoherent scattering coefficients, subshell-, shell- and total photoelectric absorption coefficients, mass attenuation coefficients and kinetic energy of photoelectrons for fundamental parameter programs.

```

Cu      Z      A      rho
29      63.54    8.9400E+00

Cu      coherent and incoherent lsf-coefficients
1.61076E+00 -7.86082E-03 -1.20265E-01 -8.47087E-02 1.97910E-02 -1.33671E-03
-5.12470E+00 1.52359E+00 -1.48407E-01 -1.82812E-02 2.05003E-03 2.37385E-05

Cu      edge-energies edge-jumps and lsf-coefficients
K
8.97890      7.59994
5.06132E+00 5.39792E+00 -4.05976E+00 1.03004E+00 -1.34157E-01 7.03190E-03
L1
1.09610      1.12790
7.12848E+00 -1.28404E+00 -4.07297E-01 7.16763E-02 -1.11716E-02 8.18537E-04
L2
0.9510       1.00000
8.03446E+00 -2.45466E+00 -2.51178E-01 1.93953E-02 -2.29673E-03 3.55470E-04
L3
0.9311       1.00000
8.69516E+00 -2.45156E+00 -2.87522E-01 3.75707E-02 -6.49420E-03 6.74545E-04
M1
0.1198       1.00000
5.53791E+00 -1.76042E+00 -1.50392E-01 3.43852E-03 -2.13485E-03 3.41960E-04
M2
0.0736       1.00000
5.60834E+00 -2.18191E+00 -3.13296E-01 2.77407E-02 -3.23429E-03 4.21111E-04
M3
0.0736       1.00000
6.27241E+00 -2.20456E+00 -3.21048E-01 3.32612E-02 -5.02599E-03 5.74792E-04
M4
0.0016       1.00000
4.80058E+00 -3.32464E+00 -2.80331E-01 1.81929E-02 -6.39701E-04 2.65036E-04
M5
0.0016       1.00000
5.17738E+00 -3.31854E+00 -3.05612E-01 3.15850E-02 -4.03917E-03 5.55743E-04
N1
0.0000       1.00000
1.78978E+00 -1.82892E+00 -9.49832E-02 -1.74157E-02 1.52049E-03 1.01834E-04
global data

Cu      lsf-coefficients of K- L- M- and N-range
5.99849E+00 4.41377E+00 -3.57877E+00 9.10946E-01 -1.19373E-01 6.30051E-03
9.36846E+00 -2.36520E+00 -7.28571E-02 -1.12747E-01 6.87008E-02 -1.23671E-02
0.00000E+00 0.00000E+00 0.00000E+00 0.00000E+00 0.00000E+00 0.00000E+00
0.00000E+00 0.00000E+00 0.00000E+00 0.00000E+00 0.00000E+00 0.00000E+00

```

Table 3.12 Numerical values of characteristic data computed by data from Table 1.

Photon energy	$\tau_{\text{coh}}/\rho$	$\sigma_{\text{inc}}/\rho$	$\tau_{L3}/\rho$	$E_{\text{kin}}$	$\tau/\rho$	$\mu/\rho$
1	5.0	0.006	5974	0.069	10385	10390
1.095	5.0	0.007	4771	0.164	8373	8378
1.097	5.0	0.007	4749	0.166	9403	9408
1.2536	5.0	0.008	3384	0.323	6830	6835
1.4866	4.9	0.011	2165	0.556	4509	4513
5	2.86	0.044	61.9	4.069	186.9	189.8
8.978	1.66	0.071	9.12	8.047	36.6	38.3
8.979	1.66	0.071	9.12	8.048	278.1	279.9
20	0.61	0.109	0.56	19.069	33.1	33.8

# CHAPTER 4 THE COMPUTING ALGORITHMS

## 4.1 SCOFFT.BAS

```

DECLARE SUB Nshell (XXS)
DECLARE SUB CNshell (XXS)
DECLARE FUNCTION splits (s$)
DECLARE FUNCTION EFToZ%(eI$)
'DECLARE FUNCTION Polynom (X#, n%, A#0)
DECLARE SUB fit (n%, X#0, Y#0, degr%, A#0)
DECLARE SUB readElement (elem AS ANY)

REM #####
REM $INCLUDE: 'MODXRF.INC'
REM #####
CLS

DIM el AS element

CLS

DEFDBL A-Z

DIM X(200), Y(200)
DIM A(10)
DIM B(10)
DIM AS(30)      The name of the subshell as written in Scofield files
DIM AAS(30)
DIM CS(30, 50)  The Photo. corss section of each subshell
DIM En(60)      The energies values of one element
DIM other(60)   The total photoelectric cross section from N1 to end.

INPUT "The element"; eI$

OPEN "D:\work\memar\tey\scofield\" + "pikevat" FOR INPUT AS #30

DO WHILE EOF(30) <> -1
  LINE INPUT #30, h$
  IF LEFT$(h$, 26) = " " THEN
    LINE INPUT #30, h$: LINE INPUT #30, h$
    Z% = VAL(MID$(h$, 10, 2))
    Nstate% = VAL(MID$(h$, 19, 2)): Nenergy% = VAL(MID$(h$, 32, 2))
    IF Z% = EFToZ%(eI$) THEN
      LINE INPUT #30, h$: LINE INPUT #30, h$: LINE INPUT #30, h$
      FOR i = 1 TO Nstate%
        AS(i) = MID$(h$, 3, 7)
        'PRINT AS(i)
        XXS = AS(i)
        CALL CNshell(XXS)
        AAS(i) = XXS
        PRINT AS(i); " = "; AAS(i)
        LINE INPUT #30, h$
      NEXT i
      LINE INPUT #30, h$: LINE INPUT #30, h$: LINE INPUT #30, h$
      FOR i% = 1 TO Nenergy%
        LINE INPUT #30, h$
        En(i%) = VAL(MID$(h$, 3, 12))
        other(i%) = VAL(MID$(h$, 63, 10))
      NEXT i%
      nn% = 0
      DO
        LINE INPUT #30, h$: LINE INPUT #30, h$
        LINE INPUT #30, h$: LINE INPUT #30, h$
        ie% = 0
        DO
          LINE INPUT #30, h$
          XS = split(h$)
          ie% = ie% + 1
          ist% = nn%
          DO UNTIL ist% = Nstate%
            XS = split(h$)
            IF XS = "" THEN EXIT DO
            ist% = ist% + 1
            CS(ist%, ie%) = VAL(XS)
          LOOP
          LOOP UNTIL ie% = Nenergy%
          nn% = ist%
          LOOP UNTIL nn% = Nstate%
        EXIT DO
      ELSE
        END IF
      END IF
    LOOP
  CLOSE #30

'END

OPEN "LSF_" + eI$ + ".dat" FOR APPEND AS #33
eI$ = eI$
eI.Z = EFToZ%(eI.eI)
CALL readElement(eI)
PRINT eI.A
PRINT #33, "Conv="; eI.A / 6.0221367D+23 * 1E+24
PRINT "Conv="; eI.A / 6.0221367D+23 * 1E+24
CLOSE #33

FOR RR = 1 TO Nstate%

XXS = AAS(RR)
CALL Nshell(XXS)

i = 1
DO UNTIL XXS = AS(i)
  i = i + 1
LOOP

OPEN "temp.dat" FOR OUTPUT AS #50
FOR V = 1 TO Nenergy%
  IF CS(i, V) > 0 THEN
    IF En(V) >= 300 THEN
      CLOSE #50: GOTO uuuu
    END IF
    PRINT #50, LOG(En(V)), LOG(CS(i, V))
  END IF
NEXT V
CLOSE #50

uuuu:
OPEN "cmd.plt" FOR OUTPUT AS #10
PRINT #10, "cd 'D:\work\shaltout'"
PRINT #10, "set grid"
PRINT #10, "plot 'temp.dat'"
PRINT #10, "pause -1"
CLOSE #10
SHELL "C:\gnuplot\wgnuplotcmd.plt"

degra% = 5
OPEN "d:\work\shaltout\" + "temp.dat" FOR INPUT AS #1
na% = 0
DO WHILE EOF(1) <> -1
  na% = na% + 1
  INPUT #1, E, tau
  X(na%) = E
  Y(na%) = tau
  LOOP
CLOSE #1

eI.eI = eI$
eI.Z = EFToZ%(eI.eI)
CALL readElement(eI)
IF AAS(RR) = "K" THEN QQ = eI.K.E
IF AAS(RR) = "L1" THEN QQ = eI.L1.E
IF AAS(RR) = "L2" THEN QQ = eI.L2.E
IF AAS(RR) = "L3" THEN QQ = eI.L3.E
IF AAS(RR) = "L3" THEN QQ = eI.L3.E
IF AAS(RR) = "M1" THEN QQ = eI.M1.E
IF AAS(RR) = "M2" THEN QQ = eI.M2.E
IF AAS(RR) = "M3" THEN QQ = eI.M3.E
IF AAS(RR) = "M4" THEN QQ = eI.M4.E
IF AAS(RR) = "M5" THEN QQ = eI.M5.E
IF AAS(RR) = "N1" THEN QQ = eI.N1.E
IF AAS(RR) = "N2" THEN QQ = eI.N2.E
IF AAS(RR) = "N3" THEN QQ = eI.N3.E
IF AAS(RR) = "N4" THEN QQ = eI.N4.E
IF AAS(RR) = "N5" THEN QQ = eI.N5.E
IF AAS(RR) = "N6" THEN QQ = eI.N6.E
IF AAS(RR) = "N7" THEN QQ = eI.N7.E
IF AAS(RR) = "O1" THEN QQ = eI.O1.E
IF AAS(RR) = "O2" THEN QQ = eI.O2.E
IF AAS(RR) = "O3" THEN QQ = eI.O3.E
IF AAS(RR) = "O4" THEN QQ = eI.O4.E
IF AAS(RR) = "O5" THEN QQ = eI.O5.E
IF AAS(RR) = "O6" THEN QQ = 0
IF AAS(RR) = "O7" THEN QQ = 0
IF AAS(RR) = "P1" THEN QQ = eI.P1.E
IF AAS(RR) = "P2" THEN QQ = eI.P2.E
IF AAS(RR) = "P3" THEN QQ = eI.P3.E
IF AAS(RR) = "P4" THEN QQ = 0
IF AAS(RR) = "P5" THEN QQ = 0
IF AAS(RR) = "Q1" THEN QQ = 0

OPEN "LSF_" + eI$ + ".dat" FOR APPEND AS #33
PRINT #33, AAS(RR); " edge"; QQ
PRINT AAS(RR); " edge"
CALL fit(na%, X(), Y(), degr%, A())
FOR i% = 0 TO degr%
  PRINT USING "a(##)#####.###"; i%, A(i%)
  PRINT #33, USING "a(##)#####.###"; i%, A(i%)
NEXT i%
CLOSE #33

INPUT "Continue (Y)es OR (N)o"; FS
IF UCASE$(FS) = "Y" THEN GOTO ZZZ
IF UCASE$(FS) = "N" THEN
  END
ELSE
  END
END IF
ZZZ:

NEXT RR

'OPEN "temp.dat" FOR OUTPUT AS #50
'FOR V = 1 TO Nenergy%
'  IF other(V) > 0 THEN

```





```

ll.Ka1.li = VAL(MID$(h$, 20, 18))
ll.Ka1.tp = VAL(MID$(h$, 39, 16))
ll.Ka1.fy = VAL(MID$(h$, 54, 16))

```

```

LINE INPUT #30, h$
ll.Ka2.E = VAL(MID$(h$, 20, 18))
ll.Ka2.tp = VAL(MID$(h$, 39, 16))

```

```

LINE INPUT #30, h$
ll.Lg3.E = VAL(MID$(h$, 20, 18))
ll.Lg3.tp = VAL(MID$(h$, 39, 16))

```

```

LINE INPUT #30, h$
ll.Lg2.E = VAL(MID$(h$, 20, 18))
ll.Lg2.tp = VAL(MID$(h$, 39, 16))

```

```

LINE INPUT #30, h$
ll.Lb3.E = VAL(MID$(h$, 20, 18))
ll.Lb3.tp = VAL(MID$(h$, 39, 16))

```

```

LINE INPUT #30, h$
ll.Lb4.E = VAL(MID$(h$, 20, 18))
ll.Lb4.tp = VAL(MID$(h$, 39, 16))

```

```

LINE INPUT #30, h$
ll.Lg6.E = VAL(MID$(h$, 20, 18))
ll.Lg6.tp = VAL(MID$(h$, 39, 16))

```

```

LINE INPUT #30, h$
ll.Lg1.E = VAL(MID$(h$, 20, 18))
ll.Lg1.tp = VAL(MID$(h$, 39, 16))

```

```

LINE INPUT #30, h$
ll.Lb1.E = VAL(MID$(h$, 20, 18))
ll.Lb1.tp = VAL(MID$(h$, 39, 16))

```

```

LINE INPUT #30, h$
ll.Ln.E = VAL(MID$(h$, 20, 18))
ll.Ln.tp = VAL(MID$(h$, 39, 16))

```

```

LINE INPUT #30, h$
ll.Lb5.E = VAL(MID$(h$, 20, 18))
ll.Lb5.tp = VAL(MID$(h$, 39, 16))

```

```

LINE INPUT #30, h$
ll.Lb215.E = VAL(MID$(h$, 20, 18))
ll.Lb215.tp = VAL(MID$(h$, 39, 16))

```

```

LINE INPUT #30, h$
ll.l.E = VAL(MID$(h$, 20, 18))
ll.tp = VAL(MID$(h$, 39, 16))

```

```

LINE INPUT #30, h$
ll.La1.E = VAL(MID$(h$, 20, 18))
ll.La1.tp = VAL(MID$(h$, 39, 16))
ll.La1.fy = VAL(MID$(h$, 54, 16))

```

```

LINE INPUT #30, h$
ll.La2.E = VAL(MID$(h$, 20, 18))
ll.La2.tp = VAL(MID$(h$, 39, 16))

```

```

LINE INPUT #30, h$
ll.Ma1.E = VAL(MID$(h$, 20, 18))
ll.Ma1.tp = VAL(MID$(h$, 39, 16))

```

```

LINE INPUT #30, h$
ll.Ma2.E = VAL(MID$(h$, 20, 18))
ll.Ma2.tp = VAL(MID$(h$, 39, 16))

```

```

END IF
END IF
LOOP

```

```

CLOSE #30

```

```

elem.Ka.E = (100 * ll.Ka1.E + 50 * ll.Ka2.E) / 150
elem.Ka.tp = ll.Ka1.tp + ll.Ka2.tp
elem.Ka.fy = ll.Ka1.fy

```

```

elem.Kb.E = (14 * ll.Kb1.E + 6 * ll.Kb3.E + .5 * ll.Kb2.E) / 20.5
elem.Kb.tp = ll.Kb1.tp + ll.Kb2.tp + ll.Kb3.tp

```

```

'elem.Kb2.E = ll.Kb2.E: elem.Kb1.E = ll.Kb1.E: elem.Kb3.E = ll.Kb3.E
'elem.Ka1.E = ll.Ka1.E: elem.Ka2.E = ll.Ka2.E: elem.Lg3.E = ll.Lg3.E
'elem.Lg2.E = ll.Lg2.E: elem.Lb3.E = ll.Lb3.E: elem.Lb4.E = ll.Lb4.E
'elem.Lg6.E = ll.Lg6.E: elem.Lg1.E = ll.Lg1.E: elem.Lb1.E = ll.Lb1.E

```

```

'elem.Ln.E = ll.Ln.E: elem.Lb5.E = ll.Lb5.E: elem.Lb215.E = ll.Lb215.E
'elem.l.E = ll.l.E: elem.La1.E = ll.La1.E: elem.La2.E = ll.La2.E
'elem.Ma1.E = ll.Ma1.E: elem.Ma2.E = ll.Ma2.E

```

```

elem.La.E = (100 * ll.La1.E + 10 * La2.E) / 110
elem.La.tp = ll.La1.tp + ll.La2.tp
elem.La.fy = ll.La1.fy

```

```

END SUB

```

```

FUNCTION split$(s$)

```

```

h$ = LTRIM$(RTRIM$(s$))
i% = INSTR(h$, " ")
IF i% = 0 THEN
  XS = LTRIM$(h$)
  s$ = ""
ELSE

```

```

  XS = LEFT$(h$, i% - 1)
  s$ = LTRIM$(RIGHT$(h$, LEN(h$) - i%))
END IF
splits = XS

```

```

END FUNCTION

```

## 4.2 MODMCM.BAS

```

DECLARE FUNCTION splits$(s$)
DECLARE FUNCTION Sigma(E, SO, SI, S2, S3, Conv)

```

```

'MODMCM V1.10 2002.06.06
'MODMCM V1.00 2001.10.30
'MODMCM V0.91 2001.10.29
'MODMCM V0.90 2001.10.24

```

The number of the elements 94  
The following functions calculate the mass absorption coefficient of the different elements

```

DECLARE FUNCTION EIToZ%(el$)
DECLARE FUNCTION TauNe!(E)
DECLARE FUNCTION TauN!(E)
DECLARE FUNCTION TauHe!(E)
DECLARE FUNCTION TauO!(E)
DECLARE FUNCTION TauAl!(E)
DECLARE FUNCTION TauAu!(E)
DECLARE FUNCTION TauB!(E)
DECLARE FUNCTION TauBa!(E)
DECLARE FUNCTION TauBe!(E)
DECLARE FUNCTION TauBi!(E)
DECLARE FUNCTION TauBr!(E)
DECLARE FUNCTION tauCl!(E)
DECLARE FUNCTION TauCa!(E)
DECLARE FUNCTION TauCd!(E)
DECLARE FUNCTION TauCe!(E)
DECLARE FUNCTION TauCh!(E)
DECLARE FUNCTION TauAr!(E)
DECLARE FUNCTION TauCo!(E)
DECLARE FUNCTION TauCr!(E)
DECLARE FUNCTION TauCs!(E)
DECLARE FUNCTION TauCu!(E)
DECLARE FUNCTION TauDy!(E)
DECLARE FUNCTION TauEr!(E)
DECLARE FUNCTION TauEu!(E)
DECLARE FUNCTION TauFe!(E)
DECLARE FUNCTION TauGa!(E)
DECLARE FUNCTION TauGd!(E)
DECLARE FUNCTION TauGg!(E)
DECLARE FUNCTION TauHg!(E)
DECLARE FUNCTION TauHf!(E)
DECLARE FUNCTION TauHl!(E)
DECLARE FUNCTION TauIn!(E)
DECLARE FUNCTION TauIr!(E)
DECLARE FUNCTION TauK!(E)
DECLARE FUNCTION TauKd!(E)
DECLARE FUNCTION TauLa!(E)
DECLARE FUNCTION TauLi!(E)
DECLARE FUNCTION TauLu!(E)
DECLARE FUNCTION TauMg!(E)
DECLARE FUNCTION TauMn!(E)
DECLARE FUNCTION TauMo!(E)
DECLARE FUNCTION TauNa!(E)
DECLARE FUNCTION TauNb!(E)
DECLARE FUNCTION TauNd!(E)
DECLARE FUNCTION TauNi!(E)
DECLARE FUNCTION TauOs!(E)
DECLARE FUNCTION TauP!(E)
DECLARE FUNCTION TauPb!(E)
DECLARE FUNCTION TauPd!(E)
DECLARE FUNCTION TauPm!(E)
DECLARE FUNCTION TauPr!(E)
DECLARE FUNCTION TauPt!(E)
DECLARE FUNCTION TauPu!(E)
DECLARE FUNCTION TauRb!(E)
DECLARE FUNCTION TauRe!(E)
DECLARE FUNCTION TauRh!(E)
DECLARE FUNCTION TauRu!(E)
DECLARE FUNCTION TauRf!(E)
DECLARE FUNCTION TauS!(E)
DECLARE FUNCTION TauSb!(E)
DECLARE FUNCTION TauSc!(E)
DECLARE FUNCTION TauSe!(E)
DECLARE FUNCTION TauSh!(E)
DECLARE FUNCTION TauSm!(E)
DECLARE FUNCTION TauSn!(E)
DECLARE FUNCTION TauSr!(E)
DECLARE FUNCTION TauTa!(E)
DECLARE FUNCTION TauTb!(E)
DECLARE FUNCTION TauTc!(E)
DECLARE FUNCTION TauTe!(E)
DECLARE FUNCTION TauTh!(E)
DECLARE FUNCTION TauTi!(E)
DECLARE FUNCTION TauTl!(E)
DECLARE FUNCTION TauTm!(E)
DECLARE FUNCTION TauU!(E)
DECLARE FUNCTION TauV!(E)
DECLARE FUNCTION TauW!(E)
DECLARE FUNCTION TauXe!(E)
DECLARE FUNCTION TauY!(E)

```

```

DECLARE FUNCTION TauYb(E)
DECLARE FUNCTION tauZ0(E, Z AS INTEGER)
DECLARE FUNCTION TauZn(E)
DECLARE FUNCTION TauZr(E)
DECLARE FUNCTION TauAs(E)
DECLARE FUNCTION TauAl(E)
DECLARE FUNCTION TauAg(E)
DECLARE FUNCTION TauRa(E)
DECLARE FUNCTION TauPa(E)
DECLARE FUNCTION TauNp(E)
DECLARE FUNCTION TauFr(E)
DECLARE FUNCTION TauAt(E)
DECLARE FUNCTION TauAc(E)
DECLARE FUNCTION TauPo(E)

INPUT "Input the element": eIS

OPEN "D:\work\shaltout\conv.dat" FOR INPUT AS #99
LINE INPUT #99, hS: LINE INPUT #99, hS
DO WHILE EOF(99) <> -1
LINE INPUT #99, hS
eIS = split(hS): Z% = VAL(split(hS)): Conv = VAL(split(hS))
IF UCASE$(eIS) = UCASE$(eIS) THEN EXIT DO
LOOP
CLOSE #99

OPEN "D:\work\shaltout\cid\CROSS-1.dat" FOR INPUT AS #70
DO WHILE EOF(70) <> -1
LINE INPUT #70, hS: XS = split(hS): XS = split(hS): XS = split(hS)
IF UCASE$(XS) = UCASE$(eIS) THEN
LINE INPUT #70, hS: LINE INPUT #70, hS: LINE INPUT #70, hS
DO
SO = VAL(split(hS)): S1 = VAL(split(hS))
S2 = VAL(split(hS)): S3 = VAL(split(hS))
LINE INPUT #70, hS
IF LEFT$(hS, 2) = "#S" THEN
EXIT DO
END IF
LOOP
EXIT DO
END IF
LOOP
CLOSE #70

OPEN "D:\work\shaltout\cid\CROSS-3.dat" FOR INPUT AS #71
DO WHILE EOF(71) <> -1
LINE INPUT #71, hS: XS = split(hS): XS = split(hS): XS = split(hS)
IF UCASE$(XS) = UCASE$(eIS) THEN
LINE INPUT #71, hS: LINE INPUT #71, hS: LINE INPUT #71, hS
DO
SSO = VAL(split(hS)): SS1 = VAL(split(hS))
SS2 = VAL(split(hS)): SS3 = VAL(split(hS))
LINE INPUT #71, hS
IF LEFT$(hS, 2) = "#S" THEN
EXIT DO
END IF
LOOP
EXIT DO
END IF
LOOP
CLOSE #71

OPEN "test1.dat" FOR OUTPUT AS #1
FOR li = 1 TO 1000 STEP .01
Tau = tauZ0(E, Z%): SSGM1 = Sigma(E, SO, S1, S2, S3, Conv)
SSGM2 = Sigma(E, SSO, SS1, SS2, SS3, Conv)
Mu = Tau + SSGM1 + SSGM2
PRINT #1, E, Tau, SSGM1, SSGM2, Mu
NEXT E
CLOSE #1

OPEN "cmd.plt" FOR OUTPUT AS #10
PRINT #10, "cd 'D:\work\shaltout'"
PRINT #10, "set grid"
PRINT #10, "set logscale"
PRINT #10, "set ylabel '2'"
PRINT #10, "set xlabel 'Photon Energy, keV'"
PRINT #10, "set ylabel 'X-ray Cross Sections, cm^2/g'"
PRINT #10, "plot[1:300] 'test1.dat' using 1:2 t 'Photoelectric cross section' w lin"
PRINT #10, "replot 'test1.dat' using 1:3 t 'Incoherent cross section' w lin"
PRINT #10, "replot 'test1.dat' using 1:4 t 'Coherent cross section' w lin"
PRINT #10, "replot 'test1.dat' using 1:5 t 'Mass absorption cross section' w lin"
PRINT #10, "pause -1"
CLOSE #10
SHELL "C:\gnuplot\wgnuplotcmd.plt"

FUNCTION EffToZ%(eIS)
IF LEN(eIS) > 2 THEN
PRINT USING "Element & not found": eIS
END
END IF

hS = RTRIM$(UCASE$(eIS))

OPEN "ELTAB.DAT" FOR INPUT AS #28
DO WHILE EOF(28) <> -1
INPUT #28, Z%, helS
IF helS = hS THEN
EffToZ% = Z%
CLOSE #28
EXIT FUNCTION
END IF

```

```

LOOP
PRINT USING "Element \ \ not found": eIS

CLOSE #28
END
END FUNCTION

SUB SGM1 (S0, S1, S2, S3)
END SUB

FUNCTION Sigma (E, SO, S1, S2, S3, Conv)
IF E >= .014 THEN
B1 = S1 * LOG(E)
B2 = S2 * LOG(E) - 2
B3 = S3 * LOG(E) - 3
BT = (1 / Conv) * EXP(SO + B1 + B2 + B3)
ELSE
PRINT "Error in Scattering: invalid E"
END
END IF

Sigma = BT

END FUNCTION

FUNCTION split$(s$)
hS = LTRIM$(RTRIM$(s$))
I% = INSTR(hS, " ")
IF I% = 0 THEN
XS = LTRIM$(hS)
sS = " "
ELSE
XS = LEFT$(hS, I% - 1)
sS = LTRIM$(RIGHT$(hS, LEN(hS) - I%))
END IF
splits = XS

END FUNCTION

FUNCTION TauAc (e)
IF e >= 106.755# THEN
S1 = .77101362# * LOG(e): S2 = -.69411987# * LOG(e) ^ 2
S3 = .047591546# * LOG(e) ^ 3
ST = 1 / 376.94 * EXP(14.299495# + S1 + S2 + S3)
ELSE
IF e >= 19.84# THEN
S1 = -.35023436# * LOG(e): S2 = .28489766# * LOG(e) ^ 2
S3 = -.030019821# * LOG(e) ^ 3
ST = 1 / 376.94 * EXP(19.316307# + S1 + S2 + S3)
ELSE
IF e >= 19.0832# THEN
S1 = -.35023436# * LOG(e): S2 = .28489766# * LOG(e) ^ 2
S3 = -.030019821# * LOG(e) ^ 3
ST = 1 / 376.94 * EXP(19.316307# + S1 + S2 + S3) / 1.154832#
ELSE
IF e >= 15.871# THEN
S1 = -.35023436# * LOG(e): S2 = .28489766# * LOG(e) ^ 2
S3 = -.030019821# * LOG(e) ^ 3
ST = 1 / 376.94 * EXP(19.316307# + S1 + S2 + S3) / 1.629284334#
ELSE
IF e >= 5.002# THEN
S1 = -.35729622# * LOG(e)
S2 = .58709782# * LOG(e) ^ 2: S3 = -.10353805# * LOG(e) ^ 3
ST = 1 / 376.94 * EXP(17.391769# + S1 + S2 + S3)
ELSE
IF e >= 4.656# THEN
S1 = -.35729622# * LOG(e)
S2 = .58709782# * LOG(e) ^ 2: S3 = -.10353805# * LOG(e) ^ 3
ST = 1 / 376.94 * EXP(17.391769# + S1 + S2 + S3) / 1.04371#
ELSE
IF e >= 3.909# THEN
S1 = -.35729622# * LOG(e)
S2 = .58709782# * LOG(e) ^ 2: S3 = -.10353805# * LOG(e) ^ 3
ST = 1 / 376.94 * EXP(17.391769# + S1 + S2 + S3) / 1.107929685#
ELSE
IF e >= 3.3702# THEN
S1 = -.35729622# * LOG(e)
S2 = .58709782# * LOG(e) ^ 2: S3 = -.10353805# * LOG(e) ^ 3
ST = 1 / 376.94 * EXP(17.391769# + S1 + S2 + S3) / 1.286939325#
ELSE
IF e >= 3.219# THEN
S1 = -.35729622# * LOG(e)
S2 = .58709782# * LOG(e) ^ 2: S3 = -.10353805# * LOG(e) ^ 3
ST = 1 / 376.94 * EXP(17.391769# + S1 + S2 + S3) / 1.864643427#
ELSE
IF e >= 1.269# THEN
S1 = -.1811576# * LOG(e)
S2 = -.29527166# * LOG(e) ^ 2: S3 = .053166901# * LOG(e) ^ 3
ST = 1 / 376.94 * EXP(14.740629# + S1 + S2 + S3)
ELSE
IF e >= 1.08# THEN
S1 = -.1811576# * LOG(e)
S2 = -.29527166# * LOG(e) ^ 2: S3 = .053166901# * LOG(e) ^ 3
ST = 1 / 376.94 * EXP(14.740629# + S1 + S2 + S3) / 1.0196557#
END IF
END IF

```







```

B2 = -.20053 * LOG(e) ^ 2
B3 = .0207248 * LOG(e) ^ 3
BT = (1 / 19.94) * EXP(10.6879 + I)1 + B2 + B3)
ELSE
  PRINT "Error in function TauC: invalid E"
END
END IF
TauC = BT

END FUNCTION

FUNCTION TauCa (e)
  IF e >= 4.0381 THEN
    S1 = -1.88644 * LOG(e); S2 = -.283647 * LOG(e) * 2
    S3 = .0226263 * LOG(e) - 3
    ST = 1 / 66.55 * EXP(14.295 + S1 + S2 + S3)
  ELSE
    IF e >= .4 THEN
      S1 = -2.55011 * LOG(e); S2 = -.0943195 * LOG(e) - 2
      ST = 1 / 66.55 * EXP(12.7044 + S1 + S2)
    ELSE
      PRINT "Error in function tauCa: invalid e"
    END
  END IF
END IF
TauCa = ST

END FUNCTION

FUNCTION TauCd (c)
  IF c >= 26.7112 THEN
    S1 = 1.07714 * LOG(c); S2 = -.831424 * LOG(e) - 2
    S3 = .057912 * LOG(e) - 3
    ST = 1 / 186.6 * EXP(12.5254 + S1 + S2 + S3)
  ELSE
    IF e >= 4.018 THEN
      S1 = -2.38363 * LOG(e); S2 = -.0801104 * LOG(c) - 2
      ST = 1 / 186.6 * EXP(15.9668 + S1 + S2)
    ELSE
      IF e >= 3.727 THEN
        S1 = -2.38363 * LOG(e); S2 = -.0801104 * LOG(e) - 2
        ST = 1 / 186.6 * EXP(15.9668 + S1 + S2) * (1 / 1.16)
      ELSE
        IF e >= 3.5375 THEN
          S1 = -2.38363 * LOG(e); S2 = -.0801104 * LOG(c) ^ 2
          ST = 1 / 186.6 * EXP(15.9668 + S1 + S2) * (1 / 1.636)
        ELSE
          IF e >= .77 THEN
            S1 = -2.52756 * LOG(e)
            ST = 1 / 186.6 * EXP(14.3497 + S1)
          ELSE
            PRINT "Error in function tauCd: invalid e"
          END
        END IF
      END IF
    END IF
  END IF
  TauCd = ST

END FUNCTION

FUNCTION TauCe (c)
  IF e >= 40.443 THEN
    S1 = 2.74562 * LOG(e); S2 = -1.14174 * LOG(e) ^ 2
    S3 = .0774162 * LOG(e) ^ 3
    ST = 1 / 232.7 * EXP(10.2725 + S1 + S2 + S3)
  ELSE
    IF e >= 6.5488 THEN
      S1 = -2.36288 * LOG(e); S2 = -.0654708 * LOG(e) ^ 2
      ST = 1 / 232.7 * EXP(16.5862 + S1 + S2)
    ELSE
      IF e >= 6.1642 THEN
        S1 = -2.36288 * LOG(e); S2 = -.0654708 * LOG(e) - 2
        ST = 1 / 232.7 * EXP(16.5862 + S1 + S2) * (1 / 1.16)
      ELSE
        IF e >= 5.7234 THEN
          S1 = -2.36288 * LOG(e); S2 = -.0654708 * LOG(e) - 2
          ST = 1 / 232.7 * EXP(16.5862 + S1 + S2) * (1 / 1.636)
        ELSE
          IF e >= 1.4346 THEN
            S1 = -2.58174 * LOG(e)
            ST = 1 / 232.7 * EXP(15.2693 + S1)
          ELSE
            IF c >= 1.2728 THEN
              S1 = -2.58174 * LOG(e)
              ST = 1 / 232.7 * EXP(15.2693 + S1) / 1.06001
            ELSE
              IF e >= 1.1854 THEN
                S1 = -2.58174 * LOG(e)
                ST = 1 / 232.7 * EXP(15.2693 + S1) / 1.15997
              ELSE
                S1 = -2.58174 * LOG(e)
                ST = 1 / 232.7 * EXP(15.2693 + S1) / 1.50988
              END IF
            END IF
          END IF
        END IF
      END IF
    END IF
  END IF
  TauCe = ST

END FUNCTION

```

```

END IF
END IF

TauCe = ST

END FUNCTION

FUNCTION TauCl (c)
  IF e >= 2.8224 THEN
    S1 = -1.71937 * LOG(e); S2 = -.354154 * LOG(e) ^ 2
    S3 = .0290841 * LOG(e) ^ 3
    ST = 1 / 58.87 * EXP(13.6188 + S1 + S2 + S3)
  ELSE
    IF e >= .238 THEN
      S1 = -2.41694 * LOG(e); S2 = -.240897 * LOG(e) ^ 2
      ST = 1 / 58.87 * EXP(12.0031 + S1 + S2)
    ELSE
      PRINT "Error in function tauCl: invalid e"
    END
  END IF
END IF
TauCl = ST

END FUNCTION

FUNCTION TauCo (c)
  IF e >= 7.7089 THEN
    S1 = -1.38933 * LOG(e); S2 = -.386631 * LOG(e) ^ 2
    S3 = .0303286 * LOG(e) ^ 3
    ST = 1 / 97.85 * EXP(14.7047 + S1 + S2 + S3)
  ELSE
    IF e >= .929 THEN
      S1 = -2.50669 * LOG(c); S2 = -.0869945 * LOG(e) ^ 2
      ST = 1 / 97.85 * EXP(13.8699 + S1 + S2)
    ELSE
      PRINT "Error in function tauCo: invalid e"
    END
  END IF
END IF
TauCo = ST

END FUNCTION

FUNCTION TauCr (c)
  IF e >= 5.9892 THEN
    S1 = -1.8243 * LOG(e); S2 = -.279116 * LOG(e) ^ 2
    S3 = .0217324 * LOG(e) ^ 3
    ST = 1 / 86.34 * EXP(14.8019 + S1 + S2 + S3)
  ELSE
    IF e >= .999 THEN
      S1 = -2.51532 * LOG(e); S2 = -.101999 * LOG(e) ^ 2
      ST = 1 / 86.34 * EXP(13.4236 + S1 + S2)
    ELSE
      PRINT "Error in function tauCr: invalid e"
    END
  END IF
END IF
TauCr = ST

END FUNCTION

FUNCTION TauCs (e)
  IF e >= 35.9846 THEN
    S1 = 1.94161 * LOG(c); S2 = -.983232 * LOG(e) ^ 2
    S3 = .0671986 * LOG(e) ^ 3
    ST = 1 / 220.7 * EXP(11.3757 + S1 + S2 + S3)
  ELSE
    IF e >= 5.7143 THEN
      S1 = -2.46363 * LOG(e); S2 = -.0542849 * LOG(e) ^ 2
      ST = 1 / 220.7 * EXP(16.5418 + S1 + S2)
    ELSE
      IF e >= 5.3594 THEN
        S1 = -2.46363 * LOG(e); S2 = -.0542849 * LOG(e) ^ 2
        ST = 1 / 220.7 * EXP(16.5418 + S1 + S2) * (1 / 1.16)
      ELSE
        IF e >= 5.0119 THEN
          S1 = -2.46363 * LOG(e); S2 = -.0542849 * LOG(e) ^ 2
          ST = 1 / 220.7 * EXP(16.5418 + S1 + S2) * (1 / 1.636)
        ELSE
          IF e >= 1.2171 THEN
            S1 = -2.53145 * LOG(e)
            ST = 1 / 220.7 * EXP(14.9713 + S1)
          ELSE
            IF e >= 1.065 THEN
              S1 = -2.53145 * LOG(e)
              ST = 1 / 220.7 * EXP(14.9713 + S1) / 1.04998
            ELSE
              IF e >= .9976 THEN
                S1 = -2.53145 * LOG(e)
                ST = 1 / 220.7 * EXP(14.9713 + S1) / 1.14951
              ELSE
                IF e >= .739 THEN
                  S1 = -2.53145 * LOG(e)
                  ST = 1 / 220.7 * EXP(14.9713 + S1) / 1.47005
                ELSE
                  PRINT "Error in function tauCs: invalid e"
                END
              END IF
            END IF
          END IF
        END IF
      END IF
    END IF
  END IF
  TauCs = ST

END FUNCTION

```



```

PRINT "Error in function TauF: invalid E"
END
END IF
TauF = BT
END FUNCTION
FUNCTION TauFe (e)
IF e >= 7.112 THEN
S1 = -1.23491 * LOG(e); S2 = -.418785 * LOG(e) ^ 2
S3 = .0321662 * LOG(e) ^ 3
ST = 1 / 92.74 * EXP(14.3456 + S1 + S2 + S3)
ELSE
IF e >= .999 THEN
S1 = -2.39195 * LOG(e); S2 = -.137648 * LOG(e) ^ 2
ST = 1 / 92.74 * EXP(13.6696 + S1 + S2)
ELSE
PRINT "Error in function taufe: invalid e"
END
END IF
END IF
TauFe = ST
END FUNCTION
FUNCTION TauFr(c)
IF e >= 101.137# THEN
S1 = .99651839# * LOG(e); S2 = -.7370386799999999# * LOG(e) ^ 2
S3 = .050139395# * LOG(e) - 3
ST = 1 / 370.3 * EXP(13.846207# + S1 + S2 + S3)
ELSE
IF e >= 18.639# THEN
S1 = -3.0122329# * LOG(e); S2 = .15276719# * LOG(e) ^ 2
S3 = -.018567205# * LOG(e) ^ 3
ST = 1 / 370.3 * EXP(18.638909# + S1 + S2 + S3)
ELSE
IF e >= 17.9065# THEN
S1 = -3.0122329# * LOG(e); S2 = .15276719# * LOG(e) - 2
S3 = -.018567205# * LOG(e) - 3
ST = 1 / 370.3 * EXP(18.638909# + S1 + S2 + S3) / 1.155423#
ELSE
IF e >= 15.0312# THEN
S1 = -3.0122329# * LOG(e); S2 = .15276719# * LOG(e) - 2
S3 = -.018567205# * LOG(e) ^ 3
ST = 1 / 370.3 * EXP(18.638909# + S1 + S2 + S3) / 1.620916352#
ELSE
IF e >= 4.652# THEN
S1 = -6.3479143# * LOG(e); S2 = 2.0011003# * LOG(e) ^ 2
S3 = -.33635566# * LOG(e) ^ 3
ST = 1 / 370.3 * EXP(19.059012# + S1 + S2 + S3)
ELSE
IF e >= 4.327# THEN
S1 = -6.3479143# * LOG(e); S2 = 2.0011003# * LOG(e) ^ 2
S3 = -.33635566# * LOG(e) ^ 3
ST = 1 / 370.3 * EXP(19.059012# + S1 + S2 + S3) / 1.0441191#
ELSE
IF e >= 3.663# THEN
S1 = -6.3479143# * LOG(e); S2 = 2.0011003# * LOG(e) ^ 2
S3 = -.33635566# * LOG(e) ^ 3
ST = 1 / 370.3 * EXP(19.059012# + S1 + S2 + S3) / 1.108875993#
ELSE
IF e >= 3.1362# THEN
S1 = -6.3479143# * LOG(e); S2 = 2.0011003# * LOG(e) ^ 2
S3 = -.33635566# * LOG(e) ^ 3
ST = 1 / 370.3 * EXP(19.059012# + S1 + S2 + S3) / 1.290090615#
ELSE
IF e >= 2.9999# THEN
S1 = -6.3479143# * LOG(e); S2 = 2.0011003# * LOG(e) ^ 2
S3 = -.33635566# * LOG(e) - 3
ST = 1 / 370.3 * EXP(19.059012# + S1 + S2 + S3) / 2.00447081#
ELSE
IF e >= 1.153# THEN
S1 = -1.8018958# * LOG(e)
S2 = -.32333809# * LOG(e) - 2; S3 = 6.861969399999999D-02 * LOG(e) - 3
ST = 1 / 370.3 * EXP(14.692429# + S1 + S2 + S3)
ELSE
S1 = -1.8018958# * LOG(e)
S2 = -.32333809# * LOG(e) ^ 2; S3 = 6.861969399999999D-02 * LOG(e) - 3
ST = 1 / 370.3 * EXP(14.692429# + S1 + S2 + S3) / 1.0214993#
END IF
END IF
END IF
END IF
END IF
END IF
END IF
END IF
TauFr = ST
END FUNCTION
FUNCTION TauGa(e)
IF e >= 10.3671 THEN
S1 = -.318459 * LOG(e); S2 = -.611348 * LOG(e) ^ 2
S3 = .0458138 * LOG(e) ^ 3
ST = 1 / 115.8 * EXP(13.6182 + S1 + S2 + S3)
ELSE

```

```

IF e >= 1.2977 THEN
S1 = -2.54469 * LOG(e); S2 = -.0757204 * LOG(e) ^ 2
ST = 1 / 115.8 * EXP(14.4795 + S1 + S2)
ELSE
IF e >= 1.1423 THEN
S1 = -2.54469 * LOG(e); S2 = -.0757204 * LOG(e) - 2
ST = 1 / 115.8 * EXP(14.4795 + S1 + S2) * (1 / 1.16)
ELSE
IF e >= 1.1154 THEN
S1 = -2.54469 * LOG(e); S2 = -.0757204 * LOG(e) - 2
ST = 1 / 115.8 * EXP(14.4795 + S1 + S2) * (1 / 1.636)
ELSE
IF e >= .158 THEN
S1 = -2.68965 * LOG(e)
ST = 1 / 115.8 * EXP(12.2646 + S1)
ELSE
PRINT "Error in function tauGa: invalid E"
END
END IF
END IF
END IF
END IF
END IF
TauGa = ST
END FUNCTION
FUNCTION TauGd(c)
IF e >= 50.24 THEN
S1 = 3.03111 * LOG(e); S2 = -1.1752 * LOG(e) ^ 2
S3 = .0786751 * LOG(e) ^ 3
ST = 1 / 261.1 * EXP(9.91968 + S1 + S2 + S3)
ELSE
IF e >= 8.376 THEN
S1 = -2.47838 * LOG(e); S2 = -.0437107 * LOG(e) ^ 2
ST = 1 / 261.1 * EXP(17.1159 + S1 + S2)
ELSE
IF e >= 7.93 THEN
S1 = -2.47838 * LOG(e); S2 = -.0437107 * LOG(e) - 2
ST = 1 / 261.1 * EXP(17.1159 + S1 + S2) / 1.16
ELSE
IF e >= 7.243 THEN
S1 = -2.47838 * LOG(e); S2 = -.0437107 * LOG(e) ^ 2
ST = 1 / 261.1 * EXP(17.1159 + S1 + S2) / 1.636
ELSE
IF e >= 1.881 THEN
S1 = -2.60843 * LOG(e)
ST = 1 / 261.1 * EXP(15.7159 + S1)
ELSE
IF e >= 1.6883 THEN
S1 = -2.60843 * LOG(e)
ST = 1 / 261.1 * EXP(15.7159 + S1) / 1.07022
ELSE
IF e >= 1.544 THEN
S1 = -2.60843 * LOG(e)
ST = 1 / 261.1 * EXP(15.7159 + S1) / 1.18022
ELSE
IF e >= 1.2172 THEN
S1 = -2.60843 * LOG(e)
ST = 1 / 261.1 * EXP(15.7159 + S1) / 1.5601
ELSE
IF e >= 1.185 THEN
S1 = -2.60843 * LOG(e)
ST = 1 / 261.1 * EXP(15.7159 + S1) / 2.29042
ELSE
S1 = -2.6085396# * LOG(e)
ST = 1 / 261.1 * EXP(13.5452754# + S1)
END IF
END IF
END IF
END IF
END IF
END IF
END IF
END IF
TauGd = ST
END FUNCTION
FUNCTION TauGe (e)
IF e >= 11.1031 THEN
S1 = -.479613 * LOG(e); S2 = -.572897 * LOG(e) - 2
S3 = .0431277 * LOG(e) - 3
ST = 1 / 120.5 * EXP(13.9288 + S1 + S2 + S3)
ELSE
IF e >= 1.4143 THEN
S1 = -2.69285 * LOG(e); S2 = -.0208355 * LOG(e) ^ 2
ST = 1 / 120.5 * EXP(14.6813 + S1 + S2)
ELSE
IF e >= 1.2478 THEN
S1 = -2.69285 * LOG(e); S2 = -.0208355 * LOG(e) ^ 2
ST = 1 / 120.5 * EXP(14.6813 + S1 + S2) * (1 / 1.16)
ELSE
IF e >= 1.2167 THEN
S1 = -2.69285 * LOG(e); S2 = -.0208355 * LOG(e) - 2
ST = 1 / 120.5 * EXP(14.6813 + S1 + S2) * (1 / 1.636)
ELSE
IF e >= .181 THEN
S1 = -2.53085 * LOG(e)
ST = 1 / 120.5 * EXP(12.4133 + S1)

```

```

ELSE
  PRINT "Error in function tauGe: invalide"
END
END IF
END IF
END IF
END IF
END IF
TauGc = ST
END FUNCTION
FUNCTION TauH(c)
IF e >= .014 THEN
  B1 = -3.34953 * LOG(e)
  B2 = -.047137 * LOG(e) ^ 2
  B3 = .00709962# * LOG(e) - 3
  BT = (1 / 1.674) * EXP(2.44964 + B1 + B2 + B3)
ELSE
  PRINT "Error in function TauH: invalide E"
END
END IF
TauH = BT
END FUNCTION
FUNCTION TauHe(e)
IF e >= .025 THEN
  B1 = -3.29053 * LOG(e)
  B2 = -.107256 * LOG(e) ^ 2
  B3 = .0144465 * LOG(e) ^ 3
  BT = (1 / 6.647) * EXP(6.06488 + B1 + B2 + B3)
ELSE
  PRINT "Error in function TauHe: invalide E"
END
END IF
TauHe = BT
END FUNCTION
FUNCTION TauHf(e)
IF e >= 65.3508 THEN
  S1 = 4.47037 * LOG(e); S2 = -1.42808 * LOG(e) ^ 2
  S3 = .0939044 * LOG(e) ^ 3
  ST = 1 / 296.4 * EXP(7.5816 + S1 + S2 + S3)
ELSE
  IF e >= 11.2707 THEN
    S1 = -1.82851 * LOG(e); S2 = -.132268 * LOG(e) ^ 2
    ST = 1 / 296.4 * EXP(16.4329 + S1 + S2)
  ELSE
    IF e >= 10.7394 THEN
      S1 = -1.82851 * LOG(e); S2 = -.132268 * LOG(e) ^ 2
      ST = 1 / 296.4 * EXP(16.4329 + S1 + S2) * (1 / 1.16)
    ELSE
      IF e >= 9.5607 THEN
        S1 = -1.82851 * LOG(e); S2 = -.132268 * LOG(e) - 2
        ST = 1 / 296.4 * EXP(16.4329 + S1 + S2) * (1 / 1.636)
      ELSE
        IF e >= 2.6009 THEN
          S1 = -2.66622 * LOG(e)
          ST = 1 / 296.4 * EXP(16.2758 + S1)
        ELSE
          IF e >= 2.3654 THEN
            S1 = -2.66622 * LOG(e)
            ST = 1 / 296.4 * EXP(16.2758 + S1) / 1.079917832#
          ELSE
            IF e >= 2.1076 THEN
              S1 = -2.66622 * LOG(e)
              ST = 1 / 296.4 * EXP(16.2758 + S1) / 1.209920679#
            ELSE
              IF e >= 1.7164 THEN
                S1 = -2.66622 * LOG(e)
                ST = 1 / 296.4 * EXP(16.2758 + S1) / 1.609647683#
              ELSE
                IF e >= 1.6617 THEN
                  S1 = -2.66622 * LOG(e)
                  ST = 1 / 296.4 * EXP(16.2758 + S1) / 2.289760107#
                ELSE
                  S1 = -2.42829 * LOG(e)
                  ST = 1 / 296.4 * EXP(14.0548 + S1)
                END IF
              END IF
            END IF
          END IF
        END IF
      END IF
    END IF
  END IF
  TauHf = ST
END FUNCTION
FUNCTION TauIg(c)
IF e >= 83.1023 THEN
  S1 = -1.9799 * LOG(e); S2 = -.276981 * LOG(e) - 2

```

```

  S3 = .0268856 * LOG(e) ^ 3
  ST = 1 / 333.1 * EXP(19.7594 + S1 + S2 + S3)
ELSE
  IF e >= 14.8393 THEN
    S1 = -2.0847 * LOG(e); S2 = -.0853294 * LOG(e) - 2
    ST = 1 / 333.1 * EXP(17.1857 + S1 + S2)
  ELSE
    IF e >= 14.2087 THEN
      S1 = -2.0847 * LOG(e); S2 = -.0853294 * LOG(e) ^ 2
      ST = 1 / 333.1 * EXP(17.1857 + S1 + S2) * (1 / 1.16)
    ELSE
      IF e >= 12.2839 THEN
        S1 = -2.0847 * LOG(e); S2 = -.0853294 * LOG(e) ^ 2
        ST = 1 / 333.1 * EXP(17.1857 + S1 + S2) * (1 / 1.636)
      ELSE
        IF e >= 3.5616 THEN
          S1 = -2.6067 * LOG(e)
          ST = 1 / 333.1 * EXP(16.5903 + S1)
        ELSE
          IF e >= 3.2785 THEN
            S1 = -2.6067 * LOG(e)
            ST = 1 / 333.1 * EXP(16.5903 + S1) / 1.0797689#
          ELSE
            IF e >= 2.8471 THEN
              S1 = -2.6067 * LOG(e)
              ST = 1 / 333.1 * EXP(16.5903 + S1) / 1.219653384#
            ELSE
              IF e >= 2.3849 THEN
                S1 = -2.6067 * LOG(e)
                ST = 1 / 333.1 * EXP(16.5903 + S1) / 1.640285869#
              ELSE
                IF e >= 2.2949 THEN
                  S1 = -2.6067 * LOG(e)
                  ST = 1 / 333.1 * EXP(16.5903 + S1) / 2.280016805#
                ELSE
                  S1 = -2.33016 * LOG(e)
                  ST = 1 / 333.1 * EXP(14.5195 + S1)
                END IF
              END IF
            END IF
          END IF
        END IF
      END IF
    END IF
  END IF
  TauIg = ST
END FUNCTION
FUNCTION TauIe(e)
IF e >= 55.6177 THEN
  S1 = 3.71822 * LOG(e); S2 = -1.29273 * LOG(e) ^ 2
  S3 = .0855026 * LOG(e) ^ 3
  ST = 1 / 273.9 * EXP(8.75203 + S1 + S2 + S3)
ELSE
  IF 0 = 9.3942 THEN
    S1 = -2.72523 * LOG(e); S2 = -8.19409E-04 * LOG(e) - 2
    ST = 1 / 273.9 * EXP(17.6583 + S1 + S2)
  ELSE
    IF e >= 8.9178 THEN
      S1 = -2.72523 * LOG(e); S2 = -8.19409E-04 * LOG(e) ^ 2
      ST = 1 / 273.9 * EXP(17.6583 + S1 + S2) / 1.16
    ELSE
      IF e >= 8.0711 THEN
        S1 = -2.72523 * LOG(e); S2 = -8.19409E-04 * LOG(e) - 2
        ST = 1 / 273.9 * EXP(17.6583 + S1 + S2) / 1.636
      ELSE
        IF e >= 2.1283 THEN
          S1 = -2.67903 * LOG(e)
          ST = 1 / 273.9 * EXP(16.014 + S1)
        ELSE
          IF e >= 1.9228 THEN
            S1 = -2.67903 * LOG(e)
            ST = 1 / 273.9 * EXP(16.014 + S1) / 1.06981
          ELSE
            IF e >= 1.7412 THEN
              S1 = -2.67903 * LOG(e)
              ST = 1 / 273.9 * EXP(16.014 + S1) / 1.17975
            ELSE
              IF e >= 1.3915 THEN
                S1 = -2.67903 * LOG(e)
                ST = 1 / 273.9 * EXP(16.014 + S1) / 1.57978
              ELSE
                IF e >= 1.3514 THEN
                  S1 = -2.67903 * LOG(e)
                  ST = 1 / 273.9 * EXP(16.014 + S1) / 2.28979
                ELSE
                  S1 = -2.6795252# * LOG(e)
                  ST = 1 / 273.9 * EXP(13.7440146# + S1)
                END IF
              END IF
            END IF
          END IF
        END IF
      END IF
    END IF
  END IF
  TauIe = ST
END FUNCTION

```







```

ST = 1 / 154.3 * EXP(13.3843 + S1 + S2 + S3)
ELSE
IF c >= 2.6977 THEN
SI = -2.20278 * LOG(e); S2 = -.136759 * LOG(e) - 2
ST = 1 / 154.3 * EXP(15.2088 + S1 + S2)
ELSE
IF e >= 2.4647 THEN
SI = -2.20278 * LOG(e); S2 = -.136759 * LOG(e) ^ 2
ST = 1 / 154.3 * EXP(15.2088 + S1 + S2) * (1 / 1.16)
ELSE
IF c >= 2.3705 THEN
SI = -2.20278 * LOG(e); S2 = -.136759 * LOG(e) ^ 2
ST = 1 / 154.3 * EXP(15.2088 + S1 + S2) * (1 / 1.636)
ELSE
IF c >= .468 THEN
SI = -2.50135 * LOG(e)
ST = 1 / 154.3 * EXP(13.5434 + S1)
ELSE
PRINT "Error in function tauNb: invalid II"
END
END IF
END IF
END IF
END IF
UND IF
TauNb = ST
END FUNCTION
FUNCTION TauNd (e)
IF c >= 43.5689 THEN
SI = 1.79481 * LOG(c); S2 = -.93666 * LOG(e) ^ 2
S3 = .0635332 * LOG(e) ^ 3
ST = 1 / 239.6 * EXP(11.7632 + S1 + S2 + S3)
ELSE
IF e >= 7.126 THEN
SI = -2.26073 * LOG(e); S2 = -.0872426 * LOG(e) ^ 2
ST = 1 / 239.6 * EXP(16.5964 + S1 + S2)
ELSE
IF e >= 6.7215 THEN
SI = -2.26073 * LOG(c); S2 = -.0872426 * LOG(e) ^ 2
ST = 1 / 239.6 * EXP(16.5964 + S1 + S2) / 1.16
ELSE
IF e >= 6.2076 THEN
SI = -2.26073 * LOG(e); S2 = -.0872426 * LOG(c) - 2
ST = 1 / 239.6 * EXP(16.5964 + S1 + S2) / 1.636
ELSE
IF e >= 1.5753 THEN
SI = -2.59006 * LOG(e)
ST = 1 / 239.6 * EXP(15.4353 + S1)
ELSE
IF e >= 1.4028 THEN
SI = -2.59006 * LOG(e)
ST = 1 / 239.6 * EXP(15.4353 + S1) / 1.05975
ELSE
IF e >= 1.29974 THEN
SI = -2.59006 * LOG(e)
ST = 1 / 239.6 * EXP(15.4353 + S1) / 1.16973
ELSE
IF e >= 1.004 THEN
SI = -2.59006 * LOG(e)
ST = 1 / 239.6 * EXP(15.4353 + S1) / 1.53965
ELSE
SI = -2.59006 * LOG(e)
ST = 1 / 239.6 * EXP(15.4353 + S1) / 2.27961
END IF
END IF
END IF
END IF
END IF
END IF
TauNd = ST
END FUNCTION
FUNCTION TauNe (e)
IF c >= .867 THEN
B1 = -2.45819 * LOG(e)
B2 = -.212591 * LOG(e) ^ 2
B3 = .0196489 * LOG(e) - 3
BT = (1 / 33.51) * EXP(12.4485 + S1 + B2 + B3)
ELSE
PRINT "Error in function TauNe: invalid E"
END
END IF
TauNe = BT
END FUNCTION
FUNCTION TauNi (e)
IF c >= 8.3328 THEN
SI = -.967736 * LOG(e); S2 = -.47807 * LOG(e) ^ 2
S3 = .0366138 * LOG(e) ^ 3
ST = 1 / 97.45 * EXP(14.2388 + S1 + S2 + S3)
ELSE
IF c >= 1.0081 THEN
SI = -2.4808 * LOG(e); S2 = -.0888115 * LOG(e) ^ 2
ST = 1 / 97.47 * EXP(13.9848 + S1 + S2)
ELSE
IF c >= .872 THEN
SI = -2.4808 * LOG(e); S2 = -.0888115 * LOG(e) ^ 2
ST = 1 / 97.47 * EXP(13.9848 + S1 + S2) / 1.16
ELSE
IF c >= .855 THEN
SI = -2.4808 * LOG(e); S2 = -.0888115 * LOG(e) ^ 2
ST = 1 / 97.47 * EXP(13.9848 + S1 + S2) / 1.636
ELSE
PRINT "Error in function tauNi: invalid e"
END
END IF
END IF
END IF
END IF
TauNi = ST
END FUNCTION
FUNCTION TauNP (e)
IF c >= 118.678 THEN
SI = .22851393# * LOG(e)
S2 = -.59343733# * LOG(e) ^ 2; S3 = .041706129# * LOG(e) - 3
ST = 1 / 393.628 * EXP(15.383751# + S1 + S2 + S3)
ELSE
IF e >= 22.4268 THEN
SI = -3.5103519# * LOG(e); S2 = .27466327# * LOG(e) - 2
S3 = -.027506946# * LOG(e) - 3
ST = 1 / 393.628 * EXP(19.53484# + S1 + S2 + S3)
ELSE
IF c >= 21.6005 THEN
SI = -3.5103519# * LOG(e); S2 = .27466327# * LOG(e) - 2
S3 = -.027506946# * LOG(e) ^ 3
ST = 1 / 393.628 * EXP(19.53484# + S1 + S2 + S3) / 1.1560598#
ELSE
IF e >= 17.61 THEN
SI = -3.5103519# * LOG(e); S2 = .27466327# * LOG(e) ^ 2
S3 = -.027506946# * LOG(e) ^ 3
ST = 1 / 393.628 * EXP(19.53484# + S1 + S2 + S3) / 1.64325785#
ELSE
IF e >= 5.7232 THEN
SI = -2.8016067# * LOG(e)
S2 = .18745434# * LOG(e) - 2; S3 = -.036336006# * LOG(e) ^ 3
ST = 1 / 393.628 * EXP(17.077399# + S1 + S2 + S3)
ELSE
IF e >= 5.3662 THEN
SI = -2.8016067# * LOG(e)
S2 = .18745434# * LOG(e) ^ 2; S3 = -.036336006# * LOG(e) ^ 3
ST = 1 / 393.628 * EXP(17.077399# + S1 + S2 + S3) / 1.0435581#
ELSE
IF e >= 4.4347 THEN
SI = -2.8016067# * LOG(e)
S2 = .18745434# * LOG(e) ^ 2; S3 = -.036336006# * LOG(e) - 3
ST = 1 / 393.628 * EXP(17.077399# + S1 + S2 + S3) / 1.10645846#
ELSE
IF e >= 3.8503 THEN
SI = -2.8016067# * LOG(e)
S2 = .18745434# * LOG(e) ^ 2; S3 = -.036336006# * LOG(e) ^ 3
ST = 1 / 393.628 * EXP(17.077399# + S1 + S2 + S3) / 1.289435598#
ELSE
IF e >= 3.6658 THEN
SI = -2.8016067# * LOG(e)
S2 = .18745434# * LOG(e) ^ 2; S3 = -.036336006# * LOG(e) ^ 3
ST = 1 / 393.628 * EXP(17.077399# + S1 + S2 + S3) / 1.82604673#
ELSE
IF e >= 1.5007 THEN
SI = -1.7546831# * LOG(e)
S2 = -.35584379# * LOG(e) ^ 1; S3 = .075525649# * LOG(e) - 3
ST = 1 / 393.628 * EXP(14.913319# + S1 + S2 + S3)
ELSE
IF c >= 1.3277 THEN
SI = -1.7546831# * LOG(e)
S2 = -.35584379# * LOG(e) - 2; S3 = .075525649# * LOG(e) - 3
ST = 1 / 393.628 * EXP(14.913319# + S1 + S2 + S3) / 1.0187777#
ELSE
IF e >= 1.0868 THEN
SI = -1.7546831# * LOG(e)
S2 = -.35584379# * LOG(e) ^ 2; S3 = .075525649# * LOG(e) ^ 3
ST = 1 / 393.628 * EXP(14.913319# + S1 + S2 + S3) / 1.032282617#
ELSE
SI = -1.7546831# * LOG(e)
S2 = -.35584379# * LOG(e) ^ 2; S3 = .075525649# * LOG(e) - 3
ST = 1 / 393.628 * EXP(14.913319# + S1 + S2 + S3) / 1.09693169#
END IF
END IF
END IF
END IF
END IF
END IF
TauNP = ST
END FUNCTION
FUNCTION TauO (e)

```







```

FUNCTION TauRb (t)
  IF e >= 15.1997 THEN
    S1 = .382736 * LOG(e); S2 = -.732427 * LOG(e) ^ 2
    S3 = .0529874 * LOG(e) ^ 3
    ST = 1 / 141.9 * EXP(13.0204 + S1 + S2 + S3)
  ELSE
    IF e >= 2.0651 THEN
      S1 = -2.39108 * LOG(e); S2 = -.0959473 * LOG(e) ^ 2
      ST = 1 / 141.9 * EXP(14.9985 + S1 + S2)
    ELSE
      IF e >= 1.8639 THEN
        S1 = -2.39108 * LOG(e); S2 = -.0959473 * LOG(e) ^ 2
        ST = 1 / 141.9 * EXP(14.9985 + S1 + S2) * (1 / 1.16)
      ELSE
        IF e >= 1.8044 THEN
          S1 = -2.39108 * LOG(e); S2 = -.0959473 * LOG(e) ^ 2
          ST = 1 / 141.9 * EXP(14.9985 + S1 + S2) * (1 / 1.636)
        ELSE
          IF e >= .322 THEN
            S1 = -2.38693 * LOG(e)
            ST = 1 / 141.9 * EXP(13.0286 + S1)
          ELSE
            PRINT "Error in functiontauRb: invalid E"
          END
        END IF
      END IF
    END IF
  END IF
  TauRb = ST
END FUNCTION

FUNCTION TauRc (e)
  IF e >= 71.6764 THEN
    S1 = 7.79444 * LOG(e); S2 = -1.99822 * LOG(e) ^ 2
    S3 = .126225 * LOG(e) ^ 3
    ST = 1 / 309.2 * EXP(13.6944 + S1 + S2 + S3)
  ELSE
    IF e >= 12.5267 THEN
      S1 = -2.61051 * LOG(e); S2 = -.0136093 * LOG(e) - 2
      ST = 1 / 309.2 * EXP(17.875 + S1 + S2)
    ELSE
      IF e >= 11.9587 THEN
        S1 = -2.61051 * LOG(e); S2 = -.0136093 * LOG(e) - 2
        ST = 1 / 309.2 * EXP(17.875 + S1 + S2) * (1 / 1.16)
      ELSE
        IF e >= 10.5353 THEN
          S1 = -2.61051 * LOG(e); S2 = -.0136093 * LOG(e) ^ 2
          ST = 1 / 309.2 * EXP(17.875 + S1 + S2) * (1 / 1.636)
        ELSE
          IF e >= 2.9317 THEN
            S1 = -2.62453 * LOG(e)
            ST = 1 / 309.2 * EXP(16.3564 + S1)
          ELSE
            IF e >= 2.6816 THEN
              S1 = -2.62453 * LOG(e)
              ST = 1 / 309.2 * EXP(16.3564 + S1) / 1.080074713#
            ELSE
              IF e >= 2.3673 THEN
                S1 = -2.62453 * LOG(e)
                ST = 1 / 309.2 * EXP(16.3564 + S1) / 1.219859254#
              ELSE
                IF e >= 1.9489 THEN
                  S1 = -2.62453 * LOG(e)
                  ST = 1 / 309.2 * EXP(16.3564 + S1) / 1.620110168#
                ELSE
                  IF e >= 1.8829 THEN
                    S1 = -2.62453 * LOG(e)
                    ST = 1 / 309.2 * EXP(16.3564 + S1) / 2.289610423#
                  ELSE
                    S1 = -2.35326 * LOG(e)
                    ST = 1 / 309.2 * EXP(14.2392 + S1)
                  END IF
                END IF
              END IF
            END IF
          END IF
        END IF
      END IF
    END IF
  END IF
  TauRc = ST
END FUNCTION

FUNCTION TauRh (e)
  IF e >= 23.2199 THEN
    R1 = 1.19682 * LOG(e); R2 = -.866697 * LOG(e) - 2
    R3 = .0606931 * (LOG(e)) ^ 3
    RT = (1 / 170.9) * EXP(12.176 + R1 + R2 + R3)
  ELSE
    IF e >= 3.4119 THEN
      R1 = -2.24976 * LOG(e)
      R2 = -.113377 * LOG(e) ^ 2
      RT = (1 / 170.9) * EXP(15.5757 + R1 + R2)
    ELSE
      IF e >= 3.1461 THEN
        R1 = -2.24976 * LOG(e)
        R2 = -.113377 * LOG(e) ^ 2
        RT = (1 / 170.9) * EXP(15.5757 + R1 + R2) * (1 / 1.16)
      ELSE
        IF e >= 3.0038 THEN
          R1 = -2.24976 * LOG(e)
          R2 = -.113377 * LOG(e) ^ 2
          RT = (1 / 170.9) * EXP(15.5757 + R1 + R2) * (1 / 1.636)
        ELSE
          IF e >= .627 THEN
            R1 = -2.61303 * LOG(e)
            RT = (1 / 170.9) * EXP(14.0312 + R1)
          ELSE
            PRINT "Error in functionTauRh: invalid E"
          END
        END IF
      END IF
    END IF
  END IF
  TauRh = RT
END FUNCTION

FUNCTION TauRn (e)
  IF e >= 98.404 THEN
    S1 = .34902 * LOG(e); S2 = -.637638 * LOG(e) - 2
    S3 = .0451377 * LOG(e) ^ 3
    ST = 1 / 368.6 * EXP(15.1782 + S1 + S2 + S3)
  ELSE
    IF e >= 18.049 THEN
      S1 = -2.13876 * LOG(e); S2 = -.0724638 * LOG(e) ^ 2
      ST = 1 / 368.6 * EXP(17.5028 + S1 + S2)
    ELSE
      IF e >= 17.3371 THEN
        S1 = -2.13876 * LOG(e); S2 = -.0724638 * LOG(e) - 2
        ST = 1 / 368.6 * EXP(17.5028 + S1 + S2) * (1 / 1.16)
      ELSE
        IF e >= 14.6194 THEN
          S1 = -2.13876 * LOG(e); S2 = -.0724638 * LOG(e) ^ 2
          ST = 1 / 368.6 * EXP(17.5028 + S1 + S2) * (1 / 1.636)
        ELSE
          IF e >= 4.482 THEN
            S1 = -2.60945 * LOG(e)
            ST = 1 / 368.6 * EXP(16.9 + S1)
          ELSE
            IF e >= 4.159 THEN
              S1 = -2.60945 * LOG(e)
              ST = 1 / 368.6 * EXP(16.9 + S1) / 1.079705187#
            ELSE
              IF e >= 3.538 THEN
                S1 = -2.60945 * LOG(e)
                ST = 1 / 368.6 * EXP(16.9 + S1) / 1.22029198#
              ELSE
                IF e >= 3.0215 THEN
                  S1 = -2.60945 * LOG(e)
                  ST = 1 / 368.6 * EXP(16.9 + S1) / 1.650106441#
                ELSE
                  IF e >= 2.8924 THEN
                    S1 = -2.60945 * LOG(e)
                    ST = 1 / 368.6 * EXP(16.9 + S1) / 2.270257778#
                  ELSE
                    IF e >= 1.097 THEN
                      S1 = -2.12905 * LOG(e)
                      ST = 1 / 368.6 * EXP(14.7243 + S1)
                    ELSE
                      IF e >= .929 THEN
                        S1 = -2.12905 * LOG(e)
                        ST = 1 / 368.6 * EXP(14.7243 + S1) / 1.01939
                      ELSE
                        IF e >= .768 THEN
                          S1 = -2.12905 * LOG(e)
                          ST = 1 / 368.6 * EXP(14.7243 + S1) / 1.03089
                        ELSE
                          S1 = -2.12905 * LOG(e)
                          ST = 1 / 368.6 * EXP(14.7243 + S1) / 1.08885
                        END IF
                      END IF
                    END IF
                  END IF
                END IF
              END IF
            END IF
          END IF
        END IF
      END IF
    END IF
  END IF
  TauRn = ST
END FUNCTION

FUNCTION TauRu (c)
  IF e >= 22.1172 THEN
    R1 = .88502 * LOG(e); R2 = -.811144 * LOG(e) - 2
    R3 = .0573759 * (LOG(e)) ^ 3
    RT = (1 / 167.8) * EXP(12.6658 + R1 + R2 + R3)
  ELSE
    IF e >= 3.224 THEN
      R1 = -2.2308 * LOG(e)
      R2 = -.119454 * LOG(e) ^ 2
      RT = (1 / 167.8) * EXP(15.4734 + R1 + R2)
    END IF
  END IF
END FUNCTION

```



```

FUNCTION TauSn (e)
  IF e >= 29.2001 THEN
    S1 = .790788 * LOG(e); S2 = -.762349 * LOG(e) ^ 2
    S3 = .0527872 * LOG(e) - 3
    ST = 1 / 197.1 * EXP(13.0323 + S1 + S2 + S3)
  ELSE
    IF e >= 4.4647 THEN
      S1 = -2.1901 * LOG(e); S2 = -.113539 * LOG(e) ^ 2
      ST = 1 / 197.1 * EXP(15.8638 + S1 + S2)
    ELSE
      IF e >= 4.1561 THEN
        S1 = -2.1901 * LOG(e); S2 = -.113539 * LOG(e) - 2
        ST = 1 / 197.1 * EXP(15.8638 + S1 + S2) / 1.16
      ELSE
        IF e >= 3.9288 THEN
          S1 = -2.1901 * LOG(e); S2 = -.113539 * LOG(e) - 2
          ST = 1 / 197.1 * EXP(15.8638 + S1 + S2) / 1.636
        ELSE
          IF e >= .884 THEN
            S1 = -2.56792 * LOG(e)
            ST = 1 / 197.1 * EXP(14.5572 + S1)
          ELSE
            PRINT "Error in function tauSn: invalid e"
          END
        END IF
      END IF
    END IF
  END IF
  TauSn = ST
END FUNCTION

FUNCTION TauSr(e)
  IF e >= 16.1046 THEN
    S1 = 2.20194E-03 * LOG(e); S2 = -.63894 * LOG(e) ^ 2
    S3 = .046007 * LOG(e) ^ 3
    ST = 1 / 145.5 * EXP(13.5888 + S1 + S2 + S3)
  ELSE
    IF e >= 2.2163 THEN
      S1 = -2.28169 * LOG(e); S2 = -.126485 * LOG(e) ^ 2
      ST = 1 / 145.5 * EXP(15.011 + S1 + S2)
    ELSE
      IF e >= 2.0068 THEN
        S1 = -2.28169 * LOG(e); S2 = -.126485 * LOG(e) - 2
        ST = 1 / 145.5 * EXP(15.011 + S1 + S2) * (1 / 1.16)
      ELSE
        IF e >= 1.9396 THEN
          S1 = -2.28169 * LOG(e); S2 = -.126485 * LOG(e) ^ 2
          ST = 1 / 145.5 * EXP(15.011 + S1 + S2) * (1 / 1.636)
        ELSE
          IF e >= .358 THEN
            S1 = -2.36655 * LOG(e)
            ST = 1 / 145.5 * EXP(13.1565 + S1)
          ELSE
            PRINT "Error in function tauSr: invalid E"
          END
        END IF
      END IF
    END IF
  END IF
  TauSr = ST
END FUNCTION

FUNCTION TauTa (e)
  IF e >= 67.4164 THEN
    S1 = 3.73117 * LOG(e); S2 = -1.26359 * LOG(e) ^ 2
    S3 = .0823539 * LOG(e) ^ 3
    ST = 1 / 300.5 * EXP(8.65271 + S1 + S2 + S3)
  ELSE
    IF e >= 11.6815 THEN
      S1 = -2.30313 * LOG(e); S2 = -.0591006 * LOG(e) ^ 2
      ST = 1 / 300.5 * EXP(17.241 + S1 + S2)
    ELSE
      IF e >= 11.1361 THEN
        S1 = -2.30313 * LOG(e); S2 = -.0591006 * LOG(e) ^ 2
        ST = 1 / 300.5 * EXP(17.241 + S1 + S2) / 1.16
      ELSE
        IF e >= 9.8811 THEN
          S1 = -2.30313 * LOG(e); S2 = -.0591006 * LOG(e) ^ 2
          ST = 1 / 300.5 * EXP(17.241 + S1 + S2) / 1.636
        ELSE
          IF e >= 2.708 THEN
            S1 = -2.66148 * LOG(e)
            ST = 1 / 300.5 * EXP(16.3038 + S1)
          ELSE
            IF e >= 2.4687 THEN
              S1 = -2.66148 * LOG(e)
              ST = 1 / 300.5 * EXP(16.3038 + S1) / 1.080023927#
            ELSE
              IF e >= 2.194 THEN
                S1 = -2.66148 * LOG(e)
                ST = 1 / 300.5 * EXP(16.3038 + S1) / 1.209960085#
              ELSE
                IF e >= 1.7932 THEN
                  S1 = -2.66148 * LOG(e)
                  ST = 1 / 300.5 * EXP(16.3038 + S1) / 1.609640671#
                ELSE

```







```

S1 = -2.45068 * LOG(e)
ST = 1 / 218 * EXP(14.7603 + S1) / 1.050148
ELSE
PRINT "Error in function tauXe: invalid e"
END
END IF
END IF
END IF
END IF
END IF
END IF
TauXe = ST
END FUNCTION

FUNCTION TauY (c)
IF c >= 17.0384 THEN
S1 = .191023 * LOG(e); S2 = -.6866116 - LOG(e) ^ 2
S3 = .0497356 - LOG(e) * 3
ST = 1 / 147.6 * EXP(13.4674 + S1 + S2 + S3)
ELSE
IF c >= 2.3725 THEN
S1 = -2.38946 * LOG(e); S2 = -.0881174 * LOG(e) - 2
ST = 1 / 147.6 * EXP(15.1822 + S1 + S2)
ELSE
IF c >= 2.1555 THEN
S1 = -2.38946 * LOG(e); S2 = -.0881174 * LOG(e) - 2
ST = 1 / 147.6 * EXP(15.1822 + S1 + S2) * (1 / 1.16)
ELSE
IF c >= 2.08 THEN
S1 = -2.38946 * LOG(e); S2 = -.0881174 * LOG(e) ^ 2
ST = 1 / 147.6 * EXP(15.1822 + S1 + S2) * (1 / 1.636)
ELSE
IF c >= .395 THEN
S1 = -2.43174 * LOG(e)
ST = 1 / 147.6 * EXP(13.2775 + S1)
ELSE
PRINT "Error in function tauY: invalid E"
END
END IF
END IF
END IF
END IF
END IF
END IF
TauY = ST
END FUNCTION

FUNCTION TauYb (e)
IF e >= 61.3323 THEN
S1 = 4.28955 * LOG(e); S2 = -1.35167 * LOG(e) ^ 2
S3 = .0866136 * LOG(e) ^ 3
ST = 1 / 287.3 * EXP(7.42791 + S1 + S2 + S3)
ELSE
IF e >= 10.4864 THEN
S1 = -2.22577 * LOG(e); S2 = -.0732557 * LOG(e) ^ 2
ST = 1 / 287.3 * EXP(16.9795 + S1 + S2)
ELSE
IF e >= 9.9782 THEN
S1 = -2.22577 * LOG(e); S2 = -.0732557 * LOG(e) ^ 2
ST = 1 / 287.3 * EXP(16.9795 + S1 + S2) / 1.16
ELSE
IF e >= 8.9436 THEN
S1 = -2.22577 * LOG(e); S2 = -.0732557 * LOG(e) ^ 2
ST = 1 / 287.3 * EXP(16.9795 + S1 + S2) / 1.636
ELSE
IF e >= 2.3981 THEN
S1 = -2.67715 * LOG(e)
ST = 1 / 287.3 * EXP(16.1794 + S1)
ELSE
IF e >= 2.173 THEN
S1 = -2.67715 * LOG(e)
ST = 1 / 287.3 * EXP(16.1794 + S1) / 1.070078979#
ELSE
IF e >= 1.9498 THEN
S1 = -2.67715 * LOG(e)
ST = 1 / 287.3 * EXP(16.1794 + S1) / 1.200227093#
ELSE
IF e >= 1.5763 THEN
S1 = -2.67715 * LOG(e)
ST = 1 / 287.3 * EXP(16.1794 + S1) / 1.599967533#
ELSE
IF e >= 1.5278 THEN
S1 = -2.67715 * LOG(e)
ST = 1 / 287.3 * EXP(16.1794 + S1) / 2.290191113#
ELSE
S1 = -2.403391 * LOG(e)
ST = 1 / 287.3 * EXP(13.9108207# + S1)
END IF
END IF
END IF
END IF
END IF
END IF
END IF
TauYb = ST
END FUNCTION

```

```

FUNCTION TauZn (c)
IF c >= 9.6586 THEN
H1 = -.933083 * LOG(e)
H2 = -.477357 * (LOG(e)) ^ 2
H3 = -.0362829 * (LOG(e)) ^ 3
h = (1 / 108.6) * EXP(14.4118 + H1 + H2 + H3)
ELSE
IF c >= 1.1936 THEN
H1 = -2.62384 * LOG(e)
H2 = -.0264926 * (LOG(e)) ^ 2
h = (1 / 108.6) * EXP(14.3221 + H1 + H2) * 1
ELSE
IF c >= 1.0428 THEN
H1 = -2.62384 * LOG(e)
H2 = -.0264926 * (LOG(e)) ^ 2
h = (1 / 108.6) * EXP(14.3221 + H1 + H2) * (1 / 1.16)
ELSE
IF c >= 1.0197 THEN
H1 = -2.62384 * LOG(e)
H2 = -.0264926 * (LOG(e)) ^ 2
h = (1 / 108.6) * EXP(14.3221 + H1 + H2) * (1 / 1.636)
ELSE
IF c >= .139 THEN
H1 = -1.10258 * LOG(e)
h = (1 / 108.6) * EXP(12.0597 + H1)
ELSE
PRINT "Error in function TauZn: invalid E"
END
END IF
END IF
END IF
END IF
TauZn = h
END FUNCTION

FUNCTION tauZO (E, Z AS INTEGER)
SELECT CASE Z
CASE 1
tauZO = TauH(E)
CASE 2
tauZO = TauIc(E)
CASE 3
tauZO = TauLi(E)
CASE 4
tauZO = TauBe(E)
CASE 5
tauZO = TauB(E)
CASE 6
tauZO = tauC(E)
CASE 7
tauZO = TauN(E)
CASE 8
tauZO = TauO(E)
CASE 9
tauZO = TauF(E)
CASE 10
tauZO = TauNe(E)
CASE 11
tauZO = TauNa(E)
CASE 12
tauZO = TauMg(E)
CASE 13
tauZO = TauAl(E)
CASE 14
tauZO = TauSi(E)
CASE 15
tauZO = TauP(E)
CASE 16
tauZO = TauS(E)
CASE 17
tauZO = TauCl(E)
CASE 18
tauZO = TauAr(E)
CASE 19
tauZO = TauK(E)
CASE 20
tauZO = TauCa(E)
CASE 21
tauZO = TauSc(E)
CASE 22
tauZO = TauTi(E)
CASE 23
tauZO = TauV(E)
CASE 24
tauZO = TauCr(E)
CASE 25
tauZO = TauMn(E)
CASE 26
tauZO = TauFe(E)
CASE 27
tauZO = TauCo(E)
CASE 28
tauZO = TauNi(E)
CASE 29
tauZO = TauCu(E)
CASE 30
tauZO = TauZn(E)
CASE 31

```

```

tauZO = TauGa(E)
CASE 32
tauZO = TauGe(E)
CASE 33
tauZO = TauAs(E)
CASE 34
tauZO = TauSe(E)
CASE 35
tauZO = TauBr(E)
CASE 36
tauZO = TauKr(E)
CASE 37
tauZO = TauRb(E)
CASE 38
tauZO = TauSr(E)
CASE 39
tauZO = TauY(E)
CASE 40
tauZO = TauZr(E)
CASE 41
tauZO = TauNb(E)
CASE 42
tauZO = TauMo(E)
CASE 43
tauZO = TauTc(E)
CASE 44
tauZO = TauRu(E)
CASE 45
tauZO = TauRh(E)
CASE 46
tauZO = TauPd(E)
CASE 47
tauZO = TauAg(E)
CASE 48
tauZO = TauCd(E)
CASE 49
tauZO = TauIn(E)
CASE 50
tauZO = TauSn(E)
CASE 51
tauZO = TauSb(E)
CASE 52
tauZO = TauTe(E)
CASE 53
tauZO = TauI(E)
CASE 54
tauZO = TauXe(E)
CASE 55
tauZO = TauCs(E)
CASE 56
tauZO = TauBa(E)
CASE 57
tauZO = TauLa(E)
CASE 58
tauZO = TauCe(E)
CASE 59
tauZO = TauPr(E)
CASE 60
tauZO = TauNd(E)
CASE 61
tauZO = TauPm(E)
CASE 62
tauZO = TauSm(E)
CASE 63
tauZO = TauEu(E)
CASE 64
tauZO = TauGd(E)
CASE 65
tauZO = TauTb(E)
CASE 66
tauZO = TauDy(E)
CASE 67
tauZO = TauHo(E)
CASE 68
tauZO = TauEr(E)
CASE 69
tauZO = TauTm(E)
CASE 70
tauZO = TauYb(E)
CASE 71
tauZO = TauLu(E)
CASE 72
tauZO = TauHf(E)
CASE 73
tauZO = TauTa(E)
CASE 74
tauZO = TauW(E)
CASE 75
tauZO = TauRe(E)
CASE 76
tauZO = TauOs(E)
CASE 77
tauZO = TauIr(E)
CASE 78
tauZO = TauPt(E)
CASE 79
tauZO = TauAu(E)
CASE 80
tauZO = TauHg(E)
CASE 81
tauZO = TauTl(E)
CASE 82
tauZO = TauPb(E)
CASE 83
tauZO = TauBi(E)

```

```

CASE 84
tauZO = TauPo(E)
CASE 85
tauZO = TauAt(E)
CASE 86
tauZO = TauRn(E)
CASE 87
tauZO = TauFr(E)
CASE 88
tauZO = TauRa(E)
CASE 89
tauZO = TauAc(E)
CASE 90
tauZO = TauTh(E)
CASE 91
tauZO = TauPa(E)
CASE 92
tauZO = TauU(E)
CASE 93
tauZO = TauNp(E)
CASE 94
tauZO = TauPu(E)
CASE ELSE
PRINT USING "Element ## not found"; Z
END
END SELECT

```

```

END FUNCTION
FUNCTION TauZr (c)

```

```

IF c >= 179976 THEN
S1 = .697409 * LOG(c); S2 = -.789307 * LOG(c) ^ 2
S3 = .0564531 * LOG(c) ^ 3
ST = 1 / 151.5 * EXP(12.7538 + S1 + S2 + S3)
ELSE
IF c >= 25316 THEN
S1 = -2.38703 * LOG(c); S2 = -.0912292 * LOG(c) ^ 2
ST = 1 / 151.5 * EXP(15.2906 + S1 + S2)
ELSE
IF c >= 23067 THEN
S1 = -2.38703 * LOG(c); S2 = -.0912292 * LOG(c) ^ 2
ST = 1 / 151.5 * EXP(15.2906 + S1 + S2) * (1 / 1.16)
ELSE
IF c >= 22223 THEN
S1 = -2.38703 * LOG(c); S2 = -.0912292 * LOG(c) ^ 2
ST = 1 / 151.5 * EXP(15.2906 + S1 + S2) * (1 / 1.636)
ELSE
IF c >= .431 THEN
S1 = -2.50201 * LOG(c)
ST = 1 / 151.5 * EXP(13.4508 + S1)
ELSE
PRINT "Error in function tauZr: invalid E"
END
END IF
END IF
END IF
END IF
END IF
END IF

```

```

TauZr = ST

```

```

END FUNCTION

```

## REFERENCES

- 1 H. G. J. Moseley, *Phil. Mag.* 26, 1024, 1913
- 2 H. G. J. Moseley, *Phil. Mag.* 27, 703, 1914
- 3 E. Gillam and H. T. Heal, *Brit. J. Appl. Phys.*, 3, 353, 1952
- 4 J. Sherman, *Spectrochim. Acta*, 7, 238, 1955
- 5 H. J. Lucas-Tooth and B. J. Price, *Metallurgia*, 54, 149, 1961
- 6 T. Shiraiwa and N. Funjino, *Jap. J. App. Phys.*, 5, 886, 1966
- 7 T. Shiraiwa and N. Funjino, *X-Ray Spectrom.*, 3, 64, 1974
- 8 J. W. Criss and L. S. Briks, *Anal. Chem.*, 40, 7, 1080, 1968
- 9 H. Ebel, *X-Ray Spectrom.*, 28, 255, 1999
- 10 C. E. Feather and J. P. Willis, *X-Ray Spectrom.*, 5, 41, 1976
- 11 P. Van Espen and F. Adams, *X-Ray Spectrom.*, 5, 123, 1976
- 12 Sheng X. Bao, *X-Ray Spectrom.*, 26, 23, 1997
- 13 D. L. Taylor and G. Andermann, *Appl. Spectrosc.*, 27, 352, 1973
- 14 R. Cesareo, *Nucl. Instruments and Methods*, 179, 545, 1981
- 15 K. K. Nielson, *Analytical Chemistry*, 49, 4, 1977
- 16 J. A. Ibers and W. C. Hamilton, *International Tables for X-Ray Crystallography*, Vol. 4, Kynoch Press, Birmingham, 1974
- 17 J. H. Hubbell, W. J. Veigele, E. A. Briggs, R. T. Brown, D. T. Cromer and R. J. Howerton, *J. Phys. Chem. Ref. Data* 4, 471, 1975
- 18 C. G. Barkla and C. A. Sadler, *Phil. Mag.* 14, 408, 1907
- 19 C. G. Barkla and C. A. Sadler, *Phil. Mag.* 17, 739, 1909
- 20 J. H. Lambert, *Photometria siva de Mensura et Gradibus Lumiere*, Le Havre, 1729
- 21 A. Beer, *Ann. Phys. (Leipzig)*, 86, 78, 1852
- 22 J. H. Hubbell, *X-Ray Spectrom.*, 28, 215, 1999
- 23 R. W. Fink, R. C. Jopson, H. Mark and C. D. Swift, *Rev. Mod. Phys.* 38, 513, 1966
- 24 W. Bambynek, B. Crasemann, R. W. Fink, H. U. Freund, H. Mark, C. D. Swift, R. E. Price and P. Venugopala Rao, *Rev. Mod. Phys.* 44, 716, 1972
- 25 J. H. Hubbell, P. N. Trehan, N. Singh, B. Chand, D. Mehta, M. L. Garg, R. R. Garg, S. Singh and S. Puhri, *J. Phys. Chem. Ref. Data* 23, 339, 1994
- 26 W. Bambynek, X-84 Proc. X-Ray and Inner-Shell Processes in Atoms. Molecules and Solids, Leipzig Aug. 20-23, 1984, edited by A. Meisel (VEB Druckerei, Thomas Münzer, Langensalza 1984) post-deadline paper P-1. A New Evaluation of K-Shell Fluorescence Yields (Fit:  $K:5 < Z < 100$ ).
- 27 D. D. Cohen, *Nucl. Instr. Meth. B* 22, 55, 1987
- 28 E. H. S. Burhop, *J. Physique et le Radium* 16, 625, 1955
- 29 G. C. Johnson, Jr., and E. W. White, *X-Ray Emission and keV Tables for Nondiffractive Analysis*. ASTM Data Series DS 46, ASTM, Philadelphia, 1970
- 30 G. Love, M. G. Cox and V. D. Scott, *J. Phys. D* 11, 7, 1978
- 31 G. Love and V. D. Scott, *J. Phys. D* 11, 1369, 1978
- 32 G. Love and V. D. Scott, *J. Phys. D* 13, 995, 1980
- 33 G. Love and V. D. Scott, *Scanning* 4, 111, 1981
- 34 J. J. Thomson, *Phil. Mag.* 45, 172, 1898
- 35 A. Sommerfeld, *Phys. Z.*, 10, 969, 1919
- 36 A. Sommerfeld, *Ann. Phys.*, 11, 257, 1931
- 37 P. Kirkpatrick and L. Wiedmann, *Phys. Rev.*, 67, 321, 1945
- 38 C. T. Ulrey, *Phys. Rev.*, 11, 401, 1918
- 39 H. A. Kramers, *Phil. Mag.*, 46, 836, 1923.
- 40 H. Kulenkampff, *Ann. Phys.*, 69, 548, 1923.
- 41 T. S. Rao-Sahib and D. B. Wittry, *Proceeding of the sixth international conference on x-ray optics and microanalysis*, University of Tokyo Press, Japan, 131, 1972.

- 42 M. C. Brunetto and J. A. Riveros, *X-Ray Spectrom.*, 13, 2, 1984
- 43 D. G. W. Smith and S. J. Reed, *X-Ray Spectrom.*, 10, 198, 1981
- 44 R. Castaing and J. Descamps, *J. Phys. Radium*, 16, 304, 1955
- 45 D. J. Whalen and D. C. Turner, *Adv. X-Ray Anal.*, 38, 299, 1995
- 46 H. Ebel, H. Wiederschwinger, J. Wernisch, P. A. Pella, *Adv. X-Ray Anal.*, 35, 721, 1992
- 47 B. Schoßmann, H. Wiederschwinger, H. Ebel, and J. Wernisch, *Adv. X-Ray Anal.* 39, 127, 1997
- 48 J. L. Pouchou and F. Pichoir, *Electron Probe Quantitation*, Ed. Heinrich and Newbury, Plenum Press, 31, 1991
- 49 J. Philibert, in *Proceedings of 3rd International Conference on X-Ray Optics and Microanalysis*, edited by H. H. Pattee, V. E. Cosslett and A. Engström, p.379, Academic Press, New York, 1963
- 50 D. A. Sewell, G. Love and V. D. Scott, *J. Phys. D, Appl. Phys.*, 18, 1269, 1985
- 51 P. A. Pella, Liangyuan Feng and J. A. Small, *X-Ray Spectrom.* 14, 125, 1985
- 52 H. Wiederschwinger, PhD Thesis, Technische Universität Wien, 1990
- 53 R. L. Myklebust, *J. Phys.* 45 (Suppl.), C2-41, 1984
- 54 H. Ebel, *Angewandte Röntgenphysik I*, TU Wien, 1998
- 55 R. Jenkins, R. W. Gould, D. Gedcke, *Quantitative X-ray Spectrometry*, 2<sup>nd</sup> edition, Marcel Dekker, Inc., 1995
- 56 C. E. Fiori, R. L. Myklebust and K. F. J. Heinrich, *Anal. Chem.*, 48, 172, 1976
- 57 E. B. Saloman, J. H. Hubbell, and J. H. Scofield, *At Data Nucl. Data Tables*, 38, 1-197, 1988
- 58 J. H. Scofield, *Phys. Rev.* 9, 179, 1969
- 59 B. L. Henke, P. Lee, T. J. Tanaka, R. Shimabukuro, and B. K. Fujikawa, *At. Data Nucl. Data Tables* 27, 1, 1982
- 60 E. Schäfer, "Massenschwächungskoeffizienten für Fundamentale Parameterprogramme", Dissertation am Institut für Angewandte und Technische Physik, der Technischen Universität Wien, 1993
- 61 J. H. Hubbell, NISTIR No. 5893, 1996
- 62 M. L. Mallikarjuna, S. B. Appaji Gowda, S. Krishnaveni, R. Gowda, and T. K. Umesh, *Nucl. Science and Engineering*, 140, 96, 2002
- 63 M. Angelone, T. Bubba, A. Esposito, *Applied Rad. and Isotopes*, 55, 505, 2001
- 64 M. Ertugrul, Ö. Simsek, O. Dogan, Ü. Turgut, *J. Radioanal. Nucl. Chem., Lett.* 213, 37, 1996
- 65 A. Karabulut, G. Budak, M. Ertugrul, *Nucl. Instrum. and Meth. in Phys. Res. B*, 152, 202, 1999
- 66 B. R. Kerur, S. R. Thontadarya and B. Hanumaiah, *X-Ray Spectrom.*, 27, 45, 1997
- 67 I. H. Suzuki, and N. Saito, *J. Electron Spectrosc. and Rel. Phen.*, 123, 239, 2002
- 68 C. T. Chantier, C. Q. Tran, Z. Barnea, D. Paterson, D. J. Cookson, D. X. Balaic, *Phys. Rev. A*, 64, 062506, 2001
- 69 P. K. Hon, and K. F. J. Heinrich, Personal Communication.
- 70 B. Nordfors, and E. Noreland, *Ark. Fys.* 20, 1, 1961.
- 71 M. H. Tuilier, D. Laporte, and J. M. Esteva, *Phys. Rev. A* 26, 372, 1982.
- 72 N. K. Del Grande, *SPIE (Int. Soc. Optical Engineering) Proc.*, 691, 2, 1986
- 73 K. Quanruzzaman, M. Hussain, and M. Sarkar, *Dhaka University Studies B* 38, 155, 1990
- 74 Wang Dachun, Yang Hua, Luo Pingan and Ding Xunliang, *Nucl. Instrum. Meth. B* 71, 249, 1992
- 75 W. H. McMaster, N. Kerr Del Grande, J. H. Mallett, J. H. Hubbel, University of California, Livermore, Publication UCRL-50174, 1969
- 76 D. T. Cromer and J. B. Mann, *Compton Scattering Factors for Spherically Free Atoms*, Los Alamos Scientific Laboratory, New Mexico, Report LA-DC-8819, 1967

- 77 D. T. Cromer and J. T. Wabet, Scattering Factors Computed from Relativistic Dirac-Slater Wave Functions, *Acta Cryst.* 18, 104, 1965
- 78 R. D. Schmickley and R. H. Pratt, *Phys. Rev.*, 164, 104, 1967
- 79 J. H. Scofield, Theoretical Photoionization Cross Sections from 1 to 1500 keV, Lawrence Livermore Laboratory, UCRL-51326, 1973
- 80 W. T. Elam, B. D. Ravel and J. R. Sieber, *Rad. Phys. Chem.*, 63, 121, 2002
- 81 American Institute of Physics Handbook, McGraw-Hill, Inc. 1972, (J. A. Bearden and J. S. Thomsen, X-Ray Wavelength and Atomic Energy Levels, The Johns Hopkins University.)
- 82 S. Brennan and P. L. Cowan, *Rev. Sci. Instr.*, 63, 1, 850, 1992
- 83 M. Ali. Memar, Werkstoffanalyse mittels Röntgenstrahlinduzierter Elektronenemission, Dissertation am Institut für Angewandte und Technische Physik, der Technischen Universität Wien, 1997
- 84 K. Siegbahn, C. Nordling, A. Fahlman, R. Nordberg, K. Hamrin, J. Hedman, G. Johansson, T. Bergmark, S. Karlsson, I. Lindgren, B. Lindberg, *Nova Acta Regiae Societatis Scientiarum Upsaliensis, Ser IV, Vol. 20, Impr. 29/12, 1967*
- 85 M. Mantler, Tabellen der Fundamentalparameter, Institut für Angewandte und Technische Physik, der Technischen Universität Wien
- 86 <http://www.ixs.iit.edu/database>
- 87 [http://www.esrf.fr/computing/scientific/dabax/tmp\\_file/FileDesc.html](http://www.esrf.fr/computing/scientific/dabax/tmp_file/FileDesc.html)
- 88 B.L. Henke, E.M. Gullikson, and J.C. Davis, *At. Data Nucl. Data Tables* 54, 181, 1993
- 89 N. K. Del Grande, "Measured 1 to 40 keV Photoabsorption Cross Section for: Fe, Ni, Sn, Ta, Pt, Au, Pb, U, *Proc. SPIE* 691, X-ray Imaging II, 2, 1990
- 90 N. K. Del Grande, *Physica Scripta* 41, 110, 1990
- 91 R. D. Deslattes, *Acta Cryst. A* 25, 89, 1969
- 92 J. H. Hubbell, *Rad. Res.* 70, 58, 1977
- 93 J. H. Hubbell, H. A. Gimm, and I. Overbo, *J. Phys. Chem. Ref. Data* 9, 1023, 1980
- 94 E. B. Saloman, J. H. Hubbell and J. H. Scofield, *At. Data Nucl. Data Tables* 38, 1, 1988
- 95 E. Storm, and H. I. Israel, *Nucl. Data Tables A* 7, 565, 1970
- 96 J. H. Hubbell, H. M. Gerstenberg, and E. B. Saloman, National Bureau of Standards Report NBSIR 86, 1986
- 97 L. Kissel and R.H. Pratt, in *Atomic Inner-Shell Physics*, B. Crasemann, ed. (Plenum Press, New York), 465, 1985
- 98 D. E. Cullen, M. H. Chen, J. H. Hubbell, S. T. Perkins, E. F. Plechaty, J. A. Rathkopf and J. H. Scofield, Tables and Graphs of Photon Interaction Cross Sections from 10 eV to 100 GeV Derived from the LLNL Evaluated Photon Data Library (EPDL), Part A: Z=1 to 50; Part B: Z=51 to 100, Lawrence Livermore National Laboratory Report UCRL-50400, Vol. 6, Rev.4, 1989
- 99 D.E. Cullen, S.T. Perkins, and J.A. Rathkopf, "The 1989 Livermore Evaluated Photon Data Library (EPDL)," UCRL-ID-103424, Lawrence Livermore National Laboratory, 1990
- 100 D.E. Cullen, S.T. Perkins and E.F. Plechaty, "The ENDF/B-VI Photon Interaction Library," Lawrence Livermore National Laboratory, UCRL-JC-109764, January 1992
- 101 D. E. Cullen, "Photon Interaction Data for ENDF/B-VI," UCRL-JC-116332 and the proceedings of the 1994 Reactor Physics Topical Meeting of the ANS, Feb. 1994
- 102 R. Jenkins, R. Manne, R. Robin, C. Senemaud, *X-Ray Spectrom.*, 20, 149, 1991
- 103 H. Ebel, R. Svagera, M.F. Ebel, A. Shaltout, H. Hubbell, *X-Ray Spectrom.*, in print 2003
- 104 M. Cardona and L. Ley, *Photoemission in Solids I, Topics in Applied Physics*, 26, Springer-Verlag Berlin Heidelberg, 1978
- 105 M. J. Berger and J. H. Hubbell, XCOM Photon Cross Sections on a Personal Computer," NBSIR 87-3597, 1987

- 106 Hubbell, J.H., Veigele, W.J., Briggs, E.A., Brown, R.T., Cromer, D.T., and Howerton, R.J., *J. Phys. Chem. Ref. Data* 4, 471, 1975); erratum in 6, 615, 1977
- 107 Hubbell, J.H. and Overbo, J. *Phys. Chem. Ref. Data* 8, 69, 1979
- 108 J. H. Hubbell, *Nad. Stand. Ref. Data Ser.* 29, 1969
- 109 R. H. Pratt, Atomic Photoelectric Effect at High Energies, *Phys. Rev.* 117, 1017, 1960
- 110 Saloman, E.B. and Hubbell, J.H., *Critical Analysis of Soft X-ray Cross Section Data*, *Nucl. Instr. Meth.* A255, 38, 1987
- 111 <http://physics.nist.gov/PhysRefData/Xcom/Text/XCOM.html>
- 112 W. H. Press, S. A. Teukolsky, W. T. Wetterling, and B. P. Flannery, *Numerical Recipes in C, The Art of Scientific Computing*, 2<sup>th</sup> Edition, Cambridge University Press, 1992
- 113 <http://www.llnl.gov/cullen/>
- 114 D.E. Cullen, et al., "Tables and Graphs of Atomic Subshell and Relaxation Data Derived from the LLNL Evaluated Atomic Data Library (EADL), Z = 1 - 100," Lawrence Livermore National Laboratory, UCRL-50400, Vol. 30, October 1991
- 115 D.E. Cullen "Program RELAX: A Code Designed to Calculate X-Ray and Electron Emission Spectra as Singly Charged Atoms Relax Back to Neutrality," Lawrence Livermore National Laboratory, UCRL-ID-110438, March 1992
- 116 D. E. Cullen, J. H. Hubbell and L. Kissel, EPDL97: The Evaluated Photon Data Library, Lawrence Livermore National Laboratory Report UCRL-50400, 6, 5, 1997
- 117 D.E. Cullen, S.T. Perkins and S.M. Seltzer, "Tables and Graphs of Electron Interaction Cross Sections from 10 eV to 100 GeV Derived from the LLNL Evaluated Electron Data Library (EEDL), Z = 1 - 100," Lawrence Livermore National Laboratory, UCRL-50400, Vol. 31, November 1991
- 118 J.H. Hubbell, *Radiat. Phys. Chem.*, 50, 1, 113, 1997
- 119 R.H. Pratt, L. Kissel and P.M. Bergstrom, Jr., "New relativistic S-Matrix results for scattering - beyond the usual anomalous factors/ beyond impulse approximation," in *Resonant Anomalous X-Ray Scattering*, G. Materlik, C.J. Sparks and K. Fischer, eds. (Elsevier Science Publishers, Amsterdam, 1994), pp 9-33
- 120 D E. Cullen, Program EPICSHOW, A computer code to allow interactive viewing of the EPIC data libraries, Lawrence Livermore National Laboratory, UCRL-ID-116819, 1994
- 121 F. Biggs and R. Lighthill, Sandia Report SANd870070 UC-34, 1988
- 122 S.Sasaki, Numerical Tables of Anomalous Scattering Factors Calculated by the Cromer and Liberman Method, KEK Report, 88-14, 1-136, 1989
- 123 C. T. Chantier, "Theoretical form factor, attenuation, and scattering tabulation for Z=1-92 from E=1-10 eV to E=0.4 -1.0 MeV", *J. Phys. Chem. Ref. Data*, Vol. 24, No. 1, pp 71-643, 1995.
- 124 S. R. Afshar, *Quantitative Röntgenfluoreszenzanalyse*, am Institut für Angewandte und Technische Physik, der Technischen Universität Wien, 1997
- 125 R.F. Reilman, A Msezane and ST Manson, *J.Electron Spectrosc.and Rel.Phen.*, 8, 389, 1976
- 126 S. Tanuma, CJ Powell and DR Penn, *Surf.Interface Anal.*, 17, 911, 1991
- 127 S. Tanuma, CJ Powell and DR Penn, *Surf.Interface Anal.*, 17, 927, 1991
- 128 S. Tanuma, CJ Powell and DR Penn, *Surf.Interface Anal.* 20, 77, 1993
- 129 H. Ebel, R Svagera, M.F. Ebel and W.S.M. Werner, *Adv.X-Ray Anal.*, 44, 380, 2001

## CURRICULUM VITA

Full Name	Abd-Allah Amin Mahmoud Shaltout																								
Family Name	Shaltout																								
Date of Birth / Place	19, April 1970, Menoufia, Egypt.																								
Marital Status	Married and have two children																								
Nationality	Egyptian																								
Addresses	<ul style="list-style-type: none"> <li>• Present address Penzingerstraße 150-166/26/2, 1140 Wien.</li> <li>• Permanent address National Research Center, Spectroscopy Dep., Dokki, Thrir Street, Cairo, Egypt. Email: shaltout_a@hotmail.at</li> </ul>																								
Educational background	<table border="0" style="width: 100%;"> <tr> <td style="vertical-align: top;">1976-1981</td> <td>Primary school in Menoufia, Egypt</td> </tr> <tr> <td style="vertical-align: top;">1981-1984</td> <td>Prep school in Menoufia, Egypt</td> </tr> <tr> <td style="vertical-align: top;">1984-1987</td> <td>Secondary school in Menoufia, Egypt</td> </tr> <tr> <td style="vertical-align: top;">July 1987</td> <td>Secondary school certificate, Egypt</td> </tr> <tr> <td style="vertical-align: top;">1987-1991</td> <td>Faculty of Science, Assiut University, Egypt</td> </tr> <tr> <td style="vertical-align: top;">May 1991</td> <td>B.Sc Degree of physics, Egypt</td> </tr> <tr> <td style="vertical-align: top;">1993-1998</td> <td>M.Sc of physics, Menoufia university, Egypt</td> </tr> <tr> <td style="vertical-align: top;">1995-1996</td> <td>Diploma of Educational computer, Cairo university, Egypt</td> </tr> <tr> <td style="vertical-align: top;">May 1996</td> <td>Diploma Degree, Cairo university, Egypt</td> </tr> <tr> <td style="vertical-align: top;">Sep. 1998</td> <td>M.Sc Degree of physics, Menoufia university, Egypt</td> </tr> <tr> <td style="vertical-align: top;">1997-1999</td> <td>Teach Assistance in Menoufia university, Egypt.</td> </tr> <tr> <td style="vertical-align: top;">Sep. 1999- Now</td> <td>Ph.D student in Vienna university of technology.</td> </tr> </table>	1976-1981	Primary school in Menoufia, Egypt	1981-1984	Prep school in Menoufia, Egypt	1984-1987	Secondary school in Menoufia, Egypt	July 1987	Secondary school certificate, Egypt	1987-1991	Faculty of Science, Assiut University, Egypt	May 1991	B.Sc Degree of physics, Egypt	1993-1998	M.Sc of physics, Menoufia university, Egypt	1995-1996	Diploma of Educational computer, Cairo university, Egypt	May 1996	Diploma Degree, Cairo university, Egypt	Sep. 1998	M.Sc Degree of physics, Menoufia university, Egypt	1997-1999	Teach Assistance in Menoufia university, Egypt.	Sep. 1999- Now	Ph.D student in Vienna university of technology.
1976-1981	Primary school in Menoufia, Egypt																								
1981-1984	Prep school in Menoufia, Egypt																								
1984-1987	Secondary school in Menoufia, Egypt																								
July 1987	Secondary school certificate, Egypt																								
1987-1991	Faculty of Science, Assiut University, Egypt																								
May 1991	B.Sc Degree of physics, Egypt																								
1993-1998	M.Sc of physics, Menoufia university, Egypt																								
1995-1996	Diploma of Educational computer, Cairo university, Egypt																								
May 1996	Diploma Degree, Cairo university, Egypt																								
Sep. 1998	M.Sc Degree of physics, Menoufia university, Egypt																								
1997-1999	Teach Assistance in Menoufia university, Egypt.																								
Sep. 1999- Now	Ph.D student in Vienna university of technology.																								